UTS UNIVERSITY OF TECHNOLOGY SYDNEY

SELECTIVE RECOVERY OF RARE EARTH ELEMENTS AND VALUABLE METALS FROM MINING WASTEWATER BY MEMBRANE/ADSORPTION HYBRID SYSTEMS

by CHARITH FONSEKA

Thesis submitted in fulfilment of the requirements for the degree of

Doctor of Philosophy

under the supervision of Emeritus Prof Saravanamuthu Vigneswaran

University of Technology Sydney

Faculty of Engineering and Information Technology

December 2023

CERTIFICATE OF ORIGINAL AUTHORSHIP

I, Charith Fonseka declare that this thesis is submitted in fulfilment of the requirements for the award of Doctor of Philosophy, in the Faculty of Engineering and Information Technology at the University of Technology Sydney.

This thesis is wholly my own work unless otherwise referenced or acknowledged. In addition, I certify that all information sources and literature used are indicated in the thesis.

This document has not been submitted for qualifications at any other academic institution.

This research is supported by the Australian Government Research Training Program.

Signature: Production Note: Signature removed prior to publication.

Date: 20/12/2023

ACKNOWLEDGEMENTS

I would like to express my deepest gratitude and appreciation to my principal supervisor, Emeritus Prof. Saravanamuthu Vigneswaran, for his invaluable guidance, support, and mentorship throughout my PhD journey. His expertise, patience, and encouragement were instrumental in shaping the direction of this research and guiding me towards achieving my academic goals.

I am also thankful to my co-supervisors A/Prof. Jaya Kandasamy and Dr. Gayathri Naidu, for providing insightful feedback, continuous motivation, which encouraged me to strive for excellence and push the boundaries of my academic pursuits. Their willingness to invest time and effort in my growth as a researcher have been truly inspiring.

I extend my heartfelt thanks to my fellow senior researcher and friend, Seongchul Ryu for his camaraderie, collaboration, and stimulating discussions, which helped me navigate challenging periods of my PhD journey.

My sincere gratitude goes to Dr. M.D. Johir, Dr. Nirenkumar Pathak and Dr. Youngwoo Choo, whose assistance and cooperation were indispensable in conducting lab experiments and accessing the necessary resources for material analysis.

Last but not least, I am deeply grateful to my loving wife Rosemary, family and friends for their unwavering love, understanding, and encouragement throughout this challenging journey.

This thesis would not have been possible without the contributions of all those mentioned above, and for that, I am sincerely thankful.

LIST OF PUBLICATIONS

Fonseka, C.; Ryu, S.; Choo, Y.; Mullett, M.; Thiruvenkatachari, R.; Naidu, G.; Vigneswaran, S. Selective Recovery of Rare Earth Elements from Mine Ore by Cr-MIL Metal–Organic Frameworks. *ACS Sustainable Chemistry & Engineering* **2021**, *9*, 16896-16904.	Published
Ryu, S.; **Fonseka, C**.; Naidu, G.; Loganathan, P.; Moon, H.; Kandasamy, J.; Vigneswaran, S. Recovery of rare earth elements (Lu, Y) by adsorption using functionalized SBA-15 and MIL-101 (Cr). *Chemosphere* **2021**, 130869.	Published
Fonseka, C.; Ryu, S.; Naidu, G.; Kandasamy, J.; Vigneswaran, S. Recovery of water and valuable metals using low pressure nanofiltration and sequential adsorption from acid mine drainage. *Environmental Technology & Innovation* **2022**, *28*, 102753	Published
Fonseka, C.; Ryu, S.; Naidu, G.; Kandasamy, J.; Ratnaweera, H.; Vigneswaran, S., 13 - Metal-organic frameworks for recovery of valuable elements. In *Nano-Enabled Technologies for Water Remediation*, Kaleekkal, N. J.; Mural, P. K. S.; Vigneswaran, S., Eds. Elsevier: 2022; pp 377-392.	Published

Fonseka, C.; Ryu, S.; Naidu, G.; Thiruvenkatachari, R.; Kandasamy, J.; Vigneswaran, S. Europium adsorption by granulated Cr-MIL-PMIDA Metal−Organic Frameworks and dynamic fixed bed column modelling. *Water Process Engineering* 2023	Published
Fonseka, C.; Ryu, S.; Choo, Y.; Naidu, G.; Foseid, L.; Thiruvenkatachari, R.; Kandasamy, J.; Ratnaweera, H.; Vigneswaran, S. Selective Recovery of Europium from real acid mine drainage by using novel SBA15-NH-PMIDA adsorbent and membrane distillation system. *Water Process Engineering* 2023	Published

CONFERENCE PRESENTATIONS

13th International Conference on the Challenges in Environmental Science and Engineering (CESE 2020), Virtual conference, oral presentation, Nov 2020	Oral Presentation
2nd International conference on Waste, Energy and Environment (ICWEE 2021), virtual conference, oral presentation, Sept 2021	Oral Presentation
14th International Conference on the Challenges in Environmental Science and Engineering (CESE 2021), Virtual conference, oral presentation, Nov 2021	Oral Presentation
ECR Membrane symposium 2021, Virtual conference, oral presentation, Nov 2021	Oral Presentation
5th UTS School of Civil and Environmental Engineering 2021 Virtual Research Showcase, Poster Presentation, Sept 2021	Poster Presentation
IWA world water congress 2022, Sept 2022	Poster pitch presentation

Circular Economy For Climate and Environment (CECE 2023) Conference, Sydney. Sept 2023 — Oral Presentation

LIST OF ABBREVIATIONS

AMD	Acid mine drainage
APTES	(3-aminopropyl)triethoxysilane
BET	Brunauer-Emmett-Teller
BJH	Barrett-Joyner-Halenda
DCC	Dicyclohexylcarbodiimide
DCMD	Direct contact membrane distillation
DMF	N,N-dimethylformamide
EC	European Commission
FE-TEM	Field emission transmission electron microscope
FT-IR	Fourier transform infrared spectroscopy
ICP-MS	Inductively coupled plasma-mass spectrometry
LDFA	Linear driving for approximation
MD	Membrane distillation
MOF	Metal-organic Frameworks
NF	Nano filtration
ODE	Ordinary differential equation
PA	Phthaloyl diamide

PDEPE	Parabolic and elliptic partial differential equations
PDM	Pore diffusion model
PMIDA	N-(phosphonomethyl) iminodiacetic acid
PSD	Pore size distribution
PTFE	Polytetrafluoroethylene
PVDF	Polyvinylidene fluoride
REE	Rare earth element
RO	Reverse osmosis
SDA	Structure direct agent
SDM	Surface diffusion model
SEM	Scanning electron microscopy
TDS	Total dissolved solids
TEOS	Tetraethyl orthosilicate
XRD	X-ray diffraction
XPS	X-ray photoelectron
VCF	Volume concentration factor

TABLE OF CONTENTS

LIST OF FIGURES

LIST OF TABLES

ABSTRACT

Rare earth elements (REEs) have become a strategic resource extensively used in renewable energy technologies and modern electronic devices. Depletion of natural REE-bearing mineral deposits has made selective recovery of REEs from alternative sources crucial in meeting the rising global demand. Among REEs, Europium (Eu) is relatively scarce in the Earth's crust compared to more abundant elements. The increasing demand for advanced electronics and technology has heightened the importance of europium. Given these factors, europium is considered critical, and its availability can impact various technological and industrial sectors, emphasizing the importance of secure and sustainable supply chains for this element. A previously reported method was used to synthesise a chromium-based metal-organic framework modified with N-(phosphonomethyl) iminodiacetic acid (PMIDA) in this study to selectively recover Eu from chemically complex zinc ore leachate. The adsorbent was characterized and comprehensively examined for Eu uptake as a function of adsorbate concentration, contact time, and pH of the solution. Cr-MIL-PMIDA showed a maximum adsorption capacity of 69.14 mg/g at pH 5.5 while adsorption kinetics best fitted the pseudo-second-order model. Furthermore, Cr-MIL-PMIDA showed exceptional selectivity (88%) toward Eu over competing transitional metal ions (Na, Mg, Al, Ca, Mn, Fe, Ni, Cu, Co, and Zn) found in the dissolved mine ore. A subsequent study was carried out to evaluate the efficiency of water recovery using low pressure Nano Filter (NF) from synthetic AMD and recovery of valuable metals from concentrated feed using novel adsorbents. NF filtration resulting in a steady flux of 15.5 L/m^2h and 80% of water was recovered from

synthetic AMD with over 95% solute rejection. Concentrated feed water was then used for selective recovery of valuable metals such as REE and Cu.

While Cr-MIL-PMIDA exhibits excellent properties for selective recovery of REE, there are practical challenges associated with its production cost and potential susceptibility to chromium leaching, making it less attractive for mass applications. To address these challenges, a highly stable, cost-effective, novel SBA15-NH-PMIDA material was then synthesized for the first time following a two-step surface modification process using 3-aminopropyl triethoxysilane (APTES) and N-(phosphonomethyl) iminodiacetic acid (PMIDA) for selective recovery of Europium (Eu). Initial, single solute Eu adsorption tests revealed that SBA15-NH-PMIDA reached equilibrium within two hours and showed a maximum Langmuir adsorption capacity of 86.21 mg/g at optimum pH 4.8. Selective adsorption tests were carried out with real acid mine drainage (AMD) collected from an abandoned mining site in northern Norway. The novel adsorbent selectively recovered over 80% of Eu from pH-adjusted real AMD at an optimum dosage of 0.8g/l.

A Direct contact membrane distillation (DCMD)/adsorption hybrid system was then developed by suspending granulated SBA15-NH-PMIDA in the feed tank to remediate pH adjusted AMD. DCMD system managed to recover 80% of clean water that can be reused for mining activities to reduce water stress, especially in arid regions. The system managed to concentrate Eu ions by over three folds to enable efficient selective recovery of Eu (over 90%), while uptake of other competing metals remained below 10%. Comprehensive chemical characterisation of pristine and spent adsorbents revealed that High selectivity of these two materials was due to the formation of strong Eu complexes with phosphonic and carboxyl functional groups. SBA15-NH-PMIDA managed to retain

over 90% of adsorption capacity over 10 regeneration cycles. The study revealed that, 193.2 g of $EuCl^3$ with 99% purity can be recovered by treating 1000 m^3 of AMD. Additionally, clean water recovered from the membrane system can be re used in mining activities to reduce water stress in arid regions.

CHAPTER 1

INTRODUCTION

1 Introduction

1.1 Background

Advancement of industries has caused severe environmental pollution over the years. Acid mine drainage (AMD) is one such challenge that has caught global attention. Acid mine drainage is caused as a result of seepage of water through ore waste piles, exposed cuts, and sulphuric-rich soils (Naidu et al, 2019). The release of untreated AMD causes contamination of downstream water bodies as it is composed of dissolved heavy metals, sulphates, and high acidity. Hence, it will pose a severe threat to the functioning of ecosystems. Consumption of water consisting above pollutants will have negative impacts on the health of people and animals. Therefore, identifying an efficient and cost-effective solution to treat AMD is of paramount importance (Naidu et al., 2019). Increasing cost of mining activities and stringent environmental regulations have made treatment of AMD an additional cost for the industry (Nordstrom, 2011). Hence, the interest on resource recovery from AMD has gained popularity within the industry. Exhaustion of natural resources have further increased the search for alternative sources for metal recovery (Gaikwad et al., 2009).

Current acid mine drainage treatment focuses on pH correction and removal of contaminants before they are released into the environment. The cost of treatment is a major factor in deciding treatment options for mining sites. Even though passive treatment is comparatively cheap, stringent environmental policies require further purification before disposal. Hence advanced treatment methods are required which comes at a high cost. Reverse osmosis, nanofiltration, and membrane distillation are some

active treatment methods that are available in the market. However, the need for pre filtration and high cost of replcement of membranes makes it unattractive for the mining industry. Hence, there is a need for resource recovery from AMD with the aim of off setting atleast a portion of the cost of treatment to make it viable for the industry.

The global demand for Rare Earth elements is rapidly increasing. Market research reports show that the market size of REE stood at 2.8 billion USD in 2018. It is expected that it will have a continuous annual growth rate of 10.4% from 2019 to 2025 (Research, 2019). Hence resource recovery from AMD has the potential to become a financially viable investment in the future which will simultaneously help reduce environmental impact. There are several methods that have been analysed for recovery of REE from Acid Mine Drainage. Precipitation, adsorption, ion exchange and liquid-liquid extraction are some of the more promising methods found in literature (Anastopoulos et al., 2016; T. Chen et al., 2014; Felipe et al., 2020; Motsi et al., 2009; Sampaio et al., 2009). Membrane separation methods such as Reverse Osmosis, nano filtration and membrane distillation were also used to pre concentrate REE (Ambiado et al., 2016). Among these methods, adsorption was found to be the most effective and simplest method for recovery of REE and heavy metals from Acid mine drainage (Anastopoulos et al., 2016). Among the promising adsorbents found in literature Nano carbon shells (Xiaoqi et al., 2016), Nano based magnetic particles (Zhang et al., 2016), metal organic frameworks (Lee et al., 2018) and silica composites (Y. Hu et al., 2017; Zheng et al., 2015) and biosorbents (Das & Das, 2013) found to be the most efficient in removing REE from aqueous solutions.

Major drawback of existing technologies is the high cost and poor regeneration capacity, which prevents this to be implemented in actual mining sites (Lèbre et al., 2017). Hence

there exist a research gap for the identification of low cost adsorbents which are highly efficient, easily sourced and high regeneration capacity to be introduced to the mining industry. Gadolinium, Europium, and Copper are valuable metals that are often targeted for recovery from waste streams due to their economic significance and potential for reuse. Efforts to recover these valuable metals from waste align with principles of resource conservation, environmental sustainability, and the circular economy. Recycling these metals not only reduces the demand for new mining but also minimizes the environmental impact associated with the extraction and processing of primary raw materials.

1.2 **Research Objectives**

Overall aim of this research is selective recovery of valuable metals such as rare earth elements (REE) and Copper (Cu) while recycling clean water from mining wastewaters. Following are specific objectives of the research

- Selective recovery of europium (Eu) from dissolved Zn mine ore using functionalized Chromium based metal Organic Frameworks.
- Analyzing the use of low pressure Nano filtration for acid mine drainage remediation through recovery of clean water and concentrating valuable metals (Eu, Gd and Cu) for selective uptake on modified adsorbents using a sequential adsorption process
- Granulation Cr-MIL-PMIDA for the first time for continuous recovery of europium (Eu) from concentrated mining wastewater for industrial application of

resource recovery.

- Synthesis and characterization of a novel modified mesoporous silica (SBA15-NH-PMIDA) material for for selective recovery of Eu from real mining wastewater.
- Designing of a Direct contact membrane distillation (DCMD)/adsorption hybrid system using granulated SBA15-NH-PMIDA for simultaneous water recovery and selective Eu adsorption

1.3 Significance

- Acid mine drainage (AMD) is highly acidic and contains toxic metals and metalloids, which can contaminate water bodies and soil, leading to severe environmental degradation. Researching remediation methods is essential to reduce the impact of AMD on ecosystems and protect biodiversity. Following points highlights the significance of this research.

- AMD contains valuable metals, including rare earth elements (REEs). Recovering these valuable resources from waste streams helps in reducing dependence on primary mining, conserving natural resources, and supporting a circular economy. Recovery of valuable metals from AMD can also lead to economic benefits by turning waste into a valuable resource. This promotes the concept of "by-product economics" and generates revenue from waste streams.

- AMD remediation and resource recovery aligns with sustainable mining practices. It encourages responsible mining activities that focus on environmental protection, waste reduction, and resource conservation. Research outcomes of this study enhances the understanding of adsorption mechanisms, membrane filtration, and metal recovery processes for AMD treatment.

1.4 Structure of thesis

The structure of this thesis is given below.

Chapter 2: A comprehensive review on the importance of acid mine drainage (AMD) treatment, review on novel adsorbents for REE recovery including metal organic frameworks and mesoporous silica materials, review on the use of membrane processes for water recovery and concentration of valuable metals are discussed in this chapter.

Chapter 3: Experimental methods used for adsorbent synthesis, preparation of synthetic AMD, material characterization and setting up of bench scale membrane systems are presented in this chapter.

Chapter 4: This chapter describes the work done on the synthesis of use of chromium based metal organic frameworks, Cr-MIL-PMIDA for selective Eu recovery from Zn mine ore leachate

Chapter 5: Granulation process of Cr-MIL-PMIDA followed by continuous adsorption experiments for Eu adsorption in a fixed bed column filter is discussed in this chapter.

Chapter 6: This chapter focuses on the use of low-pressure nano filtration for water recovery and concentration of valuable metals (Eu, Gd, Cu) in synthetic AMD. Further studies on the use of Cr-MIL-PMIDA and SBA15-NH_2 for selective adsorption of REE and Cu adsorption respectively are discussed here.

Chapter 7: Synthesis and characterization of a novel adsorbent, SBA15-NH-PMIDA for selective Eu recovery from real mining waste water is presented in this chapter.

Chapter 8: This chapter presents the work carried out on the optimization of membrane distillation/adsorption system for selective Eu recovery. This chapter also provides a cost benefit analysis on the use of this novel adsorbent.

Chapter 9: Conclusion and recommendation for future studies are presented in this chapter.

CHAPTER 2

LITERATURE REVIEW

*This chapter is based on the following published book chapter:

Fonseka, C.; Ryu, S.; Naidu, G.; Kandasamy, J.; Ratnaweera, H.; Vigneswaran, S., 13 - Metal-organic frameworks for recovery of valuable elements. In *Nano-Enabled Technologies for Water Remediation*, Kaleekkal, N. J.; Mural, P. K. S.; Vigneswaran, S., Eds. Elsevier: 2022; pp 377-392. https://doi.org/10.1016/B978-0-323-85445-0.00016-3

2 Introduction

Acid mine drainage, which is caused by seepage of water through ore waste piles, exposed earth cuts and sulphuric rich soil is a major environment concern for countries which have abandoned or active mining sites (Naidu et al., 2019). The release of untreated acid mine drainage (AMD) causes irreversible contamination downstream which effects both flora and fauna. Apart from high acidity, AMD contains high concentrations of heavy metals, rare earth elements and sulphates (Akcil & Koldas, 2006). Hence AMD pollution has the potential to cause severe threat to healthy functioning of ecosystems surrounding water sources. Consequently, accumulation of heavy metals and rare earth elements in the food chain and pose health concerns for humans as well. Hence, identifying efficient and cost effective AMD treatment method is of paramount importance (Naidu et al., 2019).

(a) (b)

Figure 2.1: (a) Active mining site and (b) pollution caused downstream due to AMD

The group Rare earth elements (REE) comprise of 17 chemical elements in the periodic table. Which includes 15 lanthanides, yttrium and scandium (Ambaye et al., 2020a). According to Ramos et al. (2016), rare earth elements occur abundantly in the earth's crust. The concentration of REE in AMD is found to be higher than that of surface water

bodies (Balaram, 2019; Felipe et al., 2020). With increased mining activities around the globe, the probability of contamination of surface and ground waters with REE is increasing. Accumulation of REE in plants and animals increases the potential of severe environmental and health impacts. Recent studies conducted by Pagano et al. (2015) and Rim (2016) shows that exposure of REE to humans can cause severe health impacts such as growth inhibition, organ specific toxicity and cytogenetic effects. Even though minute concentrations of REE is not harmful for functioning of species, elevated concentrations have reported to be toxic (Earle A. Ripley, 1995). This underlines the importance of treating AMD prior to releasing to the environment.

Increasing cost of mining activities and stringent environment regulations have made treatment of AMD an additional cost (Nordstrom, 2011). Chemical precipitation using lime is the widely used treatment method in practice (Kalin et al., 2006). Lime dosing produces excess sludge which requires periodic disposal and can lead to formation of secondary wastes. Furthermore, leaching of toxic elements to groundwater causes serious health concerns (Potgieter-Vermaak et al., 2006) Thus, identifying a sustainable and economically viable treatment method is essential to popularize AMD treatment within the mining industry. Resource recovery from AMD has long been considered a viable approach to offset cost of treatment and meet the demand for scarce metals in the international market (Naidu et al., 2019; Nordstrom et al., 2017).

The demand for rare earth elements in the global market has increased over the past decade (Research, 2019). According to Naidu et al. (2019) and Anastopoulos et al. (2016) over 90% of the global REE demand is supplied by China. Due to recent trade restrictions imposed by China over exports of REE, the global market is facing a severe shortage of

supply (Ioannis Anastopoulos et al., 2016). The European Commission included REE in the list of critical raw materials due to its high economic importance and low availability (Commission, 2014, 2017). United States of America included REE in their list of 35 critical minerals in 2018 (Interior, 2018). REE are used in the manufacturing processes of optical fibres, super magnets, super conductors, aerospace alloys etc (Hatch, 2012). Hence recovery of REE from waste such as AMD not only benefits the environment, it serves financial benefits as well.

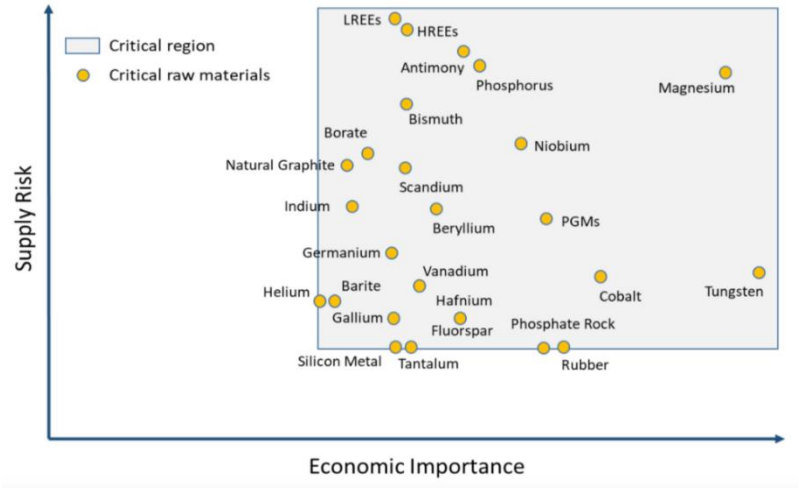

Figure 2.2: Economic importance and supply risk of critical minerals

The classification of REE into light Rare Earth Elements (LREE) and heavy Rare Earth Elements (HREE) is based on their atomic numbers, but it's important to note that the properties of individual elements within each group can vary. The rare earth elements, as a group, are critical in various technological applications, including electronics, renewable energy technologies, and defense systems. HREE are less abundant in the Earth's crust compared to LREE, and they often possess unique properties that make them

valuable in certain high-tech applications. This gives HREE higher economic importance as shown in figure 2.2.

Chemical precipitation, ion exchange, solvent extraction and adsorption are among the more promising methods proposed for REE recovery (I. Anastopoulos et al., 2016; W. Chen et al., 2014; Felipe et al., 2020; Motsi et al., 2009; Sampaio et al., 2009). According to Ambiado et al. (2016), membrane distillation and reverse osmosis methods are applied to pre concentrate AMD prior to selective recovery of REE. Among these methods, Adsorption was found to be the most effective Nano carbon shells, Nano magnetic particles, modified silica composites and bio sorbents are found to be efficient adsorbents in removing REE from aqueous media (Das & Das, 2013; Y. Hu et al., 2017; Xiaoqi et al., 2016; Zhang et al., 2016; Zheng et al., 2015). Even though the removal efficiency of these material are high, increased cost and low regeneration capacity is a barrier for implementing these technologies in practice (Lèbre et al., 2017). Hence, there is a need for development of adsorbents which are low cost, easily sourced and with high adsorption and regeneration capacity for selective recovery of REE from AMD. This will enable wide use of the technology and help create a circular economy for rare earth elements in the international market.

Technologies for industrial wastewater remediation is evolving rapidly to meet rising demand for clean water. Metal organic Frameworks (MOF), a group of new age material is extensively explored for resource recovery from wastewater owing to its high stability and accessible functionalities. This chapter discusses the use of different functionalized MOF for selective recovery of valuable metals from industrial wastewater. The role of functional groups on increasing selectivity towards targeted metals have been analysed.

The chapter also provides development on recovery of rare earth elements (REE) using MOF/mesoporous silica and the role of membrane technologies in recovering water from AMD and concentrating valuable metals for subsequent recovery. Finally, conclusions on future scope in applying membrane/adsorption systems in industrial scale has been discussed.

2.1 Acid mine drainage

Advancement of industries has caused severe environmental pollution over the years. The release of untreated industrial waste causes contamination to downstream water bodies as it is composed of dissolved heavy metals, sulphates and high acidity. It poses a severe threat to the functioning of ecosystems. Consumption of water including these pollutants will have negative impacts on the health of people and animals.

Primary Acid mine drainage (AMD) is formed when oxygen, water and pyrite in exposed rocks in mining sites react to form highly acidic water (Akcil & Koldas, 2006). Oxidation of pyrite results in the formation of dissolved sulphate, dissolved iron and H^+. The release of H^+ to water increases the acidity of AMD. Fe^{2+} that is dissolved in water, can further undergo an oxidation due to the presence of Oxygen and microbial activity under favourable pH conditions and form ferric hydroxide precipitate (Akcil & Koldas, 2006; Simate & Ndlovu, 2014). The stability of the ferric hydroxide precipitate depends on the pH of the solution. It has been found that ferric hydroxide is not stable in conditions where the pH is below 2 (Dold, 2013). In such circumstances, Fe^{3+} remains in dissolved form and it acts as a oxidizing agent for oxidation of pyrite which is contact with the solution

(Akcil & Koldas, 2006). This chain of reaction continuous until the pyrite is exhausted from the open cuts in mining sites.

Saha and Sinha (2018) have mentioned that the above phenomenon is more prevalent in abandoned mining sites than in active mines. Water level in active mines are controlled in contrary to abandoned mines. Hence open cuts in abandoned sites are prone for accelerated AMD formation. McCarthy (2011) mentions that pH of AMD varies between 2 and 3. The primary concern of AMD is the contamination of downstream water bodies with high acidity and high concentrations of dissolved metals (McCarthy, 2011). Hence environment authorities across the globe have imposed stringent regulations on disposal of AMD to the environment (Akcil & Koldas, 2006). This raises the need for sustainable AMD treatment technologies which are both efficient and financially viable.

Acid mine drainage incur high economical costs for the operation of mining sites. Discharge of untreated AMD can cost millions of dollars in remediation work. World's largest mining countries such as United States of America and China spend large amounts of money for treatment processes. Naidu et al (2019) mentions that 32 – 72 Billion USD are spent by the four major mining countries in the world. IN Australia, most mining sites are medium in terms of size. Studies have shown that operation cost of a mining site in Australia in the region of 50 million AUD (Cozzolino et al., 2017). This highlights the high costs incurred in operation and maintenance of mining sites. It was also found that treatment or remediation of abandoned mining sites is higher than that of a site in operation (Akcil & Koldas, 2006). Hence it is important to implement AMD treatment methods at the operation stage to prevent environment impacts and high remediation costs.

2.2 Chemical composition of AMD

Pyrite oxidation is the primary reaction that generates AMD. Due to high acidity, leaching of adjacent rocks causes additional metals to dissolve in water (F. Zhao et al., 2007). Fe and Al are two commonly found metals in AMD waters (Nordstrom, 2011; Simate & Ndlovu, 2014). The behaviour of heavy metals in AMD has been studied thoroughly while there are limited data on the concentrations of REE in AMD. This can be attributed to less toxicity of REE compared to heavy metals. Yet, recent studies have proved that high concentrations of REE in water can cause significant health concerns for humans and animals (Rim, 2016). Table 2.1 summarises concentrations of trace elements found in acid mine drainage across the globe.

Table 2.1: pH, Sulphate, Fe, Mn, Zn, Cu and Al concentrations (mg/l) of AMD. Data Sourced from past studies

Country	Location	pH	SO_4	Fe	Mn	Zn	Cu	Al	Reference
Spain	Odiel River	3.07	1204	23.47	13.7	24.2	7.6	NR	(Sánchez España et al., 2005)
Australia	Open pit, Mount Morgan	2.7	13600	253	71.28	21.97	44.54	780	(Edraki et al., 2005)
Portugal	S. Domingos mine	2.4	3100	497	NR	107	49	NR	(Abreu et al., 2011)
USA	Berkeley Pit mine water	2.7	2400	514	223	630	223	293	(Davis & Ashenberg, 1989)
Spain	Iberian Pyrite Belt	3.2	7884	672	35	64	15	72	(López et al., 2008)
Australia	Mount Bischoff	2.3	720	810	NR	12	2.7	NR	(Gault et al., 2005)
Slovakia	Smolnik	3.8	2938	405.25	35.5	12	8.38	108.38	(Singovszka et al., 2020)
Japan	East Japan	2.8	NR	6.58	NR	9.86	4.05	NR	(Tsuji et al., 2019)
South Korea	Daduk creek	3.3	1940	45	41	38	NR	18	(Lee & Chon, 2006)
India	Tikak, Makum Coalfield	2.4	3615	255.6	18.2	5.04	1.38	34.6	(Azad & Nesa, 2008)

Australia	Virginia, Queensland	2.6	1527	162	2.03	2.72	0.08	80.8	(Vicente-Beckett et al., 2016)
Brazil	Lauro muller, Catarina	2.71	2520	1703	42	11.2	NR	71	(Silva et al., 2011)
Cuba	Santa Lucia mine	2.6	2589	253	21.3	165	0.028	4.82	(Romero et al., 2010)
Spain	Almonaster la Real	3.08	3640	358	19	388	10	117	(Caraballo et al., 2009)
Spain	Esperanza creek	2.66	3919.5	927.5	5	26	18	147.5	(Caraballo et al., 2009)
Spain	Monte Romero	3	3430	275	18	440	5	100	(Macías et al., 2012)
USA	Williams Brothers Mines	3.9	100.67	4.6	1.23	0.13	0.07	NR	(Clyde et al., 2016)

(NR – Not Recorded)

The above table confirms the pH of AMD varies from 2 to 4 and it is influenced by the concentration of sulphates in water. The average concentration of Fe is recorded to be 421.47 mg/l while the concentration of Al is 152.26 mg/l. The dissolved concentrations of heavy metals can therefore be ranked as Fe > Al > Zn > Mn > Cu.

Studies on REE concentrations in AMD are scarce due to low toxicity compared to heavy metals. With the increased interest in REE recovery, AMD has been further analysed to study the concentrations of REE in AMD (Nordstrom et al., 2017). According to the

summary provided in table 2.2, concentrations of REE in AMD is low compared to the presence of heavy metals.

The average Concentration of total REE in AMD is recorded to be 2.169 mg/l, which is low compared to concentrations of Fe and Al. Hence the behaviour of REE in AMD is controlled by metals such as Fe, Al and Zn (Lei et al., 2008). Figure 2.3 provides the concertation of individual Rare earth elements present in AMD.

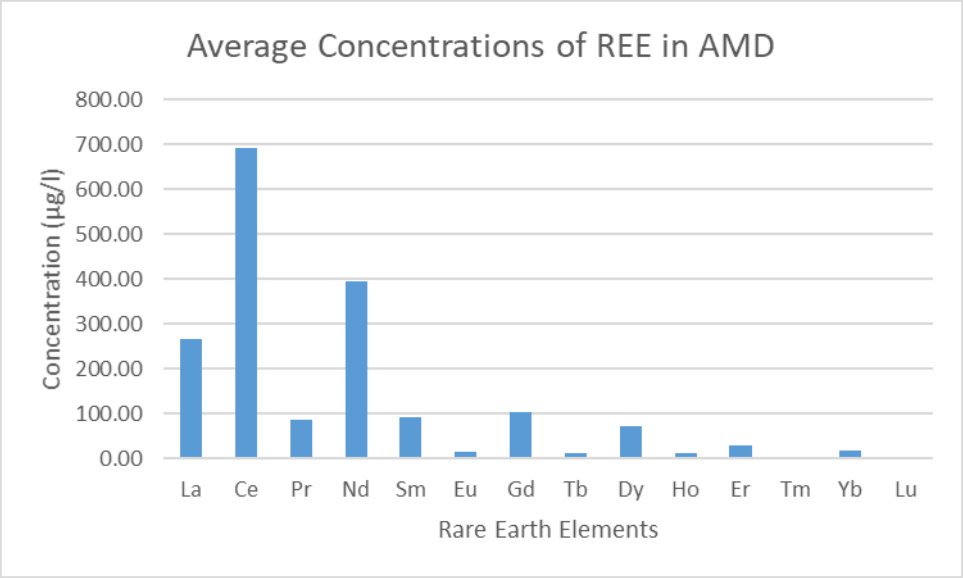

Figure 2.3: Average concentrations of REE in AMD based on data presented in table 2

Table 2.2: Concentrations of REE in AMD

Country	Location	pH	La	Ce	Pr	Nd	Sm	Eu	Gd	Tb	Dy	Ho	Er	Tm	Yb	Lu	Total REE	Reference
India	Jaintia Hills	3.0	91.8	284.9	38.4	121.0	38.4	9.1	44.2	7.3	34.4	8.8	15.7	3.6	13.2	3.4	714.7	(Sahoo et al., 2012)
China	Sitai Coal Mine	3.6	7.7	19.3	2.7	12.9	2.9	0.8	3.7	0.7	4.0	0.8	2.4	0.3	1.9	0.3	61.2	(F. Zhao et al., 2007)
Brazil	Osamu Utsumi Mine	4.4	567.0	124.0	0.0	250.0	28.5	7.7	22.6	0.0	23.2	5.2	12.2	0.0	5.5	0.5	1046.7	(Miekeley et al., 1992)
Italy	Metalliferous Hills	3.1	185.0	389.5	45.7	172.2	34.8	8.6	40.1	5.0	23.6	4.1	10.5	1.2	7.0	0.9	928.83	(Protano & Riccobono, 2002)
USA	West Virginia	4.2	11.4	41.5	7.0	39.1	13.9	3.9	19.2	3.0	16.5	2.9	7.7	1.2	5.5	1.0	174.39	(Vass et al., 2019)

Spain	Huelva Estuary	1.6	1780	4480	590.0	2580	614.0	65.4	554.0	54.7	253.0	37.2	85.9	10.2	61.7	7.6	11173	(K. L. Lecomte et al., 2017)
Spain	Odiel River	4.5	331.2	977.2	120.2	545.4	137.3	25.4	152.9	21.1	110.3	19.5	48.0	5.8	33.7	4.6	2532.9	(Olías et al., 2018)
Australia	Lake Tyrell, Victoria	3.7	90.0	279.2	39.5	153.0	31.9	7.9	50.2	5.4	40.5	4.6	13.7	1.8	6.9	0.7	725.7	(Fee et al., 1992)

pH and REE concentrations of several mining sites across the globe has been summarised in table 2.2. According to the data, Ce (693.63 µg/l) is the prominent REE present in AMD followed by Nd (394.23 µg/l) and La (268.11 µg/l). The total REE concentration varies from 61.21 µg/l to 11.17 mg/l. According to Lecomte et al. (2017), concentration of dissolved REE is inversely proportional to the pH of AMD. Low pH waters accelerate the weathering of rocks resulting in higher concentrations of dissolved metals. Several studies have shown that Sulphate complexes are the most prominent form of speciation present in AMD (Olías et al., 2018; F. Zhao et al., 2007). Sulphate complexes of REE accounts to more than 60% of dissolved concentration while Ln^{3+} cation form is prevalent 20% - 40% (F. Zhao et al., 2007). The results in figure 2.3 clearly highlights that Light REE (LREE) concentration is greater compared to heavy REE (Dutta et al.). This can be attributed to the tendency of LREE to remain dissolved sulphate form during Fe hydroxide precipitation (Olías et al., 2018). HREE is favoured to form carbonates and remain in precipitate form during this stage. Olías et al. (2018) states the above phenomenon coupled with hydro geochemical behavioural differences are the reasons behind the contrast difference in concentrations between HREE and LREE.

Untreated AMD releases significant concentrations of REE to natural water bodies resulting in a health risk to animals and humans. Even though increase of pH in downstream water bodies shifts the predominant form of presence from dissolved to particulate, complexation of HREE with carbonates causes them to remain soluble in water (F. Zhao et al., 2007). Hence, the toxicity of AMD contaminated water remains high. According to Gonzalez et al. (2014), presence of other trace metals such as Al, Cd

and As overshadows the eco toxicity of REE. Hence removing REE from AMD is essential to keep water bodies safe.

2.3 Importance of recovering REE from mining wastewater

The scarcity of natural resources is less determined by global reserves, and more by the uncertainty in international trade which impacts supply and demand (Blengini et al., 2017). In 2009, China produced 97% of global REE supply highlighting the unequal distribution of natural resources (Hennebel et al., 2015). There are many emerging technologies that depend heavily on the availability of valuable metals. Solar panels require metals such as Arsenic (Ar), Gallium (Ga), Indium (In) and wind turbine components are developed using Aluminium and REE (Xu et al., 2018; Yang et al., 2017). Furthermore, increased production of rechargeable batteries which supports growth of renewable energy sources rely on critical commodities such as Lithium (Li), Cobalt (Co) and REE (Olivetti et al., 2017). This growing demand has led to the focus on developing technologies to recover valuable metals from secondary waste sources. Among secondary waste sources, e-waste (Tan & Li, 2019), batteries (Chen et al., 2015), acid mine drainage (AMD) (Naidu et al., 2019) and ore process waste (Borra et al., 2016a) have been extensively explored for feasible recovery of valuable metals. Hydrometallurgy (H. Li et al., 2018) and precipitation (Huang et al., 2016) are two conventionally explored methods for selective recovery of metals where low purity is found to be a concern (Ambaye et al., 2020b). Ionic liquid (Wongsawa et al., 2020) is another promising technology, but recycling of secondary pollutants should be managed prior to upscaling. In this regard,

adsorption is considered to be an efficient method for selectively recovering targeted metals (Callura et al., 2018). However, conventional adsorbents such as activated carbon, alumina and zeolite show limited selectivity. Hence fine tuning the adsorption mechanism of the material by grafting beneficial organic ligands is crucial for efficient recovery. Metal organic frameworks (MOFs), a new age material, is promising in this regard, as it offers extraordinarily high surface area with flexibility of manipulating its pore geometry, size and functionality for attaining high selectivity for specific metals.

MOF was first reported in 1950s and later became popular in 1990s, especially in the field of gas adsorption. MOF is a type of nano material made with metal ions linked together by organic ligands. In the recent past, the use of MOF for recovery of valuable metals from waste sources has been extensively studied. MOF is capable of being manufactured at large scale with physiochemical properties that can be modified with functional groups for specific applications. Hence there exist an opportunity to incorporate MOF with efficient membrane technology to recover clean water and valuable metals. This chapter focuses on the use of MOF for recovery of REE and other valuable metals from industrial wastewater. Furthermore, an analysis on different functionalized MOF for selective recovery of valuable metals and scope for future application are discussed.

2.4 AMD Remediation technologies

AMD remediation technologies can be broadly categorized as active treatment and passive treatment methods (Saha & Sinha, 2018). Passive treatment approach is aimed at

improving the water quality using natural processes. Constructed wetlands is a widely used passive treatment method due low cost of operation (Clyde et al., 2016). Aerobic wetland is one of the simplest form of passive treatment method which uses shallow ponds to facilitate the oxidation of Fe. Precipitates settle at the bottom of the pond and they undergo further degradation through microbial processes. Anaerobic wetlands can be used to remove sulphates from AMD while open limestone channels can precipitate heavy metals.

Active treatment methods include chemical precipitation, aeration, microbial processes, adsorption, ion exchange and filtration. Filtration technologies include nano filtration, reverse osmosis and membrane distillation. Active treatment technologies depend on the use of external energy or resources to remove REE from AMD. From the above technologies, chemical precipitation (or Neutralization) is the widely used treatment method due to its simplicity in application (Akcil & Koldas, 2006). Due to high availability and low cost, limestone is widely used as the neutralizer. According to Saha and Sinha (2018), the aim is to increase pH of AMD and facilitate the formation of metal hydroxides. The precipitates can then be separated by gravity or by filtration methods. Accumulation of sludge is a major concern in this treatment approach. Disposal of unmanaged sludge has the potential to pose secondary soil contamination that will have adverse effects on groundwater sources.

Filtration technologies such as nano filtration and reverse osmosis have gained popularity in treating AMD, especially in arid regions. These filtration methods have the capacity to produce drinking water from waste, providing a valuable resource for people in dry lands. The major concern of this technology is the high operating cost. High concentration

contaminants of AMD increases the possibility of membrane fouling and the frequency of membrane replacement making the maintenance cost high (Zhong et al., 2007b). Akcil and Koldas (2006) has mentioned that application of pre-treatment methods can prolong the life time of the membrane. The major drawback of this technology is the high percentage of reject water. Reject water contains high concentrations of sulphates and metals which require further treatment prior to discharge. Hence this technology is preferred as the last step of a treatment process to limit the generation of reject water.

Ion exchange is a technology based on the principle of exchange of ions between an inert solid medium and a liquid (Saha & Sinha, 2018). The inert solid medium consists of functional groups which can be charged with monovalent ions such as Na or H. Feng et al. (2000) mentioned that the ion exchange process has a recovery rate of 98% with an estimated operational cost of 0.4 $\$/m^3$. This technology is widely used for treatment of ground water to remove Ca and Mg.

Adsorption is another technology which is widely used to remove contaminants from water. The advantage of adsorption over other technologies is its ability to selectively remove contaminants with modifications to the adsorbent (Xiaoqi et al., 2016). There are several studies that demonstrate the adsorption capacity of heavy metals and REE (Ioannis Anastopoulos et al., 2016; Motsi et al., 2009; Xiaoqi et al., 2016). The ability to selectively remove trace elements from aqueous solutions enables recovery of valuable resources from waste streams. This not only helps fill the demand for valuable resources in the market, it generates income from waste treatment that could offset at least part of the AMD treatment cost (Akcil & Koldas, 2006). Identifying adsorbents with high

selectivity that targets elements and with high adsorption capacity will benefit the mining industry by being able to recover resources from mining waste water.

2.5 Membrane technologies for AMD treatment

This section of the review aims to delve into the current state of membrane processes in AMD treatment, examining the challenges, ongoing research efforts, and potential strategies for their successful integration into the industry.

High cost and fouling issues associated with membrane technologies have limited their widespread application in AMD treatment (López et al., 2021). Membrane processes involve the use of semipermeable barriers to separate contaminants from water. Microfiltration, ultrafiltration, nanofiltration, and reverse osmosis are the main types of membranes used for AMD treatment (Agboola, 2019a). These technologies can effectively remove suspended solids, colloids, and heavy metals while producing clean water fit for reuse or safe discharge. Reverse osmosis and nano filtration have gained interest among researchers for AMD treatment due to high salt rejection (Kefeni et al., 2017). However, pre treatment is necessary to remove suspended solids before to reduce risk of membrane fouling or damage. AMD first undergo pH correction to precipitate scaling agents such Ca and Mg. Typically this step is followed by sedimentation and micro filtration to remove most of suspended solids (Bwapwa, 2018). Different types of membrane separation processes are used in the industry to treat industrial waste. Pressure driven membrane processes such as reverse osmosis (RO), nano filtration (NF), ultra filtration (UF) and micro filtration (MF) are the most common technologies adopted in the industry (Agboola, 2019a). Semi-permeable membrane acts as a barrier, allowing the

passage of water molecules while blocking larger particles, such as suspended solids, colloids, and heavy metal ions. Membrane's pore size determines the size of particles it can retain, making it an effective tool for removing various contaminants present in AMD.

Microfiltration (MF) membranes have a relatively large pore size, typically in the range of 0.1 to 10 micrometres. They are effective in removing suspended solids, large particles, and some bacteria from AMD (Hakami et al., 2020). Ultrafiltration membranes have smaller pore size compared to MF, ranging from 0.001 to 0.1 micrometres. UF can effectively remove smaller particles, colloids, and macromolecules present in AMD, including certain heavy metal ions (Peters, 2010). These membrane processes help in reducing the load on subsequent treatment units, improving the quality of the treated water, and minimizing fouling issues, thereby extending the lifespan of the more expensive, sophisticated membranes and reducing operational costs. Additionally, this approach promotes the successful integration of more advanced membrane technologies and other treatment methods to address the specific challenges posed by acid mine drainage.

2.5.1 Evaluation of NF and RO membranes for AMD treatment

Reverse osmosis (RO) is a membrane process that utilizes semi-permeable membranes with dense films to separate solutes and contaminants from water (Ahuchaogu et al., 2018). It is considered a pressure-driven separation process, where an external pressure is applied to the feed solution to force water molecules through the membrane, leaving behind the dissolved solids and contaminants on the feed side (Wang et al., 2021). In

reverse osmosis, the dense film or selective layer of the membrane acts as a barrier to the passage of solutes and larger particles, allowing only water molecules to pass through. The preferable mechanisms of transport in reverse osmosis are mainly attributed to two phenomena. Which are size Exclusion and solution diffusion. The dense film of the RO membrane contains extremely small pores, typically less than 0.001 micrometers in size (Pearce, 2007). These nanopores are small enough to exclude most solutes, ions, and larger particles, including heavy metals, salts, and other contaminants found in acid mine drainage (AMD). Only water molecules can pass through these tiny pores due to their small size. In addition to size exclusion, reverse osmosis operates on the principle of solution-diffusion (Lee & Lueptow, 2001). When the feed solution is subjected to high pressure, water molecules are driven to move from the region of higher concentration (feed solution) to the region of lower concentration (permeate water) across the semi-permeable membrane. This process effectively separates water from the dissolved solids and contaminants, resulting in purified water on the permeate side and a concentrated stream of contaminants on the feed side.

Zhong et al. (2007a) tested commercially available polyamide RO membranes to treat acid mine drainage. The system achieved 97% ion rejection and over 96% conductivity reduction, which shows that RO is excellent in recovering clean water. However, NF achieved 90% solute rejection in the same study, maintaining a higher permeate flux. Andrade et al. (2017) published similar results for AMD treatment, where NF produced 7 to 12 times higher flux compared to RO. Even though NF permeate quality is slightly lower than RO permeate, it has higher efficiency in operation. However, a fundamental knowledge on AMD characteristics and membrane properties is necessary to select

appropriate membrane (Agboola, 2019a). It is important to note that reverse osmosis requires a considerable amount of energy to generate the necessary pressure for water to pass through the dense membrane. The high energy demand is one of the primary challenges associated with RO, making it a more energy-intensive treatment process compared to other membrane technologies like microfiltration and ultrafiltration. A study conducted by Pearson et al. (2021) reported that brackish water RO systems have an operational cost of 0.4 -0.8 US$/$m^3$ for plant capacity of 5000m^3/day. However, cost increases further for low capacity RO plants. Nevertheless, high efficiency and effectiveness of reverse osmosis in producing high-quality water make it a valuable tool in AMD treatment, especially when the goal is to achieve near-complete removal of dissolved solids and contaminants.

Nanofiltration (NF) is another membrane technology used in the treatment of acid mine drainage (AMD). NF membranes have pore sizes ranging from approximately 0.001 to 0.01 micrometres, making them capable of selectively removing divalent ions, some multivalent ions, and larger organic molecules while allowing monovalent ions and water molecules to pass through (Jamil et al., 2021). One of the main advantages using NF in AMD treatment is its ability to selectively remove divalent ions, such as calcium (Ca^{2+}), magnesium (Mg^{2+}), and sulfate (SO_4^{2-}) (Song et al., 2020). NF can also effectively remove some heavy metal ions, such as nickel (Ni^{2+}), zinc (Zn^{2+}), copper (Cu^{2+}), ferric (Fe^{3+}), aluminium (Al^{3+}) and REE(Cheng et al., 2012). However, it may not achieve complete removal of all heavy metals present in AMD, as the removal efficiency depends on factors like pH, complexation with other ions, and the specific properties of the NF membrane. Several studies evaluated performance of NF membranes for AMD treatment.

Aguiar et al. (2015) examined commercially available NF90, NF270 and MPS-34 for treatment of gold mine wastewater. Study showed that NF90 attained high permeate flux at low pH. However, NF270 showed better solute rejection, higher flux and better fouling resistance at high pH (pH 4.2) compared to NF90. This shows that, operating conditions play a vital role in optimizing NF performance. Lower fouling observed at high pH is found to be due to unique properties of NF membranes such as intra –pore solute rejection, pore radius and effective membrane thickness (Agboola, 2019b). Wadekar et al. (2017) conducted a pilot scale study using eight commercially available NF membranes for recovery of valuable metals from abandoned mining waste. The study showed that NF membranes rejected 99% of TDS and recovered 57% of clean water after operating for 208 hours. This further confirms the feasibility of using NF for Water recovery and valuable metal concentration from acid mine drainage. Aguiar et al. (2016) conducted a study comparing RO and NF membranes for AMD treatment from a gold mine. NF membranes were more suitable for AMD treatment mainly because of extremely low permeate flux of RO membranes. NF90 membranes showed the highest solute rejection, while NF270 membranes showed higher permeate flux. Furthermore, an operational cost estimation was performed on the NF system, which showed that total operational cost of NF was 0.263 US$/$m^3$ of effluent. Which is considerable less than the operational cost of a RO system. Therefore, NF emerges as the cost effective membrane treatment solution for water recovery and valuable metal concentration.

2.5.2 Direct contact membrane distillation for AMD treatment

Membrane distillation (MD) is a membrane-based separation technology that utilizes a hydrophobic membrane to separate water vapor from the contaminants present in the feed solution (Parani & Oluwafemi, 2021). The process relies on the vapor pressure difference between the contaminated water and a cooler, less contaminated permeate stream. By applying heat to the contaminated water, water molecules vaporize and pass through the hydrophobic membrane, leaving behind the dissolved contaminants and particulates (Yadav et al., 2021). There are several advantages of using membrane distillation for AMD treatment and resource recovery. Membrane distillation can achieve high removal efficiencies for dissolved contaminants, including heavy metals and other pollutants present in AMD (Jeong et al., 2021). This allows for the production of a high quality permeate. Another critical advantage of using MD is concentration of targeted metals for subsequent recovery. Residual feed solution obtained from membrane distillation contains concentrated metals and other valuable resources, which can be processed and recovered (Ryu et al., 2020). This approach enables resource recovery and potential economic benefits. Finally, membrane distillation can be operated at low temperatures and pressures, making it energy-efficient compared to other separation processes. Furthermore, waste energy from other industrial processes can be used as an energy source to further enhance efficiency. A pilot study conducted by Dow et al., (2016) reported energy from a continuously operating 500 MW rated power station has the treatment potential up to 8000 kL/day, with 99.9% solute rejection. This highlights the potential for using waste heat sources to operate DCMD units.

There are numerous studies conducted to evaluate the efficiency of MD systems for treatment of acidic wastewaters. Kesieme et al. (2014) used direct contact membrane distillation setup with PTFE (flat sheet) was successfully used to treat acid mine leach solution. Over 99% of salts were rejected by the membrane which concentrated metals such as Al^{3+}, Ni^{2+} and Cu^{2+}. Flat sheet PVDF membrane was also tested for acid rock drainage containing Fe, Al, Cu and Zn (Hull & Zodrow, 2017). This study reported over 99% acid rejection and over 99.8% salt rejection. This further proves that MD can be successfully used as an efficient treatment method for AMD remediation (Foureaux et al., 2020). In terms of cost, Al-Obaidani et al. (2008) reported that operational cost of MD can be reduced from 1.17 US$/m3 to 0.64 US$/m3 by using a heat recovery system. Similar findings were reported by Kesieme et al. (2013), where operational cost reduced from 2.2 US$/m3 to 0.66 US$/m3 if waste heat reused in MD system. This makes membrane distillation a cost effective treatment option for AMD remediation compared reverse osmosis.

Despite the challenges, resource recovery potential of membrane processes remains a compelling incentive. Concentrated streams containing valuable metals can be further processed and extracted, converting the treatment process into a circular economy approach. Resource recovery not only offsets operational costs but also reduces the environmental impact of mining activities.

2.6 Resource recovery from industrial waste

The increasing cost of water remediation and stringent environment regulations have made treatment of industrial wastewater an additional cost to industries (Nordstrom, 2011). This has resulted in gaining popularity of resource recovery recent years. Exhaustion of natural resources have further increased the search for alternative sources for valuable metals (Gaikwad et al., 2009). Previous studies have highlighted several promising methods to recover metals such as Cu, Li, Zn, REE, etc. (Binnemans et al., 2013; L. Li et al., 2015; Ryu et al., 2019). While there are multiple methods available for selective recovery of resources, adsorption remains to be the most prefered method (Anastopoulos et al., 2016; Nagpal et al., 2013). The common feature of these adsorbents is the high surface area and adsorbent sites. Increased surface area allows more ion to be attracted to free sites which will increase removal efficiency and intervals between regeneration of adsorbent (Cardoso et al., 2019). It is essential that adsorbents have high surface area to limit intraparticle repulsion and increase adsorption (Hu et al., 2006). Progress of nano technoogy has resulted in the development of adsorbents with high adsorption capacity and selectivity. The application of MOF-based materials in wastewater treatment has gained popularity in the recent times. MOFs have been successfully used either as a photo catalyst (Chen et al., 2020) or as an adsorbent to remove pollutants from wastewater streams (Lim et al., 2020; Zheng et al., 2019). MOFs can be synthesized with unique physiochemical properties specific for the application. This can be achieved through altering the synthesis process, using different metal ion nodes and organic linkers. Organic ligands can then be altered using post synthesis modification processes to capture specific metal ions from aqueous solutions. Recently a

variety of MOF materials with different physiochemical properties have been synthesized. Among the most extensively studied groups of MOFs are MIL 47 (Rosenbach Jr et al., 2010), MIL 53 (Serre et al., 2002), MIL 101 (Lee et al., 2018), ZIF (Min et al., 2017), HKUST-1 (Zhao et al., 2020) and UiO-66 (Guo et al., 2021).

2.6.1 Metal Organic frameworks

MOFs are crystalline, microporous structures made by strong bonding of inorganic metal clusters with organic functional groups/ligands (Dias & Petit, 2015; Furukawa et al., 2013). The organic ligands act as struts while the inorganic metals are the nodes of the structure (Figure 2.4) (Safaei et al., 2019).

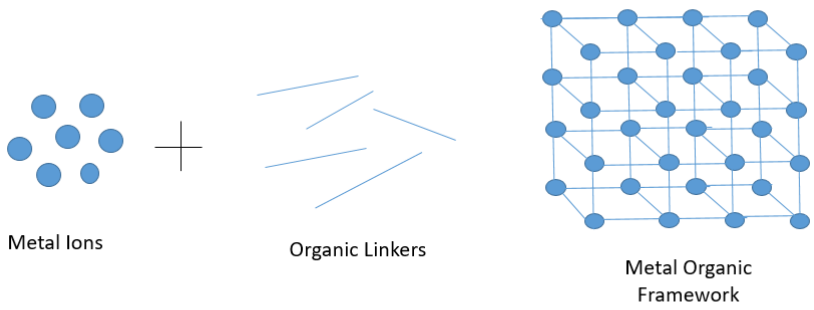

Figure 2.4: Structure of Metal organic frameworks (MOF)

Its unique features in terms of high surface area and flexibility to modify the size, pore geometry and functionality have led to the discovery of extensive types of MOFs that has

been applied in various applications such as gas separation catalytic processes, sensors and drug delivery (Bonneau et al., 2020; Dias & Petit, 2015; Furukawa et al., 2013). Combinations of different metal centres and organic ligands have been used to modify physical and chemical properties of MOF (Xing et al., 2019). Chemical modification resulting in the development of water stable MOFs has propelled research on the application of MOFs for water remediation (Wang et al., 2017; Yang et al., 2019). Specifically, the synthesis of MOFs that are water stable with characteristics such as ion exchange, surface charge binding and protonation of functional groups has enabled its application for valuable metal recovery and adsorption of heavy metal even in trace concentrations (Elsaidi et al., 2018).

Numerous studies have been conducted on recovery of valuable metals using functionalized MOFs. This chapter focuses on the development of MOFs for recovery of REE and other valuable metals.

2.6.2 Synthesis of MOFs

MOFs have beneficial physicochemical features, making them useful for various applications including water purification. MOFs have been prepared with a number of synthetic approaches such as hydrothermal (Meng et al., 2020), and solvothermal (Ghosh & Das, 2020). The properties of MOFs can be altered according to the purpose of the application. It can be achieved by changing the synthesis approach or by modifying the surface with beneficial functional groups. The most common strategy adopted is modification of MOF pores with organic functional groups for selectivity towards targeted metals. Modification with organic ligands can be carried out in situ or as a post

synthesis step. The following is a brief summary of physiochemical properties of MOFs and most widely used organic ligands for valuable metal recovery.

2.6.3 Physical and chemical properties of MOFs

MOFs are known to have high surface area which depend on the metal linkers used and the synthesis method. Modification of MOFs with beneficial ligands decreases the surface area and pore diameter. Studies have found that the reduction in surface area is overcompensated by the presence of active sites with beneficial functional groups which increases the affinity with targeted metals (Viltres et al., 2020). Another important aspect of adsorption is the ionic radius of metals and the pore diameter. For high sorption capacities, the pore diameter should be greater than the ionic radius of the metal. The pore diameter of MOFs is recorded to be within a 0.5-5.0 nm range. Therefore, MOFs are suitable for adsorption of heavy metals, REE, etc.

The water stability of an adsorbent is a fundamental prerequisite for wastewater treatment. Industrial wastewaters have a wide pH range that depends mostly on the components. Industrial wastes such as AMD has high acidity, which the adsorbent should be able to withstand. One popular approach of assessing MOFs water stability is to take the x ray diffraction (XRD) before and after soaking in solutions with different pH for a long duration. If no changes are found, the material is considered to be highly water stable.

2.7 Functional groups for selective recovery of valuable metals

Nitrogen based functional groups interact effectively with actinides and heavy metals as they are categorized as hard bases according to Hard and Soft Acid Bases (HSAB) theory. Therefore, N based functional groups have been incorporated to MOFs for high affinity towards targeted metals. A Zn based MOF, ZIF 8 was analysed for the removal of Cd from wastewater (Binaeian et al., 2020). The study found that dimethylethylenediamine functional group increased affinity towards Cd ions resulting in an 85% removal at optimum operation conditions. Another study conducted by Hasankola et al. (2020) analysed a zirconium (Zr) based MOF modified with porphyrin ligand for mercury recovery. It was found that an adsorption capacity of 233 mg/g was achieved at a contact time of less than 30 mins. Chemical characterization of adsorbent found that the presence of Nitrogen functional groups contributed to high uptake of Hg ions. A Bi-based MOF modified with triazine organic ligand (CAU-7-TATB) was analysed for Pb removal (R. Zhang et al., 2019). The study found that N in the triazine group was responsible for selective recovery of Pb over other competing heavy metals such as Ni, Co, Cr and Mn, which are categorized as hard bases. This confirms that N has affinity towards acid and soft base metals over hard base metals. Therefore, modification of MOF with nitrogen based functional groups can be utilized to selectively recover beneficial metals.

Phosphorus based functional groups such as the phosphonic group has been studied for selective recovery of REE. REEs such are typically characterized as strong acids and naturally they have an affinity towards Lewis bases. A study conducted by Lee et al. (2018) found that the presence of phosphonic groups significantly increases selectivity towards REE over heavy metals. Cr-MIL-PMIDA consist of functional phosphonic and

residual NH_2 groups, which are hard Lewis bases, which attracts REE. Therefore, phosphonic groups are beneficial for selective recovery of REE from wastewater.

Oxygen based functional groups are also widely used for selective recovery of heavy metals, lanthanides and actinides. Carboxyl group is one such functional group used to increase capacity and selectivity towards targeted metals. (Zhang et al., 2017) synthesized and explored highly porous and stable UIO-66 and its carboxyl derivatives for Th (IV) adsorption. The study found that the presence of carboxyl groups significantly enhanced the adsorption capacity of Th(IV) on UIO-66 surface. The formation of coordination bonds between Th (IV) and COO^- was found to be the main driving force behind the high adsorption capacity. Furthermore, carboxyl groups were also found to have high affinity towards REE. The study conducted by Ryu et al. (2021) found that carboxyl groups show high affinity towards REE. This has been confirmed by the study conducted by Lee et al. (2018), which showed carboxyl groups enhances selectivity towards REE over competing divalent heavy metals.

2.8 Recovery of REE from Wastewater using MOFs

REE consists of fifteen lanthanides, scandium and yttrium (Balaram, 2019). According to Balaram (2019), Scandium and Yttrium are considered as REE because they have similar chemical properties to lanthanides and they occur in the same deposits of ore. At present, the earth is facing the unprecedented challenge of global climate change. The search for sustainable energy sources has increased over the past decade. The demand for REE in the global market is increasing due to the expanded growth in production of modern technological equipment. Production of rechargeable batteries, catalysts in

vehicle exhaust systems, super conductors and fibre optics which rely heavily on REE, have increased over the past decade. According to literature, more than 90% of the demand for REE is supplied by China and due to recent trade restrictions, supply interruption exists in the global market (Ioannis Anastopoulos et al., 2016; Naidu et al., 2019). A group of REE is therefore included in the list of critical raw materials by the European Commission and United States of America due to its economic importance and supply vulnerability. The market value for REE stood at 2.8 billion USD in 2017 and it is expected to have a continuous annual growth rate of 10.4% from 2019 to 2025 (Goodenough et al., 2017). Among REEs, Gadolinium is an element that finds applications in various technologies, including medical imaging (as a contrast agent in magnetic resonance imaging or MRI), electronics, and nuclear reactors (Naidu et al., 2019). Gadolinium is used in nuclear reactors as a neutron absorber. Gadolinium rods or compounds are inserted into the reactor core to control the rate of fission reactions by absorbing excess neutrons. This helps regulate the reactor's power output. Europium is another rare earth element with unique luminescent properties. It is commonly used in the production of phosphors for color displays, LED lights, and certain types of fluorescent lamps (Fonseka et al., 2022). In addition to color displays, europium is used in CRT monitors for computers and televisions. It contributes to the generation of colors on the screen by emitting specific wavelengths of light when bombarded with electrons (Naidu et al., 2019). Copper is another widely used metal with applications in electrical wiring, construction, transportation, and various industrial processes. It is highly valued for its conductivity and versatility. It is also a key material in renewable energy technologies (Ryu et al., 2019). It is used in wiring for solar panels, wind turbines, and

electric vehicles, playing a critical role in the transition to a more sustainable energy future. Hence, valuable metal recovery from waste has the potential to become a financially viable investment which could help offset the cost of treatment. There is a need to identify adsorbents which are highly efficient, easily sourced and high regeneration capacity. This will minimize re-mining for valuable resources which will help prevent further pollution of the environment and create pathway towards a circular economy for REE.

Technologies such as nano filtration (NF) and membrane distillation (MD) were successfully studied for the pre-concentration of REEs from low-concentrated waste sources such as AMD. There is also interest in recovering REEs from discarded electronic devices, magnets and batteries. Few literature on the use of functionalized MOFs for the adsorption of trivalent renewables from waste solutions are known.

MOF is identified to be a thermally and chemically stable adsorbent which can be used for recovery of REE from aqueous solutions. Thallapally et al. (2018) has found that DETA in MOF MIL-101-SO_3 has a high capacity for REE adsorption. MIL-101-SO_3 was found to be prone to chromium leaching during the acid stripping process. DETA modified MOF was found to be a stable adsorbent with high affinity towards REE. Lee et al. (2018) studied the efficiency of REE removal using functionalized Cr-MIL-101 from aqueous solutions. MIL-101-PMIDA was found to have superior adsorption capacities for REE with high affinity towards Gd^{3+}. The highest adsorption capacity was 90 mg/g at the optimum pH of 5.5 (Lee et al., 2018). MIL-101-PMIDA also showed stable adsorption capacities over 5 regeneration cycles which confirms the high structural stability of the material.

A study conducted by Lou et al. (2019) synthesized acrylic acid functionalized MOF for Scandium (Sc) recovery. The material showed high selectivity towards Sc among competing di-valent and tri-valent metals such as Cu, Zn, Mn and Al. The formation of coordination bonds between Sc and Carboxyl groups on the surface of the adsorbent was found to be the driving force resulting in high selective uptake.

Table 2.3: Summary of MOFs used for REE recovery

MOF	**Targeted Metal**	**Adsorption Capacity (mg/g)**	**Adsorption mechanism**	**Selectivity (%) (*Competing Ions*)**	**Reference**
A-A MIL 101	Sc	90.21	Coordination bonds with carboxylic group	>90% (*Cu, Co, Zn, Mn, Al*)	(Lou et al., 2019)
Cr-MIL-PMIDA	Gd	87.7	Coordination bonds with Carboxylate and phosphonic groups	90% (*Al, Fe, Ni, Co, Zn*)	(Lee et al., 2018)
Cr-MIL-PMIDA	Lu Y	63.4 25.3	Coordination bonds with Carboxylate	-	(Ryu, Fonseka, et al., 2021)

			and phosphonic groups		
Magnetide@ MIL-101-SO3	Nd Eu Y Dy Ce	37.5 37 15 35 32.5	Complexation with diethylene triamine (DETA)	-	(Elsaidi et al., 2018)
UiO-66-EDTA	Eu	195.2	Coordination bonds with carboxylate and amine groups	No selectivity Simultaneous removal of Eu, La, Fe, Mn, Hg, cd, Pb,Cu, Co, Zn, Ni	(Wu et al., 2019)
HKUST 1	Ce	353	Ion exchange and covalent bonding with Cu	-	(Zhao et al., 2020)
MIL-101-H50	Er	57.5	Coordinative complexes with Phosphonic group	90% (Zn, Cu, Ni, Co)	(Kavun et al., 2021)
U6N@ZIF-8-20	Nd Eu	249.9 295.28	Coordination bonds with amine,	>80%	(M. Zhang et al., 2020)

	Gd	316.22	carboxyl and	(*Cd, Zn, Cu, Mn,*
	Er	340.95	hydroxyl groups	*Co*)

2.9 Opportunities and future directions for use of MOFs for REE recovery

MOFs were found to be an efficient adsorbent for recovery of REE compared to conventional adsorbents such as activated carbon, silica, etc. This is due to their large surface area, ease of modification with beneficial functional groups and high structural stability. As described in this chapter, affinity towards target metals mainly revolves around hard and soft acid bases (HSAB) theory. Here REEs are considered to be hard acids while beneficial functional groups such as amine, phosphonic and carboxyl are considered to be Lewis bases. REEs are attracted to Lewis base functional groups creating coordinating bonds. Even though modification with functional groups decreases surface area and porosity, it significantly improves affinity towards targeted metals, thus increasing the adsorption capacity. MOFs have shown high affinity towards REE supported by selectivity over competing ions. Even though MOFs have high selectivity, the adsorption capacity of REE in a single solute still remains lower compared to conventional adsorbents such as activated carbon due to reduced surface area post modification.

The cost of using MOFs in real world application is another aspect that needs to be studied. There are very few studies analysing the cost vs benefit of using MOFs for valuable metal recovery. Zhao et al. (2019) reported that the cost of producing Cys-UiO-

66 was USD 6.50 per gram of adsorbent. This shows that the cost of modifying pristine MOF with beneficial functional groups is high. In this regard, the use of MOFs for recovery of REE can still be a financially viable proposition given the high demand for REE in the international market. This will further help offset waste water treatment cost and enable its sustainable operation. Lack of real world applications of MOFs for REE recovery should not be a limiting factor for future commercialization of the product. Further studies using column experiments and pilot scale studies should be carried out to analyse the applicability of MOFs in large scale projects. The integration of MOF onto RO/NF membranes could also be analysed for simultaneous water and REE recovery. MOFs may be considered a novel approach for recovery of valuable metals from wastewater.

2.10 Functionalization of mesoporous silica for selective REE adsorption

Mesoporous silca is another emerging adsorbent which has advantages such has high adsorption capacity, high selectivity of metals in the presence of other ions such as sodium, pottasium etc, high regeneration ability and long term stability of the adsorbent structure (Da'na, 2017). Mesoporous silica possesses a well-ordered pore structure with high surface area, large pore volume, and tunable pore size. These characteristics make it an excellent candidate for REE adsorption due to the high accessibility of active sites and increased mass transfer kinetics. Furthermore, there is potential for its high affinity towards to REE further improved by introducing functional groups. Surface modification with various functional groups further enhances the adsorption capacity and selectivity of mesoporous silica towards REEs. Sulphonic, carboxyl, and amine groups have been

widely explored for their affinity to form stable complexes with REEs, promoting selective recovery (Dolatyari et al., 2016; Ryu, Fonseka, et al., 2021).

Hence this makes mesoporous silica an ideal adsorbent for slective removal of contaminents from wastewater (ALOthman, 2012; Yoshitake, 2005). The study conducted by Ryu et al. (2020) shows that multi modification of mesoporous silica with Mn and amine grafting increased adsorption capacity and selectivity for Cu. This confirms that mesoporous silica is a suitable material for modifications with high stability. The adsorption mechanism of REEs onto mesoporous silica involves a combination of ion exchange, coordination, and surface complexation (Dolatyari et al., 2016; Iftekhar et al., 2018; Ramasamy et al., 2017). The surface area and pore structure of the adsorbent play a crucial role in accommodating REEs and promoting favorable interactions. However there has been no studies conducted to evaluate the performance of PMIDA grafting on mesoporous silica materials. Previous analysis on MOF highlights that PMIDA ligand promotes highly selective adsorption towards REE. Hence, identifying a synthesis method for PMIDA grafting on to mesoporous silica surface is noteworthy.

Mesoporous silica has demonstrated superior selectivity for REEs over other metal ions present in mining wastewater. Its tailored surface chemistry allows for the selective recovery of specific REEs, minimizing interference from competing ions. Furthermore, mesoporous silica exhibits high adsorption capacities, making it a cost-effective and efficient sorbent. Despite the promising results, challenges such as regeneration, disposal of spent adsorbents, and potential competitive adsorption still exist. Addressing these

challenges will be vital for the practical implementation of mesoporous silica in large-scale REE recovery processes.

2.11 Summary

This chapter focused on the developments of MOFs and mesoporous silica materials for selective recovery of valuable metals such as REE from wastewater. Studies have highlighted different functionalization approaches for recovery of targeted metals. It was found that selectivity towards REE is significantly improved in the presence of carboxylic and phosphonic groups. This is due to the formation of coordinating structures between beneficial groups and REE. High selectivity and reusability of MOF was found to be critical factors governing the high efficiency of MOF. Despite the high cost of production, MOF is a promising material for recovery of valuable metals at industrial scale. However, functionalised mesoporous silica promises to be a cost effective solution for MOF. Mesoporous silica has highly tuneable surface, which can be modified with PMIDA. This will allow combination of high adsorption capacity of mesoporous materials to boost the selectivity of phosphonic and carboxyl groups for a better uptake of REE. Following chapters on this thesis discusses the works carried out on the performance of Cr-MIL-PMIDA, SBA15-NH-PMIDA along with the analysis of using membrane/adsorption hybrid systems for simultaneous water and valuable metal recovery.

CHAPTER 3

EXPERIMENTAL METHODS AND MATERIALS

3 Introduction

This chapter provides description on the chemicals used for synthetic AMD, procurement of Zn ore waste, adsorbent synthesis procedure, material characterization methods and experimental setup for equilibrium, kinetic and selective adsorption tests. Detailed, specific methodologies are provided within their respective chapters.

3.1 Preparation of Synthetic AMD

Chemicals used for preparation of model solutions are as follows. Europium(III) nitrate pentahydrate ($Eu(NO3)_3 \cdot 5H_2O$, 99.9%), Nickel(II) nitrate hexahydrate ($Ni(NO3)_2 \cdot 6H_2O$, 99.99%), Zinc(II) nitrate hexahydrate ($Zn(NO3)_2 \cdot 6H_2O$, 98%), Cobalt(II) nitrate hexahydrate ($Co(NO3)_2 \cdot 6H_2O$, 98%), Sodium sulfate (Na_2SO_4, 99.99%), Calcium(II) sulfate dihydrate ($CaSO_4 \cdot 2H_2O$, 99%), Manganese(II) sulfate monohydrate ($MnSO_4 \cdot H_2O$, 99%) and Copper(II) sulfate pentahydrate ($CuSO_4 \cdot 5H_2O$, 98%) were purchased from Sigma Aldrich. 0.1M HCl solution was used for regeneration of adsorbent while potassium hydroxide (KOH, 98%, Sigma Aldrich) was used for pH adjustment. Ultra pure Milli Q water for preparation of solutions were obtained from Millipak Express 40 Filter (0.22 µm membrane filter, 18 M Ωcm). All chemicals used in this study were used without further purification.

3.2 Cr-MIL-PMIDA MOF synthesis procedure

Chromium(III) nitrate nonahydrate ($Cr(NO_3)_3 \cdot 9H_2O$, 99%), N-(phosphonomethyl) iminodiacetic acid (PMIDA, 95%), 2-aminoterephthalic acid ($H_2BDC\text{-}NH_2$, 99%), N,N-dicyclohexylcarbodiimide (DCC, 99%), N,Ndimethylformamide (DMF, 99%), Ethyl alcohol (CH_3CH_2OH, 99.5%), toluene (anhydrous, 99.8%) and Methyl alcohol (CH_3OH, 99.8%) were used for synthesis of Cr-MIL-PMIDA and were purchased from Sigma Aldrich.

Cr-MIL-PMIDA MOF was prepared as follows (Figure 3.1). 1.25 g of chromium(III) nitrate nonahydrate, 0.58 g of 2-aminoterephthalic acid and 17.5 ml of Milli Q were mixed and stirred for 3 hours under room temperature (25 $\pm$ 1 ℃). The solution was then transferred to an autoclave where it was heated to 150 ℃ for 24 h in a convection oven. The autoclave was then allowed to cool to room temperature and the solution was filtered to obtain Dark green Cr-MIL-NH_2 precipitate. The filtrate was washed three times with Milli Q water and once with ethyl alcohol. The resulting product was then dried at 80 ℃ for 12 h to remove any residual solvents (Abdel-Magied et al., 2019).

Synthesized Cr-MIL-NH_2 was then modified with *N-(*phosphonomethyl) iminodiacetic acid (PMIDA). Cr-MIL-NH_2, PMIDA and *N,N*-dicyclohexylcarbodiimide (DCC) were mixed at 1:1.5:2 molar ratio and transferred to a round bottom flask containing 80 ml of *N,N*-dimethylformamide (DMF, 99%). The solution was refluxed at 150 ℃ for 48 h. DCC was used as a catalyst for the reaction between amine groups on Cr-MIL-NH_2 and carboxylic acid groups in PMIDA. The solution was cooled to room temperature and filtered to obtain light green Cr-MIL-PMIDA precipitate. It was then washed once with

toluene followed by Methyl alcohol to remove unreacted ligands from the adsorbent. Finally, the adsorbent was dried at 100 ℃ for 12 h in a convection oven.

Modified chromium based metal organic framework was granulated using sodium alginate and calcium chloride solutions (An et al., 2015; Ryu et al., 2021). 1 g of powdered Cr-MIL-PMIDA was first added to 10 ml of 1.5% sodium alginate solution. The mixture was then loaded to a 50 ml syringe and gently trickled down to 0.05M $CaCl_2$ solution with gentle stirring (100 rpm). Granulated material (dia = 2.0 ± 0.1 mm) was then sieved and dried at 70°C for 12 hours

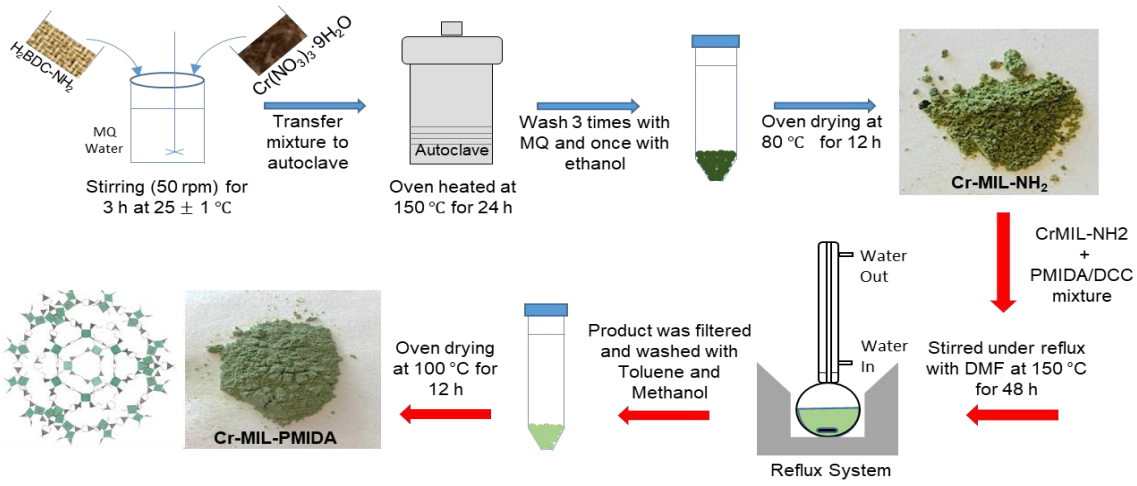

Figure 3.1: Lab synthesis of Cr-MIL-NH_2 and Cr-MIL- PMIDA

3.3 SBA15-NH-PMIDA synthesis process

Tetraethyl orthosilicate ($Si(OC_2H_5)_4$, TEOS) (98%, Sigma-Aldrich), poly(ethylene glycol)-block-poly(propylene glycol)-block-poly(ethylene glycol) (P123), (3-

aminopropyl) triethoxysilane (APTES, Sigma-Aldrich), N,N-dicyclohexylcarbodiimide (DCC, 99%), N-(phosphonomethyl) iminodiacetic acid (PMIDA, 95%), , N,N-dimethylformamide (DMF, 99%), 34% HCl solution, toluene (anhydrous, 99.8%), and Methyl alcohol (CH_3OH, 99.8%) were all purchased from sigma Aldrich for synthesis of SBA15-NH-PMIDA. Sodium alginate (Alginic acid sodium salt, medium viscosity, Sigma Aldrich) and Calcium Chloride (Anhydrous granular, ≥ 93%) were used for granulation of SBA15-NH-PMIDA powder.

SBA-15 was prepared via a hydrothermal reaction (Chang et al., 2009; Ryu et al., 2019). 120 ml of 2 M hydrochloric acid (HCl), 23 ml of deionized water (DI-water), and 3.0 g of P123, which acts as a structure-directing agent, was dissolved at ambient temperature (25 ± 1 ℃). 6.5 g of TEOS (tetraethyl orthosilicate) was then added to this solution as a silica source. The mixture was then placed in an autoclave and subjected to aging (self-assembly reaction) at 35 °C for 20 hours and 100 °C for an additional 24 hours. This step is necessary to promote formation of the mesoporous structure. The residual material was filtered and dried at 80 °C in an oven overnight. Finally, the powder was calcinated at 550 ºC for 3 h to remove any remaining water molecules and P123 surfactant (Ryu et al., 2018; Shahbazi et al., 2011).

3.3.1 **Amine grafting on SBA15**

In this step, amine groups were introduced onto the surface of SBA15, to enhance its adsorption and functional properties following a previously reported method (Da'na & Sayari, 2012; Ryu et al., 2019). 1.0 g of SBA15 was dispersed in 100 ml of dry toluene. 1 ml of APTES (3-aminopropyltriethoxysilane) was then added to the solution. The

mixture was refluxed at 110 °C for 10 hours to allow the reaction between the amino-propyl groups of APTES and OH groups on the surface of the mesoporous silica. SBA15-NH_2 precipitate was finally filtered, washed with ethanol and dried in an oven at 70 °C.

3.3.2 **Synthesis of SBA15-NH-PMIDA**

SBA15-NH2 was modified with N-(phosphonomethyl) iminodiacetic acid (PMIDA) for the first time in this study. Since previous methods for this particular modification were not reported, PMIDA grafting of chromium based MOF was used as a reference. According Lee et al. (Lee et al., 2018), 1: 1.5:2 molar ratio between NH_2, PMIDA and DCC is found to be optimum for a successful reaction. In SBA-NH_2, 3 moles of SiO_2 binds with 2 moles numbers of NH_2. Therefore, 1.5 (SBA15-NH_2): 1.5 (PMIDA): 2 (DCC) molar ratio was calculated be the optimum for synthesis. SBA15-NH_2, PMIDA and N,N-dicyclohexylcarbodiimide (DCC) were mixed at 1.5:1.5:2 molar ratio and moved to a round bottom flask containing 80 ml of N,Ndimethylformamide (DMF, 99%). The solution was refluxed at 150 ℃ for 48 h. The reaction between amine groups and PMIDA was catalysed using DCC. The solution was cooled to room temperature and filtered to obtain white colour SBA15-NH-PMIDA precipitate. It was then washed once with toluene followed by Ethyl alcohol to remove unreacted ligands from the adsorbent. Finally, the adsorbent was dried in a convection oven at 100 ℃ for 12 hours. Synthesis process for the preparation of SBA15-NH-PMIDA is summarised in figure 3.2.

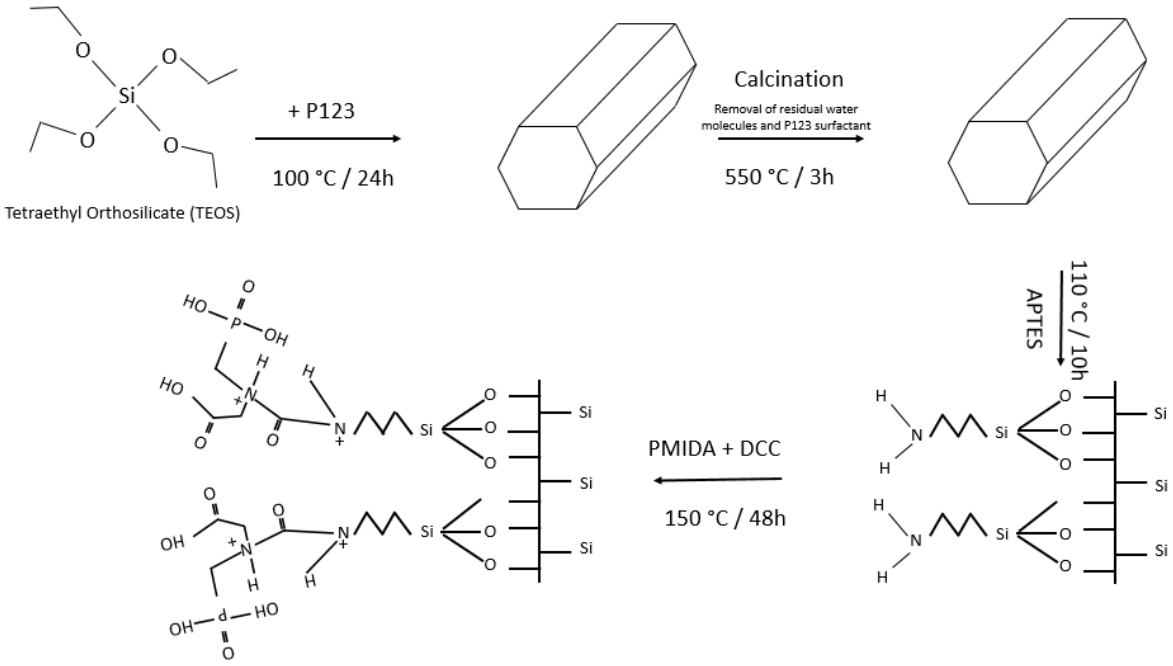

Figure 3.2: Synthesis process of SBA15-NH-PMIDA

3.4 Physical Properties

Nitrogen adsorption and desorption studies were conducted to establish physical properties of the adsorbents. Analysis were carried out using Nanoporosity Mirae (S Korea) instrument at 77K. Brunauer–Emmett–Teller (BET) surface area of samples were calculated using isotherm data obtained in $0 > P/P_0 > 0.5$ range. Barrett–Joyner–Halenda (BJH) method was adopted to estimate the pore size distribution and the pore volume.

3.5 Surface morphology

Fourier transform infrared spectroscopy (FT-IR) analysis was performed using IRAffinity-1 spectrometer (Shimadzu, Japan) with attenuated total reflection (ATR)

accessory to identify chemical bonds and vibrations on the surface of the adsorbent. Scanning electron microscopy images were obtained using Zeiss supra 55VP field emission instrument operated at 15kV. Elemental composition of adsorbent was identified and mapped using energy dispersive X-ray spectrometer (EDS). X-ray photoelectron spectroscopy (XPS) analysis was performed using a VG Multilab 2000 (Hosmed, Finland) with a 7-channeltron detector.

3.6 Adsorption experiments

3.6.1 Batch Equilibrium experiments

Maximum adsorption capacity (Qe) at equilibrium was calculated using equation (1) to (4) as described below.

Maximum adsorption capacity (Qe) at equilibrium was calculated using equation (1).

$$Qe = \frac{V}{M} * (C_i - C_e) \qquad (3\text{-}1)$$

Q_e : Adsorption capacity at equilibrium (mg/g)

V : Solution volume (L)

M : Mass of adsorbent before adsorption (g)

C_i : Initial concentration of Eu

C_e : Equilibrium concentrations of Eu

Data from adsorption experiments were fitted to Langmuir, Freundlich and Sips isotherms to analyse adsorption mechanisms.

Langmuir Isotherm: $Qe = \frac{Q_m b C_e}{1+bC_e}$ (3-2)

Freundlich Isotherm: $Qe = KC_e^{\frac{1}{n}}$ (3-3)

Sips isotherm: $\frac{Q_m b C_e{}^{1/n}}{(1+bC_e{}^{1/n})}$ (3-4)

Q_m : Maximum sorption capacity (mg/g)

b : Langmuir constant (L/mg)

K : Freundlich constant ($g^{1-n} L^n g^{-1}$)

1/n : Dimension less constant related to heterogeneity of adsorbent surface

3.6.2 **Kinetic experiments**

Pseudo-first order and pseudo-second order models were used for data analysis as described below.

Pseudo-First Order $\frac{dQ_t}{dt} = k_1(Q_e - Q_t)$ (3-5)

Pseudo-Second Order $\frac{dQ_t}{dt} = k_2(Q_e - Q_t)^2$ (3-6)

t : Contact time (h)

Q_t : Concentration of Eu (mg/l) at time t

Q_e : Concentration of Eu (mg/l) at equilibrium (24 h)

k_1 (h^{-1}) : Adsorption rate constant

k_2 (g $mg^{-1}h^{-1}$) : Adsorption rate constant

Surface diffusion model (SDM) was developed to further analyse migration mechanism of adsorbate on the surface of adsorbent (Souza et al., 2017). Adsorption from liquid phase onto a porous solid occur in three steps, which are 1) diffusion from fluid to external surface of adsorbent, 2) mass transfer from external surface to the solid phase and finally 3) physical/chemical bonding with active sites (Souza et al., 2017). Since pseudo models neglect film diffusion and intraparticle diffusion, surface diffusion model is considered to be a realistic method to predict adsorption kinetics (Souza et al., 2017). Equation for surface diffusion model are given below.

Surface Diffusion Model (SDM): $$\frac{\partial q}{\partial t} = \frac{1}{r^2}\frac{\partial}{\partial r}(r^2 D_s \frac{\partial q}{\partial r}) \quad (3\text{-}7)$$

Boundary conditions:

$$K_f(C - C_s) = D_s \rho_p \frac{\partial q}{\partial r} \quad at \quad r = R_p \quad (3\text{-}8)$$

$$\frac{\partial q}{\partial r} = 0 \quad at \quad r = 0 \quad (3\text{-}9)$$

C_s : Concentration of Eu at the surface of adsorbent (mg/l)

D_s : Effective surface diffusion coefficient (m^2/h)

r : Radius of the spherical particle (m)

Equation (7) was solved using orthogonal collocation method as proposed by McKay (2001).

3.6.3 Selective adsorption studies

The samples were prepared by spiking concentration of competing heavy metals relative to composition found in dissolved mine ore. 0.01 g of adsorbent was mixed with 50 ml of synthetic solution and was stirred on a flat shaker for 24 hrs at room temperature (20°C) to reach equilibrium. Samples were then filtered and analysed for initial and residual concentration of elements. Adsorption tests using binary mixture of metals (Eu vs competing heavy metals) were also carried out to analyse the influence of individual Al, Fe, Zn, Cu and Mn metals on selective adsorption of Eu. The recovery efficiency of dissolved ions by the adsorbent was calculated using the equation proposed by Zhao et al. (2020).

Recovery efficiency (%): $\frac{C_0 - C_t}{C_0} \times 100$ (3-10)

C_0 : Initial concentration of dissolved metal (mg/g)

C_t : Equilibrium concentration of dissolved metal (mg/g)

CHAPTER 4

SELECTIVE RECOVERY OF RARE EARTH ELEMENT FROM MINE ORE BY CR-MIL METAL ORGANIC FRAMEWORK

*This chapter is based on the following journal publication

Fonseka, C.; Ryu, S.; Choo, Y.; Mullett, M.; Thiruvenkatachari, R.; Naidu, G.; Vigneswaran, S. Selective Recovery of Rare Earth Elements from Mine Ore by Cr-MIL Metal–Organic Frameworks. *ACS Sustainable Chemistry & Engineering* **2021**, *9*, 16896-16904. https://doi.org/10.1021/acssuschemeng.1c04775

4 Introduction

Rare earth elements (REEs) have gained significant attention globally as a strategic resource essential for renewable energy application and new age electronic devices (Wu et al., 2014). Due to the localised natural presence of the REEs, many countries have categorised REE as “critical” raw materials (Naidu et al., 2019; Wu et al., 2014). The critical need to meet the demands of REE has led to much focus on alternative methods for obtaining REE through secondary waste resources

Feasible recovery of REE has been explored from secondary waste resources such as end of life consumer electronics (Ambaye et al., 2020b), acid mine drainage (AMD) (Naidu et al., 2019) and residual waste from metal ore processing (Borra et al., 2016a; Wu et al., 2018). The main challenge of REE recovery from electronic waste is the expensive chemical and physical pre-treatments required to dismantle/dissemble the electronic parts to extract REE, which generates substantial amount of slag and high losses of REE (Ambaye et al., 2020b). Likewise, REE in AMD can range into trace concentration depending on the source point (upstream/downstream of the mining area) (Naidu et al., 2019). Alternatively, REE can be directly extracted from ore leachate containing REE, namely phosphate ores, red muds (bauxites) and zinc ores (D.-r. Zhang et al., 2020). Zinc smelting is one such process where accumulation of by-products exceeds 10 million tons globally (Song et al., 2019; Ujaczki et al., 2017). Zinc smelting leachate contains valuable metals including REE which can be recovered prior to disposal. Studies found that the concentrations of REE in metal smelting leachate were significantly higher than abundance in earth’s crust (Binnemans et al., 2015; Borra et al., 2016b).

Hydrometallurgy and chemical precipitation are conventionally explored for selective REE recovery where low purity and high consumption of reagents were found to be inherent concerns (Ambaye et al., 2020b); (Vaziri Hassas et al., 2020). Ionic liquid has been widely used for REE recovery, but recycling of secondary pollutants need to be resolved before it can be practically applied (Wu et al., 2014). In recent times REE recovery with algae has also been examined. Even so, selective REE recovery in mixed acidic condition is yet to be established (Y. Zhang et al., 2019). In this regard, adsorption is considered promising due to its practical efficiency in acidic condition and low cost (Smith et al., 2016). However, majority of conventional adsorbents such as alumina, zeolite and activated carbon show low adsorption capacities or limited selectiveness towards recovering REEs (Nkinahamira et al., 2020; Ramasamy et al., 2017). Factors that can significantly enhance the performance of adsorbents towards REE selectivity includes fine tuning its selective mechanism as well as increasing its surface ratio. Metal organic frameworks (MOFs), a new age material, is highly promising in this regard, as it offers extraordinarily high surface area with flexibility of manipulating its pore geometry, size and functionality for attaining high selectivity of a specific ion.

MOFs are crystalline structures made by strong bonding of metal clusters with organic functional groups/ligands (Efome et al., 2018; Z.-Q. Li et al., 2015). Synthesis of MOFs that are water stable with characteristics such as ion exchange trapping, surface charge binding and protonation of functional groups has enabled MOFs to be used in valuable metal recovery and adsorption of heavy metal even in trace concentration (Efome et al., 2018; Z.-Q. Li et al., 2015).

Few studies have reported on the promising capacity of MOFs for REE recovery (Abdel-Magied et al., 2019; Mahmoud et al., 2019; Zhao et al., 2020). For instance zeolite MOFs evaluated for recovery of REEs (Sm, Dy), attained high adsorption capacity at 280 to 430 mg/g (Abdel-Magied et al., 2019). Likewise, a modified Zn-based MOF exhibited high capacity for yttrium REE (over 370 mg/g) and this was attributed to the mechanism of ion exchange and chemical bonding between yttrium and hydrogen ions on its surface and nitrogen ions present in the pores from the functional groups (Mahmoud et al., 2019). These studies highlight the importance of grafting metal clusters with appropriate functional groups to attain high REE selectivity in MOFs. In line with this, recent studies have reported on the high stability and capacity of chromium MIL based MOFs functionalized with phosphonic and carboxylate groups towards selective REE recovery (Kavun et al., 2021; Lee et al., 2018). Although these studies indicate MOFs adsorption capacity for REE, most of these studies were conducted with either single solute model solutions or with concentration ratios of transient metals that do not represent practical scenarios (Abdel-Magied et al., 2019; Mahmoud et al., 2019). More specifically, the performance of MOFs for recovering REE from actual zinc mine ore leachate that contain high concentration of Zn and other heavy metals is yet to be explored. It is essential to establish the capacity of applying MOFs for recovering REE in actual scenarios and understanding its selectivity mechanism to enhance its practical performance.

This study aims at examining the efficiency of modified chromium-based MOF to selectively recover REE from real zinc ore leachate and to study the impact of competing ions on REE recovery. For this reason, zinc ores were obtained from an actual mining site

and acid leaching was carried out to establish the presence of REEs from the ore leachate. Cr-MIL-PMIDA was synthesized in the lab using a previously reported method. An in-depth structural and chemical characterizations were carried out to verify the produced MOF. Factors that influence the performance of the synthesised MOF for REE recovery was examined and a detail study on the MOFs capacity to selectively recover REE from the actual zinc ore leachate was carried out. The Cr-MIL-PMIDA MOFs characterization analysis and performance trend was used to develop an understanding and represent the selective mechanism of the MOF towards REE. The feasibility of recovering REE with MOF was determined by multiple regenerative/reuse test.

4.1 Materials and Methods

4.1.1 Dissolved Mine Ore

Zinc mine ore samples obtained from an Australian mining site (SGS Minerals, Malaga, Western Australia) was used in this study. Sulphuric acid (300 ml, 2M) was added to 30 g of crushed mine ore (30g) and stirred using a magnetic stirrer at room temperature (25 $\pm$ 1 ℃) for 24 h, forming a concentrated slurry/leachate. A 0.45 µm syringe filter was used to filter the leachate and was analysed using inductively coupled plasma mass spectrometry (ICP-MS) (Agilent 4100) for dissolved ions. As indicated in table 4.1, cumulative concentration of REE in the mine ore leachate was 4.5 mg/l and it predominantly contained of Eu with trace levels of other REEs. Based on the ion characteristics, this study aims to selectively recover Eu from leached Zn mine ore.

Table 4.1 Characteristics of dissolved mine ore (pH 0.5±0.1)

Element	Concentration (mg/l)
Al	237.10 ± 0.50
Ca	440.21 ± 4.50
Fe	2922.10 ± 0.50
Mg	3141.50 ± 2.00
Mn	323.40 ± 0.50
Zn	380.31 ± 0.50
Na	18.2 ± 1.00
Cu	2.90 ± 0.20
Ni	0.20 ± 0.50
Co	0.30 ± 0.10
Ce	0.19 ± 0.01
Er	0.05± 0.01
Eu	3.50 ± 0.01
Gd	0.07 ± 0.01
La	0.04 ± 0.01
Sc	0.16 ± 0.01
U	0.03 ± 0.01
Y	0.38 ± 0.01

4.2 Cr-MIL-PMIDA MOF synthesis procedure

Chemical and detail synthesis procedure for Cr-MIL-PMIDA MOF is described in chapter 3.

4.3 Chemical decomposition

Chemical decomposition was carried out according to the method reported by Naidu et al. (2016). 0.05 g of pristine Cr-MIL-PMIDA were added to 1 ml of concentrated H_2SO_4 and heated to 200 ℃ for 5 h. The decomposed sample was then diluted to 50 ml with deionized water. The diluted sample was then filtered with 0.45 µm syringe filter and analysed for Cr, P and N using ICP-MS and IC respectively. The same procedure was repeated for Eu adsorbed Cr-MIL-PMIDA and pristine Cr-MIL-NH_2 to study the structural stability and the effect of PMIDA modification.

4.4 REE Adsorption Experiments

4.4.1 Influence of solution pH

The effect of pH on Eu adsorption on Cr-MIL-PMIDA was investigated using 10.0 mg/l Eu solutions of varying pH conditions (pH 2.0 – 6.0). 0.1 M NaOH and 0.1 M H_2SO_4 were used for pH adjustment. 0.01 g of MOF were suspended in 50 ml of pH adjusted solutions and agitated at room temperature (25 $\pm$ 1 ℃) for 24 h on a flat shaker (120 rpm). Portable multimeter (HQ40d, HACH, US) was used to measure the pH of solutions and Zetasizer (ZS Zen3600, UK) was used to measure the surface charge of Cr-MIL-PMIDA.

4.4.2 Batch Equilibrium experiments

Equilibrium adsorption studies for recovery of Eu on Cr-MIL-PMIDA were carried out using 0.01 g of MOF suspended in 50 ml of dissolved Eu solutions. Initial Eu concentrations varied from 2.5 mg/l to 30 mg/l in this study. Optimum pH of 5.5±0.5 was maintained in all samples and samples were agitated at room temperature (25 $\pm$ 1 ℃) for 24 hours to reach equilibrium. Concentrations of dissolved Eu were measured using ICP-MS. Maximum adsorption capacity (Qe) at equilibrium was calculated using equation (1) to (4).

2.4.3 Kinetic experiments

Kinetic experiments were carried out to analyse mass transfer mechanisms. Experiments were conducted by suspending 0.01 g of adsorbent in 50 ml of 10 - 20 mg/l Eu at optimum pH 5.5. The beakers were agitated on a flat shaker at room temperature (25 $\pm$ 1 ℃). Samples were recovered for analysis at selected time intervals up to 24 h and residual Eu concentrations were measured. Pseudo-first order and pseudo-second order models were used for data analysis as described in the chapter 3. The study also evaluated migration mechanism with surface diffusion model (SDM) as described in detail in the chapter 3.

4.4.3 Selective adsorption studies

Selective adsorption test was carried out with the leached solution of the mine ore (Table 4.1) to evaluate the capacity of Cr-MIL-PMIDA adsorbent towards selective Eu recovery

over significantly higher heavy metals present in the mine ore leachate. Furthermore, selectivity of adsorbent towards recovery of Eu was tested using multicomponent solutions consisting competing metals. The samples were prepared by spiking concentration of competing heavy metals relative to composition found in dissolved mine ore at pH 5.5±0.5. 0.01 g of MOF was mixed with 50 ml of synthetic solution and was stirred on a flat shaker for 24 hrs at room temperature (25 ± 1 °C) to reach equilibrium. Samples were then filtered and analyzed for initial and residual concentration of elements. Adsorption tests using binary mixture of metals (Eu vs competing heavy metals) were also carried out to analyze the influence of individual Al, Fe, Zn and Mn metals on selective adsorption of Eu.

4.5 Results and Discussion

This study evaluates the performance of Cr-MIL MOF towards selective recovery of REE, focusing on Europium (as REE), in line with its presence in the leached Zn mine ore (table 4.1). It is also worth mentioning that amongst REEs, Europium (Eu) is considered to be the one of the most expensive REEs in the international market and the rarest in nature, accounting for only 0.1 wt% in monazite and bastnasite ores (Kumari et al., 2019). This has resulted in Eu being mined only as a by product due to financial constraints (Wang et al., 2020).

4.6 Cr-MIL MOF properties and Characterization

4.6.1 XRD analysis of MOF crystalline structure

X-ray diffraction (XRD) patterns of Cr-MIL-NH_2 and end product (Cr-MIL-PMIDA) (Figure 4.1) showed that both derivatives were similar to those reported by previous studies which confirms successful synthesis of the materials (Kavun et al., 2021). Indistinguishable XRD patterns of the two MOF derivatives highlights that the crystal structure of the adsorbent was well preserved during modification with PMIDA groups.

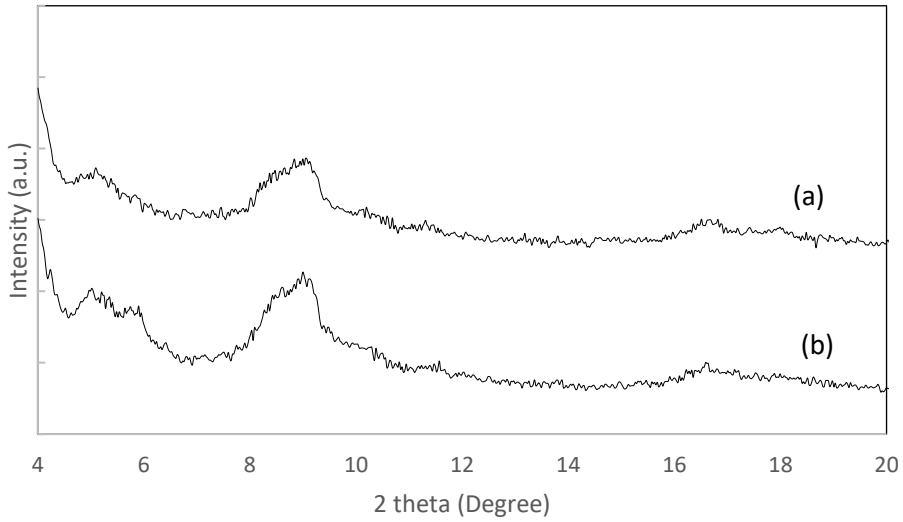

Figure 4.1: XRD patterns of (a) Cr-MIL-NH_2 and (b) Cr-MIL-PMIDA

4.6.2 BET Analysis

Physical properties reported for Cr-MIL-PMIDA in our study is similar to that reported by Lee et al. (2018) with slightly notable variations in values for Cr-MIL-NH_2. Likewise previous (Lee et al., 2018) studies on Cr-MIL indicated that the physical properties of the

prepared nanomaterials were within these value ranges. For instance, Liu et al. (2016) highlighted that the BET surface area of Cr-MIL-NH_2 was in the range of 1245 m^2/g – 2146 m^2/g. Dapaah et al. (2021) indicated that the BET surface area of the Cr MIL NH_2 prepared in their study was1443 m^2/g , which closely matched the values reported in our study. In terms of pore diameter, Babaee et al. (2020) reported that the pore diameter of Cr MIL NH_2 was less than 10 nm, that closely matches the pore diameter in our study. Hence, these validates that the pore diameter of the synthesised Cr-MIL-NH_2 in our study was within an acceptable range. It is important to highlight that modification of adsorbent with organic ligands significantly reduces physical properties such as surface area and pore volume (Bahadori et al., 2020). This explains the apparent reduction in pore diameter recorded in our study, which confirms successful grafting of beneficial ligands. Kavun et al. (2021) reported similar findings where a 60% reduction of the surface area of Cr-MIL MOF upon functionalization with organophosphorus and attributed the surface area reduction to the presence of functionalized ligand incorporated to the Cr surface. Also, the BET surface area of the organophosphorus functionalized Cr-MIL in the ranges of 970 -1200 $m^2 \cdot g^{-1}$ reported by Kavun et al. (2021) was closely similar to surface areas of functionalized Cr-MIL-NH_2 and Cr-MIL-PMIDA of our study. Physiochemical characterization of Eu loaded Cr-MIL-PMIDA shows a decrease in surface area and pore volume. This can be attributed to the pore blocking created by accumulation of Eu ion on the inner walls of pores. (Lu et al., 2016) A similar trend was reported in previous adsorption studies where decrease in pore volume and BET surface after adsorption were recorded while the pore size remained closely similar.(Lu et al., 2016; Pereira et al., 2019)

This shows the Cr-MIL-PMIDA is structurally stable which leads to increased reusability in practical applications.

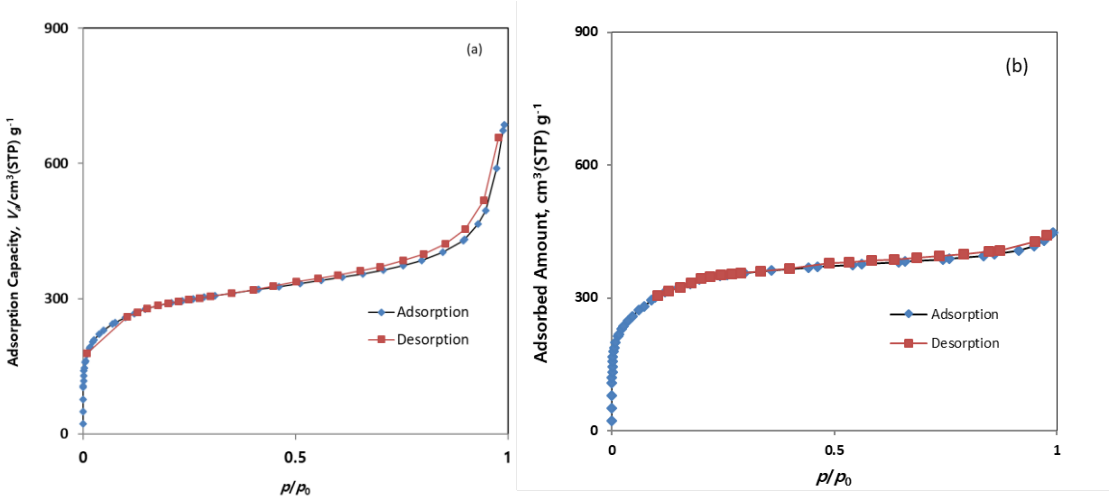

Figure 4.2: Nitrogen adsorption/desorption isotherm graphs of (a) Cr-MIL-NH_2 and (b) Cr-MIL-PMIDA

Table 4.2: Physiochemical properties of Cr-MIL-NH_2 and Cr-MIL-PMIDA

Adsorbent	**BET Surface Area** ($m^2 \cdot g^{-1}$)	**Pore Volume** ($cm^3 \cdot g^{-1}$)	**Mean Pore Diameter** (nm)
Cr-MIL-NH_2	1282.3	1.05	4.01
Cr-MIL-PMIDA	1049.4	0.69	2.15
Eu loaded Cr-MIL-PMIDA	981.18	0.59	2.12

4.6.3 SEM and element composition analysis

The elemental distribution mapping of Cr-MIL-PMIDA (Figure 4.3) obtained from SEM analysis reveals that N and P functional groups were evenly distributed on the surface of

the adsorbent. This data confirms the successful synthesis of the functional groups onto the Cr surface in Cr-MIL-PMIDA. Meanwhile the chemical decomposition analysis (Table 4.3) indicated significant increase in P content from 0.05% to 4.02% and likewise an increase of N content from 3.24% to 5.28% upon modification with PMIDA functional group. This reflects that successful bonding between amine and PMIDA groups occurred during the synthesis process. Likewise, the Cr content reduced by about 10% in Cr-MIL-PMIDA compared to Cr-MIL-NH_2, suggesting that functional groups covered the Cr surface during modification.

Table 4.3: Elemental composition of Cr-MIL-NH2 and Cr-MIL-PMIDA (based on adsorbent chemical decomposition)

Adsorbent	**Cr (wt %)**	**N (wt %)**	**P (wt %)**
Cr-MIL-NH_2	4.42	3.25	0.05
Cr-MIL-PMIDA	4.00	5.28	4.02

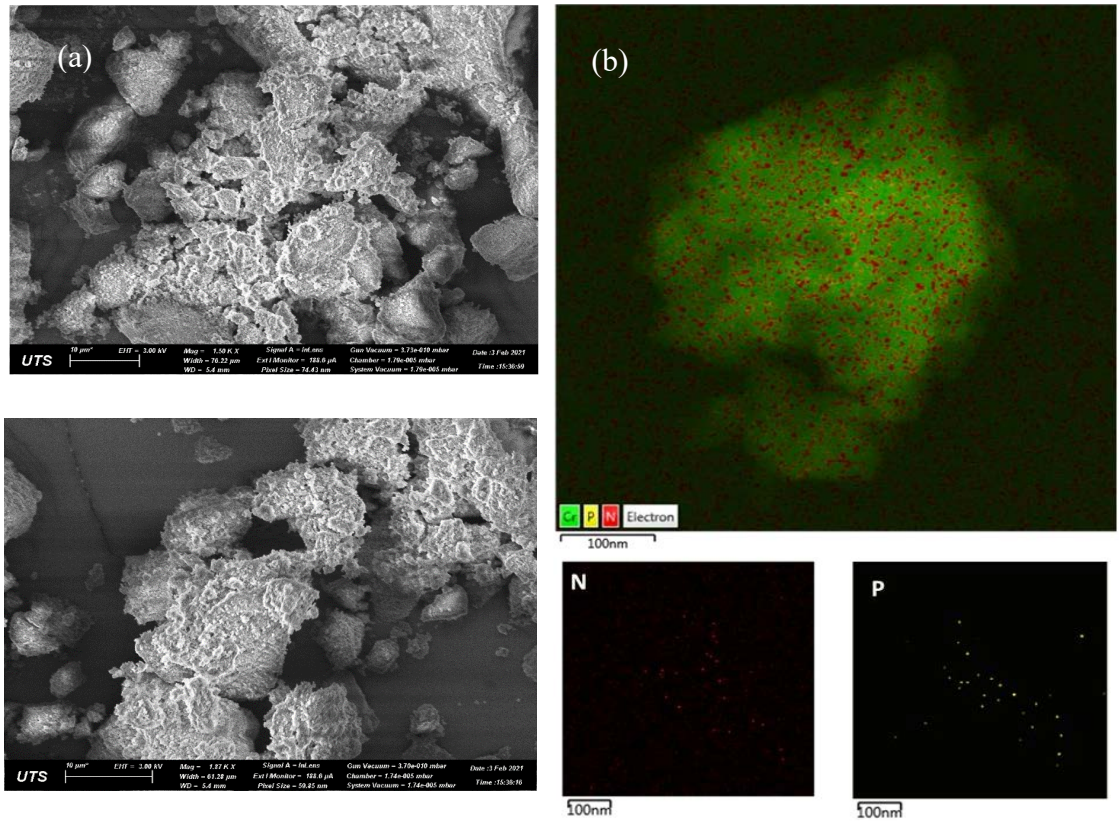

Figure 4.3: Cr-MIL-PMIDA (a) SEM images and (b) elemental distribution mapping

4.6.4 FT-IR spectra analysis

Chemical bonds and vibration patterns of MOFs were studied using FT-IR spectra analysis. The broad peak formation recorded between 3500 cm^{-1} and 3250 cm^{-1} indicates the presence of N-H bonds (Figure 4.4). The vibration located at 1258 cm^{-1} indicates the presence of C-N stretching and the hydrogen bonds between amine groups and the carboxylic acid groups are represented by the split peak recorded at 1400 cm^{-1}. Similar vibration pattern was observed in Cr-MIL-PMIDA for the range 3500 cm^{-1} to 3250 cm^{-1} highlighting the presence of N-H bonds from amide bonding. Additional peaks found in Cr-MIL-PMIDA at 2938 cm^{-1}, 900 cm^{-1} – 1100 cm^{-1} confirm the successful bonding of

phosphonic groups on the structure. Vibration peak appeared at 1589 cm^{-1}, which attributed to NH_2 scissoring, disappeared after the ligand exchange reaction confirming the formation of amide bonding which enables the tethering of PMIDA group to the adsorbent. The FT-IR spectra of Eu adsorbed Cr-MIL-PMIDA will be discussed in the later section.

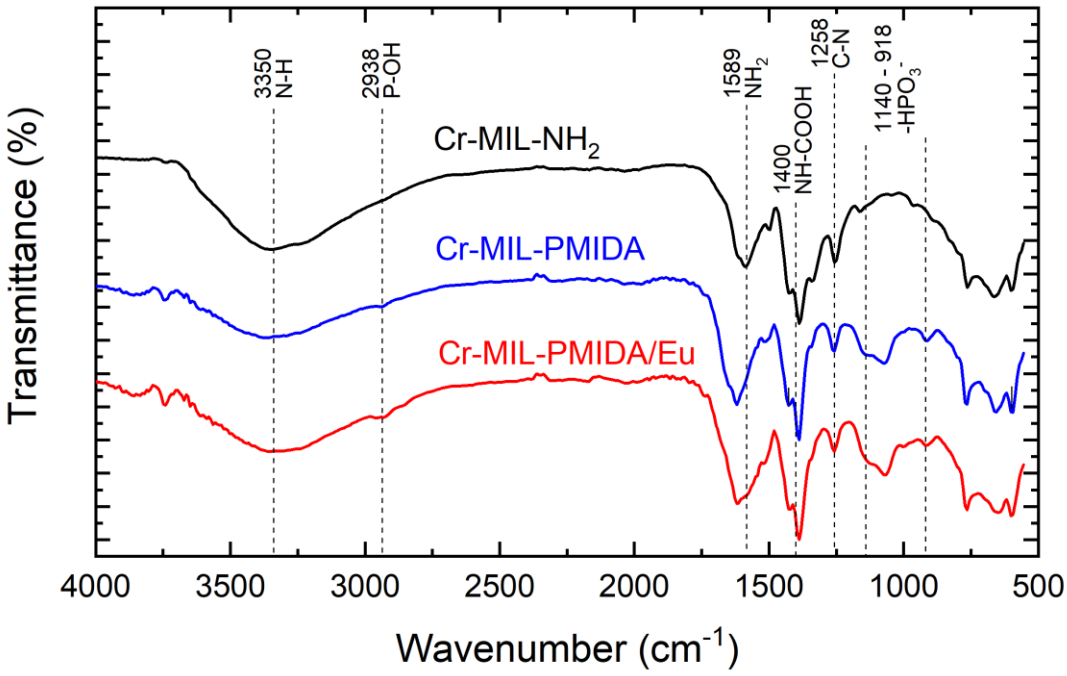

Figure 4.4: Full FT-IR spectra of Cr-MIL-NH_2 and Cr-MIL-PMIDA before and after the Eu adsorption

4.6.5 Effect of pH and surface charge on Eu recovery

The influence of pH on Eu recovery by Cr-MIL-PMIDA was examined between pH ranges of 2.0 and 6.0. A higher pH range was not selected since REEs typically form

insoluble $REE(OH)_3$ at pH above 7 (Hatanaka et al., 2017; Zhang & Honaker, 2018). The effect of pH on Eu adsorption on Cr-MIL-PMIDA was investigated using 10.0 mg/l Eu solutions of varying pH conditions (pH 2.0 – 6.0). 0.1 M NaOH and 0.1 M H2SO4 were used for pH adjustment. 0.01 g of MOF were suspended in 50 ml of pH adjusted solutions and agitated at room temperature (25 1 ± ℃) for 24 h on a flat shaker (120 rpm). Portable multimeter (HQ40d, HACH, US) was used to measure the pH of solutions and Zetasizer (ZS Zen3600, UK) was used to measure the surface charge of Cr-MIL-PMIDA.

As indicated in Figure 4.5a, recovery of Eu is highly dependent on the pH of solution. Specifically, Eu recovery increased from 13% to 93% as the pH was increased from 2.0 to 6.0. Maximum Eu recovery was achieved at pH_{eq} of 5.5±0.5. In line with the increase of Eu recovery, equilibrium pH of the solution showed a decreasing trend (Figure 4.5b). Based on this result, it is highly likely that at pH above 3, H ions were released due to deprotonation of functional groups. This resulted in a reduction of pH while the deprotonated condition created a favourable electrostatic attraction and binding capacity between the positively charged Eu and the adsorbent. In turn, Eu recovery significantly increased.

Correspondingly, the surface charge (zeta potential) showed a trend of increased negative charge when the pH was increased (Figure 4.5a). This confirms deprotonation of functional groups which resulted in increased negative surface charge at higher pH that contributed to the enhanced Eu recovery. Overall, these results identified pH_{eq} of 5.5±0.5 as optimum for attaining high Eu recovery and, therefore this optimum pH value was selected for all subsequent studies unless otherwise mentioned.

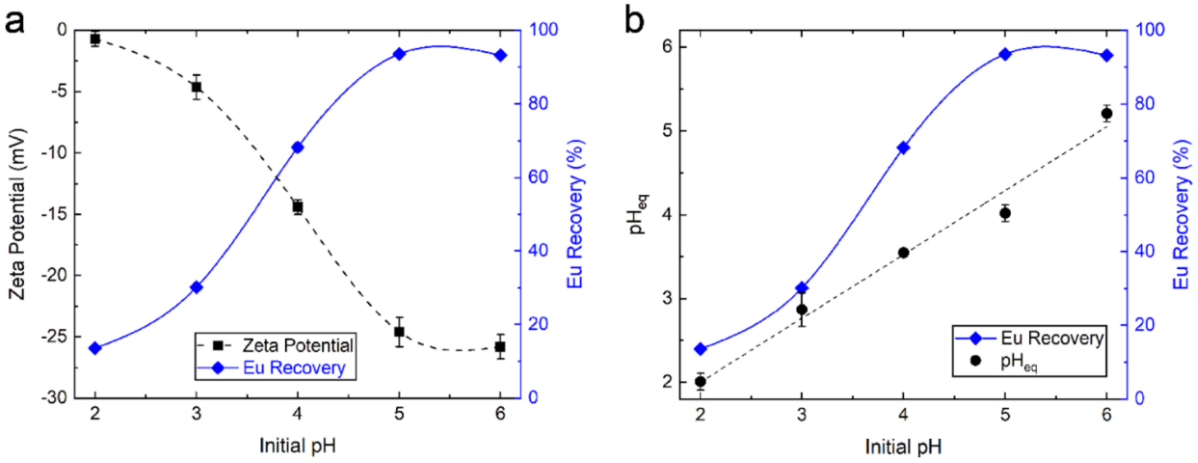

Figure 4.5: Influence of pH on (a) Eu recovery and Cr-MIL-PMIDA surface zeta potential (b) Eu recovery and pH_{eq} variation.

4.7 Adsorption Studies

4.7.1 Equilibrium Experiments

Langmuir, Freundlich and Sips isotherm models were adopted to study the interaction between Eu and Cr-MIL-PMIDA. pH of the solutions were maintained at optimum pH_{eq} 5.5±0.5 for all conditions of the equilibrium experiment.

As depicted in Figure 4.6, adsorption capacity followed a non-linear pattern and was dependent on the initial concentration of Eu. Table 4.4 summarises the isotherm parameters calculated from the models. Langmuir ($R^2 > 0.99$) and Sips ($R^2 > 0.99$) models generated the best fit with experimental data which suggest the presence of homogeneous binding sites. High correlation coefficient of Sips model too confirms monolayer adsorption at high adsorbate concentrations which results in finite molecular sorption (Elmorsi, 2011). The maximum adsorption capacity for uptake of Eu on Cr-MIL-PMIDA was calculated to be 69.14 mg/g according to Langmuir model. The Eu adsorption

capacity by Cr-MIL-PMIDA was superior to adsorbents such as activated carbon, titanate nanotubes and mesoporous molecular sieve (Gad & Awwad, 2007; Sheng et al., 2013; Zuo et al., 2011). For instance, maximum adsorption capacity of titanate nanotubes and activated carbon for Eu uptake was found to be 45.43 mg/g and 46.6 mg/g respectively (Gad & Awwad, 2007; Sheng et al., 2013). Findings from Langmuir isotherm was used to calculate the separation factor (R_L). R_L value provides an indication whether adsorption is favourable ($0 < R_L < 1$), unfavourable ($R_L > 1$), irreversible ($R_L = 0$) or linear ($R_L = 1$) (Hu et al., 2017; Meroufel et al., 2013). R_L value was observed to be $0.017 < R_L < 0.21$ for the range of initial concentrations adopted in the study. This suggests highly favourable uptake of Eu on Cr-MIL-PMIDA, especially at high initial concentrations.

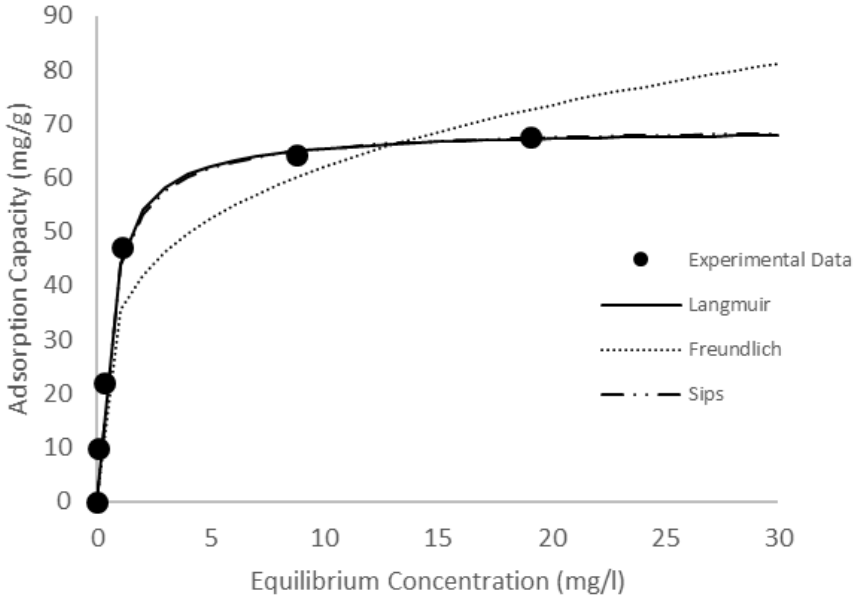

Figure 4.6: Isotherm modelling for adsorption of Eu on Cr-MIL-PMIDA

(0.01 g of adsorbent dose in 50 ml for 24 hr equilibrium time, pH = 5.5 ± 0.5)

Table 4.4: Adsorption Isotherm parameters

Langmuir			Freundlich			Sips			
Q_m (mg/g)	K_L (L/mg)	R^2	K_F (g^{1-n} $L^n g^{-1}$)	n	R^2	Q_m (mg/g)	b (L/mg)	n	R^2
69.14	1.77	0.99	35.46	4.11	0.94	69.87	1.67	1.06	0.99

4.7.2 Adsorption Kinetics

Adsorption of Eu at varying time intervals were recorded and fitted to kinetic models to obtain parameters. Non linear curves of the three models fitted with experimental data are illustrated in Figure 4.7 and rate constants obtained from kinetic models are summarised in Table 4.5. Pseudo 2nd order model produced the better fit ($R^2 > 0.96$) for both sets of samples which confirms that adsorption is controlled by chemical interaction between the adsorbent and adsorbate (Zhao et al., 2020). However, rate constants calculated from pseudo equations are unique to experimental conditions used in the study (Ryu et al., 2019). In contrast, surface diffusion model (SDM) is applicable for varying experimental conditions such as initial adsorbate concentrations, adsorbent amounts and solution volume etc. SDM assumes that pore diffusion is negligible and intraparticle diffusion is a result of surface diffusion exclusively (Souza et al., 2017). Crank-Nicolson method was used for numerical analysis and experimental data fitted well with SDM ($R^2 > 0.94$).

Equilibrium time for uptake of Eu per the kinetic models developed in this study show that 94% of adsorption capacity is reached within 2 hours of contact time. Data from kinetic models indicate that uptake of Eu ions is first carried through rapid surface adsorption followed by chemical bonding of adsorbate with functional groups, where chemisorption is the rate limiting factor. At lower initial concentrations, the concentration gradient between the bulk Eu solution and the adsorbent surface is higher. This can lead to increased mass transfer limitations if the adsorbate molecules have to diffuse through a boundary layer surrounding the adsorbent particles. In cases where adsorption is diffusion-controlled, a higher diffusion coefficient would generally result in faster mass transfer of the adsorbate to the adsorbent surface. This, in turn, could lead to higher adsorption rates, especially at lower initial concentrations. Additionally, adsorption occurred at a faster rate compared to other adsorbents under similar experimental conditions for REE recovery, such as Fe_3O_4@SiO_2(TMS-EDTA), Magnetide@ MOF composite, Zeolitic Imidazolate Frameworks (ZIF) and graphene oxide (Dupont et al.,

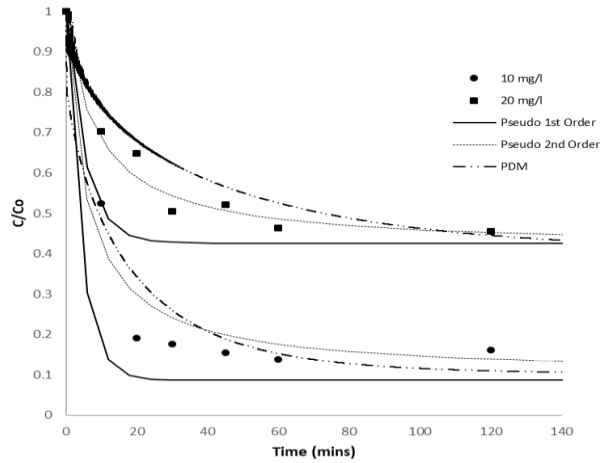

2014; Elsaidi et al., 2018; B. Hu et al., 2017; Jiang et al., 2016). For instance, REE recovery using ZIF required 24 hours (Jiang et al., 2016). The study conducted by Hu et al. (2017) demonstrated that grafted mesoporous silica has an equilibrium time of 45 mins

for adsorption of REE. Yet, the material had significantly lower adsorption capacity (8.57 mg/g) compared to Cr-MIL-PMIDA (69.14 mg/g). Hence Cr-MIL-PMIDA can be rated as a highly effective and efficient adsorbent for Eu uptake.

Figure 4.7: Kinetic adsorption studies for Eu adsorption on Cr-MIL-PMIDA (0.01 g of adsorbent suspended in 50 ml for 10 mg/l and 20 mg/l initial concentrations, pH = 5.5 ± 0.5)

Table 4.5: Kinetic adsorption parameters for adsorption of Eu on Cr-MIL-PMIDA

Initial Concentration of Eu	**Pseudo 1st Order**			**Pseudo 2nd Order**			**Surface Diffusion Model**		
	Q_e (mg/g)	k_1 (h^{-1})	R^2	Q_e (mg/g)	k_2 (g/mg·h)	R^2	k_s (m/h)	D_s (m^2/h)	R^2
20 mg/l	60.40	11.18	0.82	61.73	0.11	0.98	2.4×10^{-5}	3.0×10^{-17}	0.94
10 mg/l	50.40	14.34	0.88	49.75	0.21	0.96			0.95

4.8 Selective recovery of REE from leached mine ore

The practical application of selectively recovering Eu with Cr-MIL-PMIDA from leached zinc mine ore was evaluated. The zinc mine ores consist of high concentration of various transition metals and multivalent ions (mainly Ca, Mg, Zn, Al, Mn, Fe) with REE as a by-product (predominantly Eu) as listed in detail in Table 4.6. The mine ore leaching procedure is schematically represented in Figure 4.8. A concentrated solution was leached from the mine ore, representing the recovery of REE from a by-product of zinc mine ore leaching. The solution pH was adjusted to an optimum pH of 5.5±0.5 as per the

earlier studies. Upon pH change, changes in the concentration of metals in the leachate was observed (Table 4.6). This is primarily because of precipitation of metals such as Al, Fe and Mn (Seo et al., 2017).

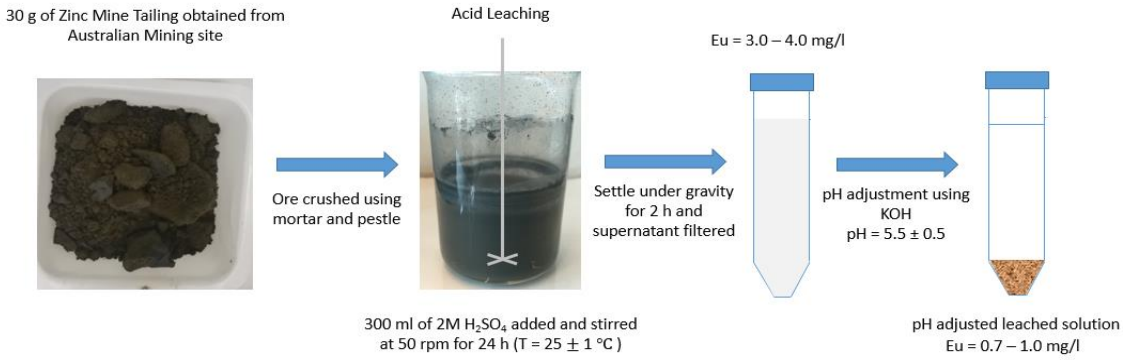

Figure 4.8: Mine ore leaching procedure

Table 4.6: Concentrations of major elements in initial and pH adjusted leachate

Major Element (mg/l)	**Al**	**Ca**	**Fe**	**Mg**	**Mn**	**Zn**	**Eu**
Initial Concentration (pH 0.5±0.1)	175.72	288.15	1495.56	3532.26	303.86	203.56	3.98
Final Concentration (pH 5.5±0.5)	13.87	50.24	35.45	455.71	73.51	88.22	0.94

Cr-MIL-PMIDA achieved 85-86% recovery of Eu from mine ore leached solution while the uptake of other metals were less than 10% (Figure 4.9a). Comparatively, Cr-MIL-PMIDA achieved 90-91% recovery with a single Eu solution. The results highlight that irrespective of significantly high concentration of competing metals, Cr-MIL-PMIDA maintained its selectivity towards Eu.

In order to understand the specific capacity of Cr-MIL-PMIDA towards selective Eu recovery, further experimental works were conducted with a mixture of individual metals and Eu in concentration ratios similar to that of the ore leached solution. The results of Eu uptake with individual metals by Cr-MIL-PMIDA (Figure 4.9b) showed a similar trend of high selectivity as found with mixed mine ore leached solution. In the presence of Zn, Eu uptake maintained about 88% recovery while Zn uptake was minimum, at around 3%. Likewise, the uptake of Al, Mn and Fe was also minimum at around 1-4%. Further, Cr-MIL-PMIDA showed significantly high Eu adsorption with minimum Ca and Mg uptake even though significantly high concentration of these elements are found in the leached ore solution.

The same high selectivity of REE over other transition metals were reported by previous studies (Callura et al., 2018; Yang et al., 2020; Zhao et al., 2020). Most of these studies attributed the selective recovery of REE to the functional group of the adsorbent, such as phosphonic, carboxyl, carbonyl groups. This is mainly because these function groups are categorized into hard base groups and therefore, they tend to exhibit high selectivity towards hard acidic groups such as REE over competing ions. Specifically, the presence of different donor species in the same ligand, such is the case with PMIDA creates high selectivity towards REE in a multi component solution (Reddy et al., 1999). It is also

noteworthy to highlight that Cu demonstrates high chelating effect with amine groups on the adsorbent, resulting in high Cu adsorption (Ryu et al., 2019). The low Cu uptake recorded in this study confirms the presence of relatively low number of amine groups on the adsorbent, which can be attributed to successful reaction between the amine and PMIDA groups during the co-synthesis process. Furthermore, heavy trivalent REE such as Eu display a tendency of higher uptake over lower valent cations due to favourable binding with functional groups (Zhao et al., 2017). This may explain the reason for the significantly higher recovery of Eu compared to divalent cations with lower molecular weight such as Ca, Mg, Cu, Mn, and Zn.

The selective recovery of Eu in the presence of Al and Fe is anticipated to be challenging, given the similar trivalent comparability of these metals and REE in acidic condition. However, at pH of 5.0 and above, these two metals predominate as hydroxylate species and precipitate (Seo et al., 2017; Zhao et al., 2007). Likewise, only minimal uptake of Al and Fe (1-2%) was observed even in high concentrations of Al and Fe (250-450 mg/g), while the recovery of Eu was maintained at 80%.

Selective recovery of REE from leached mine ore at optimum pH of 5.5 was still strongly maintained by Cr-MIL-PMIDA. These results established the favourable capacity of MOF to be applied for selective recovery of REE from leached mine ores containing high concentration of transition metals as well as alkaline divalent cations.

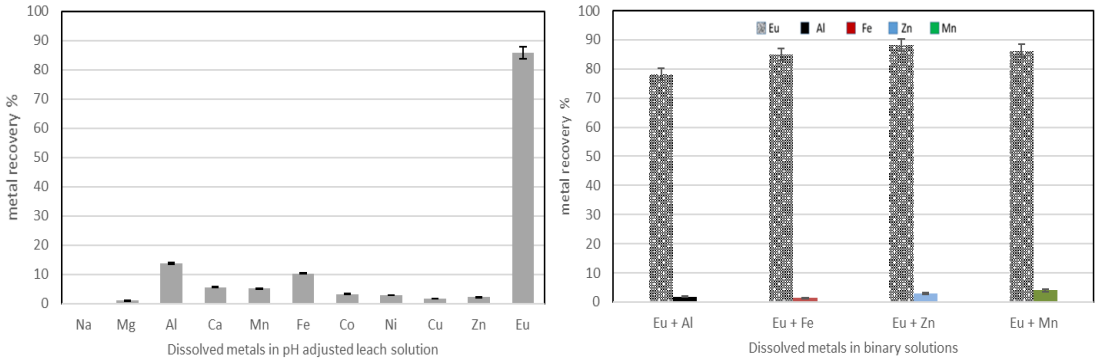

Figure 4.9: Selective recovery of Eu from: a) leached mine ore solution b) transition metals in binary mixture (model solution) (pH = 5.5 ± 0.5)

4.9 Mechanism of selective REE recovery by Cr-MIL-PMIDA

REEs such as Eu are typically characterized as strong acids and naturally they have an affinity towards Lewis bases. Cr-MIL-PMIDA consist of functional PMIDA and residual NH_2 groups, which are hard Lewis bases. In line with this, Figure 4.5 shows that pH increment resulted in increased negative surface charge of Cr-MIL-PMIDA which enhanced electrostatic adsorption of trivalent, positively charged Eu. This confirms optimum pH value of 5.5±0.5 created a favourable condition for the deprotonation of functional groups (phosphonic, carboxyl, carbonyl and amine) on the adsorbent surface, resulting in the removal of H ions and an increase of negative surface charge, which in turn, significantly increased Eu uptake. Correspondingly, a reduction of the initially set pH was observed. For lower initial pH (2-4), the final pH reduced only by 0.1-0.2, while for higher initial pH values (5-6), the equilibrium pH reduction was significantly higher (0.8-1.1). This can be attributed to the removal of H ions from the functional groups with

the increase in Eu uptake. Based on this understanding, the interaction of REE with Cr-MIL-PMIDA may likely be represented as shown in Figure 4.11.

Based on the depiction in Figure 4.11, both PMIDA and NH_2 functional groups should contribute toward the adsorption of REE. Likewise, the FT-IR analysis of the pristine Cr-MIL-PMIDA (Section 3.2.4) confirmed the presence of carboxylic, phosphonic and amine groups. Hence, the uptake of Eu at optimum pH could be attributed to strong coordinated affinity of these ligands with trivalent Eu. However, in comparing the Eu uptake of Cr-MIL-PMIDA and Cr-MIL-NH_2 in a mixed solution (Figure 4.10), while Cr-MIL-PMIDA exhibited the capacity of maintaining a high recovery of Eu over transitional metals, Cr-MIL-NH_2 did not show the similar selectivity pattern. This result suggests that high selectivity of Eu in a mixed metal solution by Cr-MIL-PMIDA is predominantly due to the presence of phosphonic and carboxylic groups.

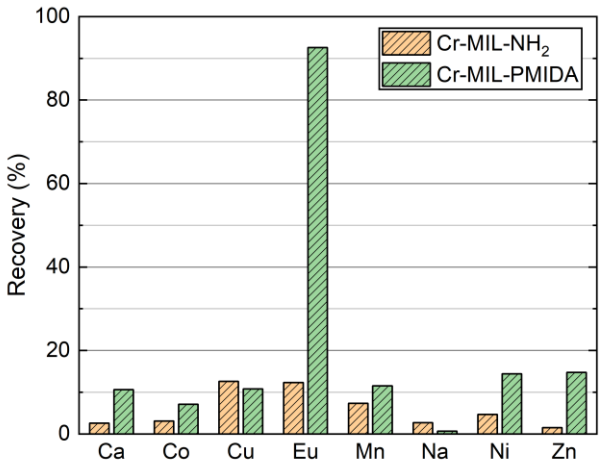

Figure 4.10: Adsorption recovery of Eu^{3+} over competing ions on Cr-MIL-PMIDA and Cr-MIL-NH_2

A detailed FT-IR examination of the pristine and Eu loaded Cr-MIL-PMIDA (Cr-MIL-PMIDA/Eu) at pH 5.5 was performed to understand the selective Eu adsorption mechanism of Cr-MIL-PMIDA. After Eu adsorption, the peak at 2938 cm^{-1}, which represents the P-OH stretching band, split into a doublet (Figure 4.12a). It suggests that Eu interact with phosphonic acid group present on the adsorbent and change the stretching symmetry of the phosphonic group (Nakamoto, 2006a). Furthermore, the vibration bands assigned to the phosphonic ($-HPO_3^-$) stretching modes (1140 – 918 cm^{-1}) showed subtle shifts to lower frequencies after the adsorption (Figure 4.12c). It is generally accepted that coordination of metal ion to the functional groups such as carboxylate or phosphonic groups shifts the peak positions to the lower frequency (Nakamoto, 2006a). Hence, the observation of the subtle red-shifts supports the chelation of the Eu ions to the phosphonic group.

Similar trend was shown in the infrared absorption bands of carboxylic groups. The carbonyl peak appeared as a shoulder at 1650 cm^{-1} and the carboxylic peak at 658 cm^{-1} disappeared and shifted post adsorption, respectively, which indicate a strong complexation of Eu(III) to the carboxylate group (Figure 4.12b, d). Interestingly, the other peak assigned to the carbonyl group from amide bond (1618 cm^{-1}, Figure 4.12b) remained unchanged before and after the Eu loading indicating the amide group did not participate in the adsorption. Also, the broad N-H stretching peaks shown in 3500 – 3250 cm^{-1} before and after adsorption are largely the same (Figure 4.4) which confirms that the N-H does not interact with Eu.

The differences in Eu interaction between the functional groups are ascribed to the pKa values. pKa values of the primary alkyl phosphonic acid ($-H_2PO_3$), alkyl carboxylic acid

(-COOH) and alkyl amide (-CONH) are ~2, ~4, and >10, respectively (Perrin et al., 1981; W. Zhang et al., 2019). At pH 5.5, we expect that primary phosphonic group and carboxylic group are fully deprotonated while the amide group is still protonated (Arai & Sparks, 2001). Hence, the Eu ions predominantly form coordination structures with phosphonate and carboxylate groups. Especially, previous reports revealed that the Eu(III) selectively coordinates with phosphonic acids in solutions with the presence of other competing ions (Wehbi et al., 2020). Thus, we speculate that the strong affinity of Eu(III) to phosphonic group and synergistic effect of carboxylic group enhanced the selectivity factor in PMIDA modified MOF against other metal ions.

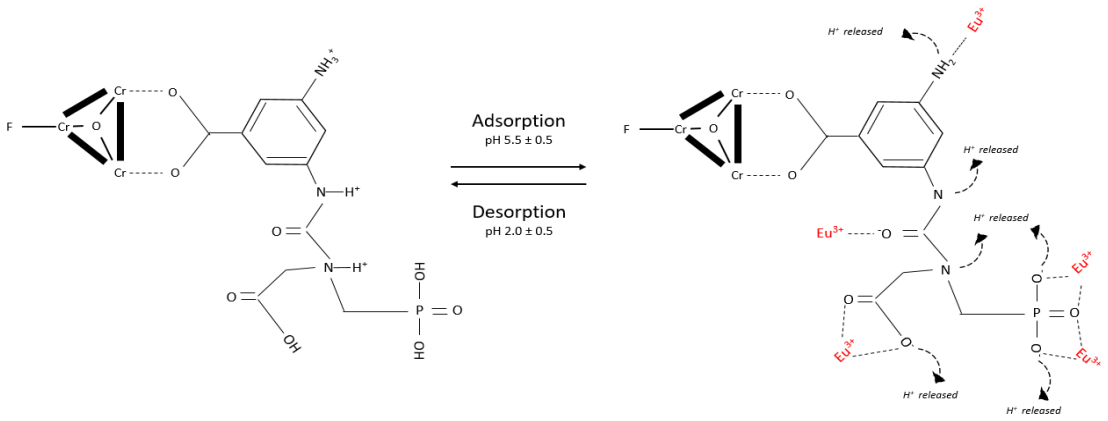

Figure 4.11: Schematic diagram of proposed adsorption mechanism

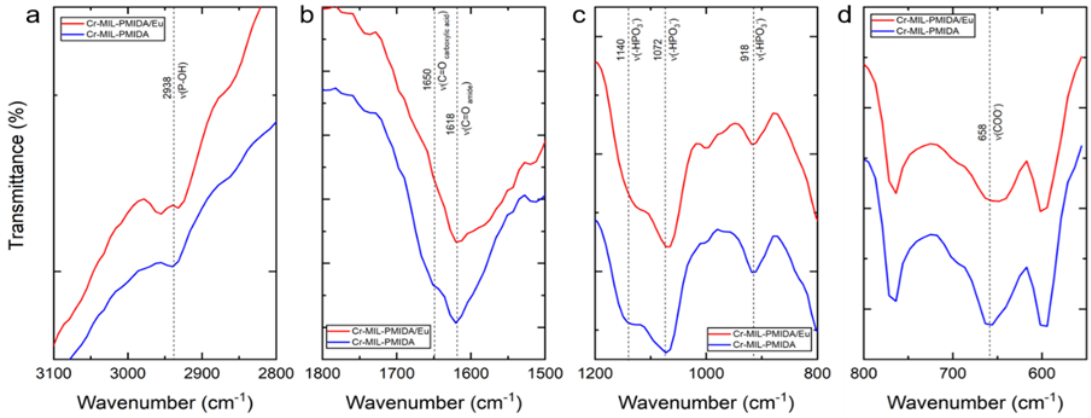

Figure 4.12: FT-IR spectra of Cr-MIL-PMIDA before and after Eu adsorption

To further investigate the adsorption mechanism, X-ray photoelectron spectroscopy (XPS) was performed before and after the adsorption of Eu. In the XPS survey (Figure 4.13a), the Eu 3d peaks appeared at binding energy (E_B) region of approximately 1150 eV, which clearly indicates that Eu ions are adsorbed on the Cr-MIL-PMIDA. In the high-resolution scan of P 2p region (Figure 4.13b, c), an additional peak at 136.2 eV appeared after the Eu^{3+} adsorption. This observation is in a good agreement with the previous literature that reports Eu^{3+} coordination with phosphonic acid-functionalized mesoporous silica.(Zhang et al., 2014) In the Eu 3d regime shown in Figure 4.13d, e, two doublet peaks appeared after the adsorption of Eu^{3+}. The peak positions of the Eu 3d appeared at (1164.7/1134.6 eV) are in a good agreement with the reported values (1165.1/1135.1 eV), respectively, confirming that Eu^{3+} are predominantly coordinated with phosphonic acid groups in bidentate motif.

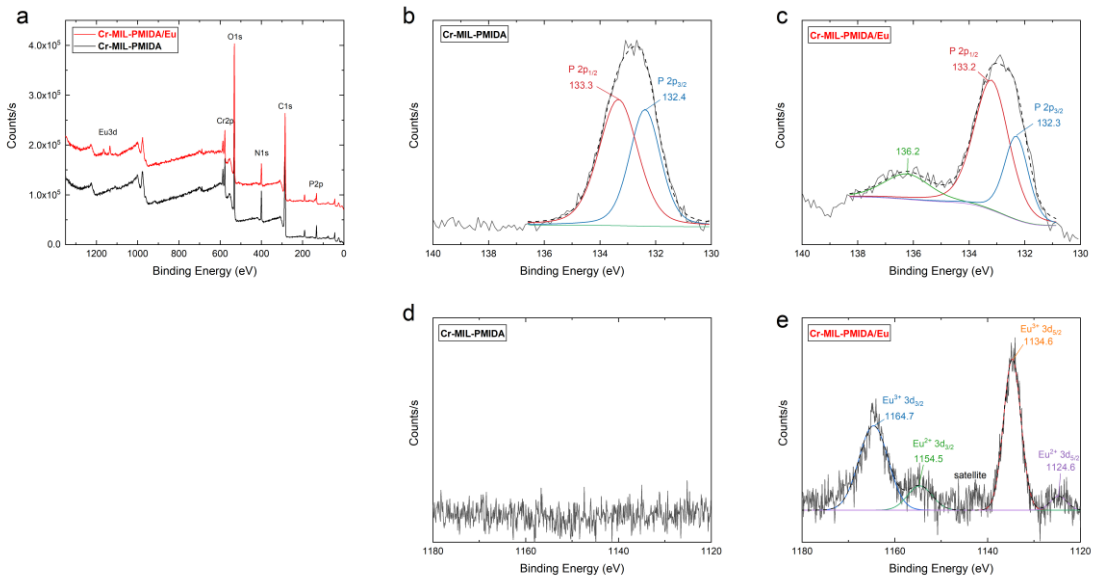

Figure 4.13: XPS analysis of the Cr-MIL-PMIDA before and after the adsorption of Eu^{3+}

Table 4.7 summarises performance of different adsorbents used for selective recovery of Eu. Huang et al. (Huang et al., 2019) states that uptake of Eu on graphene based macrostructure (GOCS) is due to inner sphere surface coordination of Eu^{3+} with functional groups containing oxygen (-COOH) and nitrogen ($-NH_2$). Surface modified mesoporous silica with sulfamic and sulfonic ligands managed to recover 30% of Eu in a mix solution with –OH bond being the favourable site for bonding (Dolatyari et al., 2016). Dousti et al. (2019) highlighted that selective adsorption of Eu is heavily influenced by the presence of Fe (III) with uptake of Eu on SBA-15/SO_3H drastically decreased from 86% to 30% in the study. This confirms the complications of selective recovery REEs when higher valent cations are competing for adsorption sites. When comparing the functional groups used in previous studies, carboxyl, amine, sulfonic and

sulfamic ligands proved to be less effective in selectively recovering Eu from mixed metal solutions. This reiterates phosphonic and carboxylic groups in Cr-MIL-PMIDA is mostly responsible for the high selectiveness towards REE.

Table 4.7: Performance Comparison of adsorbents used for selective recovery of Eu

Adsorbent	**pH**	**Adsorption Capacity (mg/g)**	**Competing Metals/Ions**	**Eu selectivity (%)**	**Ref**
Cr-MIL-PMIDA	5.5	69.14	Na, Mg, Al, Ca, Mn, Fe, Co, Ni, Cu, Zn	85	This study
Cr-MI-NH_2	5.5	-	Na, Ca, Mn, Co, Ni, Cu, Zn	12.3	This study
Graphene-Based Macrostructure	6.0	136.99	ReO_4^-, Na, Sc, Sr, Co, UO_2, Th	50	(Huang et al., 2019)
SBA-15 Mesoporous Silica	4.0	15.20	Th, Ba, Cu, Pb, Co, Ni, Mn, Cd, Cr, Fe, U	30	(Dolatyari et al., 2016)
SBA-15/SO_3H	4.0	8.60	Na, Mn, Ni, Co, Cd, Pb, Cu, Cr, Fe, Th, U	26	(Dousti et al., 2019)
TiO_2	4.5	2.69	-	-	(Tan et al., 2009)

4.10 Reusability Studies

The stability of Cr-MIL-PMIDA structure was first analyzed over five adsorption/desorption cycles using 5mg/l synthetic Eu solution. Cr-MIL-PMIDA retained over 95% of the initial adsorption capacity in recovering Eu after 5 cycles (Figure 4.14). This reflects the high reusable capacity of Cr-MIL-PMIDA. As explained earlier, protonation of functional ligands in acidic conditions creates a repulsive force with Eu which results in desorption of ions to the solution.

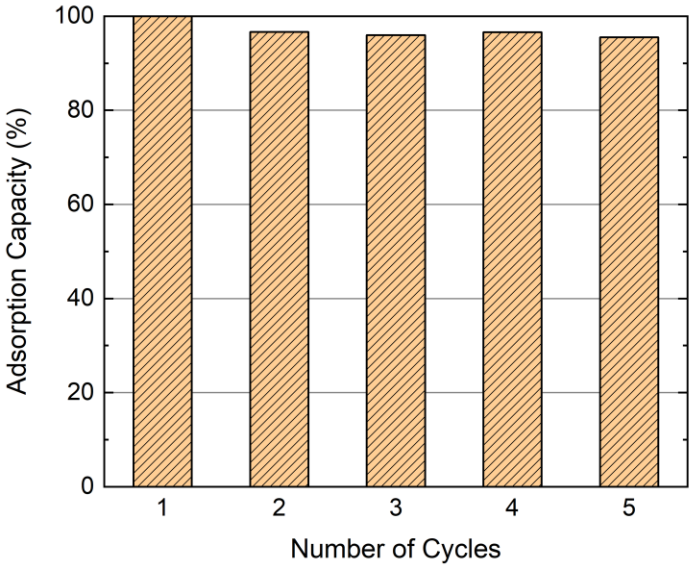

Figure 4.14: Cyclic adsorption tests for Eu^{3+} recovery at initial concentration of 5 mg/l at pH 5.5

Sequential adsorption/desorption test was then carried out to pre-concentrate Eu from leached mine ore (Table 4.8). The study showed purity of Eu in desorbed solution increases from 3.82% to 95.90% after 5 cycles (Figure 4.15). This highlights the capacity

of Cr-MIL-PMIDA in preparing concentrated Eu solution from leached mine moving towards industrial application.

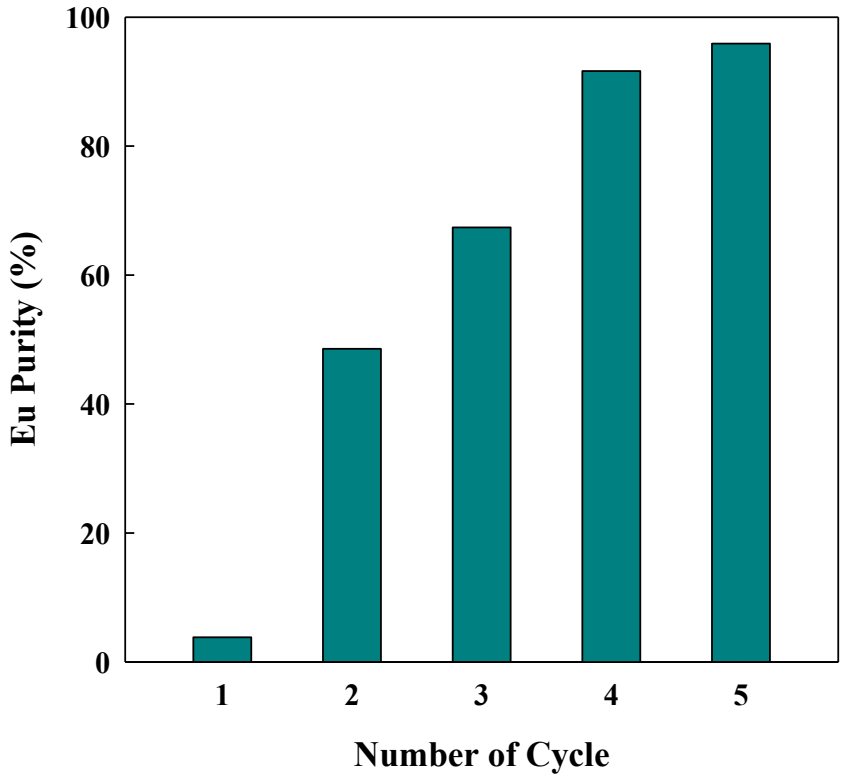

Figure 4.15: Sequential adsorption for pre-concentration of Eu from leached mine ore

Table 4.8: Pre-concentration of Eu from leached mine ore using sequential adsorption/desorption

		Mg (mg/l)	Al (mg/l)	Ca (mg/l)	Mn (mg/l)	Fe (mg/l)	Co (mg/l)	Ni (mg/l)	Cu (mg/l)	Zn (mg/l)	Eu (mg/l)	Eu Purity (%)
1st Cycle	Initial (pH 5.5)	452.45	15.37	42.84	91.60	51.93	0.01	0.01	0.61	87.07	0.857	
	Desorbed Solution (pH 2.0)	3.050	1.969	2.458	4.348	5.317	0.000	0.000	0.011	2.212	0.768	3.82
2nd Cycle	Initial (pH 5.5)	1.251	0.687	1.426	1.164	2.260	0.000	0.000	0.007	0.592	0.510	
	Desorbed Solution (pH 2.0)	0.002	0.089	0.114	0.082	0.203	0.000	0.000	0.000	0.002	0.464	48.55
3rd Cycle	Initial (pH 5.5)	0.001	0.057	0.073	0.052	0.131	0.000	0.000	0.000	0.001	0.406	
	Desorbed Solution (pH 2.0)	0.001	0.031	0.040	0.028	0.071	0.000	0.000	0.000	0.001	0.355	67.38
4th Cycle	Initial (pH 5.5)	0.000	0.011	0.010	0.015	0.024	0.000	0.000	0.000	0.000	0.308	
	Desorbed Solution (pH 2.0)	0.000	0.004	0.004	0.006	0.010	0.000	0.000	0.000	0.000	0.280	91.64
5th Cycle	Initial (pH 5.5)	0.000	0.002	0.001	0.004	0.003	0.000	0.000	0.000	0.000	0.217	
	Desorbed Solution (pH 2.0)	0.000	0.001	0.001	0.003	0.002	0.000	0.000	0.000	0.000	0.185	95.90

Also, the regenerated solution contained only trace concentration of Cr, N and P (less than 0.1 wt%), indicating insignificant leaching of adsorbents chemical contents. Likewise, the chemical decomposition of the absorbent upon multicycles of regeneration and reuse showed a chemical content of 3.6 wt% of Cr, 4.1% of N, and 3.7% of P, which was closely similar to the chemical content of the unused adsorbent (Table 4.3). These results established the chemical stability of the Cr-MIL MOF.

4.11 Summary

A chromium-based metal-organic framework was synthesized and modified with *N*-(phosphonomethyl) iminodiacetic acid (PMIDA) in this study to selectively recover REE (Europium, Eu) from chemically complex zinc ore leachate. The adsorbent was

characterized and comprehensively examined for Eu uptake as a function of adsorbate concentration, contact time, and pH of the solution.

- Cr-MIL-PMIDA showed a maximum adsorption capacity of 69.14 mg/g at pH 5.5 while adsorption kinetics best fitted pseudo second order model.

- Furthermore, the Cr-MIL-PMIDA showed exceptional selectivity (88%) towards Eu over competing transitional metal ions (Na, Mg, Al, Ca, Mn, Fe, Ni, Cu, Co, Zn) found in dissolved mine ore.

- High selectivity towards REE was attributed to the formation of coordinative complexes with grafted carboxylate, phosphonic and residual amine functional groups.
- Cr-MIL-PMIDA demonstrated excellent structural stability over multiple regeneration cycles

While the ease of synthesizing Cr-MIL-PMIDA and its high stability (multiple regenerative cycles) for selective REE is promising, further work on continuous column and detail economic cost of Cr-MIL MOF is necessary to establish its commercial and practical application for REE application**.** Next chapter discusses continuous column experiments conducted with granulated Cr-MIL-PMIDA.

CHAPTER 5

EUROPIUM ADSORPTION BY GRANULATED CR-MIL-PMIDA METAL−ORGANIC FRAMEWORKS AND DYNAMIC FIXED BED COLUMN MODELLING

*This chapter is based on the following journal publication

Fonseka, C.; Ryu, S.; Naidu, G.; Thiruvenkatachari, R.; Kandasamy, J.; Vigneswaran, S. Europium adsorption by granulated Cr-MIL-PMIDA Metal−Organic Frameworks and dynamic fixed bed column modelling. *Journal of Water Process Engineering, 56,* 104475. doi: https://doi.org/10.1016/j.jwpe.2023.104475

5 Introduction

Cr-MIL-PMIDA exhibits high adsorption capacity and selectivity towards REE due to the presence of carboxylate and phosphonic groups. However, the practical application of this promising material, particularly in terms of granulation and its use in continuous column systems, remains unexplored (Fonseka et al. 2021). The powdered form of porous adsorbents possesses inherent disadvantages in industrial applications, including handling difficulties, high pressure drop in fixed bed column systems, and low volumetric efficiency (Liu et al. 2021). Therefore, the granulation of Cr-MIL-PMIDA without compromising its inherent properties represents a significant step towards industrializing this promising material.

In this study, granulation of functionalized chromium-based Metal Organic Framework was carried out for the first time using alginic acid as a binding agent and $CaCl_2$ as a cross-linking agent. Use of sodium alginate and a $CaCl_2$ solution as a granulation method for powdered adsorbents is supported by their ability to create uniformly encapsulated, mechanically stable, and controlled-release granules (Ryu et al., 2021). This technique provides a versatile and efficient approach with benefits ranging from process simplicity to enhanced adsorption performance. Sodium alginate possesses remarkable gelling properties when exposed to divalent cations like calcium ions (Sosa Lucio et al., 2023). When sodium alginate is mixed with a $CaCl_2$ solution, it undergoes a gelation process, forming a three-dimensional matrix that encapsulates the powdered adsorbent. This matrix structure facilitates controlled granule formation. The ionic bond between sodium alginate and calcium ions is strong and efficient, resulting in robust bonding between the

adsorbent particles and the gel matrix. This strong binding minimizes the risk of granule disintegration during subsequent handling, storage, and usage (Ryu et al., 2021).

The aim of this study was to analyze the adsorption capacity, kinetics, and selectivity of the granulated Cr-MIL-PMIDA. Additionally, a suitable mathematical model was developed to predict the breakthrough curve in a single-component fixed bed column system under various operational conditions. Column experiments (upward flow) were conducted to simulate adsorption trends at different flow rates, adsorption column heights, and influent concentrations. The dynamic column modelling employed in this study serves not only to assess the performance of granulated Cr-MIL-PMIDA in continuous systems but also to determine optimal design conditions for real-world applications.

5.1 Experimental method

5.1.1 Materials

Granulated Cr-MIL-PMIDA was analysed for adsorption of Europium (Eu) in this study. All chemicals used for synthesis of the adsorbent are given in chapter 3.

A pre-determined amount of Europium(III) nitrate pentahydrate ($Eu(NO3)_3 \cdot 5H_2O$, 99.9%) and Milli Q water from Millipak Express 40 Filter (0.22 µm membrane filter, 18 M Ωcm) to prepare single component Eu solutions for batch and column tests. Potassium hydroxide (KOH, 98%, Sigma Aldrich) was used for pH correction, while 0.1M HCl was used for regeneration of adsorbent. $Na_2SO_4 \cdot 10H_2O$ (99%), $MgSO_4 \cdot 3H_2O$ (99%), $CaSO_4 \cdot 2H_2O$ (99%), $CuSO_4 \cdot 5H_2O$ (99%), $Ni(NO_3)_2 \cdot 6H_2O$ (99%), $ZnSO_4 \cdot 7H_2O$ (99%)

and $Eu(NO_3)_3 \cdot 5H_2O$ (99.9%) were dissolved in Milli Q water to prepare synthetic AMD solution for selective adsorption tests. Potassium hydroxide (KOH, 98%, Sigma Aldrich) was used was used to adjust the initial pH to 5.5 ± 0.1. All chemicals used in this study were purchased from sigma Aldrich.

5.1.2 Granulation of Cr-MIL-PMIDA

First, powdered Cr-MIL-PMIDA was synthesised as described in chapter 4. Modified chromium based metal organic framework was granulated using sodium alginate and calcium chloride solutions (An et al., 2015; Ryu, Naidu, et al., 2021). 1 g of powdered Cr-MIL-PMIDA was first added to 10 ml of 1.5% sodium alginate solution. The mixture was then loaded to a 50 ml syringe and gently trickled down to 0.05M $CaCl_2$ solution with gentle stirring (100 rpm). Granulated material (with a diameter of 2.0 ± 0.1 mm) was then sieved and dried at 70°C for 12 hours.

5.2 Adsorption study

5.2.1 Equilibrium

Equilibrium adsorption experiments were conducted with 0.01g of powdered Cr-MIL-PMIDA and 0.012g of granulated Cr-MIL-PMIDA using beakers containing 50 ml Eu solutions at optimum pH 5.5 ± 0.1 reported in a previous study (Fonseka et al., 2021). Beakers were placed in a flat shaker at room temperature (24 ± 1 °C) for 24 h to reach equilibrium. Initial concentrations ranging from 2.5 mg/l to 30 mg/l were selected considering low concentrations of Eu found in acid mine drainage (Olias et al., 2018).

Inductively Coupled Plasma Mass Spectrometry (ICP-MS, Agilent 7900, US) was used to measure initial and equilibrium Eu concentrations.

Surface diffusion model (SDM) was developed to further analyse adsorption mechanism (Suzuki & Suzuki, 1990). According to Inglezakis et al. (2019), adsorption from liquid phase onto a porous solid occur in three steps. Which are 1) diffusion from fluid to external surface of adsorbent (film diffusion), 2) mass transfer from external surface to the solid phase (Intraparticle diffusion) and finally 3) physical/chemical bonding with active sites. Since pseudo models neglect film diffusion and Intraparticle diffusion, surface diffusion model is considered to be a realistic method to predict adsorption kinetics (Souza et al., 2017). Equation for surface diffusion model are given below.

Surface Diffusion Model (SDM): $$\frac{\partial q}{\partial t} = \frac{1}{r^2}\frac{\partial}{\partial r}\left(r^2 D_s \frac{\partial q}{\partial r}\right) \quad (5\text{-}1)$$

Boundary conditions:

$$K_f(C - C_s) = D_s \rho_p \frac{\partial q}{\partial r} \quad \text{at} \quad r = R_p \quad (5\text{-}2)$$

$$\frac{\partial q}{\partial r} = 0 \quad \text{at} \quad r = 0 \quad (5\text{-}3)$$

where C_s : concentration of Eu (mg/l), D_s: effective surface diffusion coefficient (m^2/s), Kf: film transfer coefficient (m/s) and r: radial distance of the spherical particle (m). Orthogonal collocation method was adopted to solve equation

Surface Diffusion Model (McKay, 2001): $$\frac{\partial q}{\partial t} = \frac{1}{r^2}\frac{\partial}{\partial r}\left(r^2 D_s \frac{\partial q}{\partial r}\right) \quad (5\text{-}4)$$

5.2.2 Selective adsorption studies

The aim of the experiment was to compare the selectivity of Cr-MIL-PMIDA in powder and granulated forms. Table 5.1 summarises the chemical composition of synthetic AMD used for selective adsorption batch tests, which was based on previous studies that reported concentrations of REE in AMD (Fonseka et al., 2022; K. L. Lecomte et al., 2017). Synthetic AMD solution was first prepared at optimum pH of 5.5 ± 0.1. Two sets of experiments with 0.01 g of powdered Cr-MIL-PMIDA and 0.01g of granulated Cr-MIL-PMIDA were conducted, with each mixed with 50 ml of feed solution. To achieve equilibrium, the samples were stirred on a flat shaker for 24 hours at room temperature (24 $\pm$ 1 ℃). Samples were then filtered, and the initial and residual concentrations of dissolved elements were analyzed using ICP-MS (Agilent 7900, USA). Selectivity of the adsorbent towards Eu and other dissolved metals were calculated using the following equation.

$$\text{Recovery efficiency (\%):} \quad \frac{C_0 - C_t}{C_0} \times 100 \qquad (5\text{-}5)$$

Table 5.1: Chemical composition of synthetic AMD for selective adsorption batch tests

Parameters	Concentration, mg/l
Initial pH	4.8 ± 0.1
Na	100.0 ± 1.0
Mg	300.0 ± 1.0
Ca	150.0 ± 1.0
Ni	5.0 ± 0.2

Cu	100.0 ± 1.0
Zn	100.0 ± 1.0
Eu	0.5 ± 0.2

5.2.3 Column experiment

Fixed bed column adsorption experiments were carried out to evaluate Eu adsorption on granulated Cr-MIL-PMIDA. Experiments were carried out using an acrylic filter column with an inner diameter of 0.01m and length 0.1m (Figure 5.1). Granulated adsorbent was packed in the column supported on glass beads for homogeneous distribution of flow across the column. The flow rate of Eu solution was regulated using a gear pump (Shahbazi et al., 2013). At the start of the experiment, milli Q water was pumped through the column to allow granulated adsorbents to become saturated. Samples were collected at different time intervals and they were analysed using ICP MS (Agilent 7900, USA) to determine the temporal variation of residual Eu concentration. The experiment was carried out at room temperature (24 $\pm$ 1 °C).

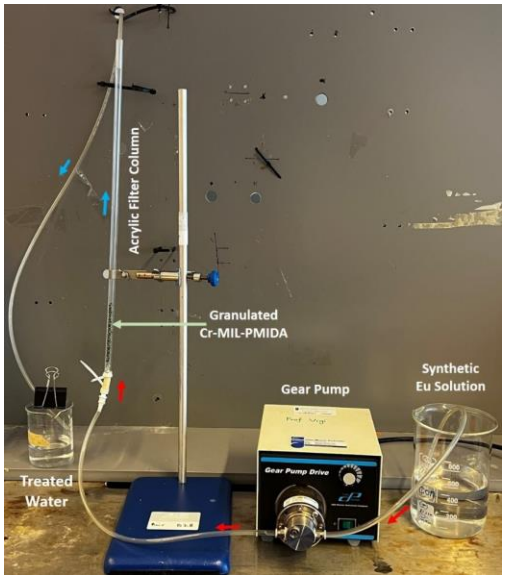

Figure 5.1: Fixed bed column adsorption experimental setup

There are several numerical models which are currently used in fixed bed column studies to simulate breakthrough curves (Chu et al., 2020; Cruz-Olivares et al., 2013; Ryu, Naidu, et al., 2021). Yoon-Nelson (YN) model, bed depth service time (BDST) model and Thomas (Th) are simple models that fit well with experimental results (Cruz-Olivares et al., 2013). In a fixed bed column, mass transfer becomes pivotal since the system is continuously moving away from the asymptotic limit. Therefore, mass transfer model is necessary to calculate solute transport parameters with few general assumptions (Ryu, Naidu, et al., 2021).

Linear driving force approximation (LDFA) is used in this study to describe adsorption in a continuous flow fixed bed column. Inglezakis et al. (2018) has mentioned that LDFA model is widely applied due to its simplicity and consistency. In this study, two

dimensional mass balance was described using the plug flow model shown in equation 11 (García-Mateos et al., 2015).

$$-D_L \frac{\partial^2 C}{\partial z^2} + \frac{\partial (vC)}{\partial z} + \frac{\partial C}{\partial t} + \left(\frac{1-\varepsilon}{\varepsilon}\right)\frac{\partial q}{\partial t} = 0 \quad (5\text{-}6)$$

where, C = Eu concentration, v=superficial velocity, D_L= axial dispersion coefficient, L = length of column and ε = bed porosity. Following are the Initial boundary conditions used to solve above equation (Lin et al., 2017).

$$C = C_0 \text{ at } z = 0 \text{ and } t = 0 \quad (5\text{-}7)$$

$$C = 0 \text{ when } 0 < z < L \text{ and } t = 0 \quad (5\text{-}8)$$

$$D_L \frac{\partial C}{\partial z} = -v(C_0 - C) \text{ when } z = 0 \text{ and } t > 0 \quad (5\text{-}9)$$

$$\frac{\partial C}{\partial Z} = 0 \text{ when } z = L \text{ and } t = 0 \quad (5\text{-}10)$$

Wakao and Funazkri (1978) equation was used to determine the external film mass transfer coefficient (k_f) of the fixed bed system (da Luz et al., 2018).

$$k_f = \frac{D_m}{2R_p}(2 + 1.1Re^{0.6}Sc^{0.33}) \quad (5\text{-}11)$$

$$Re = \frac{2R_p v_s \rho_f}{\mu} \quad (5\text{-}12)$$

$$Sc = \frac{\mu}{D_m \rho_f} \quad (5\text{-}13)$$

where, Re = Reynold's number, Sc = Schmidt number, v_s = superficial velocity, μ = viscosity of fluid (0.00089 $kgm^{-1}s^{-1}$ and ρ_f = density of fluid (1000 kg/m^3). Wilke-Chang equation was used to determine D_m (molecular diffusivity) as previously reported (Ryu et al., 2021).

$$D_m = 7.4 \times 10^{-8} \frac{\sqrt{\emptyset M_b} \times T}{\mu V_a^{0.6}} \quad (5\text{-}14)$$

$$V_a = \frac{M}{\rho} - \frac{(\rho - \rho_0)}{m\rho\rho_0} \quad \text{(Gomaa et al., 2017)} \quad (5\text{-}15)$$

where, M_b = molecular weight of Eu, $\emptyset$ = association factor, T = temperature (K), V_a = molecular volume at boiling temperature, M = molarity of solute (mol/kg), m = relative molar mass (kg/mol), ρ = density of solution (g/cm^3) and ρ_0 = density of solvent (g/cm^3).

5.3 Results and discussion

5.3.1 Characterization of adsorbent

Crystal structure

The XRD pattern of the powdered Cr-MIL-PMIDA exhibited similar peaks to those reported in previous studies, confirming the successful synthesis of the adsorbent (Fonseka et al., 2021; Lee et al., 2018). As depicted in Figure 5.2, the granulated material retained the peak in the 2θ = 8°-10° region, indicating that the crystal structure of Cr-MIL-PMIDA remained intact during the granulation process. Therefore, the successful granulation of the material was achieved in this experiment. An additional peak in the 2θ = 16°-18° region is visible, which could be attributed to the presence of Sodium Alginate ($NaC_6H_7O_6$) in the granulated adsorbent, as previously reported (Jana et al., 2015).

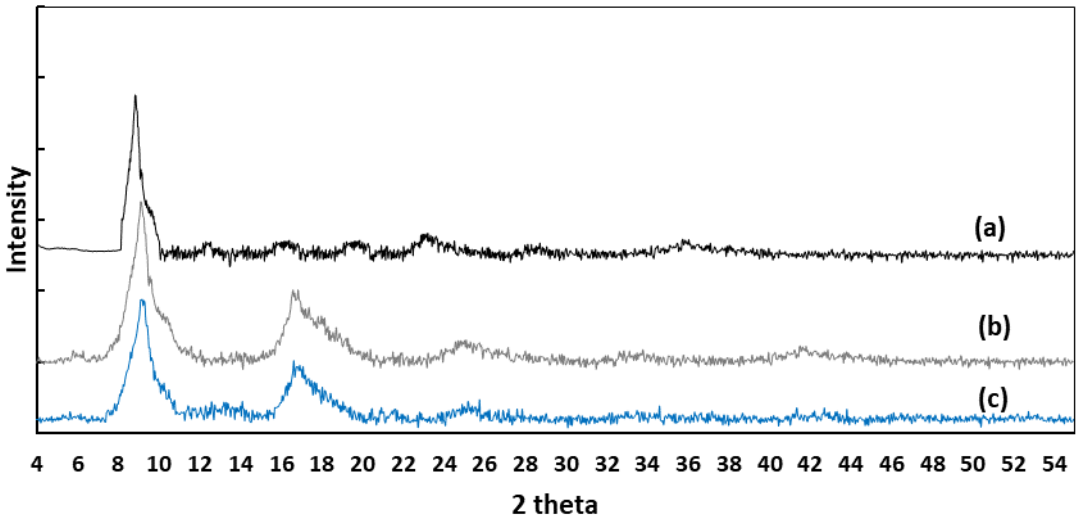

Figure 5.2: XRD patterns of a) powdered Cr-MIL-PMIDA, b) granulated Cr-MIL-PMIDA before adsorption and c) after adsorption

Chemical properties (FTIR)

To confirm the successful synthesis, FT-IR spectra analysis was conducted on the powdered Cr-MIL-PMIDA, as well as the granulated Cr-MIL-PMIDA before and after adsorption. Figure 5.3 illustrates that the chemical structure of Cr-MIL-PMIDA remained intact after granulation. Notably, peaks in the 1140-920 cm-1 range indicate the presence of P-O stretching, which plays a crucial role in the selective adsorption of Eu (Fonseka et al., 2021; Kavun et al., 2021; Lee et al., 2018). Additionally, peaks in the regions of 1400 cm-1 and 2900 cm-1 correspond to the vibration bands of N-H and P-OH, respectively. No additional peaks were observed compared to the powdered material, confirming that sodium alginate merely acted as an adhesive agent for forming spherical granules.

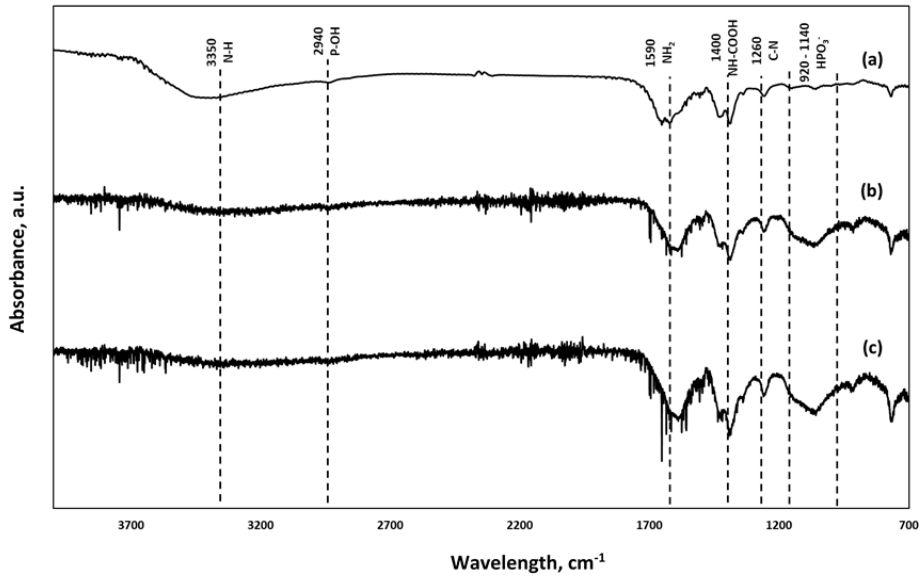

Figure 5.3: FTIR analysis of a) powdered Cr-MIL-PMIDA, granulated Cr-MIL-PMIDA b) before adsorption and c) after adsorption

Surface area and pore size distribution

Nitrogen adsorption/desorption isotherms of granulated Cr-MIL-PMIDA before and after adsorption are shown in figure 5.4. In comparison to powdered Cr-MIL-PMIDA, the granulated material exhibited a significantly lower N_2 adsorption capacity (Fonseka et al., 2021). This decrease can be attributed to pore blocking caused by the cross-linking of sodium alginate with calcium ions, resulting in the formation of insoluble calcium alginate on the surface of the adsorbent. However, it was observed that the hysteresis pattern was well-maintained after modification, indicating that the mesoporous structure of the adsorbent remained unaffected by the granulation process. Additionally, the N_2 adsorption further decreased after adsorption, confirming that the adsorption of Eu led to further blockage of the free pores in the material.

The physical properties of the adsorbents, as summarized in Table 5.2, indicates a significant decrease in the BET surface area and pore volume following granulation. The BET surface area decreased from 1040 m^2/g to 624 m^2/g, while the addition of sodium alginate to achieve a spherical shape slightly reduced the pore volume compared to the powdered form. However, the mean pore diameter remained consistent, as the granulation process did not affect the size of the pores in the adsorbent.

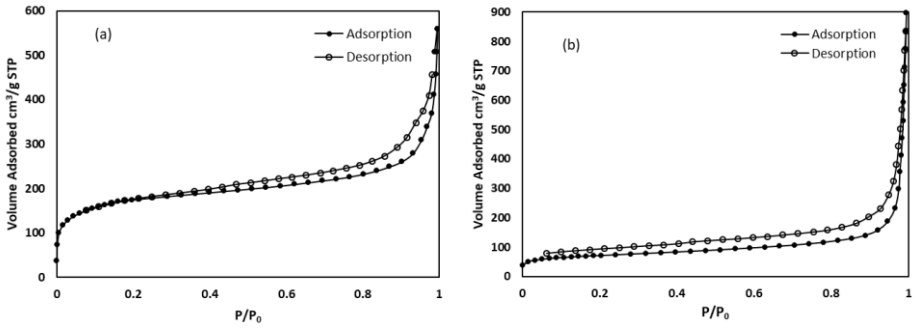

Figure 5.4: Nitrogen adsorption/desorption isotherm graphs of (a) Granulated Cr-MIL-PMIDA before adsorption and (b) Granulated Cr-MIL-PMIDA after adsorption

Table 5.2: Physical properties of adsorbent

Adsorbent	**BET Surface Area** ($m^2.g^{-1}$)	**Pore Volume** ($cm^3.g^{-1}$)	**Mean Pore Diameter** (nm)
Cr-MIL-PMIDA Powder	1040	0.72	1.95
Granulated Cr-MIL-PMIDA	624	0.55	2.01

Surface morphology and element content

Scanning electron microscopy (SEM) was utilized to investigate the structural morphology of granulated Cr-MIL-PMIDA. Successful preparation of spherical granules with a particle size of approximately 2 mm was achieved, as depicted in Figure 5.5a. The SEM image of the adsorbent's surface revealed rough surfaces with layered cracks, facilitating increased contact between Eu ions and the adsorption sites, as shown in Figure 5.5b. These uneven surfaces contributed to a higher adsorption capacity by enhancing the contact area between Eu and the adsorbent (Yu et al., 2019). Furthermore, the energy-dispersive X-ray spectroscopy (EDS) chart of the granulated Cr-MIL-PMIDA after adsorption demonstrated the presence of Phosphorus, Chromium, and Oxygen, confirming the successful granulation while maintaining the chemical structure of the adsorbent, as illustrated in Figure 5.6a and 5.6b. The EDS chart of the loaded adsorbent revealed the presence of Eu, confirming the successful adsorption onto the surface of the granulated material.

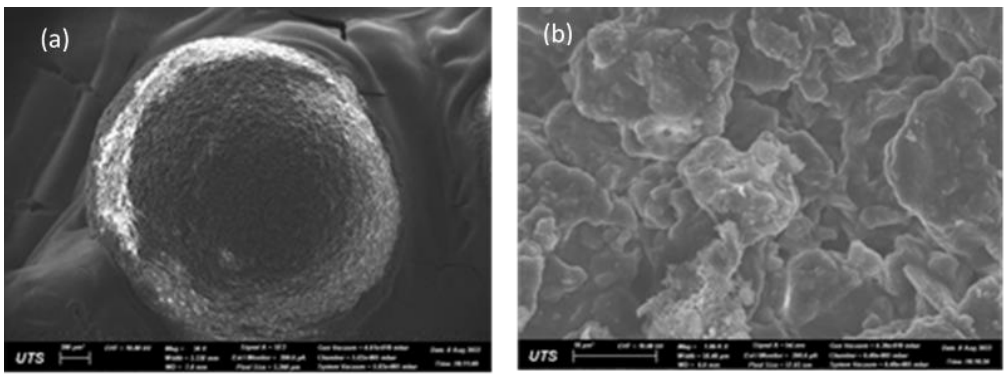

Figure 5.5: SEM-images of granulated Cr-MIL-PMIDA

5.4 Adsorption study

5.4.1 Equilibrium

The adsorption equilibrium characteristics of powdered Cr-MIL-PMIDA and granulated Cr-MIL-PMIDA were analysed using the Langmuir and Freundlich isotherm models (Figure 5.7). These models were employed to evaluate the adsorption behaviour and establish the relationship between the adsorbate concentration and the adsorption capacity of the adsorbent. The experiment was conducted at pH equilibrium (pHeq) of 5.5±0.1, which has been identified as the optimal pH for Cr-MIL-PMIDA in previous studies (Fonseka et al., 2021; Lee et al., 2018). Deprotonation of phosphonic and carboxyl groups in Cr-MIL-PMIDA at high pH values (pH 5.5) was found to significantly enhance the adsorption of Eu^{3+} due to the high negative surface charge (Fonseka et al., 2021).

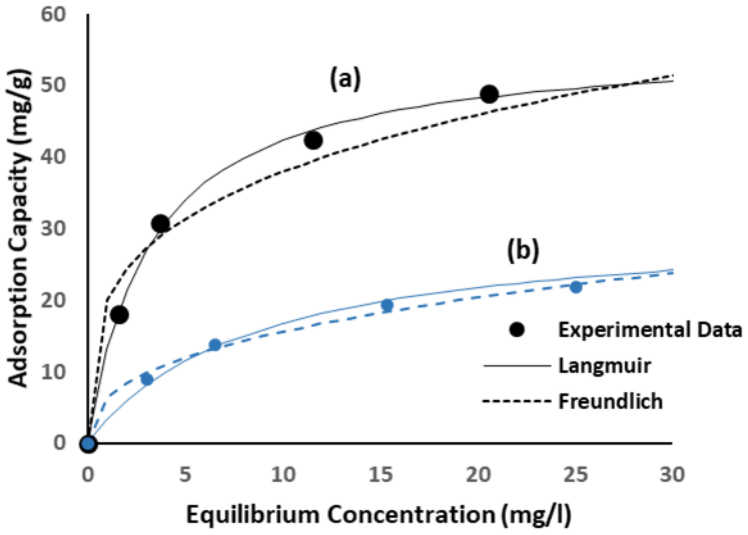

Figure 5.6: Adsorption Isotherm for (a) Powdered Cr-MIL-PMIDA and (b) Granulated Cr-MIL-PMIDA

According to Table 5.3, both the Langmuir and Freundlich models provided excellent fits to the experimental data (R^2>0.99), indicating that the adsorbent surface possessed homogeneous binding sites. The maximum Langmuir adsorption capacity calculated for powdered Cr-MIL-PMIDA was 56.01 mg/g, which is consistent with data reported in the literature for the adsorption of rare earth metals on chromium-based metal organic frameworks (Fonseka et al., 2021; Kavun et al., 2021; Ryu, Fonseka, et al., 2021). However, the maximum adsorption capacity of granulated Cr-MIL-PMIDA dropped to 31.05 mg/g, representing a 44% reduction compared to the powdered adsorbent. This decrease can be attributed to the reduction in surface area, chemical groups, and pore volume, as reported in Table 5.2. Ryu et al. (2021) also reported a 41.2% reduction in the adsorption capacity for granulated modified SBA15 compared to the powdered product when sodium alginate was used as the binding agent. Therefore, the findings of this experiment align with the literature, where the loss of surface area is the primary reason for the reduction in adsorption capacity for granulated materials.

Table 5.3: Adsorption isotherm parameters

Adsorbent	Langmuir			Freundlich		
	Q_m (mg/g)	**b (L/mg)**	**R^2**	**K_F ($g^{1-n}L^ng^{-1}$)**	**n**	**R^2**
Cr-MIL-PMIDA Powder	56.0	0.31	0.99	20.1	3.63	0.97
Cr-MIL-PMIDA Granules	31.1	0.12	0.99	6.4	2.60	0.99

5.4.2 Kinetics

Kinetic experiments were conducted to study the adsorption of Eu under similar conditions as the equilibrium study, using two initial concentrations (10 mg/l and 5 mg/l).

Samples were collected at various time intervals up to 24 hours and fitted to three kinetic models. As depicted in Figure 5.7, more than 90% of the adsorption occurred within the first 4 hours, and equilibrium was reached within 24 hours.

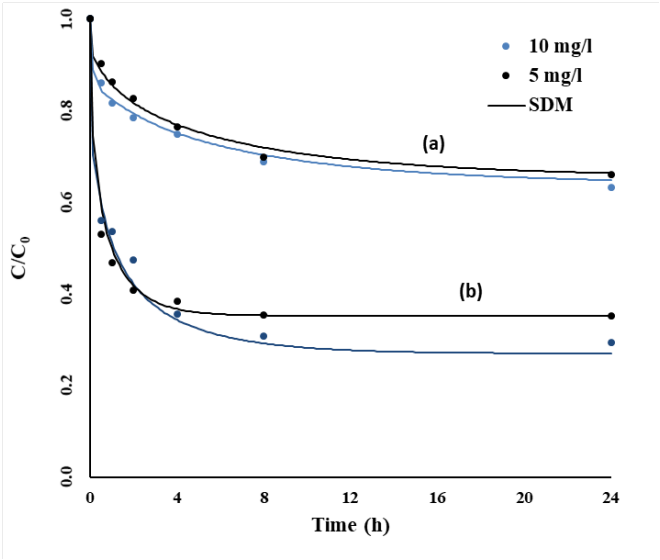

Figure 5.7: Adsorption kinetics for (a) Granulated Cr-MIL-PMIDA and (b) Powdered Cr-MIL-PMIDA

All three models provided successful fits to the experimental data. The pseudo 2nd order model exhibited a better fit with an R^2 value exceeding 0.99 (Table 5.4). According to Zhao et al. (Zhao et al., 2020), when kinetic data aligns well with the pseudo 2^{nd} order model, the adsorption process is predominantly governed by chemical interactions. However, it is important to note that pseudo models are not universally applicable and can depend on experimental conditions (Souza et al., 2017). Therefore, in this study, the surface diffusion model was adopted to analyse mass transfer in detail. The surface diffusion model not only predicts results under different experimental conditions but also facilitates the modelling of fixed bed adsorption systems (Ryu, Naidu, et al., 2021). The

coefficients for film diffusion (k_f) and surface diffusivity (D_s) calculated from the surface diffusion model were determined to be 5.50 x 10-5 m/s and 1.50 x 10-17 m^2/s, respectively.

Table 5.4: Adsorption kinetic parameters of granulated Cr-MIL-PMIDA (Pseudo 1st, 2nd and SDM)

Initial Concentration of Eu	Pseudo 1st Order			Pseudo 2nd Order			Surface Diffusion Model		
	Q_e (mg/g)	k_1(s^{-1})	R^2	Q_e (mg/g)	k_1(g/mg.s)	R^2	K_f (m/s)	Ds (m^2/s)	R^2
10 mg/l	33.7	6.97	0.97	34.1	0.19	0.99	5.50 x 10^{-5}	1.50 x 10^{-17}	0.94
5 mg/l	17.6	4.83	0.77	18.9	0.14	0.99			0.95

The kinetic data suggest that the uptake of Eu initially occurs through surface adsorption, followed by chemisorption. The surface diffusivity (D_s) of the granulated media, as calculated in this study, is lower than the value reported for powdered Cr-MIL-PMIDA by Fonseka et al.(2021). This can be attributed to the reduced BET surface area of the granulated media, which limits the initial rate of surface adsorption. Consequently, the adsorption rate of granulated Cr-MIL-PMIDA is lower compared to powdered media under similar experimental conditions.

5.4.3 Selective adsorption studies

This study aimed to investigate the selective adsorption capacity of granulated Cr-MIL-PMIDA for Eu. Two experiments were conducted, where 50 ml of synthetic AMD

solution was mixed with 0.01g of powdered Cr-MIL-PMIDA and 0.01g of granulated Cr-MIL-PMIDA, respectively, to compare the selectivity before and after granulation. Figure 5.9 shows that the selectivity towards Eu slightly decreased from 92% to 83% after granulation. The uptake of other competing ions remained below 10% in both cases. The minor reduction in Eu uptake on granulated Cr-MIL-PMIDA can be attributed to the decreased number of free sites resulting from the loss of pore volume, which correlates with a lower quantity of functional groups present on the surface of the granulated media.

The successful recovery of rare earth elements (REE) is closely associated with the presence of functional groups within the adsorbent material, as indicated in prior research (Callura et al., 2018; Zhao et al., 2020). These functional groups, including phosphonic, carboxyl, and carbonyl groups, have been recognized to play a critical role in the selective adsorption process. Due to their classification as hard base groups, they exhibit a strong affinity for binding with hard acidic groups such as REE, even in the presence of competing ions (Fonseka et al., 2021). Additionally, trivalent Eu ions exhibit a preferential binding to available active sites compared to lower valence cations in the solution. This characteristic accounts for the high selectivity of Cr-MIL-PMIDA over other competing ions. The findings of this study provide evidence that granulated Cr-MIL-PMIDA can be effectively utilized for selective recovery of REE in various industrial applications.

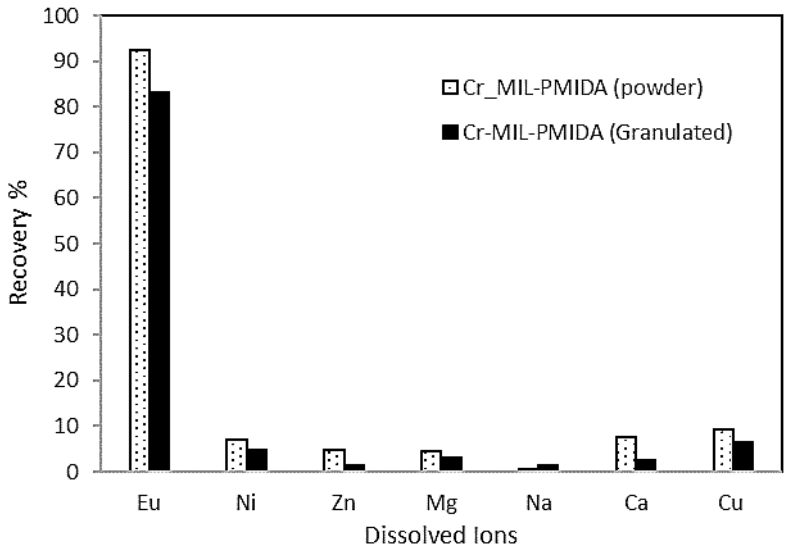

Figure 5.8: Selective adsorption of Eu from a multi component solution by powdered and granulated Cr-MIL-PMIDA

5.4.4 Cyclic adsorption/desorption

The reusability or multiple application potential of granulated Cr-MIL-PMIDA was assessed through five consecutive adsorption/desorption cycles. In the regeneration process, 0.01M HCl served as the stripping agent, followed by a washing step with Milli Q water before the subsequent use. The protonation of functional ligands under low pH conditions resulted in a positively charged surface of the adsorbent, creating a repulsive force that facilitated the desorption of Eu^{3+} ions into the HCl solution.

As depicted in Figure 5.10, granulated Cr-MIL-PMIDA exhibited a retention of over 95% of its initial adsorption capacity throughout the five adsorption/desorption cycles. This indicates minimal loss of functional groups during the regeneration process. Previous studies conducted by Lee et al. (2018) and Fonseka et al. (2021) have also demonstrated the high stability of Cr-MIL-PMIDA in repetitive adsorption/desorption cycles. Thus, this study confirms that granulated Cr-MIL-PMIDA maintains similar stability and effectiveness across multiple applications.

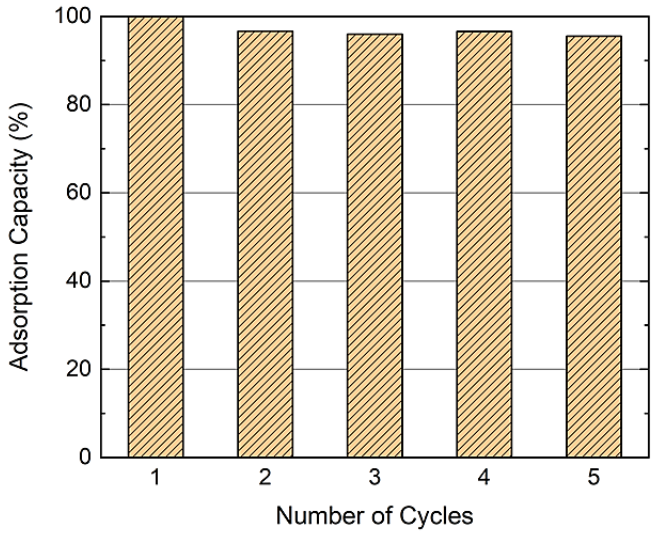

Figure 5.9: Cyclic adsorption tests for Eu^{3+} recovery at initial concentration of 0.2 mg/l at pH 5.5±0.1

5.5 Column experiment

5.5.1 Modelling of single component breakthrough curve

The LDFA (Linear Driving Force Approximation) model has gained widespread use in the modelling of breakthrough curves due to its simplicity and accuracy, as mentioned in studies by Kim et al. (2008) and Nguyen et al. (2022). According to the LDFA, the rate of mass transfer is directly proportional to the concentration difference between the bulk and outer surface of the granulated adsorbent particle, as demonstrated by Ryu et al. (2021).

The coefficients required for the simulation were obtained using equations 5-11 to 5-15 and are listed in table 5.5. The values of the parameters k_f and D_s were derived from the surface diffusion model (SDM) utilized in the adsorption kinetic modelling. The LDFA model, incorporating the surface diffusion model, successfully described the single-component breakthrough curves for Eu adsorption in the upward flow (i.e. Influent pumped from the bottom) fixed-bed system (Figure 5.1). Initially, the lower layers of the fresh adsorbent predominantly adsorb Eu, forming the primary adsorption zone (Patel, 2019). Consequently, the effluent's Eu concentration is close to zero during this stage, resulting in very low C/C_0 values. As the bottom layers of the Cr-MIL-PMIDA granules become saturated, the primary adsorption zone gradually shifts towards the fresher granules at the top. As the adsorption zone continuously moves, Eu tends to breakthrough with the effluent at a certain point, commonly referred to as the breakthrough point. Once the granules are completely exhausted, the C/C_0 value reaches 1, as illustrated in Figure 5.11.

The axial dispersion coefficient was first determined to be 6.00×10^{-5} m^2/s for the experimental condition given in Figure 5.11. These values were utilized to simulate breakthrough curves under different experimental conditions. In this study, multiple breakthrough curves were simulated for various system conditions, including initial feed concentration, flow rate, and the length of the fixed-bed column. These simulated curves were then compared with experimental results to evaluate the accuracy of the model.

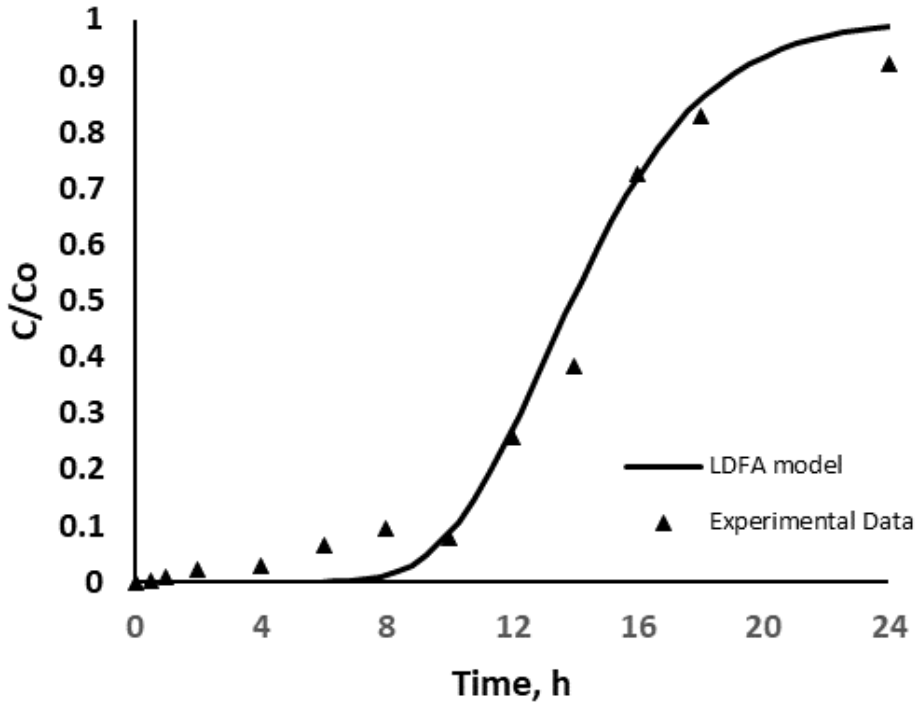

Figure 5.10: Validation of single component breakthrough curve to calibrate the model (Bed Length: 0.1m, Linear velocity 0.637 m/h, R^2=0.94)

Table 5.5: Parameters used for breakthrough column modelling

Parameters	**Value**	**Unit**
Bed length, L	0.1	m
D_L (axial dispersion coefficient)	6.00E-05	m^2/s
Area	7.85E-05	m^2
V (Linear velocity)	0.637	m/h
C_0 (initial concentration in the fluid within the column)	0	mmol/L
C_{in} (inflow concentration)	0.001316	mol/m^3
k_f	5.50E-05	m/s
D_s	1.50E-17	m^2/s

5.5.2 Analysis of the effect of initial concentration

Figure 5.12a presents the experimental results and breakthrough curve obtained at a linear flow velocity 0.637 m/h, bed height of 0.1 m and at 0.4 mg/l initial concentrations of Eu to verify the column model. A high R^2 value of 0.92 between the simulated and experimental data confirmed the accuracy of the model.

Simulation of the breakthrough curves for initial Eu concentrations between of 0.2 to 0.4 mg/l at a linear flow velocity of 0.637 m/h, a bed height of 0.1 m is presented in figure 5.13a. As the initial concentration of Eu is increased, breakthrough curves developed sharper profiles and shifted to the left. This resulted in breakthrough times decreasing

from 24 to less than 12 hours. Exhaustion time was also impacted, as it dropped from 24 to less than 12 hours upon doubling the influent Eu concentration. The diffusion process of Eu uptake onto the granulated Cr-MIL-PMIDA caused by steeper adsorbate concentration gradients was the primary cause of the observed changes in the breakthrough and exhaustion curves (García-Mateos et al., 2015; Nguyen et al., 2022; Ryu et al., 2021).

5.5.3 Analysis on the effect of flowrate

At a bed height of 0.1 m, an initial Eu concentration of 0.2 mg/l, and a linear flow velocity of 0.796 m/h, a column experiment was carried out and the results are depicted in Figure 5.12b. The R2 value of 0.92 shows that the experiment's data fits well with the simulation model. Simulation of breakthrough curves at higher flowrates in figure 5.13b shows that the breakthrough times were shortened and the curves became steeper, indicating rapid saturation post-breakthrough. This is likely due to the shorter contact time between the adsorbate and adsorbent not being sufficient to reach equilibrium for granulated Cr-MIL-PMIDA (Lin et al., 2017). When the simulation model was run at a slower linear flow velocity of 0.478 m/h, the breakthrough time was shifted to the right and the slope of the curve was made shallower and the breakthrough time was longer. This indicates that the saturation period was longer.

5.5.4 Analysis on the effect of bed height

The depth of granulated adsorbent bed was found to be an important factor as shown by simulation curves in Figure 5.13c. To prove the model's accuracy, an experiment was conducted, with an inflow of 0.2 mg/l Eu, flow rate of 0.637 m/h and a bed depth of 7.5cm (Figure 5.12c). The outcomes were consistent with the simulation model (R^2=0.94). Figure 5.12c demonstrated that the curves shifted to the right and had higher breakthrough depths as the bed was increased from 7.5 cm to 12.5 cm, indicating that a larger assembled adsorbent yielded more binding sites for the Eu ions. Brion-Roby et al. (2018) and Ryu et al. (2021) reported similar findings. This study proves that a LDFA model can be successfully developed for Eu adsorption on granulated SBA15-PMIDA using one column experiment to find the axial dispersion coefficient and simulate breakthrough

curves for varying operating conditions with the same value of the coefficient with high accuracy.

Figure 5.11: Validation of simulation curves with experimental data (inlet concentration, bed height, flow rate)

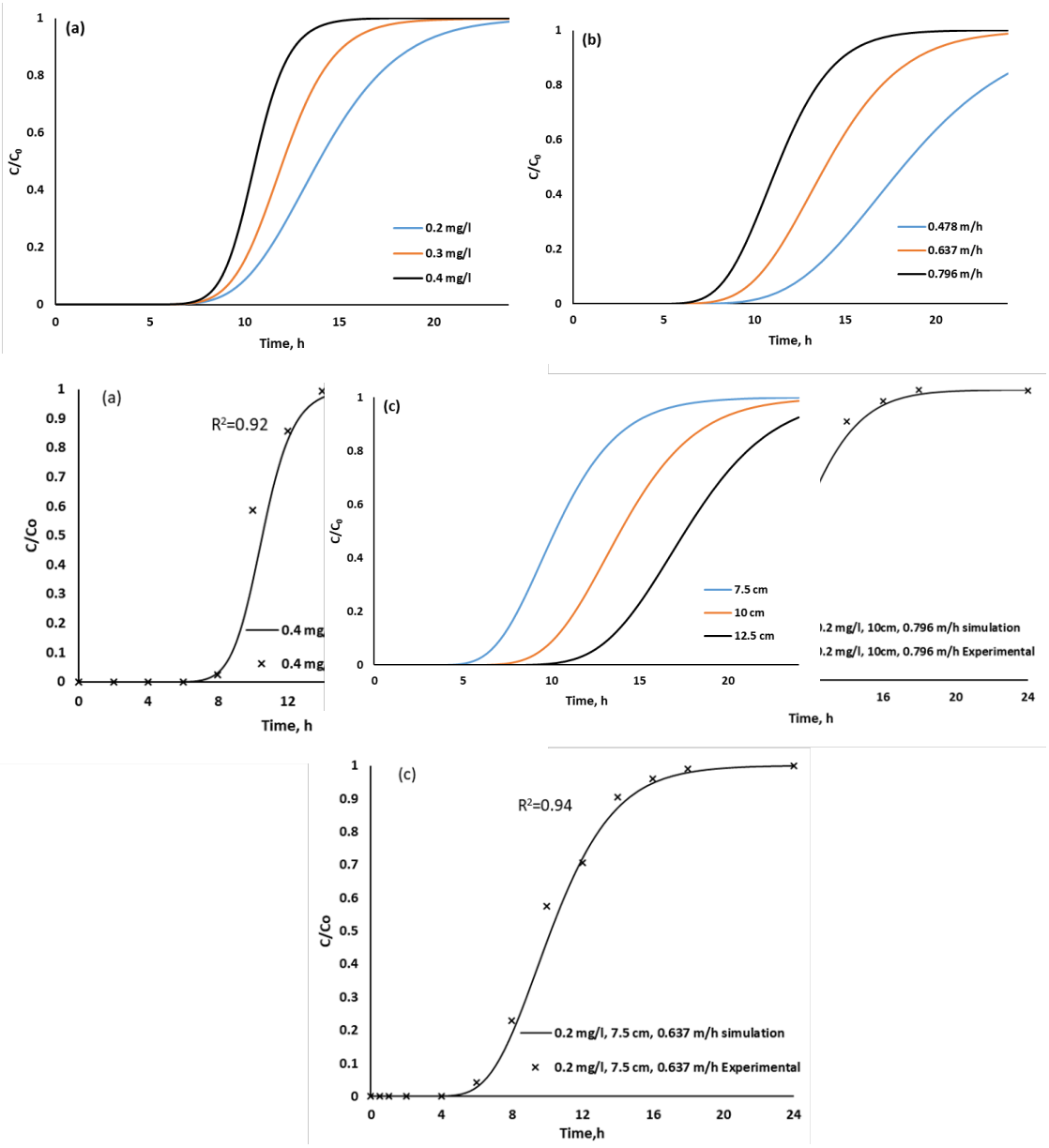

Figure 5.12: Simulation of breakthrough curves for single component adsorption of Eu in terms of (a) feed concentration, (b) flow rate and (c) length of bed

5.6 Summary

In this study, the synthesis of Cr-MIL-PMIDA was achieved through a hydrothermal reaction, followed by successful granulation using alginic acid and $CaCl_2$ for the first time. The prepared material was characterised using XRD, SEM and FTIR measurements to validate successful granulation.

- Adsorption capacity of powdered Cr-MIL-PMIDA, 56.01 mg/l decreased to 36.05 mg/l after granulation due to reduction of surface area and pore volume.
- However, granulated Cr-MIL-PMIDA recorded only a 8% reduction in selectivity towards Eu in a multi component solution compared to the ungranulated version, indicating granulation has minimal impact on performance.
- The material exhibited the ability to be reused for five cycles while maintaining over 90% of its initial adsorption capacity.
- a dynamic model based on the surface diffusion model was developed to validate and predict the results of single-component fixed bed adsorption. Experimental

tests were conducted, varying the column length, feed concentration, and linear flow rate, successfully confirming the simulations generated by the model.

- This study demonstrates that the dynamic column model developed for granulated Cr-MIL-PMIDA can be reliably utilized to design industrial-scale systems with a single adsorption column experiment.

Conducting membrane filtration before adsorption in the treatment of AMD can significantly improve the efficiency and effectiveness of REE concentration processes. It helps remove of impurities, enhances selectivity, and contributes to a more environmentally sustainable approach to managing AMD and recovering valuable REEs. The inclusion of membrane filtration preceding the adsorption stage can yield remarkable enhancements in both the efficiency and efficacy of Rare Earth Elements (REE) concentration process, as well as in water recovery. Reusing recycled water for mining activities represents a proactive and strategic approach to address water stress in mining operations. This practice not only aids in water conservation and cost reduction but also aligns with broader sustainability objectives. The next chapter evaluates the use of low pressure nano filtration for recovery of water and concentration of REE and Cu for subsequent adsorption.

CHAPTER 6

RECOVERY OF WATER AND VALUABLE METALS USING LOW PRESSURE NANOFILTRATION AND SEQUENTIAL ADSORPTION FROM ACID MINE DRAINAGE

*This chapter is based on the following journal publication

Fonseka, C.; Ryu, S.; Naidu, G.; Kandasamy, J.; Vigneswaran, S. Recovery of water and valuable metals using low pressure nanofiltration and sequential adsorption from acid mine drainage. *Environmental Technology & Innovation* **2022**, *28*, 102753. https://doi.org/10.1016/j.eti.2022.102753

6 Introduction

The use of membrane technologies has increased in popularity throughout the mining industry for AMD treatment (Agboola, 2019a). Most mines are located in arid regions where water is a scarce resource, thus recovering potable water from AMD generates a distinct advantage. The treated water can be reused for mining activities or for drinking with further purification. The major drawback of this technology is its high operational cost and production of reject water which consists of highly concentrated metal ions and sulphates (Saha & Sinha, 2018). Additionally, fouling of membranes due to the presence of organic matter (OM) can increase membrane replacement frequency and cost (Zhong et al., 2007b). OM can cause membrane fouling resulting in flux reduction. Studies report that high acidity and sulphates concentrations in AMD increase interaction with OM (Lazareva et al., 2019). (Gillmor, 2011) found that dissolved organic content in AMD can increase up to 12 mg/l. For this reason, identifying methods to reduce membrane fouling due to dissolved organics is critical for the successful practical application of membrane technology for AMD filtration.

Among membrane fouling mitigation strategies, feed water pre-treatment such as Microfiltration (MF) and Coagulation (Ohno et al., 2010), membrane modification (Bagheripour et al., 2019) and chemical washing (Al-Amoudi & Lovitt, 2007) have proved to be effective. High cost was a limiting factor for membrane modification, while generation of secondary chemical pollutants was an inherent disadvantage of chemical washing (Zhao & Yu, 2015). It is necessary to identify efficient and cost-effective pre-treatment technologies. Among pre-treatment methods, successful application of powdered eggshell for removal of organic pollutants was reported by (Zulfikar et al.,

2013). Their study found that 95% of humic acid was successfully adsorbed onto powdered eggshell. Furthermore, the experiment was conducted at low pH range (pH 2) similar to that of AMD found near mining sites (Vass et al., 2019). The use of powdered eggshell is a promising low-cost solution for: firstly, reducing organic content in feed water to the NF membrane; and secondly, reducing organic fouling and associated flux reduction.

Nanofiltration is a promising technology investigated for concentrating dissolved metal ions and recovering water from AMD (Mullett et al., 2014; Pino et al., 2020; Wadekar et al., 2017). NF offers advantages such as low operating pressure, high permeate flux over reverse osmosis (RO) leading to lower operational and maintenance costs (Zhao et al., 2018). Wadekar et al. (2017) tested eight commercially available NF membranes for filtration of synthetic and real AMD. NF90 membrane was found to be the most efficient with high ion rejection (> 97%) and stable permeate flux (3 LMH/bar). The study conducted by Pino et al. (2020) compared the performance of NF90 and NF270 for filtration of AMD from an active copper mine. NF90 showed higher metal rejection at low operating pressures, while NF270 was prone to fouling. NF90 is reported as a weakly hydrophilic membrane with positively charged functional groups on the surface (Jamil et al., 2021; Pino et al., 2020). This results in excellent cation rejection enabling valuable trace metals such as REE to be concentrated.

Modified chromium-based Metal Organic Frameworks such as Cr-MIL-PMIDA are regarded as highly efficient adsorbents for the removal of REE from aqueous solutions (Lee et al., 2018; Ren et al., 2016). High stability, large pore area and ability for modification with functional groups make the recovery of REE economically feasible.

Mesoporous silica is another adsorbent efficient at removing pollutants from waste streams (Cashin et al., 2017). Mesoporous silica too has a high surface area coupled with stable physical, chemical and thermal characteristics (Liu et al., 2019). Ryu et al. (2019) noted that amine-grafted mesoporous silica selectively adsorbed copper in the presence of competing ions such as Zn, Ni and Mg while maintaining its chemical structure over multiple loading/stripping cycles.

While several studies have been conducted on the recovery of water from AMD, relatively few focused on the optimization of NF/adsorption hybrid system for selective recovery of valuable metals from the concentrated retentate. This study aims to evaluate the efficiency of low-pressure NF in recovering fresh water from AMD while concentrating valuable metals. These will subsequently be selectively adsorbed using metal organic frameworks and mesoporous silica materials.

6.1 Materials and Method

6.1.1 Preparation of AMD solution

Low Pressure NF filtration and adsorption analyses of valuable metals were conducted using synthetic AMD. The composition of AMD prepared for experiments was based on previous studies (Karina Leticia Lecomte et al., 2017; Ryu et al., 2020) and is summarized in Table 6.1.

Table 6.1: Chemical composition of synthetic AMD

Parameters	Concentration, mg/l
pH	2.0 ± 0.2

TOC	10.00
Na	112.92
Mg	300.95
Al	101.64
Ca	168.54
Fe	302.90
Ni	6.02
Cu	107.48
Zn	104.34
Eu	0.14
Gd	0.51

Synthetic AMD was prepared using $Na_2SO_4 \cdot 10H_2O$ (99%), $MgSO_4 \cdot 3H_2O$ (99%), $Al_2(SO_4)_3 \cdot 18H_2O$ (99%), $CaSO_4 \cdot 2H_2O$ (99%), $Fe(SO_4) \cdot 7H_2O$ (99%), $Ni(NO_3)_2 \cdot 6H_2O$ (99%), $CuSO_4 \cdot 5H_2O$ (99%), $ZnSO_4 \cdot 7H_2O$ (99%), $Eu(NO_3)_3 \cdot 5H_2O$ (99.9%) and $Gd(NO_3)_3 \cdot 6H_2O$ (99.9%). Humic acid (HA) (53680, CAS No. 1415-93-6, Sigma-Aldrich) was used to replicate dissolved organic matter (OM) in AMD as previously reported by Holland et al. (2014). All chemical compounds were purchased from Sigma-Aldrich. 2 M H_2SO_4 was used to adjust the initial pH to 2.0 ± 0.2. pH of the solution was measured using HQ40d multimeter, Hach, USA, while the concentrations of dissolved metals were measured using ICP-MS, Agilent 7900, USA.

6.2 NF membrane and operation

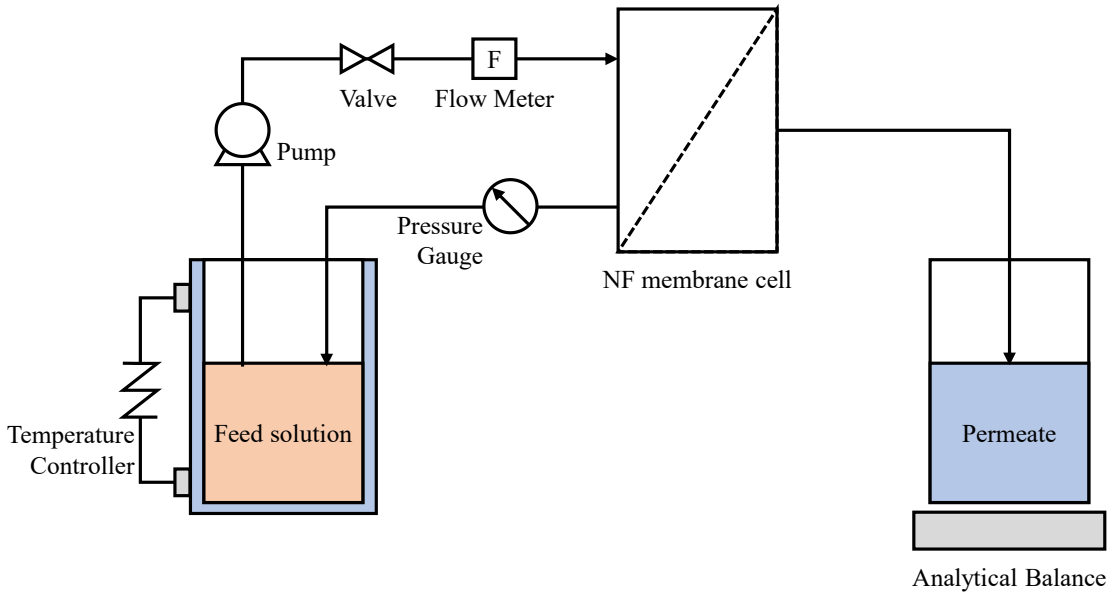

Figure 6.1: Schematic diagram of NF setup

The NF membranes used in this experiment were purchased from Sterlitech Corporation, WA, USA. The properties of this membrane are listed in Table 6.2 and were obtained from Jamil et al. (2021).

Table 6.2: Characteristics of NF membrane (Jamil et al., 2021)

Membrane	Manufacturer (Material)	MWCO (Da)	Zero Point Charge (ZPC) pH	Contact Angle (Degrees)
NF90	DOW (Polyamide TFC)	90 – 180	3.5	79

A feed volume of 2 L and a rectangular cross-flow cell with an area of 54 cm^2 (9 cm x 6 cm) was used for experiments. A schematic diagram of the NF set-up is shown in Figure 6.1. Several studies have been conducted at transmembrane pressure of above 10 bar for AMD filtration using NF90 membrane (Wadekar et al., 2017; Pino et al., 2020). Jamil et al. (2021) documented that NF90 demonstrated excellent inorganic salt and dissolved organic rejection at low operational pressure of 2 -5.5 bar. Therefore, a low trans-membrane pressure of 3 bar was chosen for this study to analyse performance of NF90 for AMD filtration at a temperature of 25±1°C. The feed solution was continuously circulated while permeate was collected and its increase in mass measured using analytical balance. Permeate flux and water recovery were calculated based on readings measured from analytical balance at constant intervals. At completion, initial feed, final feed (concentrated feed) and permeate were analysed for metal concentrations, pH and TOC.

The volume concentrating factor (VCF) of the concentrated feed was determined using the following equation:

$$VCF = \frac{V_i}{V_c} \qquad (6\text{-}1)$$

Where,

V_i - Initial AMD feed volume (L)

V_c - Final concentrated AMD volume (L)

Permeate flux of the membrane was calculated by measuring the permeate volume collected at 5 min intervals using the following equation:

$$J = \frac{V}{A\ x\ \Delta t} \quad (6\text{-}2)$$

J - Permeate Flux (l/m^{2}h)

A - Effective filter area of membrane (m^2)

Δt - Time interval (h)

Osmotic pressure (bar) across the membrane was calculated using Van't Hoff equation as reported by Zhang et al. (2020b):

$$\pi = iMRT \quad (6\text{-}3)$$

i - Van't Hoff Factor

M - Molarity of Solute (mol/L^{-1})

R - Universal gas constant (0.08315 L.bar.mol^{-1}.K^{-1})

T - Temperature (K)

Solute rejection was calculated from the concentration of dissolved metals in feed AMD and filtered permeate measured using ICP MS (Agilent 7900, USA):

$$R(\%) = \frac{C_i - C_p}{C_i} \quad (6\text{-}4)$$

R - Solute Rejection (%)

C_i - Initial solute concentration (mg/l)

C_p - Permeate solute concentration (mg/l)

6.3 Preparation of powdered Eggshell for TOC removal

Eggshell was examined as a cost-effective solution for selective removal of OM as discussed in the introduction (Zulfikar et al., 2013). The eggshell sample was first washed with detergent and the inner thin membrane under the shell was then removed. The cleaned eggshell was further washed with Milli Q water and air dried for 48 hours. The dried eggshell was then ground to a particle size of 75 μm using a mortar and pestle.

6.4 MOF synthesis procedure

Cr-MIL-PMIDA was synthesized using Chromium (III) nitrate nonahydrate, H_2BDC-NH_2 and PMIDA as previously reported by Fonseka et al. (2021). The synthesis procedure is described in detail in chapter 3.

6.5 SBA15 synthesis procedure

SBA15 was synthesized through hydrothermal reactions and modified with amine ligands following toluene reflux with APTES as previously and recently reported by Ryu et al. (2021). The details of the synthesis are provided in chapter 3.

6.6 REE and Cu selective Adsorption Experiments

6.6.1 Influence of pH

Concentrated feed solution obtained from the NF filtration was used in this study. Initial pH of concentrated feed-was found to be 2.0 ± 0.2. pH was then adjusted to values ranging

from pH 2 to 7 using 1 M KOH to: firstly, precipitate competing ions from solution; and secondly, establish the best pH level for the adsorbents to recover REE and Cu. The precipitate was allowed to settle under gravity for 12 h and then the supernatant was filtered using a 0.45 µm syringe filter.

6.6.2 Selective recovery of REE (Gd and Eu)

Optimum pH of 5 was used in these experiments. Cr-MIL-PMIDA adsorbent, ranging from 0.02 g to 0.32 g was used to find the desired adsorbent dosage for selective REE recovery. The adsorbent was mixed with 50 ml of pH adjusted NF concentrated feed solution and then stirred on a flat shaker for 24 h at room temperature (25 ± 1 °C) to reach equilibrium. Samples were then filtered and analysed for initial and residual concentration of elements (ICP-MS, Agilent 7900, USA).

6.6.3 Selective recovery of Cu

Residual solution after Cr-MIL-PMIDA adsorption was used in this experiment. Dosages of 0.02 g to 0.32 g of SBA15 were mixed with residual solution and similar experimental conditions to REE adsorption was maintained. Initial and residual concentrations of elements were measured to find the optimum adsorbent dosage (ICP-MS, Agilent 7900, USA).

6.7 Results and Discussion

6.7.1 Physical characterization of adsorbents

Cr-MIL-PMIDA, Cr-MIL-NH_2, pristine SBA15 and amine grafted SBA15 were tested for their physical characteristics before and after modification. Figure 6.2 shows the X-ray diffraction patterns of prepared adsorbents at low angles in the 2-theta range. They were found to be similar to Ryu, Fonseka, et al. (2021) findings. Cr-MIL-PMIDA was synthesized following a co-synthesis process where Cr-MIL-NH_2 was modified with N-(phosphonomethyl) iminodiacetic acid (PMIDA) in the presence of N,N-dicyclohexylcarbodiimide (DCC) as a dehydrating agent. XRD patterns for SBA15 shows one sharp 110 peak followed by two small peaks. This XRD pattern is associated with the hexagonal structure of SBA15 as reported in previous studies (El-Nahhal et al., 2018; Ryu, Fonseka, et al., 2021). Amine grafted SBA15 shows a decrease in peaks at 110 and 200 while the first sharp peak remained unchanged. This is a reflection of pore blocking due to amine grafting on SBA15 surface. However the structure of amine grafted SBA15 was well preserved as confirmed by TEM images in Figure 6.4.

The XRD patterns for Cr based MOF were also similar to those reported in previous studies (Lee et al., 2018; Ryu, Fonseka, et al., 2021). Indistinguishable XRD patterns of the two MOF derivatives highlights that the crystal structure of the adsorbent was well preserved during modification with PMIDA groups.

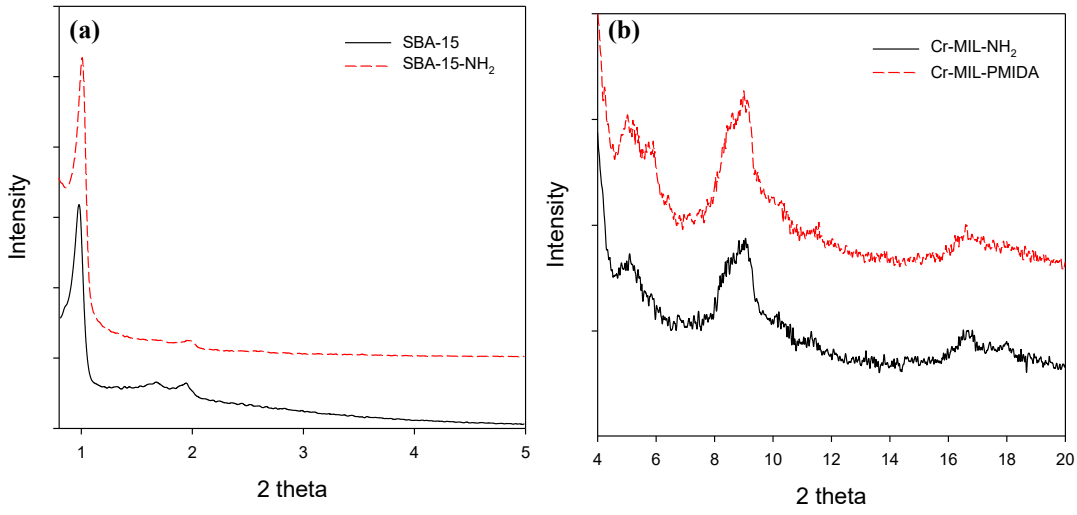

Figure 6.2: XRD patterns of (a) SBA15 and (b) MOF samples

Nitrogen adsorption/desorption isotherms of SBA15 and Cr based MOF samples are shown in figure 6.3. Modified samples showed decreased N_2 adsorption compared to respective pristine structures. This again reflects successful grafting of beneficial ligands which reduced pore volume. However, the hysteresis in both SBA15 derivatives were well maintained after modification confirming that the mesoporous structure was undamaged during synthesis (Moritz & Łaniecki, 2012).

According to 6.3, the BET surface area and the pore volume was found to be lower for SBA15 samples compared to Cr based MOF. The BET surface area of Cr-MIL-PMIDA was recorded as 1040 $m^2.g^{-1}$, which was higher than that of amine grafted SBA15 (300 $m^2.g^{-1}$). These values were similar to findings from previous studies (Lee et al., 2018; Ryu et al., 2019). The reduction in surface area is due to pore blocking by functional groups grafted onto the two adsorbents. Mean pore diameter of amine grafted SBA15 (4.2

nm) is two fold higher than Cr-MIL-PMIDA (1.95 nm). Studies have shown that the small pore size of MOF enables size exclusion and promote selective adsorption of REE (Lee et al., 2018). This was confirmed by the study by Ryu et al. (2021), which found that Cr-MIL-PMIDA had superior adsorption capacities towards REE (Lu, Y) compared to amine grafted SBA15.

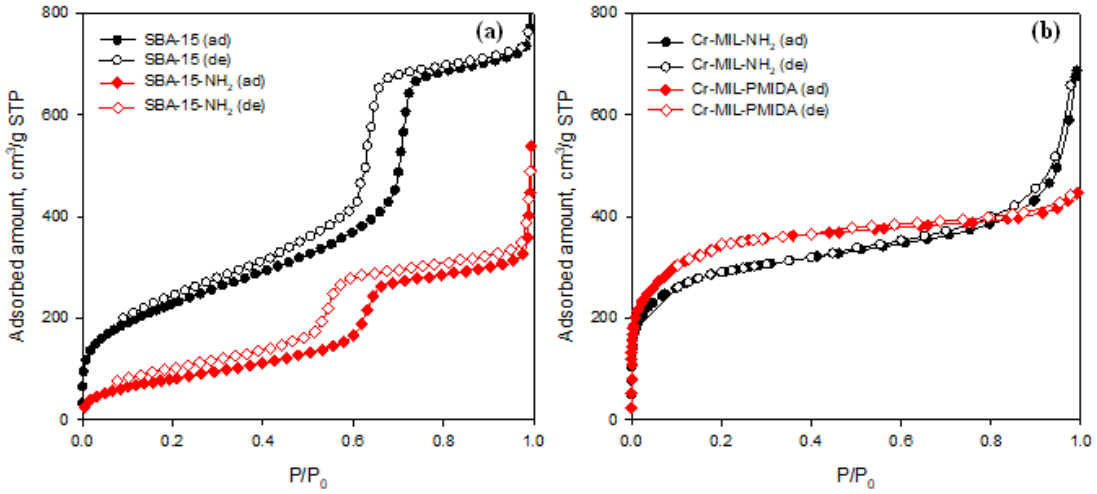

Figure 6.3: Nitrogen adsorption/desorption isotherm graphs of (a) SBA15 samples and (b) MOF samples

Table 6.3: Physical properties of prepared adsorbents

Adsorbent	BET Surface Area $m^2.g^{-1}$	Pore Volume $cm^3.g^{-1}$	Mean Pore Diameter nm
SBA 15	810	0.95	7.21
SBA15-NH_2	300	0.80	4.20

Cr-MIL-NH_2	1285	1.07	4.08
Cr-MIL-PMIDA	1040	0.72	1.95

The morphology of the adsorbent was analysed using SEM. Elemental distribution mapping of Cr-MIL-PMIDA (Figure 6.4a) reveals that nitrogen and phosphorus functional groups are evenly distributed on the surface of the adsorbent. This data confirms the successful synthesis of Cr-MIL-PMIDA in line with Lee et al. (2018). Furthermore, TEM images of SBA15 show the hexagonal structure of the adsorbent has been preserved after amine grafting. The results confirmed that physical and chemical structure of both materials remained strong which is necessary for successive loading/stripping cycles.

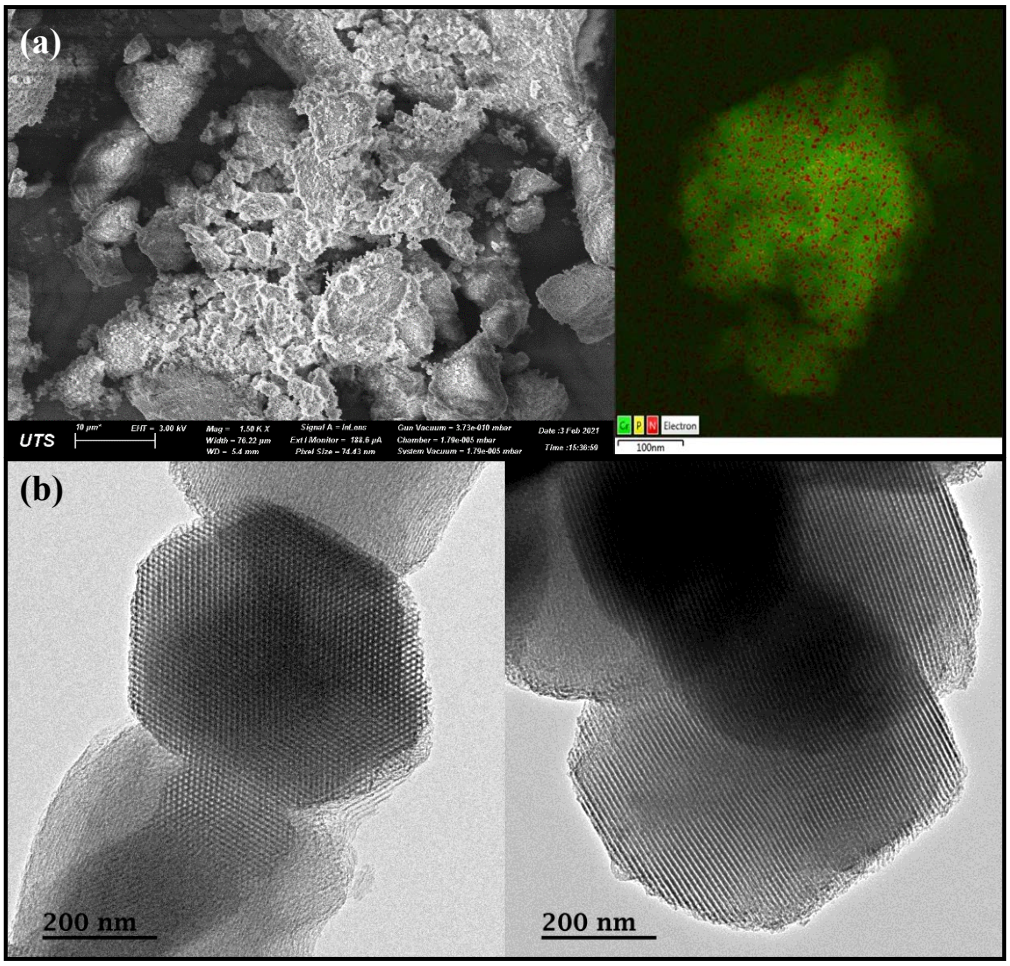

Figure 6.4: (a) SEM image and Elemental distribution mapping of Cr-MIL-PMIDA and (b) TEM images of SBA15 and SBA15-NH_2

6.7.2 Chemical characterization

FT-IR spectra analysis was carried out to study the chemical bonds present on the surface of both adsorbents (Figure 6.5). The vibration pattern recorded for SBA15 showed that Si-O stretching vibration was located at 900 cm^{-1}. The reduction in Si-O vibration on SBA15-NH_2 can be attributed to bonding of –OH with silica groups (Li et al., 2007). New

peaks at 2850 cm^{-1} and 1400 cm^{-1} corresponds to N-H vibration which confirms NH_2 was successfully grafted onto pristine SBA15 (Ryu et al., 2019).

The vibration peaks of MOF located at 1600 cm^{-1} are assigned to carbonyl (C=O) and carboxyl (-COOH) stretching in the adsorbent and they remained relatively unchanged after modification (Babaee et al., 2020). A similar vibration pattern was observed in Cr-MIL-PMIDA as reported in previous studies (Ryu et al., 2021). The peaks assigned for amine groups at 1400 cm^{-1} showed significant decrease after modification with PMIDA. This confirms that chemical reaction between NH_2 and PMIDA under reflux condition was successful. Additional peaks in the range of 900–1100 cm^{-1} in Cr-MIL-PMIDA confirm the presence of phosphonic groups on the structure (Lee et al., 2018; Pramanik & Bhaumik, 2014).

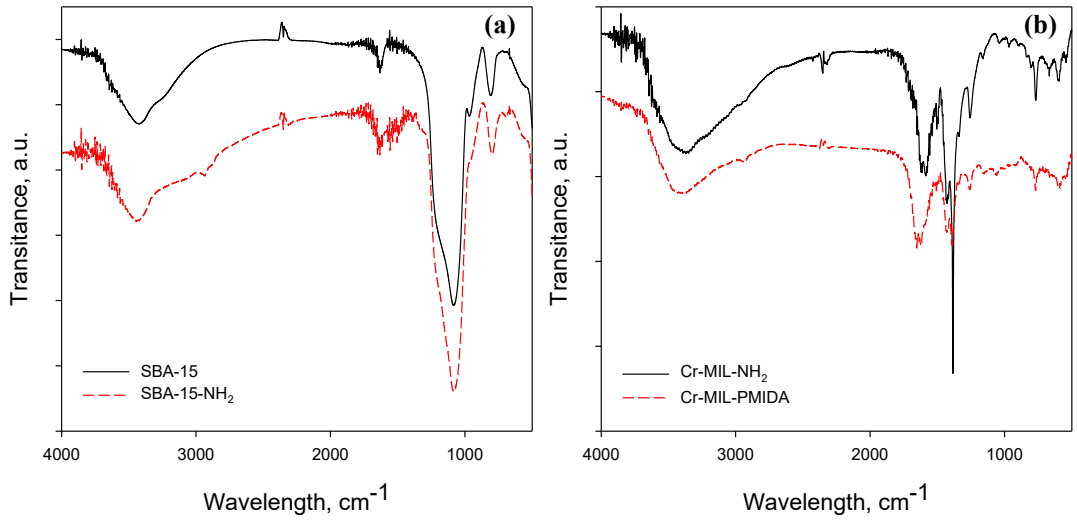

Figure 6.5: FT-IR spectra of (a) SBA-15 and (b) MOF samples

6.8 Performance of low-pressure NF

The performance of bench scale low-pressure NF was analysed using the NF90 membrane supplied by Sterlitech Corporation, WA, USA. Experiments were carried out to evaluate AMD remediation and its ability to produce clean water while increasing the concentration of REE and Cu in the feed. A low feed pressure of 3 bar with a cross-flow velocity of 0.35 m/s (Reynolds Number = 4635) was used in the experiment. The performance of NF was measured using synthetic AMD with and without organic matter.

The results from the experiment show that the NF system achieved steady permeate flux of 15.5 ± 0.2 L/m^{2}h (LMH) for AMD feed without organic matter (Figure 6.6). The initial permeate flux for AMD feed with organic matter was 10.2 ± 0.3 L/m^{2}h (LMH), which is considerably lower compared to the experiment without organic matter. The initial osmotic pressure on the feed side was calculated using equation 3 and it was found to be 0.895 bar. Both sets of samples maintained a steady flux up to a volume concentration factor (VCF, equation 1) of 5, recovering 80% of permeate. Solute rejection (equation 2) in both cases were found to be high (> 98%) with the exception of Na (Table 6.4). MWCO (molecular weight cut off) value is the molecular weight of the smallest solute of which at least 90% is rejected by the membrane (Drioli et al., 2016). The NF90 membrane consists of positively charged functional groups on its surface. This creates an electrostatic field within the membrane matrix known as the Donnan potential (Mehiguene et al., 1999). This significantly contributes to membrane potential which inhibits transfer of positively charged ions across the membrane. This may be the main reason for the high rejection rates recorded for higher valent cations in AMD. In theory, solutes of lower molecular weights than MWCO should pass on to the permeate side

(Franke et al., 2019). According to Franke et al. (2019), when electrostatic repulsion dominates size exclusion, solutes with lower molecular weights were found to be rejected more than expected. This explains the slightly higher rejection rate found for positively charged Na in this study.

Table 6.4: Permeate quality and solute rejection rates

Element	**Initial Concentration (mg/l)**	**Permeate quality (mg/l) (AMD with Organic)**	**Rejection %**	**Permeate quality (mg/l) (AMD without Organic)**	**Rejection %**
Na	112.92	11.23	90.05	10.56	90.65
Al	101.64	1.33	98.69	1.69	98.34
Ca	168.54	1.92	98.86	1.65	99.02
Cu	107.48	1.52	98.59	1.08	99.00
Fe	302.90	5.20	98.28	2.64	99.13
Mg	300.95	3.65	98.79	3.12	98.96
Ni	6.02	0.08	98.67	0.07	98.84
Zn	101.34	0.95	99.06	0.81	99.20
Gd	0.51	0.0149	97.08	0.0009	99.82
Eu	0.14	0.0034	97.57	0.0042	97.00

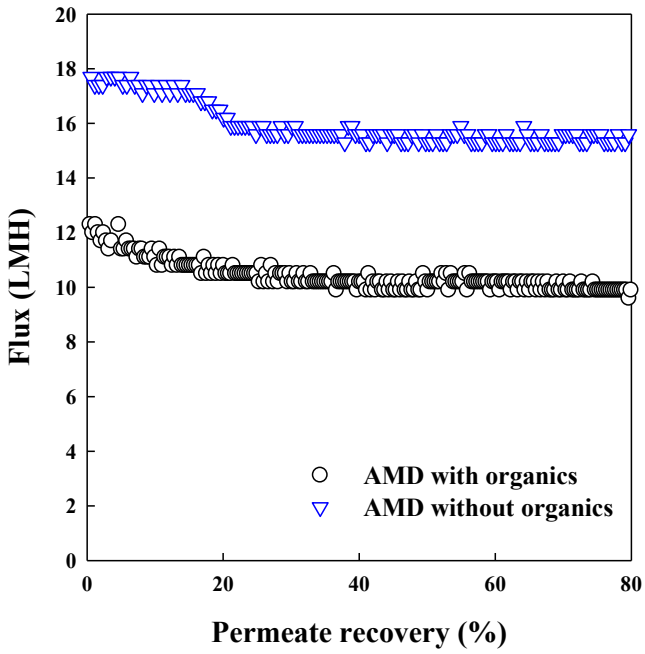

Figure 6.6: Permeate flux for AMD with organics and AMD without organics

The reduction in permeate flux can be attributed to the presence of organic matter which increased pore blocking due to membrane fouling. According to Jamil et al. (2021), NF90 has a contact angle of 79° making it weakly hydrophilic. Studies also found that NF90 is one of the roughest (63 nm) measured using the atomic force microscopic measurement (Xu et al., 2005; Jamil et al., 2021). The rough surface promotes higher deposition of organic matter on the membrane leading to more severe flux decline. Therefore, identifying a cost-effective method to remove organic matter prior to the NF process can significantly increase permeate flux and reduce operation time.

6.9 Adsorption of organic matter using powdered eggshell

Coagulation (Callegari et al., 2017), adsorption using activated carbon (Korotta-Gamage & Sathasivan, 2017) and Ultra Filtration (UF) (Brehant et al., 2002) were conventional methods explored for OM removal prior to NF. Coagulation requires the addition of reagents which could increase cost while there is a risk of valuable metals settling out with flocs. Utilizing an UF system could result in higher operational and maintenance costs, while activated carbon has a high affinity to heavy metals which hinders selective recovery of valuable metals (Zhao and Yu, 2015).

Powdered eggshell, which can be easily sourced, was analysed as a low-cost adsorbent for removal of organic matter from synthetic AMD. According to Zulfikar et al. (2013), powdered eggshell has a crystalline structure with a similar morphology to calcite. The point of zero zeta potential for eggshell was found at pH 8.7 ± 0.2, where surface charge becomes positive in acidic conditions (Labidi, 2008). It was also found that close to 50% (initial concentration of 238 mg/l) of organic matter from a solution can be removed in less than 15 min using powdered eggshell (5g mixed in 50 ml solution). The high initial removal rate is attributed to abundant free sites available for uptake of organic matters. Egg shell reaches equilibrium in about 60 min of contact time (Zulfikar et al., 2013). This contact time was used in our experiment. In their research, Zulfikar et al. (2013) discovered that highest organic removal was recorded at pH 2, which is a similar pH value to synthetic AMD used in our experiment. Here, powdered eggshell could be used without adding chemical reagents for pH correction.

Varying quantities of powdered eggshell were added to 50 ml of AMD solution with organics to assess the removal efficiency and optimum dosage. Adsorbent dosage ranging

from 0.1 g/L to 1.6 g/L were used in this experiment to identify the optimum dosage to increase removal of organics with minimum loss of REE and Cu. Figure 6.7 shows that an eggshell dosage of 0.2 g/L was optimum. Eggshell adsorbed all organics present in AMD while the loss of REE was relatively minimal. It was discovered that adsorption of REE and Ca leaching significantly increased at higher eggshell doses. The increase in the Ca concentration in AMD was due to eggshell leaching where calcite is rapidly dissolved under acidic conditions. Furthermore, eggshell adsorbed Fe in the solution as illustrated in Figure 6.7. Consequently, it was very evident that eggshell treatment managed to remove two membrane fouling agents (Fe & dissolved OM) without affecting concentrations of targeted valuable metals.

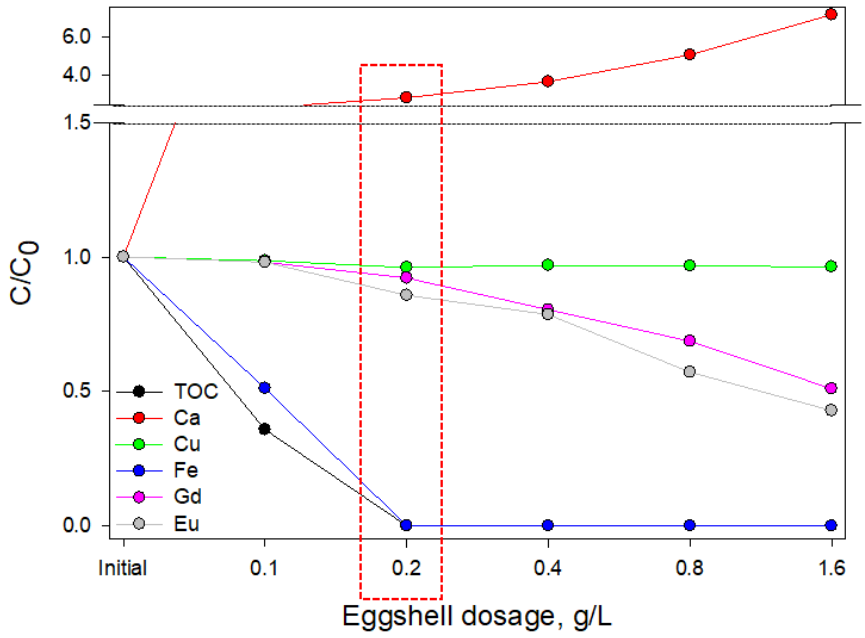

Figure 6.7: Adsorption of TOC and dissolved metals onto eggshell (Contact time: 1 hr)

6.10 Influence of pH on adsorption

Adsorption capacity is highly influenced by the pH of the solution. According to Lee et al. (2018), REE forms coordinated bonding between deprotonated phosphonic, carboxyl, carbonyl and ammine groups on the adsorbent surface. Highly acidic conditions would therefore protonate functional groups in the adsorbent resulting in the formation of repulsive force with trivalent REE ions. Subsequently, high pH values are favoured for enhanced binding capacity. Ashour et al. (2017) state that REE can form electrostatic bonds with $–NH_2$-OH^- functional groups at high pH conditions. At pH>7 REE are found to form insoluble $REE(OH)_3$ (Hatanaka et al., 2017). Lee et al. (2018) showed that optimum Gd^{3+} adsorption on Cr-MIL-PMIDA was achieved at pH 5–5.5. Zeta potential analysis conducted on Cr-MIL-PMIDA also shows that negative charges on the surface significantly increase at pH >5 (Lee et al., 2018). Prior studies conducted on Cu adsorption onto mesoporous silica found that pH>4 should be maintained to avoid protonation of amine ligands (Shahbazi et al., 2013). In their work, Ryu et al. (2019) found that solution pH in the 5.0–5.5 range yielded the maximum adsorption capacity for Cu uptake onto modified mesoporous silica. Furthermore, the pH of concentrated feed was 2.0 ± 0.3 and it was adjusted to values ranging 2.0 – 7.0 using 1M KOH. The composition of concentrated feed at different pH levels are tabulated in Table 6.5.

High concentrations of heavy metals (Ca, Mg, Zn, Cu, Al) were present in the concentrated feed of this experiment along with REE (predominantly Eu). Prior to adsorption, the pH of concentrated feed was increased to analyse solubility of dissolved

metals. pH correction experiment for concentrated feed was then performed to identify optimum pH at which Al will be fully precipitated while the targeted valuable metals remained dissolved. Ryu et al. (2019) found that the type of alkaline material used for pH correction influenced adsorption capacity. It was reported that using NaOH can reduce adsorption capacity since Na ions which have a small ionic radius and higher electronegativity interact with active sites of the adsorbent, competing with targeted metals (Ryu et al., 2019). Therefore, 1 M KOH was used to raise the solution's pH and the sample was left undisturbed for 2 h to allow precipitates to settle.

Figure 6.8 shows Fe and Al were completely precipitated at pH 5, while 70% of REE and Cu still remained dissolved. At pH 6, the majority of REE had precipitated which made recovery inefficient. Therefore, pH 5 appears to be the optimum condition for concentrated feed where a majority of targeted metals remain dissolved while all competing trivalent cations are precipitated. The study conducted by Balintova and Petrilakova. (2011) found that 97% of Fe is precipitated at pH 4, while 93% of Al is precipitated at pH 5. Furthermore, the study conducted by Ryu et al. (2020) reported both Fe and Al completely precipitates at pH >5 due to the two metals' low solubility limits. The finding is beneficial as Fe and Al were found to reduce selective adsorption capacities of both SBA15 and Cr-MIL-PMIDA (Lee et al., 2018; Ryu et al., 2019). Hence, pH 5.0 was determined as the best for valuable metal recovery and it coincides with optimum pH required for the adsorbents for maximum uptake.

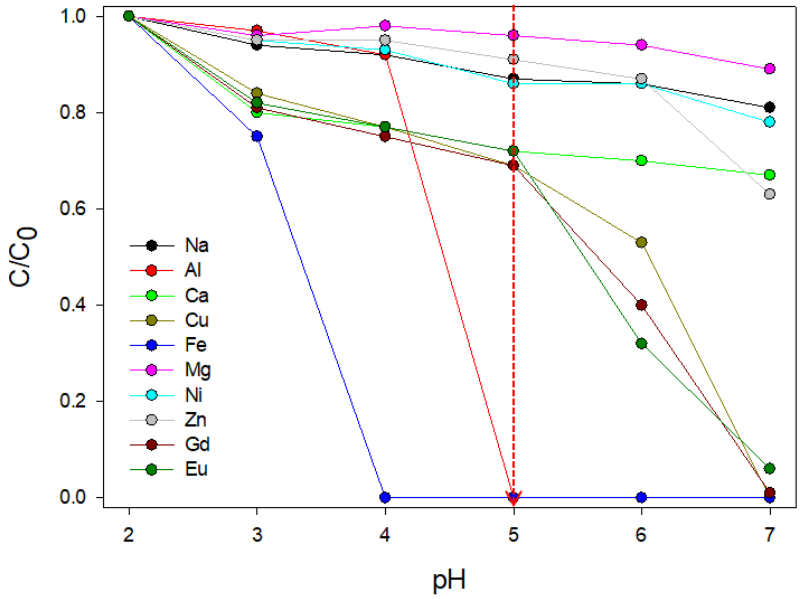

Figure 6.8: Precipitation of metal ions with increase in solution pH

Table 6.5: Composition of pH adjusted concentrated NF feed

	C_i (mg/l)	C_f/C_i				
	pH 2	pH 3	pH 4	pH 5	pH 6	pH 7
Na	283.87	0.9	0.9	0.9	0.9	0.8
Al	283.13	1.0	0.9	0.0	0.0	0.0
Ca	1157.06	0.8	0.8	0.7	0.7	0.7
Cu	392.24	0.8	0.8	0.7	0.5	0.0
Fe	0.40	0.8	0.0	0.0	0.0	0.0
Mg	1088.44	1.0	1.0	1.0	0.9	0.9
Ni	28.63	1.0	0.9	0.9	0.9	0.8
Zn	397.65	1.0	0.9	0.9	0.9	0.6
Gd	2.06	0.8	0.7	0.7	0.4	0.0
Eu	0.39	0.8	0.8	0.7	0.3	0.1

6.11 Selective Adsorption Studies

6.11.1 Selective adsorption of REE

The practical application of selectively recovering REE with Cr-MIL-PMIDA from pH adjusted concentrated feed was evaluated. 50 ml of pH adjusted solution was mixed with different Cr-MIL-PMIDA doses to identify the optimum adsorbent dose to selectively recover REE. Results from the experiment reveal that an adsorbent dosage of 3.2 g/L yields the best outcomes for selective recovery of REE (Figure 6.9). At 6.4 g/L dosage the uptake of REE increased slightly, yet the uptake of Cu and Zn also increased more than 10%. This is attributed to the increased number of free sites present due to high adsorbent dosage. Also, Cr-MIL-PMIDA has residual or unreacted amine groups on its surface which is a beneficial functional group for Cu and Zn uptake (Ryu et al., 2019; Ryu et al., 2021). Cr-MIL-PMIDA was also able to maintain significantly high REE uptake with very minimal Ca and Mg uptake, in spite of the high concentration of these elements over REE in the solution.

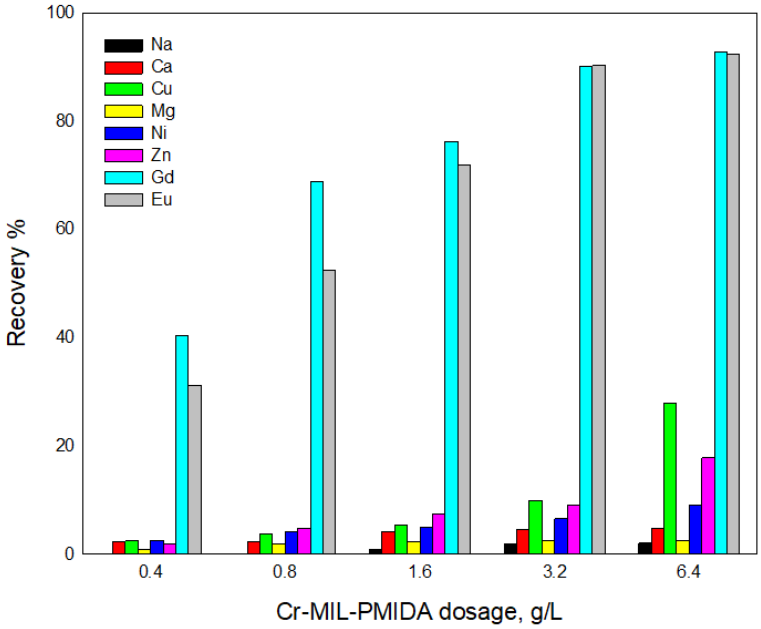

Figure 6.9: Selective recovery of REE from pH adjusted concentrated NF feed (pH 5)

Similar high selectivity of REE over other transition metals were reported in recent research (Callura et al., 2018; Yang et al., 2020; Zhao et al., 2020). Most of these studies attributed selective recovery of REE to the functional group of the adsorbent, such as phosphonic, carboxyl and carbonyl groups. These functional groups are categorized into hard base groups and therefore, tend to exhibit high selectivity towards hard acidic groups such as REE over competing ions. Specifically, the synergistic effect created by the presence of different donor species in the same ligand, such as is the case with PMIDA, creates high selectivity towards REE in a multi-component solution (Reddy et al., 1999). It is also worth noting that a recent study conducted by Ryu et al. (2019) found that Cu demonstrates high chelating effect with amine groups on the adsorbent which results in high Cu adsorption. The low Cu uptake recorded in this experiment confirms the presence

of a relatively low number of amine groups on the adsorbent, which can be attributed to successful reaction between the amine and PMIDA groups during the co-synthesis process. Furthermore, heavy trivalent REE such as Eu display a tendency for higher recovery due to favorable binding with active sites on the adsorbent surface compared to lower valent cations ((Zhao et al., 2017). This may explain the reason for the significantly higher recovery of Gd and Eu as it favorably binds with active sites on the adsorbent surface compared to divalent cations with lower molecular weight such as Ca, Mg, Cu, Mn, and Zn.

Solvent extraction using organophosphorus acids is a widely used method to separate rare earth elements. A study conducted by Vera & Braga. (2019) successfully used 2-ethylhexyl phosphonic acid mono-2-ethylhexyl ester (P507) to separate Gd and Eu from chloride media. Another study by S.-C. Li et al. (2018) found that combination of photochemical reduction and extraction chromatography can be successfully used to separate Gd and Eu with high purity.

6.11.2 Selective Adsorption of Cu

The residual solution post-Cr-MIL-PMIDA adsorption was used in the experiment for Cu recovery. The experiment was conducted at pH 5.2 which was earlier identified as the optimum pH for selective Cu uptake. Varying dosages of SBA15-NH_2 were mixed with 50 ml of the solution and the residual metal concentration was measured to determine the removal percentage. Figure 6.10 shows Cu removal at more than 90% was recorded for adsorbent dosage above 3.2 g/L where the removal of other metals remained below 10%. At dosages of 6.4 g/L and beyond, Zn uptake on to SBA15 significantly increased. Hence

SBA15-NH_2 dosage of 3.2 g/L was used. Previous studies show that Cu, Ni and Zn do not show any significant difference in chemical properties (Ryu et al., 2019). The ionic radius of all three metals was between 0.69 Å to 0.74 Å (Ryu et al., 2019).

Furthermore, all three metals have similar valence, and they appear next to each other in the periodic table. The absolute electro-negativity with amine groups for Cu and Zn was also found to be similar, i.e. 28.6 and 28.8, respectively (Liu et al., 2008). Ryu et al. (2019) go on to mention that theoretically Zn should have higher affinity towards ammine ligands because of its higher absolute hardness compared to Cu. Yet the high selectivity towards Cu in the presence of Zn in this experiment demonstrates that ion characteristics are not the dominant force in competitive adsorption.

High affinity of Cu towards ammine ligands can also be due to the formation of coordination complexes. Koong et al. (2013) mention that Cu forms strong chelating bonds with amine groups. Other studies also confirm that ammine ligands form strong coordination complexes that enable high selectivity (Aguado et al., 2009; Sierra and Pérez-Quintanilla, 2013). This further confirms that the formation of strong chelating bonds with amine ligands on SBA15 makes possible high selective recovery of Cu from competing metals.

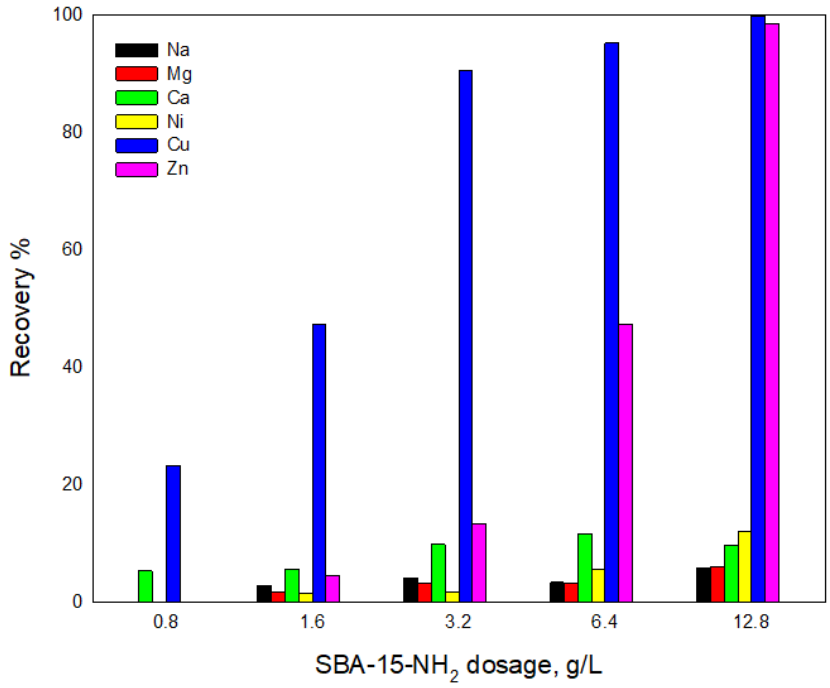

Figure 6.10: Selective recovery of Cu from MOF-treated NF feed

6.12 Re-usability studies

The stability of Cr-MIL-PMIDA and SBA15-NH_2 was analysed over 5 adsorption/desorption cycles. Reusability of adsorbents is critical for practical application of this technology in industry. 0.01 M HCl solution served as the stripping agent for both adsorbents. Alkaline regeneration was used for SBA15-NH_2 to deprotonate ammine groups prior to subsequent application (Ryu et al., 2019). At pH below 3, protonation of ammine and phosphonic ligands occur which creates a repulsive force with positively charged REE and Cu ions (Ryu et al., 2019; Ryu et al., 2021). This desorbs adsorbed metals onto the acidic solution. It has been reported that SBA15-NH_2 should be washed with NaOH to neutralize ammine charge (Ryu et al., 2019). Over 5 cycles, both Cr-MIL-

PMIDA and SBA15-NH_2 retained over 95% of its initial adsorption capacity (Figure 6.11). This confirms the high structural stability of these adsorbents after repetitive use.

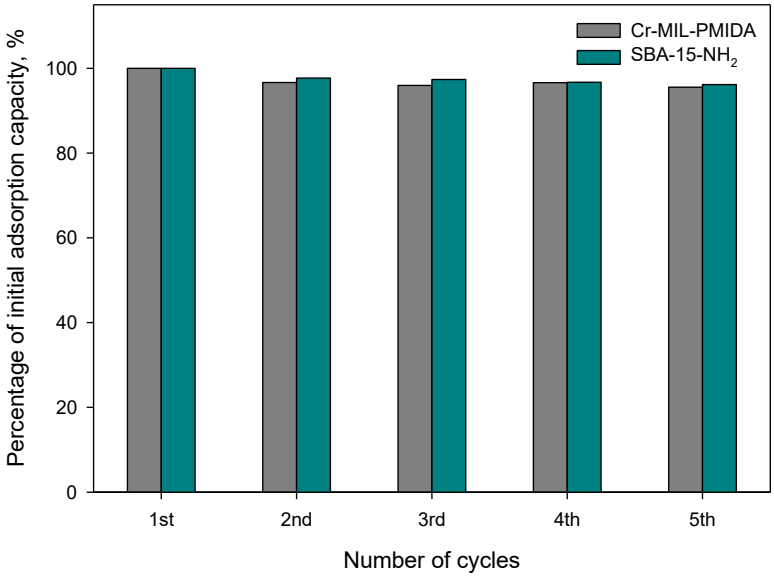

Figure 6.11: Cyclic adsorption tests for REE and Cu recovery at initial concentration of 5 mg/l at pH 5.5

Table 6.6 shows that 0.06 mg, 0.015 mg and 10.24 mg of Gd, Eu and Cu can be recovered, respectively, by processing 1L of AMD using this treatment process. This enables financially viable and sustainable treatment of AMD approaching zero liquid discharge.

Table 6.6: Mass Balance for recovery of Valuable metals

(for AMD characteristics listed in table 6.1)

		Concentration (mg/l)		
Treatment Step	**Volume (L)**	**Gd**	**Eu**	**Cu**
Initial Concentration in Synthetic AMD	1	0.51	0.14	107.48
After Egg Shell Treatment	1	0.459	0.126	104.26
After NF process (Concentrated Feed)	0.2	2.29	0.611	516.06
After pH adjustment	0.2	1.6	0.428	361.24
After 5 cycles of Adsorption/Desorption (As reported by Fonseka et al. (2021))	0.2	0.32	0.077	51.215
Amount of Metals recovered by 1 L of AMD (mg)		0.064 (13.9% recovery)	0.0154 (12.6% recovery)	10.243 (9.9% recovery)

Discharge of untreated AMD has become a global environment concern. The sustainable approach to resolve this issue is through active industry participation. The study demonstrates that combining low pressure NF and adsorption for AMD treatment not only enables recovery of clean water for industrial operations, it also creates additional income through recycling of valuable metals which can offset at minimum a portion of treatment costs. Since lab-scale experiments using 1L volumes indicate promising results for valuable metal recovery, the next logical step is to scale up the process to pilot scale to validate and optimize the recovery process under conditions more representative of practical applications.

6.13 Summary

Low pressure nanofiltration with commercially available NF90 membrane was first studied to recover fresh water from synthetic AMD and concentration of dissolved metals for subsequent efficient selective recovery. Subsequently, Cr-MIL-PMIDA and an amine-grafted mesoporous silica (SBA15) material was synthesized for selective recovery of REE and Cu, from the concentrated feed solution.

- A steady permeate flux of 15.5 ± 0.2 L/m^{2}h (LMH) was achieved for pre-treated AMD with a solute rejection rate of more than 98%.
- The two adsorbents were used sequentially to selectively adsorb REE (91%) and Cu (90%) from pH adjusted concentrated feed.
- The formation of coordinating complexes with carboxylate and phosphonic groups on MOF was found to be the primary driving force for selective REE adsorption. Selective uptake of Cu onto amine-grafted SBA15 was due to the formation of strong chelating bonds between Cu and amine ligands.
- Both adsorbents remained structurally stable over 5 regeneration cycles.
- The findings here highlight the practical potential of membrane/adsorption hybrid systems for water and valuable metal (REE) recovery from AMD.

Chromium-based Metal-Organic Frameworks (MOFs) have shown promising properties for selective REE adsorption, but their suitability for industrial use is limited due to two main factors: high production cost and environmental concerns related to chromium leaching. In response to these issues, researchers and industries have been exploring

alternative MOF materials that offer similar or improved performance without the drawbacks associated with chromium-based MOFs. Next chapter of this thesis evaluates the performance of a novel, mesoporous silica based adsorbent for selective REE removal from mining wastewater.

CHAPTER 7

SELECTIVE RECOVERY OF EUROPIUM FROM REAL ACID MINE DRAINAGE BY USING NOVEL SBA15-NH-PMIDA ADSORBENT

*This chapter is based on the following journal publication

Fonseka, C.; Ryu, S.; Choo, Y.; Naidu, G.; Foseid, L.; Thiruvenkatachari, R.; Kandasamy, J.; Ratnaweera, H.; Vigneswaran, S. Selective Recovery of Europium from real acid mine drainage by using novel SBA15-NH-PMIDA adsorbent and membrane distillation system. *Journal of Water Process Engineering, 56, 104551.* doi:https://doi.org/10.1016/j.jwpe.2023.104551

7 Introduction

Increasing demand for high-tech products, clean energy technologies, and defense applications has elevated the importance of rare earth elements (REEs) in the global market. As countries aim to secure stable and sustainable access to these critical elements, research and development in mining, processing, recycling, and diversification of supply sources continue to be areas of interest and investment. Among REEs, Europium (Eu) is considered to be the most expensive and the rarest, accounting for only 0.1 % w/w in monazite and bastnaesite ores (Kumari et al., 2019). This has resulted in Europium being mined only as a byproduct due to financial constraints. Europium is widely used in the production of phosphors, alloys, additives and is a critical raw material for development of smart devices from high-resolution color screens to its circuitry (Wang et al., 2020). Furthermore, Europium oxide is widely used in control rods as neutron absorber in fast breeder nuclear power plants.

Chemical precipitation (Li et al., 2013), solvent extraction (Seyyed Alizadeh Ganji et al., 2016), ion exchange (Khawassek et al., 2019), adsorption (Fonseka et al., 2021), and membrane filtration (Murthy & Choudhary, 2011) are some of the widely researched technologies for REE recovery. While these technologies offer distinct advantages, they also present their unique challenges, such as high cost of solvents, matrix interferences, membrane pore blocking and the need for residue waste management. Therefore, adsorption is considered to be the most promising due to high efficiency and low cost (Callura et al., 2018).

However, majority of traditional adsorbents show limited selectiveness towards REE recovery (Zhao et al., 2020). Hence, modification with favorable functional groups is necessary to increase performance. In this regard, metal-organic framework (MOF) materials functionalized with specific ligands have shown high affinity towards REEs (Abdel-Magied et al., 2019; Fonseka et al., 2021; Zhao et al., 2020). Specifically, functionalized chromium based MOF selectively recovered Eu from zinc ore leachate due to the formation of strong chelating complexes with phosphonic and carboxylate ligands (Fonseka et al., 2021; Lee et al., 2018). However, high cost of production, coupled with concerns over long-term stability hinders industrial scale application of these promising materials. Mesoporous silica materials, such as SBA15 (Santa Barbara Amorphous-15), offer excellent tunability and modification capabilities, making them an attractive, low cost alternative (Rivas-Sanchez et al., 2022). Hence, there is considerable potential for incorporating ligands with high affinity towards REEs into SBA15 to enhance selectivity and efficiency.

The main objectives of this study was to study the performance of a novel, functionalized SBA15-NH-PMIDA material for selective Eu recovery. N-(phosphonomethyl) iminodiacetic acid (PMIDA) ligand was selected for modification due to high affinity towards REE reported in previous studies (Fonseka et al., 2021; Lee et al., 2018). First, detailed adsorption studies for removal of REE were carried out using single solute synthetic Eu solutions at different pH values to find optimum conditions. Real AMD samples collected from an abandoned mining site in northern Norway was then used for selective adsorption tests. Detailed physical and chemical characterization of SBA15-NH-PMIDA were performed to determine the selective adsorption mechanisms.

7.1 Adsorption studies

7.1.1 Equilibrium

Adsorption experiments for Europium (Eu) recovery on powdered SBA15-NH-PMIDA (0.01 g) and granulated SBA15-NH-PMIDA (0.012 g) were carried out using beakers containing 50 ml Eu solutions at optimum pH found in the previous experiment. Equilibrium adsorption experiments were carried out with 5 mg/l single-solute synthetic Eu solutions. This allows for a clearer understanding of the interaction between SBA15-NH-PMIDA and Eu ions without the interference contaminants present in complex mixtures. The beakers were kept on a flat shaker at room temperature (24 ± 1 °C) for 24 h. Initial concentrations were limited to 2.5 mg/l -30 mg/l for this experiment, considering low concentrations of Eu reported in acid mine drainage (Olias et al., 2018). Initial and equilibrium concentrations of Eu were measured using Inductively Coupled Plasma Mass Spectrometry (ICP-MS, Agilent 7900, US).

7.1.2 Kinetics

Mass transfer mechanisms and the rate of adsorption were evaluated through kinetic experiments. 0.01 g of powdered and granulated SBA15-NH-PMIDA was mixed with with 50 ml of 10 and 20 mg/l single-solute synthetic Eu solutions at optimum pH. The beakers placed on a flat shaker at room temperature (24 ± 1 ℃) and agitated for 24h. Samples were collected at various time intervals up to 24 hours, and residual Eu concentrations were measured using ICP-MS.

Surface diffusion model (SDM) was also used to further analyse adsorption mechanism (Suzuki & Suzuki, 1990). According to Inglezakis et al. (2019), adsorption from liquid

phase onto a porous solid occur in three steps which are 1) diffusion from fluid to external surface of adsorbent (film diffusion), 2) mass transfer from external surface to the solid phase (Intraparticle diffusion) and finally 3) physical/chemical bonding with active sites. Since pseudo models neglect film diffusion and Intraparticle diffusion, surface diffusion model is considered to be a realistic method to predict adsorption kinetics (Souza et al., 2017). In this study, PDEPE function on Matlab was used to solve the SDM equation.

Equation for surface diffusion model are given below.

Surface Diffusion Model (SDM): $$\frac{\partial q}{\partial t} = \frac{1}{r^2}\frac{\partial}{\partial r}(r^2 D_s \frac{\partial q}{\partial r}) \quad (7\text{-}1)$$

Boundary conditions:

$$K_f(C - C_s) = D_s \rho_p \frac{\partial q}{\partial r} \quad at \quad r = R_p \quad (7\text{-}2)$$

$$\frac{\partial q}{\partial r} = 0 \quad at \quad r = 0 \quad (7\text{-}3)$$

Where

D_s: effective surface diffusion coefficient (m^2/s) r: radial distance of the spherical particle (m)

C_s : concentration of Eu at the surface of adsorbent (mg/l)

7.1.3 Recovery of Eu from real AMD

Solubility of dissolved metals in real AMD at varying pH values:

Acid mine drainage samples from an abandoned mining site in northern Norway was collected for this study. AMD samples were characterized to determine the initial metal concentrations and pH levels. Then, pH of the solution was adjusted using 0.01M NaOH to find optimum conditions for subsequent selective adsorption process. Chemical composition of the original and pH adjusted samples were analysed using Inductively Coupled Plasma Mass Spectrometry (ICP-MS, Agilent 7900, US). Analysing solubility of dissolved metals in real AMD with pH adjustment is critical for achieving selective Eu recovery. Results from this study will be critical to understand the pH-dependent speciation, optimize recovery conditions, and design effective separation and purification strategies for Eu.

Selective adsorption study:

Based on the optimum pH conditions identified in the previous study, selective adsorption studies were conducted using pre determined quantities of powdered SBA-NH_2-PMIDA. The objective of this experiment was to find the optimum dosage to maximize Eu recovery while minimizing the uptake of other dissolved metals. Experiments were carried out using 50 ml beakers containing ph adjusted real AMD. Samples were agitated on flat shaker at room temperature (24 ± 1°C) for 24 h to provide sufficient time for the adsorption process to reach equilibrium, ensuring accurate and consistent results. pH and temperature of the samples were measured using a multimeter (HQ40d, HACH, USA)

and Inductively coupled plasma-mass spectrometry (ICP-MS, Agilent 7900, USA) was used to determine the cation concentrations before and after adsorption.

Further selective adsorption experiments were conducted using binary synthetic solutions to understand specific capacity of SBA15-NH-PMIDA for selective Eu recovery in the presence of individual tri-valant (Fe, AL) and di-valant (Zn, Cu) metal ions. In each binary solution, similar concertations of Eu and other metals found in real AMD were kept to the same values as found in real AMD was maintained. All samples were agitated for 24h at room temperature (24 ± 1°C). Concentrations of metals before and after adsorption were analysed using ICP-MS

7.2 Results and discussion

7.2.1 Characterization of adsorbents

Crystal structure:

XRD patterns of pristine SBA15-NH2, pristine SBA15-NH-PMIDA and spent SBA15-NH_2-PMID were analysed. The XRD pattern (Figure 7.1) of SBA15-NH_2 shows two clear peaks at (1 0 0) and (2 0 0), which corresponds to the hexagonal structure of mesoporous silica (Kim et al., 2015). The peak at (1 0 0) decreased for SBA15-NH-PMIDA, which is a sign of reduction in the mesoscopic order of the structure (Aguado et al., 2009). This may be due to the pore reduction caused by grafted phosphonic groups. XRD pattern of spent SBA15-NH-PMIDA remained similar to that of the fresh adsorbent. This suggests that the hexagonal structure remained unchanged during adsorption, which is beneficial for repetitive adsorption/desorption.

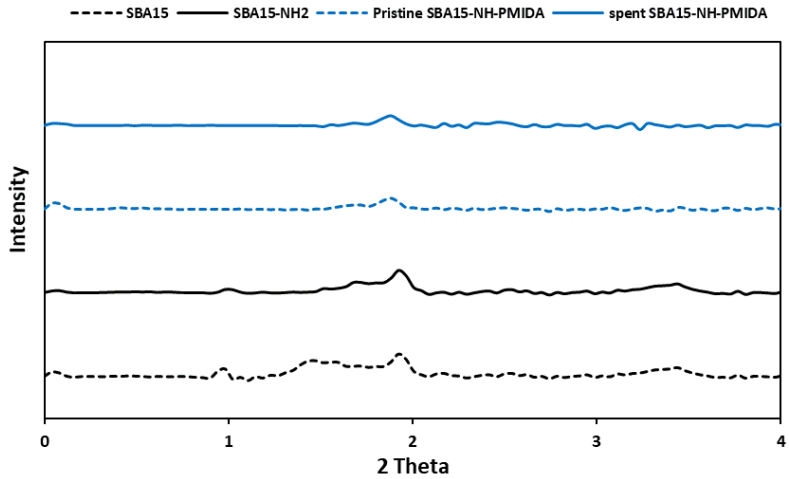

Figure 7.1: XRD patterns of pristine SBA15, pristine SBA15-NH_2, pristine SBA15-NH-PMIDA and spent SBA15-NH-PMIDA

Chemical properties (FTIR):

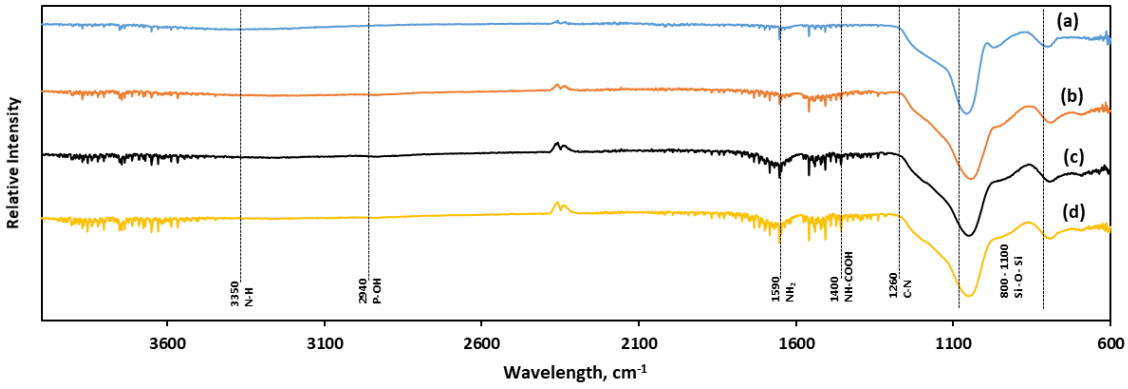

Figure 7.2: FTIR spectrums of a) SBA15, b) SBA15- NH_2, c) SBA15-NH-PMIDA before adsorption and d) SBA15-NH-PMIDA after adsorption

FTIR analysis (Figure 7.2) was carried out to investigate the chemical properties of SBA15 and its modifications. The observed peaks at 1080 and 800 cm^{-1} signify the

presence of Si–O–Si bonds, which are characteristic constituents of SBA15 material. The presence of these peaks in both the virgin and modified SBA15 samples confirms that the structure of SBA15 remained intact and undamaged after the two modification processes (Ryu et al., 2019; Wang et al., 2015). The reduction in the peak at 970 cm^{-1} suggests that a reaction has occurred between silica and hydroxyl groups, as reported by Ali et al. (Ali et al., 2023). This implies the successful amine modification of SBA-15, as evidenced by the reaction between NH2 and Si–OH (Nie et al., 2020). Peaks at 2900 and 1400 cm^{-1} in the curves corresponding to SBA15-NH-PMIDA indicates the presence of P–OH and NH-COOH vibrations respectively. This confirms that PMIDA reacted successfully with the amine groups and were successfully grafted onto the surface of SBA15. Further analysis on adsorption mechanisms using FTIR analysis have been discussed in subsequent sections.

Surface area and pore size distribution:

BET surface area and BJH pore size distribution analysis of pristine SBA15, SBA15-NH2 and SBA15-NH-PMIDA were carried out to determine physical properties. According to Table 7.1, pristine SBA15 recorded a BET surface area of 826 m^2/g, which reduced to 113 m^2/g after modification. This can be due to pore blocking as a result of amine and PMIDA functional groups grafted onto the surface of SBA15. Similar findings were reported by ryu et al. (2019), where BET surface area reduced from 830 m^2/g to 310 m^2/g after amine grafting. Isotherm graph of N_2 adsorption/desorption at 77 K for SBA15-NH-PMIDA is presented in figure 7.3a and the clear hysteresis implies the adsorption on mesopores of the material (Dolatyari et al., 2016; Moritz & Łaniecki, 2012)

Table 7.1: Physical properties of adsorbents

Adsorbent	BET Surface Area ($m^2.g^{-1}$)	Pore Volume ($cm^3.g^{-1}$)	Mean Pore Diameter (nm)
Pristine SBA15	826	1.27	6.16
SBA15- NH_2	330	0.78	9.45
SBA15-NH- PMIDA	113	0.26	9.16
Cr-MIL-PMIDA	1049.4	0.69	2.15

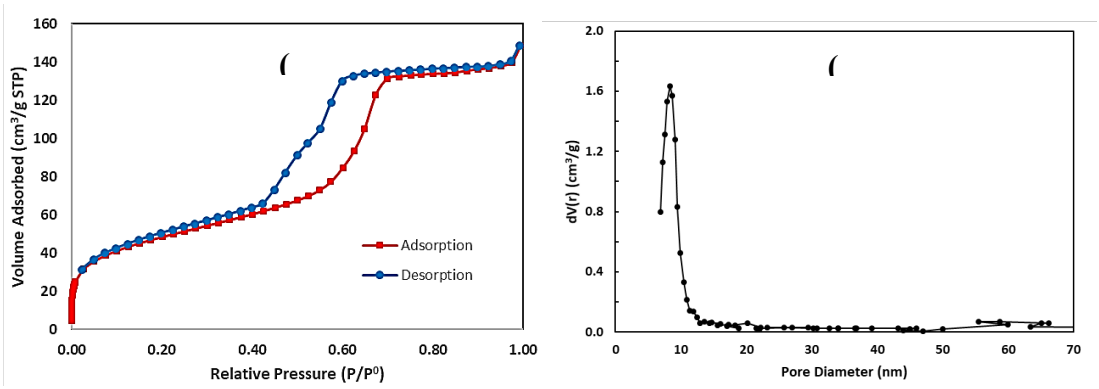

Figure 7.3: (a) N adsorption and desorption isotherm and (b) pore size distribution of SBA15-PMIDA

Pore size distribution graph of SBA15-NH-PMIDA exhibits a prominent peak in the pore diameter range of 7-8 nm (Figure 7.3b). Study conducted by Ryu et al. (2019) reported that virgin SBA15 showed peaks around 6nm. The slight shift of the peak to the right post modification can be due to partial or complete blocked pores due to functionalization

reactions. This effect can reduce the number of smaller pores and increase the proportion of larger pores, resulting in a shift of the peak towards larger sizes (Shi et al., 2023). This outcome explains that amine groups and PMIDA ligands were grafted well on the pores of SBA15 structure.

SEM and EDS analysis:

Scanning Electron Microscopy (SEM) and Energy-Dispersive X-ray Spectroscopy (EDS) analyses were conducted on pristine SBA15-NH-PMIDA to observe surface morphology, elemental composition, and structural characteristics. SEM images (Figure 7.4a) exhibit the well-ordered , 2D hexagonal structured array of the mesoporous material. The spheres observed are likely to be the particles or aggregates of the mesoporous silica material itself (Ijaz et al., 2020). Results indicated that the modified adsorbents were able to maintain well-ordered structure as that of the virgin SBA-15, as previously reported by Ryu et al. (2019). EDS chart of pristine SBA15-NH-PMIDA (Figure 7.4b) confirms the presence of phosphorous, carbon and oxygen with distinct peaks at respective energy bands. This further confirms successful reaction between amine ligands and PMIDA during synthesis.

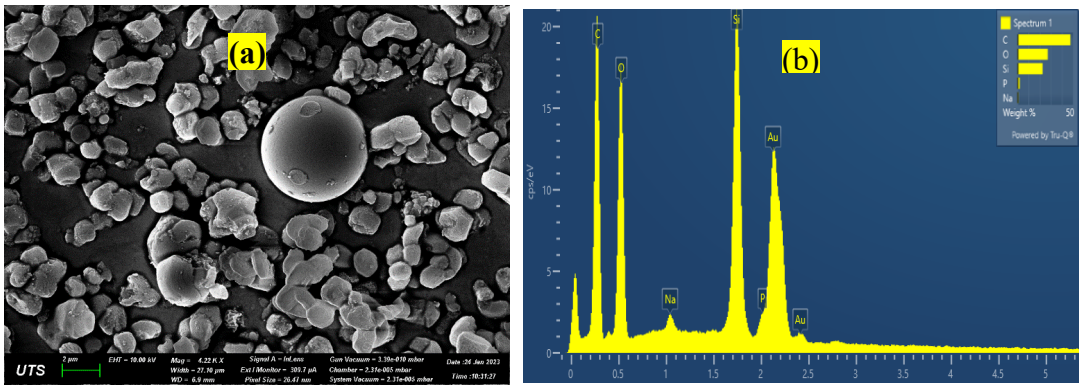

Figure 7.4: (a) SEM image and (b) EDS chart of pristine SBA15-NH-PMIDA

7.3 Influence of pH

7.3.1 Influence of pH and surface charge on Eu uptake by SBA15-PMIDA

The pH of the solution dictates the surface condition of adsorbent and adsorbate in an aqueous media (Iftekhar et al., 2018). The effect of pH on Eu recovery by SBA15-PMIDA was investigated within the pH range of 2 to 6 using single-solute synthetic Eu solutions. Higher pH values were avoided since REEs tend to form insoluble $REE(OH)_3$ species above pH 6, which would hinder the adsorption process.(Abdel Maksoud et al., 2022; Hatanaka et al., 2017; Zhang & Honaker, 2018).

The results revealed a significant correlation between Eu recovery on SBA15-NH-PMIDA and the solution pH (Figure 7.5). As pH increased from 2 to 6, Eu recovery showed a notable improvement, rising from 11% to 96%. The maximum Eu recovery was attained at a pH value of approximately 4.75 ± 0.1 (pHeq). The corresponding surface charge (zeta potential) exhibited an increasing trend of negative charge with higher pH values (Fig. 7.5). This observation suggests that the enhanced Eu recovery is likely due to the deprotonation of functional groups on the adsorbent surface. The pH of 4.75 ± 0.1 was identified as the optimum condition for achieving high Eu recovery. This optimum pH value was selected for all subsequent adsorption studies.

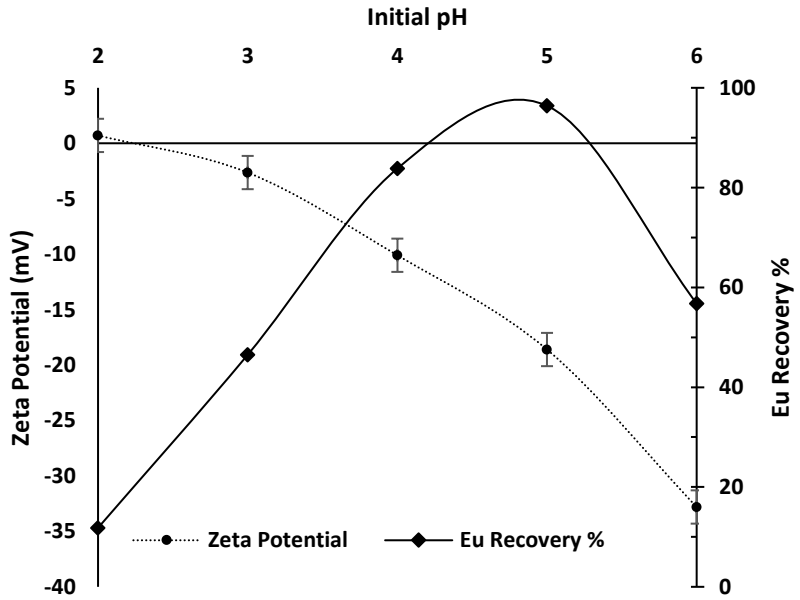

Figure 7.5: Influence of pH on Eu uptake and SBA15-PMIDA surface charge (Initial Eu Concentration: 5 mg/l)

7.4 Adsorption study

7.4.1 Equilibrium experiments

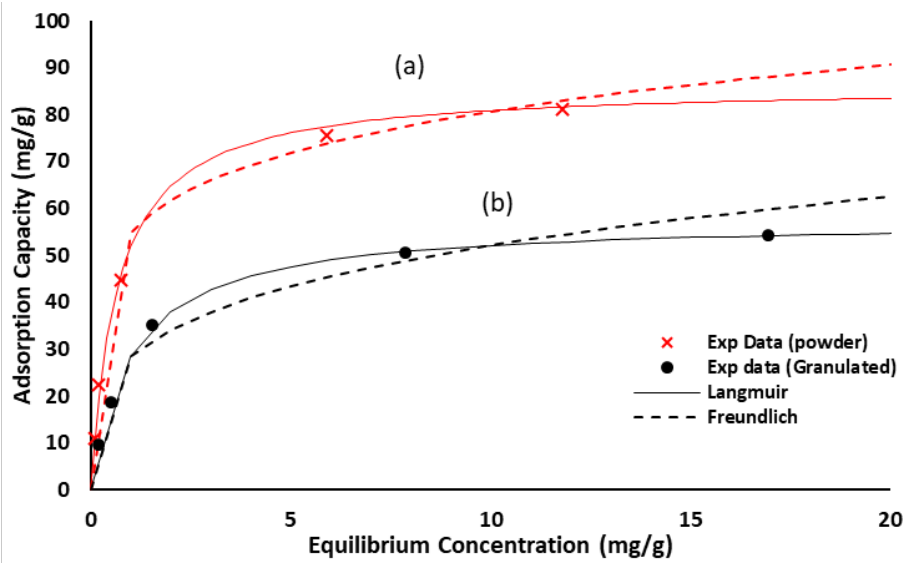

Figure 7.6: Adsorption of Eu on (a) powdered SBA15-NH-PMIDA and (b) granulated SBA15-NH-PMIDA

Table 7.2: Adsorption isotherm parameters

	Langmuir			Freundlich		
	Q_m (mg/g)	b (L/mg)	R^2	K_F (g^{1-n} $L^n g^{-1}$)	n	R^2
Powder	86.21	1.51	0.99	54.90	5.98	0.96
Granulated	57.47	0.97	0.99	28.40	3.80	0.93

Adsorption experiments were conducted with powdered and granulated SBA15-NH-PMIDA at room temperature (25 ± 1 °C) and corresponding isotherms were plotted for

initial Eu concentrations ranging from 2.5 mg/l to 30 mg/l at an optimum pH 4.75 ± 0.1 (Figure 7.6). Adsorption data showed good fit to both Langmuir and Freundlich models high R^2 values (Table 7.2). Hence, the adsorption process exhibit characteristics of both monolayer adsorption and multilayer adsorption with interactions between adsorbed Eu molecules. The Langmuir isotherm assumes a monolayer adsorption mechanism, while the Freundlich isotherm allows for multilayer adsorption and considers the adsorption intensity (Kalam et al., 2021). The maximum Langmuir adsorption capacity (Q_m) for powdered SBA15-NH-PMIDA was calculated to be 86.21 mg/g which is a significant improvement compared to previous studies on REE adsorption (Fonseka et al., 2021; Ryu et al., 2021). Study conducted by Fonseka et al. (Fonseka et al., 2021) reported that Cr-MIL-PMIDA maximum adsorption capacity of 69.21 mg/g. SBA15 is a mesoporous silica material with a well-defined pore structure, providing a large surface area and accessible pore volume for adsorption (Ryu et al., 2019). N-(phosphonomethyl) iminodiacetic acid (PMIDA) is a ligand that can form complexation or coordination interactions with REE ions (Fonseka et al., 2021; Lee et al., 2018). Therefore, the functionalization of SBA15 with PMIDA offer favourable conditions for Eu adsorption.

7.4.2 Kinetics experiments

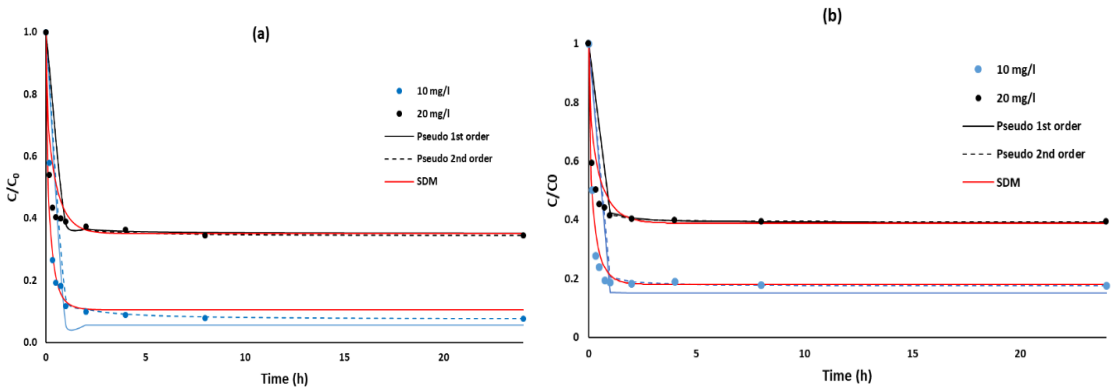

Figure 7.7: Pseudo 1st order and Pseudo 2nd order Eu adsorption kinetic graphs for a) Powdered SBA15 -NH_2-PMIDA and b) granulated SBA15-NH_2- PMIDA

(Where, C_0 – Initial concentration of Eu, C – Concentration of Eu at time t)

Table 7.3: Adsorption kinetic parameters of powdered SBA15-PMIDA

Adsorbent	Initial Concentration of Eu	Pseudo 1st Order			Pseudo 2nd Order			Surface diffusion model	
		Q_e (mg/g)	k_1(s^{-1})	R^2	Q_e (mg/g)	k_1 (g/mg.s)	R^2	Ks (m/s)	Ds (m^2/s)
Powdered SBA15-PMIDA	10 mg/l	47.45	11.43	0.97	46.51	0.27	0.99	6.50 E-05	4.50 E-17
	20 mg/l	65.11	20.97	0.98	65.79	0.23	0.99		
Granulated SBA15-PMIDA	10 mg/l	35.53	6.10	0.94	34.60	0.70	0.99	5.50 E-05	4.00 E-17
	20 mg/l	50.97	17.68	0.99	50.76	0.43	0.99		

The kinetic studies for both powdered SBA15 PMIDA and granulated SBA15 PMIDA were carried out for Eu(III) adsorption at pH 4.75 ± 0.1, with initial concentrations of 10 mg/l and 20 mg/l (Figure 7.7). For both adsorbents, the equilibrium was reached within 2 h, followed by a stable plateau. The kinetic data were analysed by pseudo-first-order, pseudo-second-order and surface diffusion models. For both materials, experiment data had a better fit to pseudo-second-order model (Table 7.3). Based on the kinetic models and data analysis, it appears that the uptake of Eu ions on SBA15 follows a two-step process. Initially, there is rapid surface adsorption, where Eu ions quickly adhere to the surface of SBA15. This step is likely driven by physical interactions such as electrostatic forces. In the second step, the Eu ions undergo chemisorption onto the functional groups present on the highly porous surface of SBA15. This chemical sorption step is the rate-limiting factor in the overall uptake process, meaning it is the slower step that determines the overall kinetics. The presence of hydroxyl (-OH), carboxyl (-COOH) and phosphonic (-NH2-C-$PO(OH)_2$) groups on the porous surface of SBA15 provides sites for strong chemical interactions with the Eu ions. The surface diffusion model is of great importance in understanding adsorption kinetics. It improves the accuracy of predicting adsorption kinetics compared to simpler models that do not consider surface diffusion. By taking into account the mobility of adsorbate molecules on the surface, the surface diffusion model allows for a more realistic representation of the adsorption process (Putranto & Aziz, 2020). The coefficients K_f and D_s for powdered SBA15-NH-PMIDA from surface diffusion model were calculated to be 6.50 x 10^{-5} m/s and 4.5 x 10^{-17} m^2/s respectively. These values were higher than what was previously reported for powdered Cr-MIL-PMIDA by Fonseka et al. (Fonseka et al., 2021). High film diffusion rates lead to more

rapid delivery of adsorbate molecules to the surface, which can result in faster adsorption kinetics. Meanwhile, high surface diffusivity enables adsorbates to move more freely on the surface, increasing the chances of finding energetically favorable sites for adsorption (Liu et al., 2023).

Moreover, Eu uptake on SBA15-NH-PMIDA occurred at a faster rate compared to conventional adsorbents under similar experimental conditions (Dupont et al., 2014; Elsaidi et al., 2018; B. Hu et al., 2017; Jiang et al., 2016). Fonseka et al.(Fonseka et al., 2021) reported similar rapid equilibrium time for Eu uptake on Cr-MIL-PMIDA. However, Cr-MIL-PMIDA had lower adsorption capacity (69.14mg/g) compared to SBA15-NH-PMIDA (86.21 mg/g). Hence, SBA15-PMIDA can be considered a highly effective and efficient adsorbent for removal of Eu from aqueous solutions.

7.5 Recovery of Eu from real Acid Mine Drainage (AMD)

This study also focused on assessing the practical application of selective Eu recovery from acid mine drainage (AMD) using SBA15-PMIDA. Acid mine drainage from an abandoned mining site in northern Norway was first collected and then analyzed for chemical composition (Table 7.4).

Table 7.4: Chemical composition of AMD (pH = 2.0 ±0.2)

Parameters	Concentration (mg/l)
Na	37

Mg	220
Al	170
S	1300
Ca	190
Cr	0.4
Mn	6.3
Fe	620
Ni	0.53
Cu	65
Zn	41
Eu	3.2

AMD consists of high concentration of Sulphur (in the form of SO_4^{-3}), transition metals and multivalent ions (Fe, Mg, Al, Ca, Cu, Zn) with low pH (2.0 ± 0.1). Rare earth elements were found to be present in low concentrations, with Eu being the predominant, with a concentration of 3.2 mg/l (Table 7.4). Selective recovery of Eu using SBA15-PMIDA can become challenging with high concentrations of trivalent Fe and Al in AMD (Naidu et al., 2019). Hence, careful consideration and optimization of the operating conditions, such as pH adjustment are necessary to overcome these challenges and improve the selectivity towards Eu.

7.5.1 Influence of pH on solubility of dissolved metals in AMD

This experiment was conducted to investigate the effect of pH on the leaching and solubility of metals present in the AMD (Figure 7.8). NaOH, a commonly used alkaline agent in the industry, was utilized to adjust the pH of AMD from 2.0 to 5.0. Dissolved metals at different pH values were measured to obtain optimum conditions. The presence of trivalent Fe and Al in high concentrations can detrimentally affect the selectivity of SBA15-NH-PMIDA towards Eu (Fonseka et al., 2021). Since Fe^{3+} and Al^{3+} have similar ionic properties to Eu^{3+}, they can occupy the functional groups on the adsorbent surface and thereby reduce the adsorption capacity of SBA15-NH-PMIDA specifically for Eu. Since trivalent Fe^{3+} and Al^{3+} ions carry positive charges, similar to Eu^{3+}, electrostatic interactions between positively charged metal ions and the negatively charged functional groups of SBA15-PMIDA can interfere with the selective adsorption of Eu ions, reducing the overall selectivity of the adsorbent. pH of 4.5 – 5.0 favoured maximum precipitation of Fe and Al by more than 99%, while around 38% of Eu remained dissolved (Table 7.5. This phenomenon is attributed to the relatively low solubility limit of Fe and Al at this pH range. (Miranda et al., 2022).

These results confirm that adjusting the pH of AMD to 4.5 – 5.0 was favourable since it precipitated almost all of Fe/Al and it coincides with the optimum pH range for maximum uptake of Eu onto SBA15-NH-PMIDA. Therefore, pH of 4.75 ±0.1 was selected for all selective adsorption experiments.

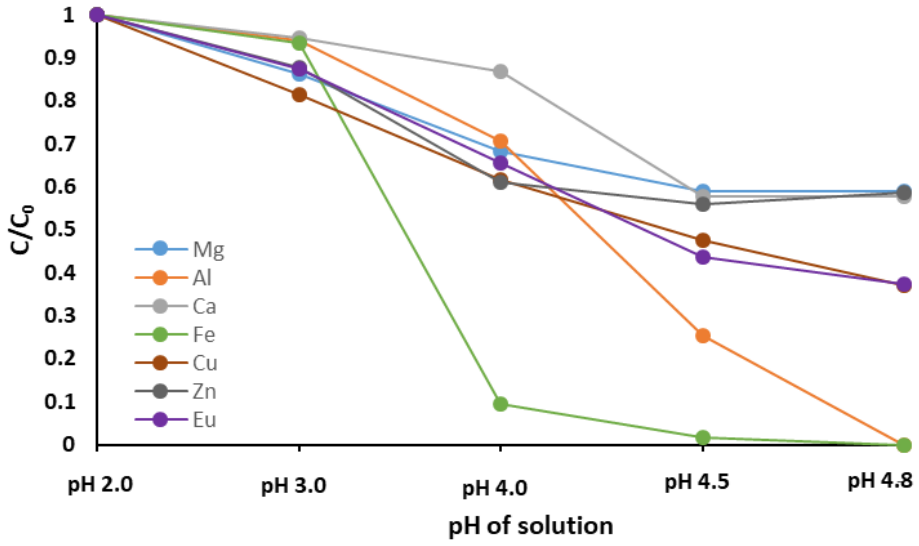

Figure 7.8: Precipitation of dissolved metals in AMD through pH correction

(Where C = Concentration at initial pH, C_0= Concentration at adjusted pH)

Table 7.5: Concentration of dissolved metals in AMD at different pH values (mg/l)

	Initial (pH 2.0)	**pH 3.0**	**pH 4.0**	**pH 4.5**	**pH 4.8**
Mg	220.0 ± 5.0	190.0 ±7.0	150.0 ±5.0	130.0 ±5.0	130.0 ±5.0
Al	170.0 ± 7.0	160.0 ±5.0	120.0 ±5.0	43.0 ±2.0	ND
Ca	190.0 ± 5.0	180.0 ±5.0	165.0 ±5.0	110.0 ±5.0	110.0 ±5.0
Cr	0.4 ± 0.1	0.4 ± 0.1	0.3 ± 0.1	0.1 ± 0.05	ND
Mn	6.3 ± 0.3	5.8 ± 0.5	5.5 ± 0.3	3.5 ± 0.1	3.2 ± 0.1
Fe	620.0 ± 5.0	580.0 ±7.0	58.0 ±5.0	9.7 ±1.0	ND

Ni	0.5 ± 0.1	0.5 ± 0.1	0.5 ±0.1	0.3 ±0.1	0.3 ±0.1
Cu	65.0 ± 2.0	53.0 ±3.0	40.0 ±3.0	31.0 ±3.0	24.0 ±2.0
Zn	41.0 ± 3.0	36.0 ±3.0	25.0 ±2.0	23.0 ±3.0	24.0 ±2.0
Eu	3.2 ± 0.1	2.8 ± 0.1	2.1 ± 0.1	1.4 ± 0.1	1.2 ± 0.1

7.5.2 Selective adsorption tests

Application of SBA15-NH-PMIDA for recovery of Eu from real mining wastewater was analysed. Mining wastewater is often complex and contains various pollutants, including heavy metals, metalloids, organic compounds, and other contaminants. Using real wastewater provides a more accurate representation of the challenges involved in treating such industrial effluents.

Pre determined amounts of powdered SBA15-NH-PMIDA was mixed with 50 ml of pH adjusted (pH 4.8) real acid mine drainage and stirred in room temperature for 24 hours. Samples were then filtered and analysed for residual concentrations of dissolved metals. Adsorption trends of metals at different adsorbent doses are shown in figure 7.9. Europium uptake remained at less than 20% with low adsorbent dosage of 0.2g/l. However, this value increased to over 80% at higher adsorbent amounts. This can be attributed to higher number of free adsorption sites with increased adsorbent dosage. Higher adsorbent dose can lead to faster kinetics and shorter contact times. With more

adsorbent available, the rate of europium adsorption onto the surface increases, facilitating quicker attainment of the equilibrium adsorption capacity. At 0.8 g/l of SBA15-NH-PMIDA dosage, Eu adsorption was reported to be over 80% while the uptake of other metals remained below 20%. According to fig.11, uptake of competing heavy metals increased considerably at dosage of 1.6 g/l, while Eu uptake increased marginally to 84%. While a higher adsorbent dose initially increased the recovery rate, further increases in adsorbent dosage do not significantly improve the recovery rate beyond a saturation point (Al-dhawi et al., 2023). At this point, the adsorbent becomes fully loaded with europium ions, and adding more adsorbent will not lead to additional europium recovery. Hence, it can be concluded that 0.8 g/l dosage is optimum to selectively recover Europium from AMD. Study conducted by Fonseka et al (Fonseka et al., 2022) reported that 3.2 g/l of powdered Cr-MIL-PMIDA is necessary for optimum selective recovery of Eu from a synthetic AMD solution. Therefore, SBA15-NH-PMIDA can achieve similar recovery rate with considerably lower amounts of adsorbent. Higher use of adsorbent material can significantly increase the cost of recovery process. Balancing the cost of the adsorbent with the desired recovery rate is crucial for practical and economically viable europium recovery from AMD.

The chelating properties of phosphonic and carboxyl groups play a critical role in enhancing the selectivity of europium recovery processes (Chen et al., 2022). These ligands have lone pairs of electrons that can coordinate with the europium ion, leading to the formation of strong bonds between the ligands and Eu ions (Li et al., 2020; Qiang et al., 2021). The affinity of aforementioned ligands towards europium is higher compared to di valant heavy metal ions (Figure 7.9). Therefore, phosphonic and carboxyl groups

preferentially coordinate with europium ions, forming stable chelate complexes. It's important to note that the success of selective recovery depends not only on the ligand's affinity but also on other factors, such as pH, temperature, and the presence of competing metal ions (Romal & Ong, 2023).

Futher experiments were carried out with binary mixtures of Eu and heavy metals, with similar concentration ratios found in AMD. SBA15-NH-PMIDA displayed high selectivity over competing divalent cations similar to findings in the previous experiment. Around 90% of selective Eu uptake was maintained, while Zn and Cu uptake remained below 4%. However, selectivity of SBA15-NH-PMIDA reduced considerably in the presence of trivalent cations such as Fe and Al (Figure 7.10). Uptake of Eu was found to be 68% in the presence of Al and 54% against Fe. Fe^{3+} and Al^{3+} ions have strong affinities for oxygen-containing ligands, such as phosphonic and carboxyl groups, due to their high charge densities and Lewis acid properties (Hao et al., 2022; Lee et al., 2018). This strong affinity allows Fe^{3+} and Al^{3+} to outcompete europium for coordination with the ligands. Study conducted by Fonseka et al. (2021) reported similar findings for Cr-MIL-PMIDA. However, it showed higher Eu recovery rates in the presence of Fe and Al in binary systems (Fe + Eu, Al + Eu). This can be due to the appropriate pore size of Cr-MIL-PMIDA (2 nm) and geometries that favor the selective uptake of europium ions while limiting the access of larger metal ions like Fe and Al (Lee et al., 2018). In contrast, SBA15-NH-PMIDA have a more open pore structure with pore diameter around 9 nm, allowing easier access for Fe and Al ions to its surface. Furthermore, Cr-MIL-PMIDA, have a much robust and stable structure that can retain its selectivity even under challenging conditions (Fonseka et al., 2021; Lee et al., 2018). In contrast, the stability

and selectivity of SBA15-NH-PMIDA might be more susceptible presence of competing tri valant metal ions. Therefore, it is critical to precipitate Fe and Al from AMD by pH corrrection prior to adsorption to improve selectivity towards Eu.

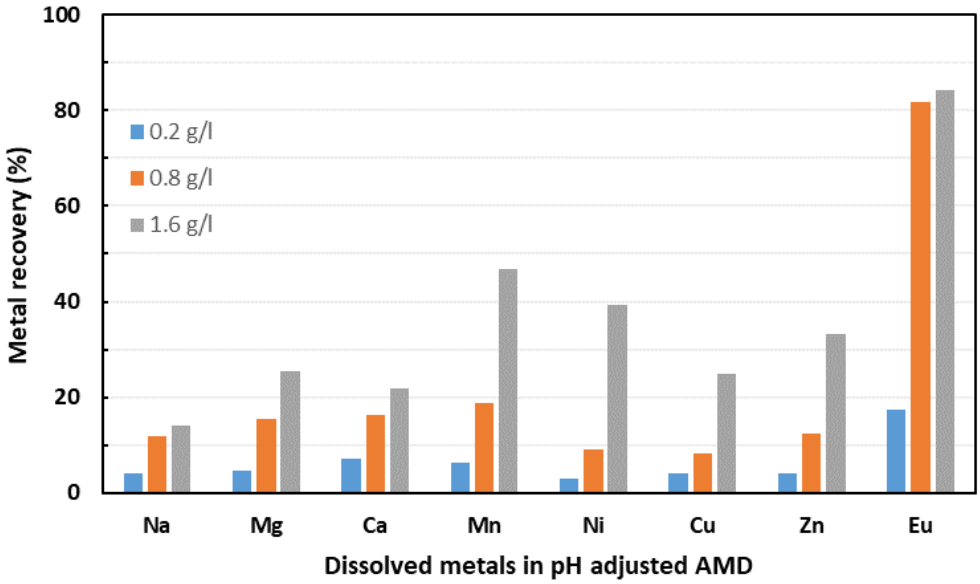

Figure 7.9: Adsorption of dissolved metals from pH adjusted acid mine drainage

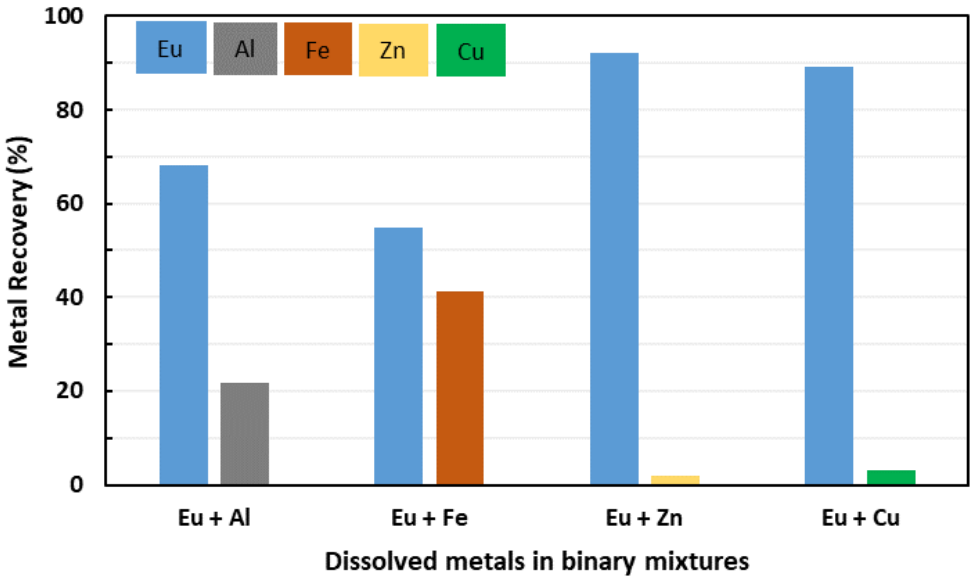

Figure 7.10: Adsorption of dissolved metals from synthetic binary solutions using SBA15-NH-PMIDA

7.6 Comparison of selective adsorption of Eu between Cr-MIL-PMIDA and SBA15-NH-PMIDA

A comparative analysis of the selectivity for europium (Eu) uptake between Cr-MIL-PMIDA and SBA15-NH-PMIDA was carried out using real AMD obtained from northern Norway (Table 7.4). The study aimed to discern and evaluate the differential capabilities of these two materials in terms of their preferential adsorption of Eu ions. Cr-MIL-PMIDA, characterized by its metal-organic framework nature, exhibited well-defined crystalline structures with inherent porosity and tunable functionalities.

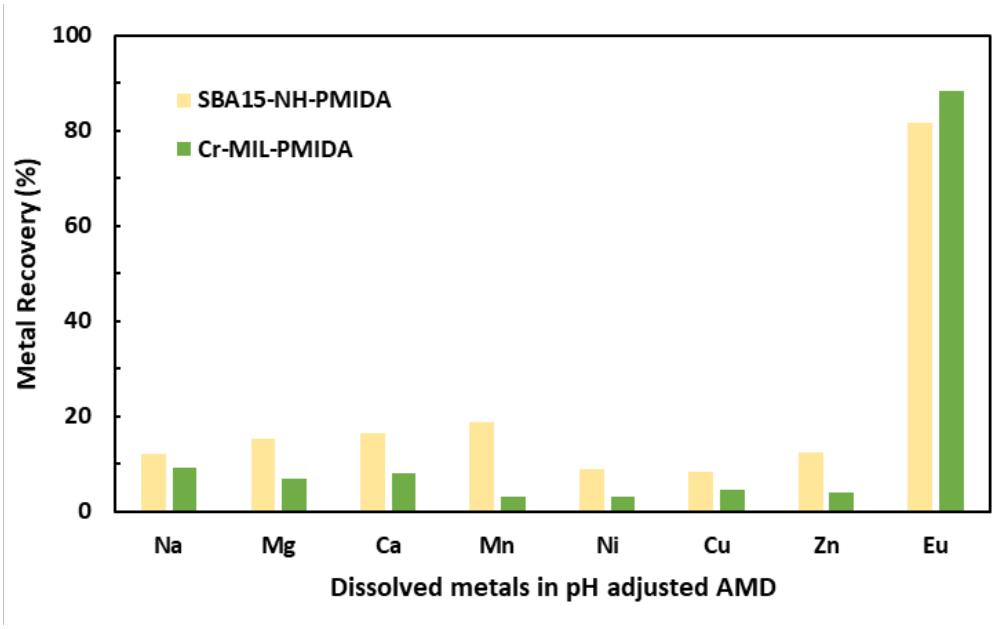

Figure 7.11: Recovery of Eu from pH adjusted real AMD using Cr-MIL-PMIDA and SBA15-NH-PMIDA

(Experimental condition: 50 ml AMD volume, 0.8 g/l adsorbent dose, 24 h equilibrium time, pH = 4.8 ± 0.1)

According to figure 7.11, Cr-MIL-PMIDA shows superior selectivity towards Eu (88%) compared to SBA15-NH-PMIDA (81%). Since the two materials possess the same PMIDA functional ligands, differences in selectivity can be attributed to variations in physical properties, such as pore size, surface area, and structural characteristics (Callura et al., 2018). These physical properties influence the interactions between the ligands and the adsorbed species, ultimately affecting the materials' adsorption behaviour.

Coordination sites within the Cr-MIL-PMIDA structure demonstrated significant affinity for Eu ions due to tailored ligand properties and metal links, resulting in strong adsorption. SBA15-NH-PMIDA, characterized by its mesoporous silica nature, possess a well-ordered, large-pore structure with accessible surface area. According to table 7.1,

Cr-MIL-PMIDA has a larger surface area (more than 9 folds) and pore volume (more than 2 folds). However, SBA15-NH-PMIDA has a larger pore size (9.16 nm) compared to Cr-MIL-PMIDA (2.15 nm). The higher single-solute Eu adsorption capacity observed in SBA15-NH-PMIDA (86.21 mg/g, table 7.2) compared to Cr-MIL-PMIDA (69.14 mg/g, table 4.4) can be attributed to the combination of larger pore size and the structural characteristics that promote multi-layer adsorption and the formation of bulkier complexes. On the other hand, Cr-MIL-PMIDA's size-selective adsorption and potentially stronger ligand-metal interactions might contribute to its slightly lower adsorption capacity. The interplay of these factors underlines the importance of understanding the materials' structural and surface properties when interpreting and optimizing their adsorption performance.

The larger pore size allows for increased spatial freedom within the pores, potentially enabling more diverse coordination and binding interactions between the adsorbent's functional groups and various metal species. The smaller pore size of Cr-MIL-PMIDA restricts the entry of larger metal ions or complex species, leading to size-selective adsorption (Fonseka et al., 2021). The significant difference in pore sizes between SBA15-NH-PMIDA and Cr-MIL-PMIDA can significantly impact the selectivity. The larger pore size of SBA15-NH-PMIDA allows for the accommodation of larger metal species and complex molecules, broadening its selectivity profile. In contrast, the smaller pore size of Cr-MIL-PMIDA restricts the entry of larger species, contributing to its size-selective adsorption. Although both materials contain the same PMIDA ligand, the arrangement of the ligands on the surface of the material can differ. Even slight variations

in the orientation or density of ligands can lead to differences in the steric effects and electrostatic interactions with adsorbed species (Lu et al., 2021).

In conclusion, the combination of low production cost and high reusability lends SBA15-NH-PMIDA a broad applicability that transcends its slightly lower selectivity compared to Cr-MIL-PMIDA. Economic advantages and sustainable features of SBA15-NH-PMIDA make it a practical and attractive choice for various industries seeking efficient and cost-effective separation solutions. Detailed cost analysis for the production of SBA15-NH-PMIDA is presented in chapter 8. Ultimately, the selection between these materials should be based on a holistic evaluation of their performance, cost-effectiveness, and compatibility with the specific demands of the intended application.

7.7 Reusability of SBA15-NH-PMIDA

Reusability is critical for industrial application of novel adsorbents such as SBA15-NH-PMIDA. In this study, granulated SBA15-NH-PMIDA was analysed over ten adsorption/desorption cycles using 5 mg/l synthetic Eu solution. 0.01M HCl was used as the stripping agent and Milli Q water was used for washing. As explained earlier, protonation of functional ligands in acidic conditions creates a repulsive force with Eu^{3+} which results in desorption of ions to the solution. As shown in Figure 7.12, SBA15-NH-PMIDA retained over 89% of the initial Eu adsorption capacity after 10 cycles. This reflects negligible loss of functional groups during regeneration process, confirming successful surface modification with PMIDA.

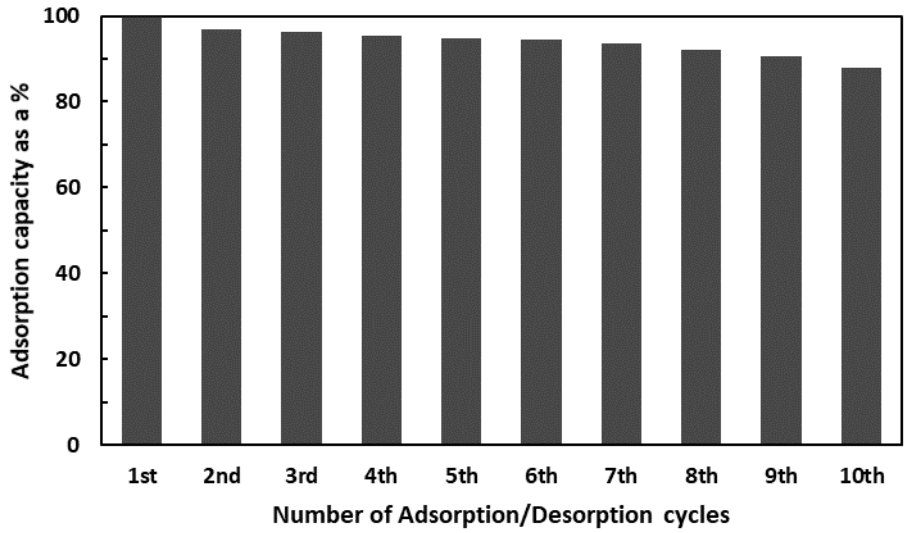

Figure 7.12: Cyclic adsorption tests for Eu recovery at initial concentration of 5 mg/l at pH 4.75 ± 0.1

7.8 Mechanism for Selective Eu recovery with SBA15-NH-PMIDA

Selectivity of SBA15-NH-PMIDA towards europium over competing metal ions is a result of specific chemical interactions and complex formation between europium ions and the ligand's coordination sites, as well as the overall stability and properties of the resulting chelate complex (Fonseka et al., 2021; Lee et al., 2018). Other factors, such as solution conditions, pH, and the presence of competing metal ions, also influence the selectivity of PMIDA for europium. According to figure 7.5, optimum pH of 4.75 ±0.1 resulted in maximum Eu uptake at which favourable conditions for deprotonation of functional groups were present. At low pH, surface of SBA15-NH-PMIDA have a net

positive charge due to the protonation of amino groups. As pH increases, surface becomes negatively charged due to the deprotonation of NH^{3+}, P-OH and COOH groups.

FT-IR analysis of pristine SBA15-NH-PMIDA confirmed the presence of phosphonic, carboxylic and amine groups. The carboxylic and phosphonic acid groups in PMIDA provide multiple coordination sites, enabling them to bind to Eu ions through coordination bonds (Liu & Chen, 2021; Wan et al., 2023). Oxygen atoms in these functional groups act as electron donors, forming coordinate covalent bonds with the Eu ions, which act as electron acceptors (Li et al., 2023). This coordination interaction results in the formation of stable complexes between Eu and PMIDA. FTIR analysis of spent SBA15-NH-PMIDA were carried out to further establish selective adsorption mechanisms. Peaks in the vibration bands assigned to phosphonic group (1100 – 900 cm^{-1}) and carboxylic group (600 -700 cm^{-1}) shifted to lower frequencies after adsorption (Figure 7.13a). In the context of Eu coordination with the phosphonic ligand, the shift of the peak at 1055 cm^{-1} to a lower frequency likely corresponds to a change in the vibrational frequency of the phosphonate (PO) stretching vibration. The coordination of Eu with the phosphonic ligand alters the local bonding environment around the phosphonate groups, resulting in the observed shift to lower frequencies (Nakamoto, 2006b). Similarly, a shift in peak at 600-700 cm^{-1} to a lower frequency likely suggests a weakening of the C-O bond due to the coordination with Eu (Figure 7.13b). This weakening can be associated with the formation of a coordination complex between the carboxylic group and the adsorbate. The coordination bond typically involves the donation of electron pairs from the carboxylic oxygen to the Eu, which results in a decrease in the vibrational frequency (Vijayaraghavan et al., 2018). However, there was

no change observed in vibration range assigned to N-H stretching (3200 -3500 cm^{-1}) after adsorption, suggesting that Eu ions did not interact with amine ligands.

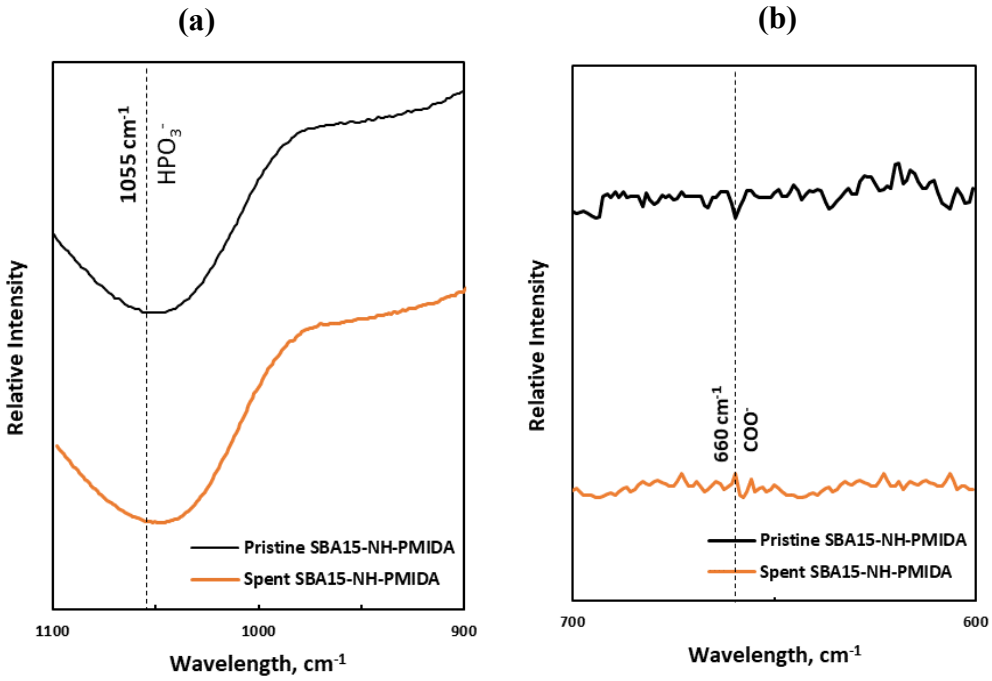

Figure 7.13: FTIR spectra of SBA15-NH-PMIDA before and after adsorption

Physical properties of the adsorbent plays a key role in selectivity towards a target metal. SBA15-NH-PMIDA, being a mesoporous material, have larger and more open pores compared to MOFs like Cr-MIL-PMIDA (Fonseka et al., 2021). The larger pore size allows for easier diffusion and access of various metal ions, including Al and Fe, to the adsorbent surface. Consequently, SBA15-NH-PMIDA may have lower selectivity for europium over Al and Fe compared to Cr-MIL-PMIDA.

Table 7.6 summarises the Eu adsorption capacities of different novel adsorbents. Titanate nanorings and graphene oxide-maghemite-chitosan composites reported superior single

component Eu adsorption capacities. However, SBA15-NH-PMIDA was observed to have high selectivity for Eu in complex multicomponent solutions, such as Acid Mine Drainage (AMD). This confirms that the presence of phosphonic and carboxylic groups in SBA15- NH_2-PMIDA is primarily responsible for its high selectivity toward Rare Earth Elements (REEs), including europium (Eu).

Table 7.6: Comparison of Eu adsorption capacities of different adsorbents

Adsorbent	pH	Adsorption Capacity (mg/g)	Reference
SBA15-NH-PMIDA	4.8	86.21	This study (Chapter 7)
Cr-MIL-PMIDA	5.5	69.14	(Fonseka et al., 2021)
Al-substituted goethite	5.5	4.24	(Li et al., 2017)
GO-MGH-CS III	5.0	160.00	(Lujanienė et al., 2022)
SBA-15 Mesoporous Silica	4.0	15.20	(Dolatyari et al., 2016)
SBA-15/SO_3H	4.0	8.60	(Dousti et al., 2019)
Titanate Nanorings	5.0	115.30	(Zheng et al., 2020)
TiO_2	4.5	2.69	(Tan et al., 2009)
mesoporous Al_2O_3/EG composites	6.0	5.14	(Sun et al., 2012)

7.9 Summary

In this study, a novel SBA15-NH-PMIDA material was synthesized following a two step surface modification process using 3- aminopropyl triethoxysilane (APTES) and N-(phosphonomethyl) iminodiacetic acid (PMIDA) for selective recovery of Europium (Eu) from real AMD. First, a comprehensive physical and chemical characterisation of the

material was conducted to verify successful synthesis of the material followed by detailed adsorption studies.

- Single solute Eu adsorption tests revealed that SBA15-NH-PMIDA reached equilibrium within two hours and showed maximum Langmuir adsorption capacity of 86.21 mg/g at optimum pH 4.8.
- Furthermore, the material selectively recovered over 80% of Eu from pH adjusted real AMD at optimum dosage of 0.8 g/l.
- High selectivity was due to the formation of strong Eu complexes with phosphonic and carboxyl functional groups.
- A comparative study showed that Cr-MIL-PMIDA (88%) has a slightly higher selectivity towards Eu compared to SBA15-NH-PMIDA (81%) from real mining wastewater.
- SBA15-NH-PMIDA managed to retain over 90% of adsorption capacity over 10 regeneration cycles, making it an economically viable adsorbent for industrial scale applications.

However, granulation of SBA15-NH-PMIDA is necessary for industrial applications to improve handling, reduce pressure drop, enhance mass transfer and ensure reproducibility and scalability. Next chapter of this thesis analyses the performance of a membrane distillation/adsorption hybrid system, using granulated SBA15-NH-PMIDA for simultaneous water and Eu recovery.

CHAPTER 8

MEMBRANE DISTILLATION/ADSORPTION SYSTEM FOR SELECTIVE EU RECOVERY FROM MINING WASTEWATERS

*This chapter is based on the following journal publication

Fonseka, C.; Ryu, S.; Choo, Y.; Naidu, G.; Foseid, L.; Thiruvenkatachari, R.; Kandasamy, J.; Ratnaweera, H.; Vigneswaran, S. Selective Recovery of Europium from real acid mine drainage by using novel SBA15-NH-PMIDA adsorbent and membrane distillation system. *Journal of Water Process Engineering, 56, 104551.* doi:https://doi.org/10.1016/j.jwpe.2023.104551

8 Introduction

Increasing the concentration of REE within AMD is a crucial step toward efficient and selective recovery. This strategy not only enhances the technical feasibility of recovery processes but also contributes to the overall economic viability and sustainability of the selective adsorption process. In this regard, membrane distillation is a thermal separation process that relies on differences in vapour pressure to separate dissolved metals (such as REE) from highly concentrated waste streams (Foureaux et al., 2020). Kesieme et al. (Kesieme et al., 2014) used direct contact membrane distillation setup with PTFE (flat sheet membrane) to successfully treat acid mine leach solution. Furthermore, Naidu et al. (Naidu et al., 2017) and Ryu et al. (Ryu et al., 2020) successfully explored membrane distillation/adsorption systems to selectively recover valuable metals (Rb and Cu) from the concentrated feed using granulated adsorbents. Therefore, integration of membrane distillation and adsorption offers a holistic solution that not only improves water quality but also maximizes the value derived from waste streams containing valuable resources.

This research aimed to achieve two primary objectives: (a) an exploration of the performance of granulated SBA15-NH-PMIDA, for the selective recovery of Eu, and (b) a comprehensive analysis of the efficacy of membrane distillation in amplifying Eu concentration while concurrently yielding purified water from AMD. An assessment encompassing the physical and chemical characterization of granulated SBA15-NH-PMIDA was conducted to unravel the underlying mechanisms governing its selective adsorption capabilities. Finally, a hybrid system coupling direct contact membrane distillation (DCMD) with adsorption, employing granulated SBA15-NH-PMIDA, was operated to achieve simultaneous water and Eu recovery from a synthetic AMD solution

mirroring the composition of actual AMD samples. The economic viability of this novel adsorbent was gauged through multiple tests and sequential adsorption experiments.

8.1 Granulation of SBA15-NH-PMIDA

SBA15-NH-PMIDA was granulated using sodium alginate and calcium chloride solutions (Ryu et al., 2021). 1 g of powdered SBA15-NH-PMIDA was first added to 10 ml of sodium alginate (1.5%) solution. Mixture was then loaded to a 50 ml syringe and gently trickled down to 0.05M $CaCl_2$ solution with gentle stirring (100 rpm). Granulated material (diameter = 2.0 ± 0.1 mm) was then sieved and dried at 70°C for 12 hours.

8.2 Direct Contact Membrane Distillation (DCMD)/adsorption system setup

DCMD experiments were carried out with synthetic AMD with similar chemical composition to real AMD. Aim of this experiment was to analyse the efficiency of conventional DCMD in recovering clean water from AMD and to concentrate Eu, which would otherwise exist in trace concentrations. The setup comprises of a flat sheet membrane module (40 cm^2), integrated with a double wall jacket reactor. Commercially available, polytetrafluoroethylene (PTFE) hydrophobic flat-sheet membrane was purchased acquired from General Electric, US. The membrane had an average pore size of 0.22 µm, a porosity ranging from 70% to 80%, and a thickness of 179 µm. Temperature of the feed tank was maintained at 60 ± 0.5 °C using a double-walled bottle and a heat sink. The permeate temperature was maintained at 20 ± 0.5 °C using a chiller. Selective adsorption experiments were carried out with varying, Both feed and permeate streams were circulated at a flow rate of 1.0 L/min, regulated by a gear pump. Temporal increment

of mass of the permeate tank was continuously measured using an analytical balance connected to a data logging software (AdamDU). Samples were collected at the beginning and at the end of experiments (Feed tank and permeate tank). All samples were first filtered using 0.45 µm syringe filters and dissolved metals were analysed using ICP-MS (Agilent 7900, USA).

First, DCMD experiments were carried out to determine solute rejection and concentration of Eu in the feed tank. Next, experiments were carried out with pre determined amounts granulated SBA15-NH-PMIDA suspended in the feed tank as depicted in Figure 8.1. A steel mesh was fixed to the end of the feed water circulation pipe in the feed tank to prevent granules entering the membrane module.

Following equation were used to calculate he volume concentrating factor (VCF) of the concentrated feed.

$$VCF = \frac{V_i}{V_c} \qquad (8\text{-}1)$$

Where,

V_c: Final concentrated AMD volume (L) V_i: Initial AMD feed volume (L)

Membrane permeate flux (equation 10) was calculated by continuously measuring permeate volume collected at 2 min intervals.

$$J = \frac{V}{A\,x\,\Delta t} \qquad (8\text{-}2)$$

A: Effective filter area of membrane (m^2) J: Permeate Flux (l/m^2h)

Δt: Time interval (h)

The following equation was used to calculate solute rejection of the membrane for each dissolved metal.

$$R(\%) = \frac{C_i - C_p}{C_i} \quad (8\text{-}3)$$

C_i: Initial solute concentration (mg/l) C_p: Permeate solute concentration (mg/l)

R: Solute Rejection (%)

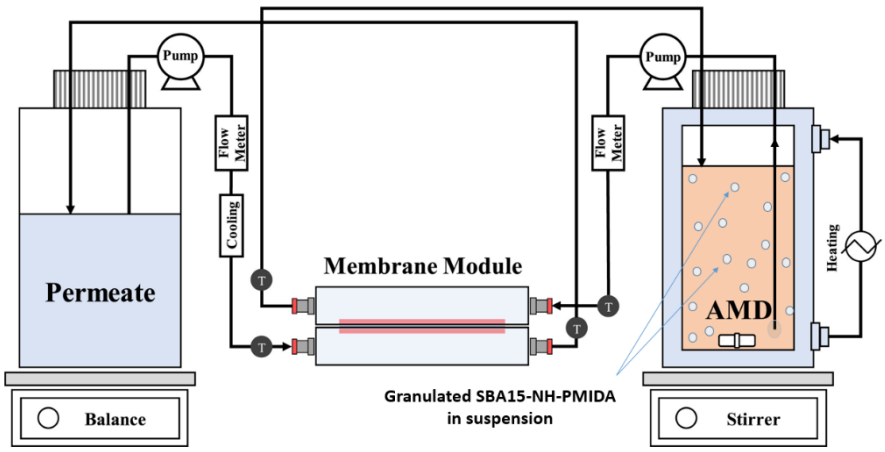

Figure 8.1: Schematic diagram of integrated DCMD/Adsorption system

8.3 Results and Discussion

8.3.1 Membrane Distillation for Eu concentration

DCMD experiments were carried out with pH adjusted synthetic AMD, with similar chemical composition as real mining wastewater listed in Table 7.4. This was due to the difficulty in transporting large volumes real AMD and to maintain a uniform chemical composition for all DCMD experiments. These experiments were carried out to evaluate AMD remediation for recovery of clean water and potentially increase Eu concentration for higher EU recovery.

Two sets experiments were carried out to assess the system. First, DCMD was operated without adsorbents in feed tank to analyse the solute rejection. The second set of experiments were conducted with pre determined amounts of granulated adsorbents suspended in the feed tank to analyse selective Eu adsorption and optimum dosage. The results showed that DCMD managed to recover 80% of clean water in 11.8 hours, with an initial constant permeate flux around 7.0 ± 0.5 L/m^{2}h (Figure 8.2). However, a steady flux decline was recorded from VCF 2 until 4.3 followed by a rapid flux decline. The results suggests that pH adjustment of AMD was found to reduce metal solubility limit (Ryu et al., 2020; Warsinger et al., 2015). Divalent metal cations such as Fe^{2+}, Ca^{2+}, Mg^{2+}, Mn^{2+} exhibit lower solubility limit at higher pH (Huang et al., 2017; Zoungrana et al., 2016). Ryu et al. (Ryu et al., 2020) reported significant reduction in permeate flux when treating pH adjusted AMD. This can be the reason for low flux rate and rapid flux decline observed in this experiment.

Over 99% of solute rejection was found when analysing the permeate water quality. Concentrations of metals in feed tank are reported in table 8.1. Concentration of Eu increased from 1.06 mg/l to 3.9 mg/l in this experiment. Therefore, membrane distillation can be successfully used to concentrate and recover Eu from acid mine drainage.

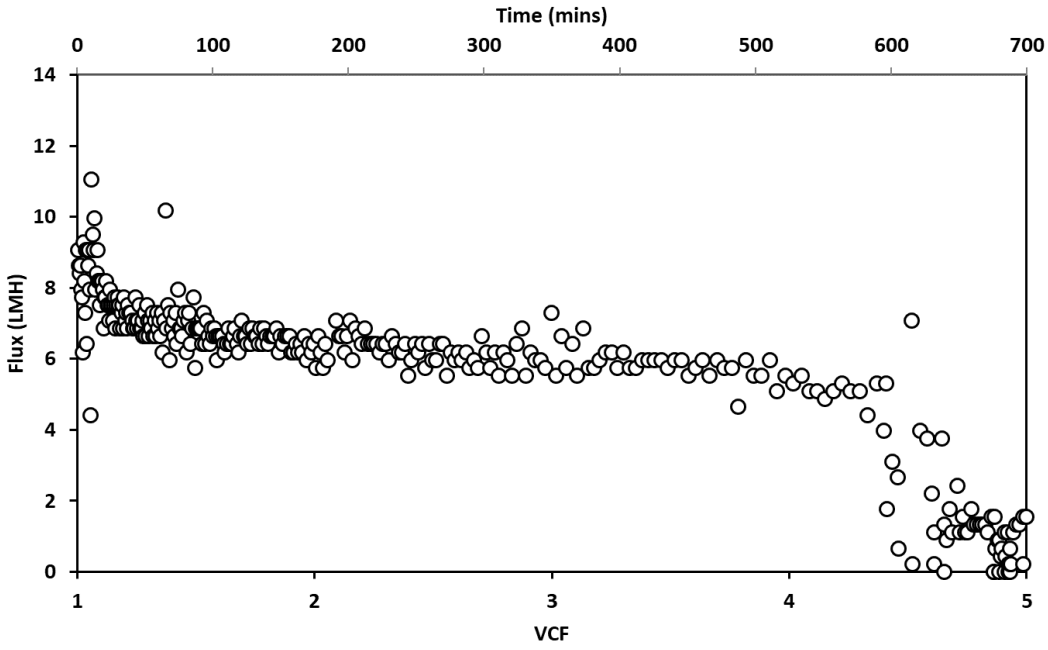

Figure 8.2: DCMD permeate flux for pH adjusted (pH 4.8) synthetic AMD solution. Flux (LMH) vs VCF vs Time (min)

.

Table 8.1: Concentrations of metals (mg/l) in pH adjusted initial synthetic solution and concentrated feed (DCMD experiment without adsorbents in feed tank)

Element	Na	Mg	Ca	Mn	Cu	Zn	Eu
pH adjusted Initial AMD	746.0	136.5	202.0	3.9	5.9	8.2	1.1
Concentrated feed	2218.0	490.0	455.0	15.9	18.7	22.6	3.9

8.3.2 Selective adsorption of Eu onto granulated SBA15-NH-PMIDA

The practical application of selectively recovering Eu using granulated SBA15-PMIDA from the concentrated feed was then evaluated. Four DCMD experiments with varying granulated SBA15-NH-PMIDA amounts in the feed tank were carried out to determine the optimum adsorbent dosage for maximum Eu recovery with minimum impurities. In all four experiments, samples were taken at the end of DCMD experiment for analysis, after allowing the feed tank to cool down to room temperature.

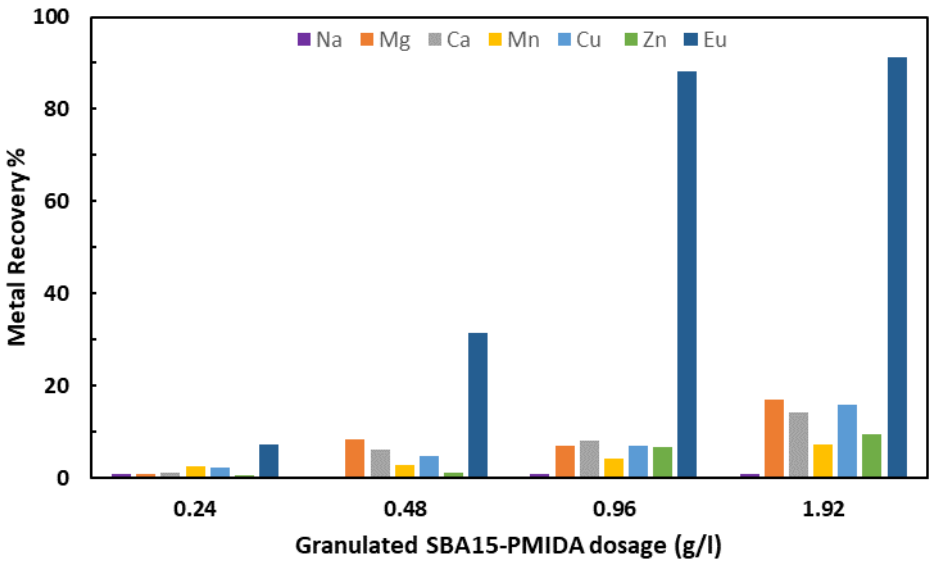

Figure 8.3: Selective Eu recovery from DCMD concentrated feed tank

According to the Figure 8.3, 0.96 g/l of granulated SBA15-NH-PMIDA dose yielded close to 90% Eu recovery with minimum uptake of competing metals. Thus, making it

the optimum dosage. This value is similar to the optimum dosage found for powdered SBA15-NH-PMIDA reported in section 3.4.2. At 1.92 g/l dosage, Eu recovery was found to be over 90%, while the uptake of Mg, Cu and Ca was above 15%. This phenomenon is a result of excessive free adsorption sites as result of higher dosage. Concentrating Eu before adsorption is a crucial preparatory step that enhances the efficiency, selectivity, and cost-effectiveness of the recovery process. It increases the concentration in the feed solution, making it easier for the adsorbent to interact with and capture higher number of Eu ions. This leads to improved adsorption efficiency and higher Eu recovery rates. Combining membrane distillation with granulated SBA15-NH-PMIDA in the feed tank can be an effective and sustainable approach for recovering europium from solutions containing this valuable metal. Proper optimization of the process parameters, including temperature, flow rates, and adsorbent dosage, is crucial for achieving efficient and selective europium recovery.

8.4 Cyclic adsorption/desorption tests for granulated SBA15-NH-PMIDA

Further tests were carried out to increase the purity of Eu in the dissolved solution. Adsorbents separated from the DCMD feed tank was first desorbed using 0.01M HCL solution (50 ml) and analysed for dissolved metals using ICP-MS. pH of desorbed solution was then adjusted again to 4.7 – 4.9 using NaOH and similar adsorbent dosage (0.96 g/l) of granulated SBA15-NH2 was added and stirred at room temperature. These steps were repeated four times to increase purity of Eu in the desorbed solution.

Table 8.2: Concentration of Eu from using sequential adsorption/desorption

Number of Adsorption/desorption cycles	Concentration of Eu (mg/l)	Purity of Eu %
1st Cycle	3.59	8.23
2nd Cycle	2.29	64.66
3rd Cycle	1.43	97.33
4th Cycle	0.92	99.9

According to data from table 8.2, purity of Eu can be significantly improved using 4 sequential adsorption/desorption steps. Purity increased to 99.9% after the 4th cycle. However, this process results in a loss of nearly 75% of Eu ions. During the adsorption process, Eu ions form soluble complexes with ligands present on the adsorbent surface (Sheng et al., 2012). However, during desorption, these complexes may break down or rearrange, leading to the formation of less soluble europium compounds. Furthermore, concentration of Eu in the solution may become too high after multiple adsorption-desorption cycles, reaching a point of oversaturation. When the solution is supersaturated with europium, the excess ions can precipitate out of the solution as solid phases (Lakshtanov & Stipp, 2004). Therefore, further studies should be carried out on optimising desorption conditions, such as pH and temperature, to avoid conditions that promote Eu precipitation.

8.5 Cost benefit analysis

Conducting a cost-benefit analysis for a novel adsorbent such as SBA15-NH-PMIDA is essential to evaluate economic feasibility and potential benefits of its application in the industry. This analysis was performed by calculating the costs and potential revenue of treating 1000 m^3/day of AMD with chemical composition listed in table 7.4.

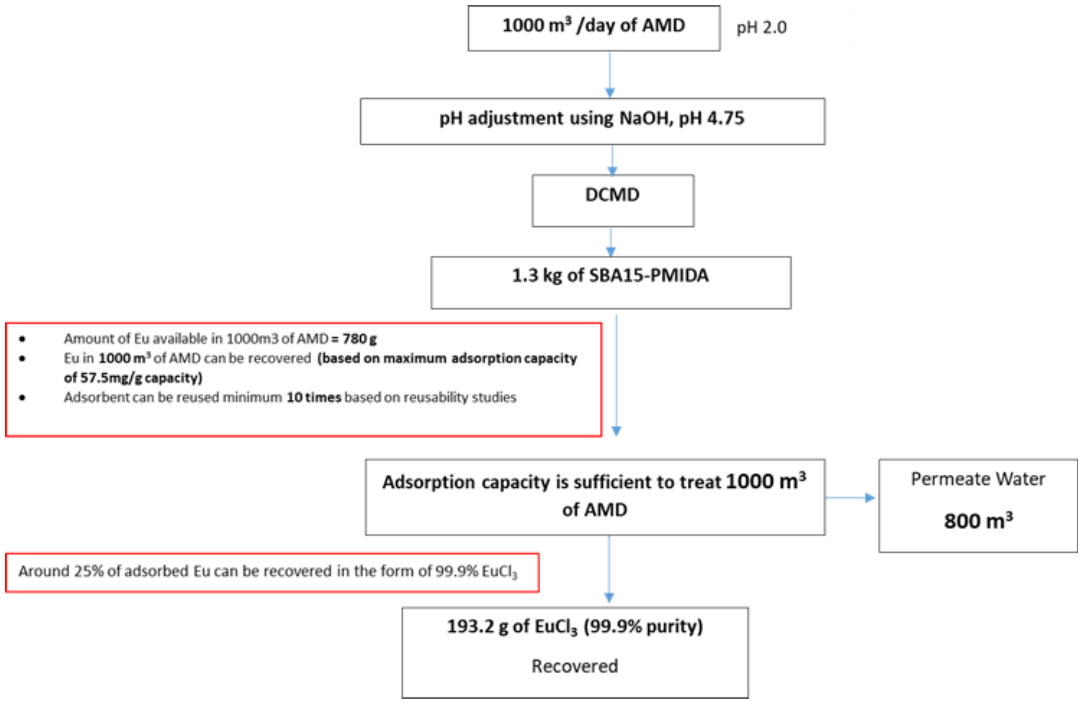

Figure 8.4: Estimated recovery of clean water and Eu from 1000 m^3/day of AMD

As depicted in figure 8.4, NaOH is first used for pH correction. Then, the resultant supernatant water will be passed through membrane distillation/adsorption system. Assuming 1.3 kg of granulated SBA15-NH-PMIDA is available, and based on its maximum adsorption capacity, 57.5 mg/g, Eu available in 1000 m^3 of AMD can be

recovered. Based on 80% water recovery rate, 800 m3 of clean water can be recovered from this process. Based on the calculation provided in table 8.2, approximately 193.2 g of $EuCl_3$ (99% purity) can be recovered through this process. Table 8.3 summarises predicted revenue and expenses sheet for this system.

Table 8.3: Predicted cost/revenue to treat 1000 m^3 of AMD

Item	Revenue (A$)	Expenses (A$)
Adsorbent Preparation (1.3 kg)		2683.87
pH adjustment (NaOH)-*(Industrial Supplier)*		325.50
Desorption (HCl)- *(Industrial Supplier)*		312.55
Sale of $EuCl_3$ (193.2 g)	11,881.90	
Sale of permeate water (800 m^3)	2000.00	
Total	**13,881.90**	**3,321.92**

According to the above calculation, DCMD/adsorption hybrid system can yield a positive monetary return excluding associated labour costs, DCMD operation and maintenance costs. However, this is a significant finding since no studies have been conducted to evaluate the financial benefits of selectively recovering valuable metals. Expenses can be further reduced when purchasing chemicals in bulk. This system can be further extended to recover other valuable metals such as Cu, Mg to further increase revenue.

Additional set of column experiments were conducted to develop a mathematical model to predict breakthrough curve for single solute Eu adsorption using granulated SBA15-NH-PMIDA. These experiments yield valuable insights that aid in optimizing column

filter processes, validating models, and guiding practical applications of adsorption technology. Findings are presented in the appendix.

8.6 Summary

A Direct contact membrane distillation (DCMD)/adsorption hybrid system was then developed by suspending granulated SBA15-NH-PMIDA in the feed tank to treat pH adjusted synthetic AMD.

- DCMD system managed to recover 80% of clean water and concentrated Eu ions by over three folds.
- Granulated SBA15-NH-PMIDA selectively recovered of over 90% of Eu, while the uptake of other competing metals remained below 10% at optimum dosage of 0.96 g/l.
- Cost benefit analysis showed that 1.3 kg of granulated SBA15-NH-PMIDA is sufficient to treat 1000 m^3 of AMD. This will produce 800 m^3 of permeate water and 193.2 g of $EuCl_3$ with 99.9% purity.
- This confirms that the novel SBA15-NH-PMIDA is a highly efficient and low cost adsorbent for REE recovery from mining wastewaters.
- Application of granulated SBA15-NH-PMIDA in an upward flow column setup for Eu recovery was analysed and data are presented in the appendix.

This shows that by embracing resource recovery practices and technologies, we can move towards a more sustainable and circular approach to resource management. This not only attract financial benefits, but also addresses environmental challenges, supports the transition to renewable energy, and fosters a more sustainable and equitable society. It is

an essential component of achieving global sustainability goals and building a more resilient and regenerative future.

CHAPTER 9

CONCLUSION AND RECOMMENDATIONS

9 Conclusion and recommendations

9.1 Conclusion

Rare Earth elements (REEs) have become a strategic resource extensively used in renewable energy technologies and modern electronic devices. Depletion of natural REE bearing mineral deposits has made selective recovery of REE from alternative sources crucial in meeting the rising global demand. The primary objective of this study was to evaluate the efficacy of Cr-MIL-PMIDA and novel SBA15-NH-PMIDA adsorbents for Eu adsorption and explore the potential of combining membrane seperation with adsorption for acid mine drainage (AMD) remediation. While detailed conclusions have been presented at the end of each individual chapter, the following is an overall conclusion that encompasses the overarching findings and key takeaways from the entire study.

Cr-MIL-PMIDA metal organic framework (MOF) was synthesised in this study, which was subsequently characterized and studied for selective recovery of europium (Eu) from zinc ore obtained from a mining site in Western Australia. The physical and chemical characterization analysis of the synthesised Cr-MIL-PMIDA material outlined the presence of chromium (Cr), Nitrogen (N) and Phosphorous (P) as main elements of the material. The Cr-MIL MOF possessed high surface area (over 1000 $m^2.g^{-1}$) and the FT-IR (Fourier-Transform Infrared) spectra indicated the chemical bonds of hydrogen, carbonyl, carboxyl and amine present on adsorbent surface, established the tethering of PMIDA (N-(phosphonomethyl) iminodiacetic acid) group to the adsorbent. Eu recovery by Cr-MIL-PMIDA was highly influenced by pH. Maximum Eu recovery was achieved

at pH_{eq} of 5.5±0.5 which was mainly due to deprotonation of the functional groups that resulted in high negatively charged Cr-MIL-PMIDA surface (zeta value of -25 mV) at this pH range. At the optimum pH_{eq} of 5.5±0.5, adsorption of Eu by Cr-MIL-PMIDA fitted well with Langmuir isotherm and yielded an adsorption capacity of 69.14 mg/g. A rapid Eu recovery was attained (within 2 h) and the kinetic data fitted well with pseudo-second order model. Cr-MIL-PMIDA exhibited highly selective recovery of Eu from leached mine containing substantial amount of transition metals as well as alkaline divalent cations. The high selectivity is attributed to the presence of carboxylate and phosphonic groups, coupled with electrostatic bonding with residual ammine groups that enables to maintain high selective affinity towards hard acidic groups of REE over other transition metals.

Given the impractical nature of using powdered adsorbents in the industry, Cr-MIL-PMIDA was then granulated for the first time using alginic acid and $CaCl_2$ for a study on continuous adsorption of Eu in a fixed bed column. Physical and chemical characteristics of both powdered and granulated Cr-MIL-PMIDA were first conducted. A reduction in surface area and pore volume were reported for granulated media, but FTIR and XRD analysis highlighted the presence of the same functional groups, which confirmed successful granulation process. Equilibrium and kinetic experiments were carried out on the uptake of Eu onto granulated media and the results confirm that the adsorption equilibrium and kinetics data fitted well with Langmuir, Freundlich and surface diffusion (SDM) models. Adsorption capacity of granulated Cr-MIL-PMIDA reduced by 44% compared to performance of powdered media primarily due to pore blocking and reduction of active surface area. However, the study on regeneration indicated that

granular Cr-MIL-PMIDA was able to retain over 95% of its initial adsorption capacity over five adsorption/desorption cycles. Therefore, the granulated material has the potential to be reused in multiple column experiments to compensate for the slight reduction in adsorption capacity. Selectivity studies conducted with both powdered and granulated media shows only a slight reduction of Eu uptake. 92% selective adsorption of Eu by powdered Cr-MIL-PMIDA from a multi component solution dropped to 83% after granulation, which can be attributed to reduction of pore volume during synthesis. High affinity of phosphonic and carboxyl groups towards Eu was found to be the main reason for high selectivity over competing ions. Results from a kinetic experiment using a single-component Eu solution demonstrated that Fixed Bed Column (FBC) breakthrough curves can be accurately simulated using parameters (Ds and kf) from the surface diffusion model. Axial dispersion coefficient was calculated using one column experiment and it was successfully applied to simulate breakthrough curves for other experimental conditions. When varying inlet concentrations, flow rates and bed lengths, the Linear Driven Force Approximation (LDFA) model showed a good fit (R^2>0.92). The successful application of the LDFA model proves that it is an effective tool to both simulate and optimise FBC experiments utilizing granulated Cr-MIL-PMIDA for Eu recovery.

Since REE exist at trace concentrations in AMD, a study to evaluate the efficiency of water recovery using low pressure Nano filtration (NF) from synthetic AMD and recovery of valuable metals from concentrated feed using novel adsorbents was conducted. The presence of organic pollutants decreased the flux of NF. Powdered eggshell was successfully employed as a low-cost adsorbent to remove organic matter (OM) prior to

NF filtration resulting in a 52% flux increase (10.2 L/m^2h to 15.5 L/m^2h). 80% of water was recovered from synthetic AMD with over 95% solute rejection. Concentrated feed water was then used for selective recovery of valuable metals such as REE and copper (Cu). Cr-MIL-PMIDA and amine-grafted SBA15 were successfully prepared in the lab and detailed characterization of the material was performed to determine their chemical and physical properties. The pH of concentrated feed was then adjusted to 5, where it was found that most of the Aluminium (Al) and ferric (Fe) precipitate while a majority of valuable metals remained dissolved.

Cr-MIL-PMIDA was found to recover over 90% of REE over highly concentrated competing ions present in pH adjusted solution. The optimum dosage was 3.2 g/L at which the uptake of competing ions remained below 10%. High selectivity towards Eu is attributed to affinity with carboxylate and phosphonic groups, coupled with electrostatic bonding with residual amine groups. Amine-grafted SBA15 was then used as an adsorbent to selectively recover Cu from residual solution. At 3.2 g/L dosage of SBA15-NH_2, over 90% of Cu was recovered while the uptake of other competing metals remained below 10%. Formation of coordination complexes between Cu and amine ligands was found to be the driving force behind the high selectivity. Cyclic adsorption and desorption study showed that both Cr-MIL-PMIDA and SBA15-NH_2 retained over 95% of the initial adsorption capacity for recovering REE and Cu, respectively, even after 5 cycles.

While chromium-based MOFs show promise for selective REE adsorption, their suitability for industrial applications is constrained by factors such as toxicity, stability, scalability, and cost-effectiveness. The next study aimed to assess the effectiveness of novel SBA15-NH-PMIDA for Eu adsorption. SBA15-NH-PMIDA was synthesized for

the first time following a two-step sequential functionalization method. A comprehensive chemical and physical characterisation of the material was carried out to confirm successful synthesis and to establish adsorption mechanism. Single solute synthetic Eu solutions were used for initial screening tests, where optimal pH for Eu adsorption was found to be 4.8. Adsorption equilibrium was reached within 2 hours with a maximum capacity of 86.21 mg/g. Selective adsorption experiments were then carried out with real acid mine drainage obtained from an abandoned mining site in northern Norway. At optimum adsorbent dosage of 0.8 g/l, over 80% of Eu in AMD was selectively recovered, whilst the uptake of other metals remained below 10%. Adjusting the pH of AMD was found necessary not only to avoid undesired protonation of functional groups, but to promote precipitation of interfering metal ions (Fe and Al) and enhance the overall selectivity for Eu. Detailed FTIR analysis of spent adsorbent confirmed that high selectivity of SBA15-NH-PMIDA was due to the formation of stable coordination complexes between Eu ions and phosphonate, carboxyl groups. Furthermore, the adsorbent maintained over 90% of initial adsorption capacity over 10 cycles, making SBA15-NH-PMIDA an efficient and low cost adsorbent for Eu recovery. However, granulation of this highly efficient adsorbent was necessary to improve flow properties, ease of handling and transport in industrial processes.

Finally, a direct contact membrane distillation (DCMD)-adsorption system was developed by suspending granulated SBA15-NH-PMIDA in the feed tank for simultaneous water and REE recovery. The study showed that at optimum dosage of 0.96 g/l, the adsorbent recovered 90% of Eu in the feed tank while uptake of competing ions remained below 10%. Furthermore, the purity of recovered Eu can be increased upto 99%

using a 4 step sequential adsorption-desorption process. A cost-benefit analysis was then conducted to quantify the advantages of using this novel material. The study revealed that, 193.2 g of $EuCl^3$ with 99% purity can be recovered by treating 1000 m^3 of AMD. Additionally, clean water recovered from the membrane system can be re used in mining activities to reduce water stress in arid regions.

Recovery of Eu, a valuable rare earth element, from AMD offers significant economic incentives for both AMD treatment and environmental remediation endeavours. By extracting and recycling europium from AMD, companies can effectively transform a waste stream into a valuable resource, thereby generating additional revenue and fostering sustainable resource management practices. Following are specific conclusions of this study.

9.2 Recommendations

The successful adoption and widespread implementation of novel AMD treatment and resource recovery methods will depend on their ability to demonstrate improved performance, economic viability, and environmental sustainability compared to traditional approaches. Continuous research, development, and pilot-scale testing are essential to validating the effectiveness and competitiveness of these innovative solutions. Following are recommendations for future studies based on experiences from this research.

- SBA15-NH-PMIDA has highly tuneable pores, which can be adjusted in terms of pore size, pore volume, and surface functionalization. Further analysis on this allows researchers to tailor this adsorbent to have specific characteristics that favour REE uptake, while excluding competing tri valant cations (Fe, Al) based on their size and chemical properties
- Functional ligands play a critical role in selectivity and the search for new ligands for the selective extraction of rare earth elements (REEs) is a promising area of study. This requires designing of ligands with specific properties, such as high affinity towards REEs, stability in various conditions, and compatibility with different extraction methods.

- Investigation into the synthesis and characterization of SBA15-NH-PMIDA integrated membranes for Acid Mine Drainage (AMD) treatment is a promising area of research. Understanding the structural properties, surface chemistry, and morphology of the membranes can provide insights into their adsorption capabilities and potential applications.

- Conducting pilot and field-scale studies to validate the laboratory results and assess the practicality and scalability of the developed adsorption processes is necessary. This will help bridge the gap between lab-scale research and real-world applications.

APPENDIX

Column experiment for Eu adsorption using granulated SBA15-NH-PMIDA

Application of granulated SBA15-NH-PMIDA in a column adsorption study was performed to develop a LDFA model for prediction of breakthrough curves at different operational conditions. The accuracy of the model was validated with experiments at different operational conditions. Since a similar study using granulated Cr-MIL-PMIDA is presented in chapter 5 of the thesis, findings of this study are given in the appendix.

Column experiments were conducted using upward flow, to study adsorption behaviors under various operating conditions. These experiments enable the analysis of design parameters such as flow rates, column heights, and influent concentrations on the adsorption breakthrough trends. Initial screening column experiment was carried out with inflow Eu concentration of 1 mg/l, flowrate of 1.39E-08 m^3/s and bed height of 0.1 m. Experiment was conducted for 20 hours, where samples were collected from the outlet at regular intervals and were then analysed for Eu concentration using ICP MS. Table A1 gives a summary of data collected. The Linear Driving Force Approximation (LDFA) model was adopted to describe the behaviour of Eu breakthrough curves. The model was developed using equations 5-11 to 5-15 and the equations were solved using the PDEPE function on Matlab. Table A2 presents the coefficients obtained from the analysis.

Table A.1: Raw data obtained from the preliminary column experiment for adsorption of Eu

(Inflow Eu Concentration 1 mg/l, flowrate 1.39E-08 m^3/s, bed height 0.1 m)

Time, hr	C_t	C_t/C_0
0.5	0.0014	0.0014
1	0.0062	0.0059
2	0.0094	0.0059
4	0.0298	0.0286
6	0.0667	0.0640
8	0.0545	0.0523
10	0.0980	0.0942
12	0.1267	0.1216
14	0.2200	0.2113
16	0.5887	0.5653
18	0.8842	0.8491
20	0.9842	0.9451

**Where C_t : concentration of Eu at outlet at time t, C_0 : Inflow Eu Concentration*

Table A.2: Parameters obtained from LDFA analysis

Parameters	**Unit**	**value**
Bed height	m	0.10
Bed diameter	m	0.01
Bed surface area	m^2	7.85E-05
Flow rate	m^3/s	1.39E-08
Linear velocity	m/s	1.77E-04
k_f	m/s	5.50E-05
Ds	m^2/s	4.00E-17
D_L (axial dispersion coefficient)	m^2/s	3.00E-06
C_0	mg/l	1.04

Modelling of single component breakthrough curve

Coefficients obtained from the preliminary column experiment were utilized to simulate breakthrough curves under different experimental conditions. In this study, multiple breakthrough curves were simulated for various system conditions, including initial feed concentration, flow rate, and the length of the fixed-bed column. These simulated curves were then compared with experimental results to evaluate the accuracy of the model. Figure A.1 presents the validation simulation curve obtained for initial experimental conditions given in table A.2.

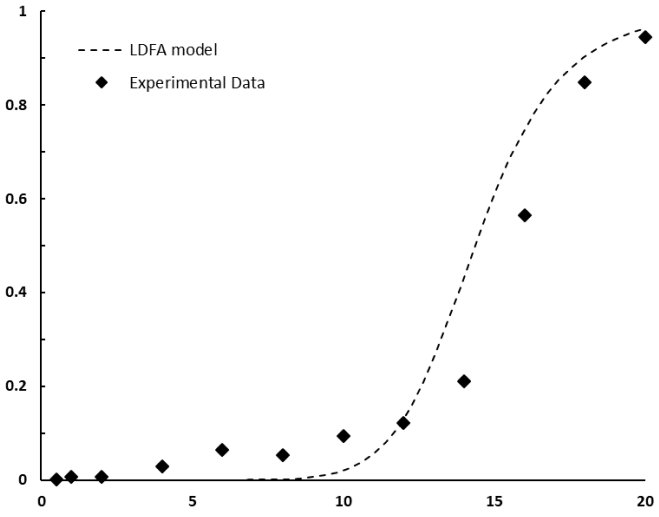

Figure A.1: Validation of single solute Eu breakthrough curve for granulated SBA15-NH-PMIDA

(Bed Length: 0.1m, Linear velocity 0.637 m/h, R^2=0.95)

As shown in figure A.1, experimental results provided a good fit for LDFA model. The

values for constants obtained from this model (Table A.2) were used to simulate various operating conditions

Analysis of the effect of initial concentration

Figure A.2 presents the experimental results and breakthrough curve obtained for initial Eu concentration of 3 mg/l. This value was selected based on the availability of Eu in AMD as presented in chapter 7. Remaining parameters were kept constant to assess the influence of concentration on the breakthrough curve (linear flow velocity 0.637 m/h, bed height of 0.1 m). R^2 value of 0.92 between the simulated and experimental data confirmed the accuracy of the model. As the initial concentration of Eu was increased, breakthrough curves developed a sharper profile and shifted to the left. This resulted in breakthrough times decreasing from 12 to less than 7 hours. Exhaustion time was also impacted, as it dropped to less than 10 hours upon doubling the influent Eu concentration.

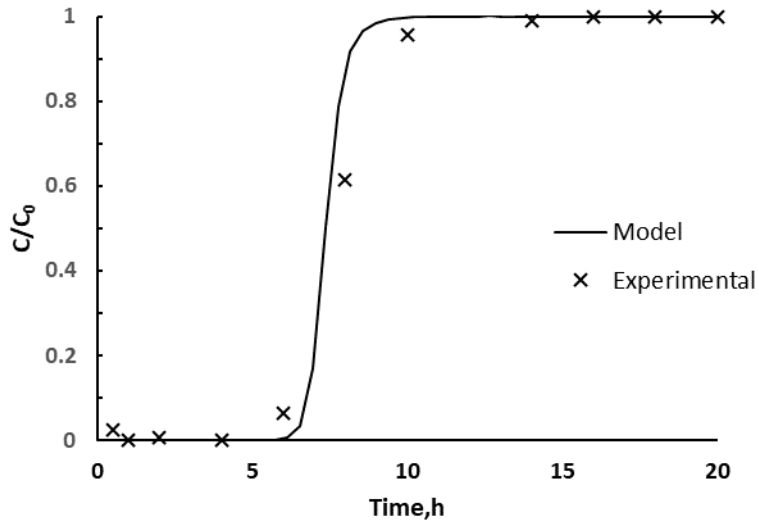

Figure A.2: Validation of simulation model for inlet concentration of 3 mg/l

(Bed Height: 0.1m, Linear velocity 0.637 m/h, R^2=0.92)

Analysis on the effect of flowrate

An experiment with higher flowrate (0.955 m/h) was conducted to analyse the effect of flowrate on the breakthrough curve. The R2 value of 0.91 shows that the experiment's data fits well with the simulation model (Figure A.3). Simulation of breakthrough curves at higher flowrates shows that the breakthrough times were shortened and the curves became steeper, indicating rapid saturation post-breakthrough. This is likely due to the shorter contact time between the adsorbate and adsorbent not being sufficient to reach equilibrium for granulated SBA15-NH-PMIDA.

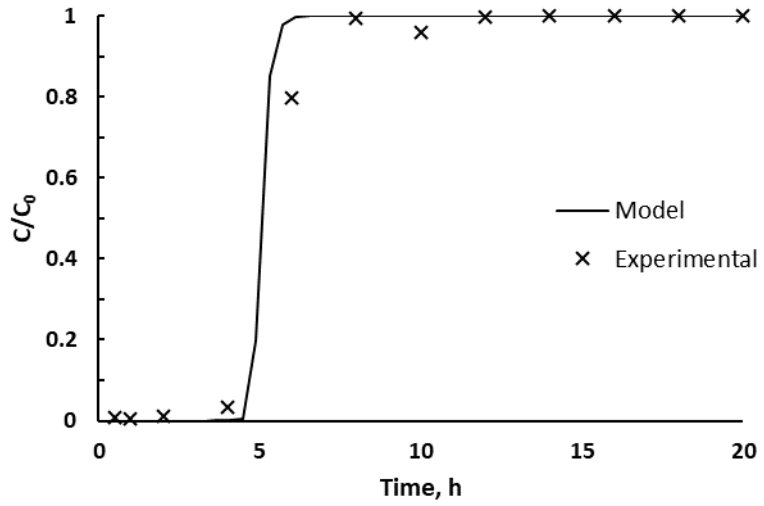

Figure A.3: Validation of simulation model for flow rate of 0.955 m/h

(Inlet concentration 3 mg/l, bed height 0.1 m, R^2=0.94)

Analysis on the effect of bed height

The depth of granulated adsorbent bed is a critical factor as found in chapter 7. To prove the model's accuracy, an experiment was conducted, with an inflow of 3 mg/l Eu, flow rate of 0.637 m/h and a bed depth of 12.5 cm (Figure A.4). The experimental results were consistent with the simulation model (R^2=0.91). Comparison of results shows that the curves shifted to the right and had higher breakthrough depths as the bed was increased from 10 cm to 12.5 cm, indicating that a larger assembled adsorbent yielded more binding sites for the Eu ions.

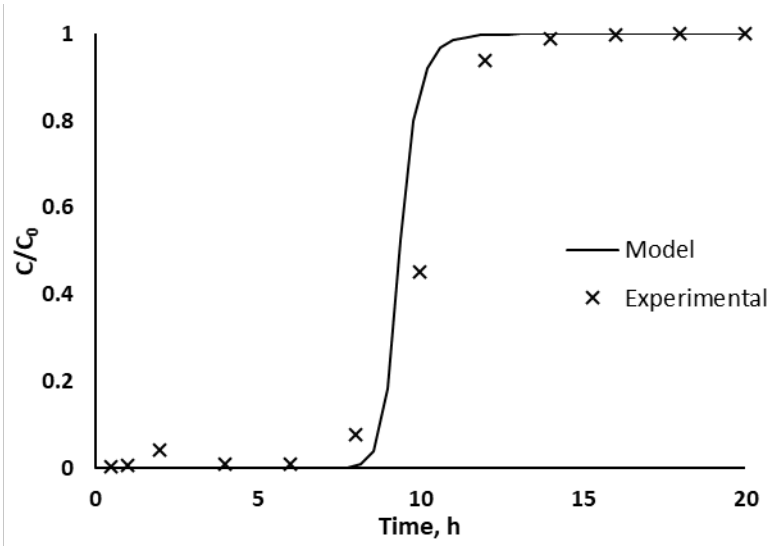

Figure A.4: Validation of simulation model for bed height of 0.125 m

(Inlet Concentration 3 mg/l, Linear velocity 0.637 m/h, R^2=0.91)

This study proves that a LDFA model can be successfully developed for Eu adsorption

on granulated SBA15-NH-PMIDA using one column experiment to find the axial dispersion coefficient and simulate breakthrough curves for varying operating conditions with the same value of the coefficient with high accuracy.

Conclusion

In this study, SBA15-NH-PMIDA was granulated using alginic acid and $CaCl_2$ for continuous adsorption of Eu in a fixed bed column. Physical and chemical characteristics of both powdered and granulated SBA15-NH-PMIDA were conducted and are presented in chapter 7. Results from a kinetic experiment using a single-component Eu solution was used to develop a fixed bed column breakthrough model. Axial dispersion coefficient was calculated using one column experiment and it was successfully applied to simulate breakthrough curves for other experimental conditions. Linear Driven Force Approximation (LDFA) model showed a good fit (R^2>0.91) for varying operational conditions. The successful application of the LDFA model proves that it is an effective tool to both simulate and optimise column experiments utilizing granulated SBA15-NH-PMIDA for Eu recovery

REFERENCES

Abdel-Magied, A. F., Abdelhamid, H. N., Ashour, R. M., Zou, X., & Forsberg, K. (2019). Hierarchical porous zeolitic imidazolate frameworks nanoparticles for efficient adsorption of rare-earth elements. *Microporous and Mesoporous Materials*, *278*, 175-184.

Abdel Maksoud, M. I. A., Sami, N. M., Hassan, H. S., Bekhit, M., & Ashour, A. H. (2022). Novel adsorbent based on carbon-modified zirconia/spinel ferrite nanostructures: Evaluation for the removal of cobalt and europium radionuclides from aqueous solutions. *Journal of Colloid and Interface Science*, *607*, 111-124.

Abreu, M., Batista, M., Magalhaes, M. C., & Matos, J. (2011). Acid mine drainage in the Portuguese Iberian Pyrite Belt. *Mine Drainage and Related Problems*, 71-118.

Agboola, O. (2019a). The role of membrane technology in acid mine water treatment: a review. *Korean Journal of Chemical Engineering*, *36*(9), 1389-1400.

Agboola, O. (2019b). The role of membrane technology in acid mine water treatment: a review. *Korean Journal of Chemical Engineering*, *36*, 1389-1400.

Aguado, J., Arsuaga, J. M., Arencibia, A., Lindo, M., & Gascón, V. (2009). Aqueous heavy metals removal by adsorption on amine-functionalized mesoporous silica. *Journal of Hazardous Materials*, *163*(1), 213-221.

Aguiar, A., Andrade, L., Pires, W., & Amaral, M. (2015). Effect of feed pH in the nanofiltration of gold acid mine drainage. *Agreeing on Solutions for More Sustainable Mine Water Management*, *1*, 1-10.

Aguiar, A. O., Andrade, L. H., Ricci, B. C., Pires, W. L., Miranda, G. A., & Amaral, M. C. S. (2016). Gold acid mine drainage treatment by membrane separation

processes: An evaluation of the main operational conditions. *Separation and Purification Technology*, *170*, 360-369.

Ahuchaogu, A. A., Chukwu, O. J., Obike, A., Igara, C. E., Nnorom, I. C., & Echeme, J. B. O. (2018). Reverse osmosis technology, its applications and nano-enabled membrane. *International Journal of Advanced Research in Chemical Science*, *5*(2), 20-26.

Akcil, A., & Koldas, S. (2006). Acid Mine Drainage (AMD): causes, treatment and case studies. *Journal of Cleaner Production*, *14*(12), 1139-1145.

Al-Amoudi, A., & Lovitt, R. W. (2007). Fouling strategies and the cleaning system of NF membranes and factors affecting cleaning efficiency. *Journal of Membrane Science*, *303*(1-2), 4-28.

Al-dhawi, B. N. S., Kutty, S. R. M., Baloo, L., Alawag, A. M., Almahbashi, N. M. Y., Naji, G. M. A., . . . Jagaba, A. H. (2023). Lithium adsorption from aqueous solution using aluminum hydroxide: Characterization, optimization by response surface methodology, kinetic modelling, and isotherm studies. *Case Studies in Chemical and Environmental Engineering*, *7*, 100350.

Al-Obaidani, S., Curcio, E., Macedonio, F., Di Profio, G., Al-Hinai, H., & Drioli, E. (2008). Potential of membrane distillation in seawater desalination: thermal efficiency, sensitivity study and cost estimation. *Journal of Membrane Science*, *323*(1), 85-98.

Ali, H. H., Mihsen, H. H., & Hussain, K. A. (2023). Synthesis, Characterization and Antimicrobial Studies of Modified Silica Materials Derived from Rice Husks. *BioNanoScience*, 1-14.

ALOthman, Z. A. (2012). A review: fundamental aspects of silicate mesoporous materials. *Materials*, *5*(12), 2874-2902.

Ambaye, T. G., Vaccari, M., Castro, F. D., Prasad, S., & Rtimi, S. (2020a). Emerging technologies for the recovery of rare earth elements (REEs) from the end-of-life electronic wastes: a review on progress, challenges, and perspectives. *Environmental Science and Pollution Research*, *27*(29), 36052-36074.

Ambaye, T. G., Vaccari, M., Castro, F. D., Prasad, S., & Rtimi, S. (2020b). Emerging technologies for the recovery of rare earth elements (REEs) from the end-of-life electronic wastes: a review on progress, challenges, and perspectives. *Environmental Science and Pollution Research*, 1-23.

Ambiado, K., Bustos, C., Schwarz, A., & Bórquez, R. (2016). Membrane technology applied to acid mine drainage from copper mining. *Water Science and Technology*, *75*(3), 705-715.

An, B., Lee, H., Lee, S., Lee, S.-H., & Choi, J.-W. (2015). Determining the selectivity of divalent metal cations for the carboxyl group of alginate hydrogel beads during competitive sorption. *Journal of Hazardous Materials*, *298*, 11-18.

Anastopoulos, I., Bhatnagar, A., & Lima, E. C. (2016). Adsorption of rare earth metals: A review of recent literature. *Journal of Molecular Liquids*, *221*, 954-962.

Anastopoulos, I., Bhatnagar, A., & Lima, E. C. (2016). Adsorption of rare earth metals: a review of recent literature. *J Mol Liq*, *221*.

Andrade, L., Aguiar, A., Pires, W., Miranda, G., Teixeira, L., Almeida, G., & Amaral, M. (2017). Nanofiltration and reverse osmosis applied to gold mining effluent treatment and reuse. *Brazilian Journal of Chemical Engineering*, *34*, 93-107.

Arai, Y., & Sparks, D. L. (2001). ATR–FTIR Spectroscopic Investigation on Phosphate Adsorption Mechanisms at the Ferrihydrite–Water Interface. *Journal of Colloid and Interface Science*, *241*(2), 317-326.

Azad, P., & Nesa, N. (2008). Studies on trace metal levels in soil and water of Tipong, Tirap and Tikak collieries of Makum Coal Field, Tinsukia, Assam. *Poll Res.*, *27*, 237-239.

Babaee, S., Zarei, M., Sepehrmansourie, H., Zolfigol, M. A., & Rostamnia, S. (2020). Synthesis of metal–organic frameworks MIL-101 (Cr)-NH2 containing phosphorous acid functional groups: Application for the synthesis of N-Amino-2-pyridone and pyrano [2, 3-c] pyrazole derivatives via a cooperative vinylogous anomeric-based oxidation. *ACS omega*, *5*(12), 6240-6249.

Bagheripour, E., Moghadassi, A., Parvizian, F., Hosseini, S., & Van der Bruggen, B. (2019). Tailoring the separation performance and fouling reduction of PES based nanofiltration membrane by using a PVA/Fe3O4 coating layer. *Chemical Engineering Research and Design*, *144*, 418-428.

Bahadori, M., Marandi, A., Tangestaninejad, S., Moghadam, M., Mirkhani, V., & Mohammadpoor-Baltork, I. (2020). Ionic Liquid-Decorated MIL-101 (Cr) via Covalent and Coordination Bonds for Efficient Solvent-Free CO2 Conversion and CO2 Capture at Low Pressure. *The Journal of Physical Chemistry C*, *124*(16), 8716-8725.

Balaram, V. (2019). Rare earth elements: A review of applications, occurrence, exploration, analysis, recycling, and environmental impact. *Geoscience Frontiers*, *10*(4), 1285-1303.

Binaeian, E., Maleki, S., Motaghedi, N., & Arjmandi, M. (2020). Study on the performance of Cd2+ sorption using dimethylethylenediamine-modified zinc-based MOF (ZIF-8-mmen): optimization of the process by RSM technique. *Separation Science and Technology*, *55*(15), 2713-2728.

Binnemans, K., Jones, P. T., Blanpain, B., Van Gerven, T., & Pontikes, Y. (2015). Towards zero-waste valorisation of rare-earth-containing industrial process residues: a critical review. *Journal of Cleaner Production*, *99*, 17-38.

Binnemans, K., Jones, P. T., Blanpain, B., Van Gerven, T., Yang, Y., Walton, A., & Buchert, M. (2013). Recycling of rare earths: a critical review. *Journal of Cleaner Production*, *51*, 1-22.

Blengini, G. A., Nuss, P., Dewulf, J., Nita, V., Peirò, L. T., Vidal-Legaz, B., . . . Pennington, D. (2017). EU methodology for critical raw materials assessment: Policy needs and proposed solutions for incremental improvements. *Resources Policy*, *53*, 12-19.

Bonneau, M., Lavenn, C., Ginet, P., Otake, K.-i., & Kitagawa, S. (2020). Upscale synthesis of a binary pillared layered MOF for hydrocarbon gas storage and separation. *Green Chemistry*, *22*(3), 718-724.

Borra, C. R., Blanpain, B., Pontikes, Y., Binnemans, K., & Van Gerven, T. (2016a). Recovery of Rare Earths and Other Valuable Metals From Bauxite Residue (Red Mud): A Review. *Journal of Sustainable Metallurgy*, *2*(4), 365-386.

Borra, C. R., Blanpain, B., Pontikes, Y., Binnemans, K., & Van Gerven, T. (2016b). Smelting of bauxite residue (red mud) in view of iron and selective rare earths recovery. *Journal of Sustainable Metallurgy*, *2*(1), 28-37.

Brehant, A., Bonnelye, V., & Perez, M. (2002). Comparison of MF/UF pretreatment with conventional filtration prior to RO membranes for surface seawater desalination. *Desalination*, *144*(1-3), 353-360.

Brion-Roby, R., Gagnon, J., Deschênes, J.-S., & Chabot, B. (2018). Investigation of fixed bed adsorption column operation parameters using a chitosan material for treatment of arsenate contaminated water. *Journal of Environmental Chemical Engineering*, *6*(1), 505-511.

Bwapwa, J. K. (2018). A review of acid mine drainage in a water-scarce country: case of South Africa. *Environ. Manag. Sustain. Dev*, *7*, 1-20.

Callegari, A., Boguniewicz-Zablocka, J., & Capodaglio, A. G. (2017). Experimental application of an advanced separation process for NOM removal from surface drinking water supply. *Separations*, *4*(4), 32.

Callura, J., Perkins, K., Noack, C., Washburn, N., Dzombak, D., & Karamalidis, A. (2018). Selective Adsorption of Rare Earth Elements onto Functionalized Silica Particles. *Green Chemistry*, *20*.

Caraballo, M. A., Rötting, T. S., Macías, F., Nieto, J. M., & Ayora, C. (2009). Field multi-step limestone and MgO passive system to treat acid mine drainage with high metal concentrations. *Applied Geochemistry*, *24*(12), 2301-2311.

Cardoso, C. M. M., Zavarize, D. G., Lago, P. d. A., Pedroza, M. M., Brum, S. S., & Mendonça, A. R. V. (2019). Evaluating adsorbent properties of drinking water treatment plant sludge-based carbons activated by K2CO3/CH3COOH: a low-cost material for metal ion remediation. *SN Applied Sciences*, *1*(7), 686.

Cashin, V., Eldridge, D., Zhao, D., & Yu, A. (2017). Surface functionalization and manipulation of mesoporous silica adsorbents for improved removal of pollutants: A Review. *Environ. Sci.: Water Res. Technol.*, *4*.

Chang, F.-Y., Chao, K.-J., Cheng, H.-H., & Tan, C.-S. (2009). Adsorption of CO2 onto amine-grafted mesoporous silicas. *Separation and Purification Technology*, *70*(1), 87-95.

Chen, T., Yan, B., Lei, C., & Xiao, X. (2014). Pollution control and metal resource recovery for acid mine drainage. *Hydrometallurgy*, *147-148*, 112-119.

Chen, W., Wang, L., Zhuo, M., Wang, Y., Fu, S., Li, Y., & Wu, S. (2014). Reusable colloidal graphene oxide suspensions combined with dialysis bags for recovery of trace Y (III) from aqueous solutions. *RSC Adv*, *4*.

Chen, X., Luo, C., Zhang, J., Kong, J., & Zhou, T. (2015). Sustainable recovery of metals from spent lithium-ion batteries: a green process. *ACS Sustainable Chemistry & Engineering*, *3*(12), 3104-3113.

Chen, Y., Zhai, B., Liang, Y., & Li, Y. (2020). Hybrid photocatalysts using semiconductor/MOF/graphene oxide for superior photodegradation of organic pollutants under visible light. *Materials Science in Semiconductor Processing*, *107*, 104838.

Chen, Z., Li, Z., Chen, J., Kallem, P., Banat, F., & Qiu, H. (2022). Recent advances in selective separation technologies of rare earth elements: A review. *Journal of Environmental Chemical Engineering*, *10*(1), 107104.

Cheng, S., Oatley, D. L., Williams, P. M., & Wright, C. J. (2012). Characterisation and application of a novel positively charged nanofiltration membrane for the treatment of textile industry wastewaters. *Water research*, *46*(1), 33-42.

Chu, J.-H., Kang, J.-K., Park, S.-J., & Lee, C.-G. (2020). Application of the anion-exchange resin as a complementary technique to remove residual cyanide complexes in industrial plating wastewater after conventional treatment. *Environmental Science and Pollution Research*, *27*(33), 41688-41701.

Clyde, E. J., Champagne, P., Jamieson, H. E., Gorman, C., & Sourial, J. (2016). The use of a passive treatment system for the mitigation of acid mine drainage at the Williams Brothers Mine (California): pilot-scale study. *Journal of Cleaner Production*, *130*, 116-125.

Commission, E. (2014). Report on critical raw materials for the EU: Report of the ad-hoc working group on defining critical raw materials, May 2014, 41 pp.

Commission, E. (2017). Communication from the commission to the European parliament, the council, the European economic and social committee and the committee of the regions on the 2017 list of Critical Raw Materials for the EU, Brussels, 13.9.2017.

Cozzolino, D., Chandra, S., Roberts, J., Power, A., Rajapaksha, P., Ball, N., . . . Chapman, J. (2017). There is gold in them hills: Predicting potential acid mine drainage events through the use of chemometrics. *Science of The Total Environment*, *619*.

Cruz-Olivares, J., Pérez-Alonso, C., Barrera-Díaz, C., Ureña-Nuñez, F., Chaparro-Mercado, M. C., & Bilyeu, B. (2013). Modeling of lead (II) biosorption by residue of allspice in a fixed-bed column. *Chemical Engineering Journal*, *228*, 21-27.

Da'na, E. (2017). Adsorption of heavy metals on functionalized-mesoporous silica: A review. *Microporous and Mesoporous Materials*, *247*, 145-157.

Da'na, E., & Sayari, A. (2012). Adsorption of heavy metals on amine-functionalized SBA-15 prepared by co-condensation: Applications to real water samples. *Desalination*, *285*, 62-67.

da Luz, C., Ulson, S. M. d. A. G., de Souza, A. A. U., Dervanoski, A., Moraes, A. d. O. S., & Wood, B. D. (2018). A multiscale model for carbon adsorption of BTX compounds: Comparison of volume averaging theory and experimental measurements. *Chemical Engineering Science*, *184*, 285-308.

Dapaah, M. F., Liu, B., & Cheng, L. (2021). Adsorption of organic compounds from aqueous solution by pyridine-2-carboxaldehyde grafted MIL-101(Cr)-NH2 metal-organic frameworks. *Journal of Environmental Chemical Engineering*, *9*(4), 105275.

Das, N., & Das, D. (2013). Recovery of rare earth metals through biosorption: an overview. *Journal of Rare Earths*, *31*(10), 933-943.

Davis, A., & Ashenberg, D. (1989). The aqueous geochemistry of the Berkeley Pit, Butte, Montana, U.S.A. *Applied Geochemistry*, *4*(1), 23-36.

Dias, E. M., & Petit, C. (2015). Towards the use of metal–organic frameworks for water reuse: a review of the recent advances in the field of organic pollutants removal and degradation and the next steps in the field. *Journal of Materials Chemistry A*, *3*(45), 22484-22506.

Dolatyari, L., Yaftian, M. R., & Rostamnia, S. (2016). Adsorption characteristics of Eu(III) and Th(IV) ions onto modified mesoporous silica SBA-15 materials. *Journal of the Taiwan Institute of Chemical Engineers*, *60*, 174-184.

Dold, B. (2013). ChemInform Abstract: Basic Concepts in Environmental Geochemistry of Sulfidic Mine-Waste Management. In (Vol. 44).

Dousti, Z., Dolatyari, L., Yaftian, M. R., & Rostamnia, S. (2019). Adsorption of Eu (III), Th (IV), and U (VI) by mesoporous solid materials bearing sulfonic acid and sulfamic acid functionalities. *Separation Science and Technology*, *54*(16), 2609-2624.

Dow, N., et al. (2016). Pilot trial of membrane distillation driven by low grade waste heat: Membrane fouling and energy assessment. *Desalination, 391*, 30-42. doi:https://doi.org/10.1016/j.desal.2016.01.023

Dupont, D., Luyten, J., Bloemen, M., Verbiest, T., & Binnemans, K. (2014). Acid-Stable Magnetic Core–Shell Nanoparticles for the Separation of Rare Earths. *Industrial & Engineering Chemistry Research*, *53*(39), 15222-15229.

Dutta, T., Kim, K.-H., Uchimiya, M., Kwon, E. E., Jeon, B.-H., Deep, A., & Yun, S.-T. (2016). Global demand for rare earth resources and strategies for green mining. *Environmental Research*, *150*, 182-190.

Earle A. Ripley, R. E. R., Adele A. Crowder. (1995). A Review of: "Environmental Effects of Mining (1995):" Earle A. Ripley, Robert E. Redmann, Adele A. Crowder, St. Lucie Press, Delray Beach, Florida 33483 USA. *International Journal of Surface Mining, Reclamation and Environment*, *9*(4), III-III.

Edraki, M., Golding, S., Baublys, K., & Mg, L. (2005). Hydrochemistry, mineralogy and sulfur isotope geochemistry of acid mine drainage at the Mt. Morgan mine environment, Queensland, Australia. *Applied Geochemistry*, *20*, 789-805.

Efome, J. E., Rana, D., Matsuura, T., & Lan, C. Q. (2018). Insight studies on metal-organic framework nanofibrous membrane adsorption and activation for heavy metal ions removal from aqueous solution. *ACS Applied Materials & Interfaces*, *10*(22), 18619-18629.

El-Nahhal, I. M., Salem, J. K., Tabasi, N. S., Hempelmann, R., & Kodeh, F. S. (2018). Synthesis and structural characterization of ZnO-and CuO-NPs supported mesoporous silica materials (hexagonal SBA-15 and lamellar-SiO2). *Chemical Physics Letters*, *691*, 211-218.

Elmorsi, T. M. (2011). Equilibrium isotherms and kinetic studies of removal of methylene blue dye by adsorption onto miswak leaves as a natural adsorbent. *Journal of Environmental Protection*, *2*(06), 817.

Elsaidi, S. K., Sinnwell, M. A., Devaraj, A., Droubay, T. C., Nie, Z., Murugesan, V., . . . Thallapally, P. K. (2018). Extraction of rare earth elements using magnetite@ MOF composites. *Journal of Materials Chemistry A*, *6*(38), 18438-18443.

Fee, J. A., Gaudette, H. E., Lyons, W. B., & Long, D. T. (1992). Rare-earth element distribution in Lake Tyrrell groundwaters, Victoria, Australia. *Chemical Geology*, *96*(1), 67-93.

Felipe, E. C. B., Batista, K. A., & Ladeira, A. C. Q. (2020). Recovery of rare earth elements from acid mine drainage by ion exchange. *Environ Technol*, 1-12.

Feng, D., Aldrich, C., & Tan, H. (2000). Treatment of acid mine water by use of heavy metal precipitation and ion exchange. *Minerals Engineering*, *13*(6), 623-642.

Fonseka, C., Ryu, S., Choo, Y., Mullett, M., Thiruvenkatachari, R., Naidu, G., & Vigneswaran, S. (2021). Selective Recovery of Rare Earth Elements from Mine Ore by Cr-MIL Metal–Organic Frameworks. *ACS Sustainable Chemistry & Engineering*, *9*(50), 16896-16904.

Fonseka, C., Ryu, S., Naidu, G., Kandasamy, J., & Vigneswaran, S. (2022). Recovery of water and valuable metals using low pressure nanofiltration and sequential adsorption from acid mine drainage. *Environmental Technology & Innovation*, *28*, 102753.

Foureaux, A. F. S., Moreira, V. R., Lebron, Y. A. R., Santos, L. V. S., & Amaral, M. C. S. (2020). Direct contact membrane distillation as an alternative to the conventional methods for value-added compounds recovery from acidic effluents: A review. *Separation and Purification Technology*, *236*, 116251.

Furukawa, H., Cordova, K. E., O'Keeffe, M., & Yaghi, O. M. (2013). The chemistry and applications of metal-organic frameworks. *Science*, *341*(6149).

Gad, H., & Awwad, N. (2007). Factors affecting on the sorption/desorption of Eu (III) using activated carbon. *Separation Science and Technology*, *42*(16), 3657-3680.

Gaikwad, D. R., S.A, M., Dhirendra, & D.V, G. (2009). REMOVAL OF COPPER IONS FROM ACID MINE DRAINAGE (AMD) BY ION EXCHANGE RESINS: INDION 820 AND INDION 850. *Journal of Applied Sciences in Environmental Sanitation*.

García-Mateos, F. J., Ruiz-Rosas, R., Marqués, M. D., Cotoruelo, L. M., Rodríguez-Mirasol, J., & Cordero, T. (2015). Removal of paracetamol on biomass-derived activated carbon: Modeling the fixed bed breakthrough curves using batch adsorption experiments. *Chemical Engineering Journal*, *279*, 18-30.

Gault, A. G., Cooke, D. R., Townsend, A. T., Charnock, J. M., & Polya, D. A. (2005). Mechanisms of arsenic attenuation in acid mine drainage from Mount Bischoff, western Tasmania. *Science of The Total Environment*, *345*(1), 219-228.

Ghosh, A., & Das, G. (2020). Green synthesis of Sn (II)-BDC MOF: Preferential and efficient adsorption of anionic dyes. *Microporous and Mesoporous Materials*, *297*, 110039.

Gillmor, A. M. (2011). Attenuation of acid mine drainage enhanced by organic carbon and limestone addition: a process characterization.

Gomaa, E. A., Negm, A., & Tahoon, M. A. (2017). Conductometric and volumetric study of copper sulphate in aqueous ethanol solutions at different temperatures. *Journal of Taibah University for Science*, *11*(5), 741-748.

Gonzalez, V., Vignati, D. A., Leyval, C., & Giamberini, L. (2014). Environmental fate and ecotoxicity of lanthanides: are they a uniform group beyond chemistry? *Environ Int*, *71*, 148-157.

Goodenough, K., Wall, F., & Merriman, D. (2017). The Rare Earth Elements: Demand, Global Resources, and Challenges for Resourcing Future Generations. *Natural Resources Research*.

Guo, J., Fan, X., Wang, J., Yu, S., Laipan, M., Ren, X., . . . Li, Y. (2021). Highly efficient and selective recovery of Au (III) from aqueous solution by Bisthiourea

immobilized UiO-66-NH2: performance and mechanisms. *Chemical Engineering Journal*, 130588.

Hakami, M. W., Alkhudhiri, A., Al-Batty, S., Zacharof, M.-P., Maddy, J., & Hilal, N. (2020). Ceramic microfiltration membranes in wastewater treatment: Filtration behavior, fouling and prevention. *Membranes*, *10*(9), 248.

Hao, Y., Ma, H., Wang, Q., Zhu, C., & He, A. (2022). Complexation behaviour and removal of organic-Cr (III) complexes from the environment: A review. *Ecotoxicology and Environmental Safety*, *240*, 113676.

Hasankola, Z. S., Rahimi, R., Shayegan, H., Moradi, E., & Safarifard, V. (2020). Removal of Hg2+ heavy metal ion using a highly stable mesoporous porphyrinic zirconium metal-organic framework. *Inorganica Chimica Acta*, *501*, 119264.

Hatanaka, T., Matsugami, A., Nonaka, T., Takagi, H., Hayashi, F., Tani, T., & Ishida, N. (2017). Rationally designed mineralization for selective recovery of the rare earth elements. *Nature communications*, *8*(1), 1-10.

Hatch, G. P. (2012). Dynamics in the Global Market for Rare Earths. *Elements*, *8*(5), 341.

Hennebel, T., Boon, N., Maes, S., & Lenz, M. (2015). Biotechnologies for critical raw material recovery from primary and secondary sources: R&D priorities and future perspectives. *New Biotechnology*, *32*(1), 121-127.

Hu, Drouin, E., Larivière, D., Kleitz, F., & Fontaine, F.-G. (2017). Highly Efficient and Selective Recovery of Rare Earth Elements Using Mesoporous Silica Functionalized by Pre-Organized Chelating Ligands. *ACS Applied Materials & Interfaces*, *9*, 38584-38593.

Hu, B., Hu, Q., Li, X., Pan, H., Tang, X., Chen, C., & Huang, C. (2017). Rapid and highly efficient removal of Eu(III) from aqueous solutions using graphene oxide. *Journal of Molecular Liquids*, *229*, 6-14.

Hu, J., Chen, G., & Lo, I. M. C. (2006). Selective Removal of Heavy Metals from Industrial Wastewater Using Maghemite Nanoparticle: Performance and Mechanisms. *Journal of Environmental Engineering*, *132*(7), 709-715.

Hu, Y., Drouin, E., Larivière, D., Kleitz, F., & Fontaine, F.-G. (2017). Highly Efficient and Selective Recovery of Rare Earth Elements Using Mesoporous Silica Functionalized by Preorganized Chelating Ligands. *ACS Applied Materials & Interfaces*, *9*(44), 38584-38593.

Huang, Li, Z.-J., Zheng, L.-R., Wu, W.-S., Chai, Z.-F., & Shi, W.-Q. (2019). Adsorption of Eu(III) and Th(IV) on three-dimensional graphene-based macrostructure studied by spectroscopic investigation. *Environmental Pollution*, *248*, 82-89.

Huang, J., Yuan, F., Zeng, G., Li, X., Gu, Y., Shi, L., . . . Shi, Y. (2017). Influence of pH on heavy metal speciation and removal from wastewater using micellar-enhanced ultrafiltration. *Chemosphere*, *173*, 199-206.

Huang, Y., Han, G., Liu, J., Chai, W., Wang, W., Yang, S., & Su, S. (2016). A stepwise recovery of metals from hybrid cathodes of spent Li-ion batteries with leaching-flotation-precipitation process. *Journal of Power Sources*, *325*, 555-564.

Hull, E. J., & Zodrow, K. R. (2017). Acid rock drainage treatment using membrane distillation: impacts of chemical-free pretreatment on scale formation, pore wetting, and product water quality. *Environmental Science & Technology*, *51*(20), 11928-11934.

Iftekhar, S., Srivastava, V., Casas, A., & Sillanpää, M. (2018). Synthesis of novel GA-g-PAM/SiO2 nanocomposite for the recovery of rare earth elements (REE) ions from aqueous solution. *Journal of Cleaner Production*, *170*, 251-259.

Ijaz, A., Yagci, M. B., Ow-Yang, C. W., Demirel, A. L., & Miko, A. (2020). Formation of mesoporous silica particles with hierarchical morphology. *Microporous and Mesoporous Materials*, *303*, 110240.

Inglezakis, V. J., Fyrillas, M. M., & Park, J. (2019). Variable diffusivity homogeneous surface diffusion model and analysis of merits and fallacies of simplified adsorption kinetics equations. *Journal of Hazardous Materials*, *367*, 224-245.

Inglezakis, V. J., Fyrillas, M. M., & Stylianou, M. A. (2018). Two-phase homogeneous diffusion model for the fixed bed sorption of heavy metals on natural zeolites. *Microporous and Mesoporous Materials*, *266*, 164-176.

Interior, U. D. o. (2018). Final List of Critical Minerals 2018. Office of the Federal Register, National Archives and Records Administration, 83(97): 23295–23296.

Jamil, S., Loganathan, P., Kandasamy, J., Ratnaweera, H., & Vigneswaran, S. (2021). Comparing nanofiltration membranes effectiveness for inorganic and organic compounds removal from a wastewater-reclamation plant's micro-filtered water. *Materials Today: Proceedings*.

Jana, S., Trivedi, M. K., Tallapragada, R. M., Branton, A., Trivedi, D., Nayak, G., & Mishra, R. (2015). Characterization of physicochemical and thermal properties of chitosan and sodium alginate after biofield treatment. *Pharmaceutica Analytica Acta*, *6*(10).

Jeong, S., Song, K. G., Kim, J., Shin, J., Maeng, S. K., & Park, J. (2021). Feasibility of membrane distillation process for potable water reuse: A barrier for dissolved organic matters and pharmaceuticals. *Journal of Hazardous Materials*, *409*, 124499.

Jiang, L., Zhang, W., Luo, C., Cheng, D., & Zhu, J. (2016). Adsorption toward trivalent rare earth element from aqueous solution by zeolitic imidazolate frameworks. *Industrial & Engineering Chemistry Research*, *55*(22), 6365-6372.

Kalam, S., Abu-Khamsin, S. A., Kamal, M. S., & Patil, S. (2021). Surfactant Adsorption Isotherms: A Review. *ACS omega*, *6*(48), 32342-32348.

Kalin, M., Fyson, A., & Wheeler, W. N. (2006). The chemistry of conventional and alternative treatment systems for the neutralization of acid mine drainage. *Science of The Total Environment*, *366*(2), 395-408.

Kavun, V., van der Veen, M. A., & Repo, E. (2021). Selective recovery and separation of rare earth elements by organophosphorus modified MIL-101 (Cr). *Microporous and Mesoporous Materials*, *312*, 110747.

Kefeni, K. K., Msagati, T. A. M., & Mamba, B. B. (2017). Acid mine drainage: Prevention, treatment options, and resource recovery: A review. *Journal of Cleaner Production*, *151*, 475-493.

Kesieme, U. K., Milne, N., Aral, H., Cheng, C. Y., & Duke, M. (2013). Economic analysis of desalination technologies in the context of carbon pricing, and opportunities for membrane distillation. *Desalination*, *323*, 66-74.

Kesieme, U. K., Milne, N., Cheng, C. Y., Aral, H., & Duke, M. (2014). Recovery of water and acid from leach solutions using direct contact membrane distillation. *Water Science and Technology*, *69*(4), 868-875.

Khawassek, Y. M., Eliwa, A. A., Haggag, E. S. A., Omar, S. A., & Abdel-Wahab, S. M. (2019). Adsorption of rare earth elements by strong acid cation exchange resin thermodynamics, characteristics and kinetics. *SN Applied Sciences*, *1*, 1-11.

Kim, J., Balathanigaimani, M., & Moon, H. (2015). Adsorptive Removal of Nitrate and Phosphate Using MCM-48, SBA-15, Chitosan, and Volcanic Pumice. *Water, Air, & Soil Pollution*, *226*.

Kim, S.-H., Ngo, H. H., Shon, H., & Vigneswaran, S. (2008). Adsorption and photocatalysis kinetics of herbicide onto titanium oxide and powdered activated carbon. *Separation and Purification Technology*, *58*(3), 335-342.

Korotta-Gamage, S. M., & Sathasivan, A. (2017). A review: Potential and challenges of biologically activated carbon to remove natural organic matter in drinking water purification process. *Chemosphere*, *167*, 120-138.

Kumari, A., Jha, M. K., Pathak, D. D., Chakravarty, S., & Lee, J.-c. (2019). Processes developed for the separation of europium (Eu) from various resources. *Separation & Purification Reviews*, *48*(2), 91-121.

Labidi, N. (2008). Studies of the mechanism of polyvinyl alcohol adsorption on the calcite/water interface in the presence of sodium oleate. *Journal of Minerals and Materials Characterization and engineering*, *7*(02), 147.

Lakshtanov, L., & Stipp, S. (2004). Experimental study of europium (III) coprecipitation with calcite. *Geochimica et Cosmochimica Acta*, *68*(4), 819-827.

Lazareva, E., Myagkaya, I., Kirichenko, I., Gustaytis, M., & Zhmodik, S. (2019). Interaction of natural organic matter with acid mine drainage: In-situ accumulation of elements. *Science of The Total Environment*, *660*, 468-483.

Lèbre, É., Corder, G., & Golev, A. (2017). The role of the mining industry in a circular economy: a framework for resource management at the mine site level. *Journal of Industrial Ecology*, *21*(3), 662-672.

Lecomte, K. L., Sarmiento, A., Borrego, J., & Nieto, J. (2017). Rare earth elements mobility processes in an AMD-affected estuary: Huelva Estuary (SW Spain). *Marine pollution bulletin*, *121*(1-2), 282-291.

Lecomte, K. L., Sarmiento, A. M., Borrego, J., & Nieto, J. M. (2017). Rare earth elements mobility processes in an AMD-affected estuary: Huelva Estuary (SW Spain). *Marine Pollution Bulletin*, *121*(1), 282-291.

Lee, J. S., & Chon, H. T. (2006). Hydrogeochemical characteristics of acid mine drainage in the vicinity of an abandoned mine, Daduk Creek, Korea. *Journal of Geochemical Exploration*, *88*(1), 37-40.

Lee, S., & Lueptow, R. M. (2001). Reverse osmosis filtration for space mission wastewater: membrane properties and operating conditions. *Journal of Membrane Science*, *182*(1-2), 77-90.

Lee, Y.-R., Yu, K., Ravi, S., & Ahn, W.-S. (2018). Selective adsorption of rare earth elements over functionalized Cr-MIL-101. *ACS Applied Materials & Interfaces*, *10*(28), 23918-23927.

Lei, L.-q., Song, C.-a., Xie, X.-l., & Li, Y.-h. (2008). REE behavior and effect factors in AMD-type acidic groundwater at sulfide tailings pond, BS nickel mine, W.A. *Transactions of Nonferrous Metals Society of China*, *18*(4), 955-961.

Li, C., Zhuang, Z., Huang, F., Wu, Z., Hong, Y., & Lin, Z. (2013). Recycling rare earth elements from industrial wastewater with flowerlike nano-Mg (OH) 2. *ACS Applied Materials & Interfaces*, *5*(19), 9719-9725.

Li, G.-M., Liang, Z.-G., Liu, Y., Li, J.-H., Pan, J., & Han, S.-D. (2023). Ligand Tailoring and Functional Group Fusion Strategy for Developing Photochromic Compounds: A Case Study for Pyridinedicarboxylic Acid. *Crystal Growth & Design*, *23*(4), 2182-2189.

Li, H., Eksteen, J., & Oraby, E. (2018). Hydrometallurgical recovery of metals from waste printed circuit boards (WPCBs): Current status and perspectives–A review. *Resources, Conservation and Recycling*, *139*, 122-139.

Li, J., Qi, T., Wang, L., Liu, C., & Zhang, Y. (2007). Synthesis and characterization of imidazole-functionalized SBA-15 as an adsorbent of hexavalent chromium. *Materials Letters*, *61*(14-15), 3197-3200.

Li, L., Qu, W., Zhang, X., Lu, J., Chen, R., Wu, F., & Amine, K. (2015). Succinic acid-based leaching system: a sustainable process for recovery of valuable metals from spent Li-ion batteries. *Journal of Power Sources*, *282*, 544-551.

Li, M., Liu, H., Chen, T., Hayat, T., Alharbi, N. S., & Chen, C. (2017). Adsorption of Europium on Al-substituted goethite. *Journal of Molecular Liquids*, *236*, 445-451.

Li, R., Tian, X., Ashraf, I., & Chen, B. (2020). Fluoride removal using a chelating resin containing phosphonic-sulfonic acid bifunctional group. *Journal of Chromatography A*, *1613*, 460697.

Li, S.-C., Kim, S.-C., Kang, C.-S., Kim, C.-J., & Kang, C.-J. (2018). Separation of samarium, europium and gadolinium in high purity using photochemical reduction-extraction chromatography. *Hydrometallurgy*, *178*, 181-187.

Li, Z.-Q., Yang, J.-C., Sui, K.-W., & Yin, N. (2015). Facile synthesis of metal-organic framework MOF-808 for arsenic removal. *Materials Letters*, *160*, 412-414.

Lim, C.-R., Lin, S., & Yun, Y.-S. (2020). Highly efficient and acid-resistant metal-organic frameworks of MIL-101 (Cr)-NH2 for Pd (II) and Pt (IV) recovery from acidic solutions: Adsorption experiments, spectroscopic analyses, and theoretical computations. *Journal of Hazardous Materials*, *387*, 121689.

Lin, X., Huang, Q., Qi, G., Shi, S., Xiong, L., Huang, C., . . . Chen, X. (2017). Estimation of fixed-bed column parameters and mathematical modeling of breakthrough behaviors for adsorption of levulinic acid from aqueous solution using SY-01 resin. *Separation and Purification Technology*, *174*, 222-231.

Liu, B., Peng, Y., & Chen, Q. (2016). Adsorption of N/S-heteroaromatic compounds from fuels by functionalized MIL-101 (Cr) metal–organic frameworks: the impact of surface functional groups. *Energy & Fuels*, *30*(7), 5593-5600.

Liu, H., Zhang, X., Hou, L., Zheng, H., Niu, B., Weng, K., . . . Fu, J. (2023). Nitrogen-rich hierarchical porous polyphosphazene for rapid and efficient adsorption of anionic contaminants: Kinetics, isotherm, thermodynamics and mechanism. *Applied Surface Science*, *616*, 156538.

Liu, P., Huang, R., & Tang, Y. (2019). Comprehensive Understandings of Rare Earth Element (REE) Speciation in Coal Fly Ashes and Implication for REE Extractability. *Environmental Science & Technology*, *53*(9), 5369-5377.

Liu, T., & Chen, J. (2021). Extraction and separation of heavy rare earth elements: A review. *Separation and Purification Technology*, *276*, 119263.

López, J., Gibert, O., & Cortina, J. (2021). Integration of membrane technologies to enhance the sustainability in the treatment of metal-containing acidic liquid wastes. An overview. *Separation and Purification Technology*, *265*, 118485.

López, M., González, I., & Romero, A. (2008). Trace elements contamination of agricultural soils affected by sulphide exploitation (Iberian Pyrite Belt, Sw Spain). *Environmental Geology*, *54*(4), 805-818.

Lou, Z., Xiao, X., Huang, M., Wang, Y., Xing, Z., & Xiong, Y. (2019). Acrylic Acid-Functionalized Metal–Organic Frameworks for Sc (III) Selective Adsorption. *ACS Applied Materials & Interfaces*, *11*(12), 11772-11781.

Lu, H., Zhang, Q., Dong, Y., Li, J., & Zhang, X. (2016). The adsorption capacity, pore structure, and thermal behavior of the modified clay containing SSA. *Advances in Materials Science and Engineering*, *2016*.

Lu, L., Zou, S., & Fang, B. (2021). The Critical Impacts of Ligands on Heterogeneous Nanocatalysis: A Review. *ACS Catalysis*, 11(10), 6020-6058. https://doi.org/10.1021/acscatal.1c00903

Lujanienė, G., Novikau, R., Joel, E. F., Karalevičiūtė, K., Šemčuk, S., Mažeika, K., . . . Jokšas, K. (2022). Preparation of Graphene Oxide-Maghemite-Chitosan

Composites for the Adsorption of Europium Ions from Aqueous Solutions. *Molecules*, *27*(22), 8035.

Macías, F., Caraballo, M. A., Nieto, J. M., Rötting, T. S., & Ayora, C. (2012). Natural pretreatment and passive remediation of highly polluted acid mine drainage. *Journal of Environmental Management*, *104*, 93-100.

Mahmoud, M. E., Mohamed, A. K., Amira, M. F., & Seleim, S. M. (2019). Novel Nanostructured Metal–Organic Framework-Bonded Silica Amine and Polymer: Facile Synthesis, Kinetics, Isotherms, and Thermodynamics Evaluation for Adsorption of Yttrium (III) Ions. *Journal of Chemical & Engineering Data*, *64*(12), 6060-6070.

McCarthy, T. (2011). The impact of acid mine drainage in South Africa. *South African Journal of Science*, *107*, 01-07.

McKay, G. (2001). Solution to the homogeneous surface diffusion model for batch adsorption systems using orthogonal collocation. *Chemical Engineering Journal*, *81*(1), 213-221.

Mehiguene, K., Garba, Y., Taha, S., Gondrexon, N., & Dorange, G. (1999). Influence of operating conditions on the retention of copper and cadmium in aqueous solutions by nanofiltration: experimental results and modelling. *Separation and Purification Technology*, *15*(2), 181-187.

Meng, L., Yang, L., Chen, C., Dong, X., Ren, S., Li, G., . . . Feng, S. (2020). Selective Acetylene Adsorption within an Imino-Functionalized Nanocage-Based Metal–Organic Framework. *ACS Applied Materials & Interfaces*, *12*(5), 5999-6006.

Meroufel, B., Benali, O., Benyahia, M., Benmoussa, Y., & Zenasni, M. (2013). Adsorptive removal of anionic dye from aqueous solutions by Algerian kaolin: Characteristics, isotherm, kinetic and thermodynamic studies. *J. Mater. Environ. Sci*, *4*(3), 482-491.

Miekeley, N., Coutinho de Jesus, H., Porto da Silveira, C. L., Linsalata, P., & Morse, R. (1992). Rare-earth elements in groundwaters from the Osamu Utsumi mine and Morro do Ferro analogue study sites, Poços de Caldas, Brazil. *Journal of Geochemical Exploration*, *45*(1), 365-387.

Min, X., Yang, W., Hui, Y.-F., Gao, C.-Y., Dang, S., & Sun, Z.-M. (2017). Fe3O4@ ZIF-8: a magnetic nanocomposite for highly efficient UO22+ adsorption and selective UO22+/Ln3+ separation. *Chemical Communications*, *53*(30), 4199-4202.

Miranda, L. S., Ayoko, G. A., Egodawatta, P., & Goonetilleke, A. (2022). Adsorption-desorption behavior of heavy metals in aquatic environments: Influence of sediment, water and metal ionic properties. *Journal of Hazardous Materials*, *421*, 126743.

Moritz, M., & Łaniecki, M. (2012). Application of SBA-15 mesoporous material as the carrier for drug formulation systems. Papaverine hydrochloride adsorption and release study. *Powder technology*, *230*, 106-111.

Motsi, T., Rowson, N. A., & Simmons, M. J. H. (2009). Adsorption of heavy metals from acid mine drainage by natural zeolite. *International Journal of Mineral Processing*, *92*(1), 42-48.

Mullett, M., Fornarelli, R., & Ralph, D. (2014). Nanofiltration of mine water: impact of feed pH and membrane charge on resource recovery and water discharge. *Membranes*, *4*(2), 163-180.

Murthy, Z., & Choudhary, A. (2011). Application of nanofiltration to treat rare earth element (neodymium) containing water. *Journal of rare earths*, *29*(10), 974-978.

Nagpal, G., Bhattacharya, A., & Singh, N. (2013). Removal of copper (II) from aqueous solution by Khangar. *Int. J. Eng. Res. Technol.*, *2*(12), 3624-3631.

Naidu, G., Jeong, S., Johir, M. A. H., Fane, A. G., Kandasamy, J., & Vigneswaran, S. (2017). Rubidium extraction from seawater brine by an integrated membrane distillation-selective sorption system. *Water Research*, *123*, 321-331.

Naidu, G., Loganathan, P., Jeong, S., Johir, M. A. H., To, V. H. P., Kandasamy, J., & Vigneswaran, S. (2016). Rubidium extraction using an organic polymer encapsulated potassium copper hexacyanoferrate sorbent. *Chemical Engineering Journal*, *306*, 31-42.

Naidu, G., Ryu, S., Thiruvenkatachari, R., Choi, Y., Jeong, S., & Vigneswaran, S. (2019). A critical review on remediation, reuse, and resource recovery from acid mine drainage. *Environmental Pollution*, *247*, 1110-1124.

Nakamoto, K. (2006a). Infrared and R aman spectra of inorganic and coordination compounds. *Handbook of vibrational spectroscopy*.

Nakamoto, K. (2006b). Infrared and Raman Spectra of Inorganic and Coordination Compounds. In *Handbook of Vibrational Spectroscopy*.

Nguyen, T. H., Ryu, S., Loganathan, P., Kandasamy, J., Nguyen, T. V., & Vigneswaran, S. (2022). Arsenic adsorption by low-cost laterite column: Long-term experiments

and dynamic column modeling. *Process Safety and Environmental Protection*, *160*, 868-875.

Nie, W., Luo, Y., Yang, Q., Feng, G., Yao, Q., & Lu, Z.-H. (2020). An amine-functionalized mesoporous silica-supported PdIr catalyst: boosting room-temperature hydrogen generation from formic acid. *Inorganic Chemistry Frontiers*, *7*(3), 709-717.

Nkinahamira, F., Alsbaiee, A., Zeng, Q., Li, Y., Zhang, Y., Feng, M., . . . Sun, Q. (2020). Selective and fast recovery of rare earth elements from industrial wastewater by porous β-cyclodextrin and magnetic β-cyclodextrin polymers. *Water research*, *181*, 115857.

Nordstrom, D. K. (2011). Hydrogeochemical processes governing the origin, transport and fate of major and trace elements from mine wastes and mineralized rock to surface waters. *Applied Geochemistry*, *26*(11), 1777-1791.

Nordstrom, D. K., Bowell, R. J., Campbell, K. M., & Alpers, C. N. (2017). Challenges in recovering resources from acid mine drainage. Mine Water and Circular Economy. Proceedings of the 2017 International Mine Water Association Conference held,

Ohno, K., Matsui, Y., Itoh, M., Oguchi, Y., Kondo, T., Konno, Y., . . . Magara, Y. (2010). NF membrane fouling by aluminum and iron coagulant residuals after coagulation–MF pretreatment. *Desalination*, *254*(1-3), 17-22.

Olias, M., Canovas, C. R., Basallote, M. D., & Lozano, A. (2018). Geochemical behaviour of rare earth elements (REE) along a river reach receiving inputs of acid mine drainage. *Chemical Geology*, *493*, 468-477.

Olías, M., Cánovas, C. R., Basallote, M. D., & Lozano, A. (2018). Geochemical behaviour of rare earth elements (REE) along a river reach receiving inputs of acid mine drainage. *Chemical Geology*, *493*, 468-477.

Olivetti, E. A., Ceder, G., Gaustad, G. G., & Fu, X. (2017). Lithium-ion battery supply chain considerations: analysis of potential bottlenecks in critical metals. *Joule*, *1*(2), 229-243.

Pagano, G., Guida, M., Tommasi, F., & Oral, R. (2015). Health effects and toxicity mechanisms of rare earth elements-Knowledge gaps and research prospects. *Ecotoxicol Environ Saf*, *115*, 40-48.

Parani, S., & Oluwafemi, O. S. (2021). Membrane distillation: recent configurations, membrane surface engineering, and applications. *Membranes*, *11*(12), 934.

Patel, H. (2019). Fixed-bed column adsorption study: a comprehensive review. *Applied Water Science*, *9*(3), 45.

Pearce, G. (2007). Introduction to membranes: Filtration for water and wastewater treatment. *Filtration & separation*, *44*(2), 24-27.

Pearson, J. L., Michael, P. R., Ghaffour, N., & Missimer, T. M. (2021). Economics and Energy Consumption of Brackish Water Reverse Osmosis Desalination: Innovations and Impacts of Feedwater Quality. *Membranes (Basel)*, *11*(8).

Pereira, R. C., Anizelli, P. R., Di Mauro, E., Valezi, D. F., da Costa, A. C. S., Zaia, C. T. B., & Zaia, D. A. (2019). The effect of pH and ionic strength on the adsorption of glyphosate onto ferrihydrite. *Geochemical transactions*, *20*(1), 1-14.

Perrin, D. D., Dempsey, B., & Serjeant, E. P. (1981). *pKa prediction for organic acids and bases* (Vol. 1). Springer.

Peters, T. (2010). Membrane technology for water treatment. *Chemical engineering & technology*, *33*(8), 1233-1240.

Pino, L., Beltran, E., Schwarz, A., Ruiz, M. C., & Borquez, R. (2020). Optimization of nanofiltration for treatment of acid mine drainage and copper recovery by solvent extraction. *Hydrometallurgy*, *195*, 105361.

Potgieter-Vermaak, S. S., Potgieter, J. H., Monama, P., & Van Grieken, R. (2006). Comparison of limestone, dolomite and fly ash as pre-treatment agents for acid mine drainage. *Minerals Engineering*, *19*(5), 454-462.

Pramanik, M., & Bhaumik, A. (2014). Phosphonic acid functionalized ordered mesoporous material: a new and ecofriendly catalyst for one-pot multicomponent Biginelli reaction under solvent-free conditions. *ACS Applied Materials & Interfaces*, *6*(2), 933-941.

Protano, G., & Riccobono, F. (2002). High contents of rare earth elements (REEs) in stream waters of a Cu–Pb–Zn mining area. *Environmental Pollution*, *117*(3), 499-514.

Putranto, A., & Aziz, M. (2020). Mass transfer of adsorption of methylene blue into biomass-based activated carbons: heterogeneous surface diffusion model. *Separation Science and Technology*, *55*(13), 2269-2280.

Qiang, H., Xia, M., Wang, F., Lei, W., Lu, X., & Ni, Y. (2021). The highly specific detection and mechanism of Cu-MOF-74 fluorescent probe to amino trimethylene phosphonic acid: Experimental study and theoretical calculation of quantum chemistry. *Journal of Molecular Liquids*, *341*, 117442.

Ramasamy, D. L., Repo, E., Srivastava, V., & Sillanpää, M. (2017). Chemically immobilized and physically adsorbed PAN/acetylacetone modified mesoporous silica for the recovery of rare earth elements from the waste water-comparative and optimization study. *Water research*, *114*, 264-276.

Ramos, S. J., Dinali, G. S., Oliveira, C., Martins, G. C., Moreira, C. G., Siqueira, J. O., & Guilherme, L. R. G. (2016). Rare Earth Elements in the Soil Environment. *Current Pollution Reports*, *2*(1), 28-50.

Reddy, M., Bharathi, J. B., Peter, S., & Ramamohan, T. (1999). Synergistic extraction of rare earths with bis (2, 4, 4-trimethyl pentyl) dithiophosphinic acid and trialkyl phosphine oxide. *Talanta*, *50*(1), 79-85.

Ren, J., Dyosiba, X., Musyoka, N. M., Langmi, H. W., North, B. C., Mathe, M., & Onyango, M. S. (2016). Green synthesis of chromium-based metal-organic framework (Cr-MOF) from waste polyethylene terephthalate (PET) bottles for hydrogen storage applications. *International Journal of Hydrogen Energy*, *41*(40), 18141-18146.

Research, G. V. (2019). *Rare Earth Elements Market Size, Share & Trends Analysis Report By Product (Cerium, Dysprosium, Erbium), By Application (Magnets, Catalyst), By Region, And Segment Forecasts, 2019 - 2025*.

Rim, K. (2016). Effects of rare earth elements on the environment and human health: A literature review. *Toxicology and Environmental Health Sciences*, *8*, 189-200.

Rivas-Sanchez, A., Cruz-Cruz, A., Gallareta-Olivares, G., González-González, R. B., Parra-Saldívar, R., & Iqbal, H. M. (2022). Carbon-based nanocomposite materials

with multifunctional attributes for environmental remediation of emerging pollutants. *Chemosphere*, *303*, 135054.

Romal, J. R. A., & Ong, S. K. (2023). Marine polysaccharide-based hydrogels for critical materials selective removal and recovery: A review. *Coordination chemistry reviews*, *482*, 215054.

Romero, F. M., Prol-Ledesma, R. M., Canet, C., Alvares, L. N., & Pérez-Vázquez, R. (2010). Acid drainage at the inactive Santa Lucia mine, western Cuba: Natural attenuation of arsenic, barium and lead, and geochemical behavior of rare earth elements. *Applied Geochemistry*, *25*(5), 716-727.

Rosenbach Jr, N., Ghoufi, A., Deroche, I., Llewellyn, P., Devic, T., Bourrelly, S., . . . Maurin, G. (2010). Adsorption of light hydrocarbons in the flexible MIL-53 (Cr) and rigid MIL-47 (V) metal–organic frameworks: a combination of molecular simulations and microcalorimetry/gravimetry measurements. *Physical Chemistry Chemical Physics*, *12*(24), 6428-6437.

Ryu, S., Fonseka, C., Naidu, G., Loganathan, P., Moon, H., Kandasamy, J., & Vigneswaran, S. (2021). Recovery of rare earth elements (Lu, Y) by adsorption using functionalized SBA-15 and MIL-101 (Cr). *Chemosphere*, 130869.

Ryu, S., Naidu, G., Moon, H., & Vigneswaran, S. (2019). Selective copper extraction by multi-modified mesoporous silica material, SBA-15. *Science of The Total Environment*, *697*, 134070.

Ryu, S., Naidu, G., Moon, H., & Vigneswaran, S. (2020). Selective copper recovery by membrane distillation and adsorption system from synthetic acid mine drainage. *Chemosphere*, *260*, 127528.

Ryu, S., Naidu, G., Moon, H., & Vigneswaran, S. (2021). Continuous and selective copper recovery by multi-modified and granulated SBA-15. *Chemosphere*, *271*, 129820.

Ryu, S. C., Kim, J. Y., Hwang, M. J., & Moon, H. (2018). Recovery of nitrate from water streams using amine-grafted and magnetized SBA-15. *Korean Journal of Chemical Engineering*, *35*(2), 489-497.

Safaei, M., Foroughi, M. M., Ebrahimpoor, N., Jahani, S., Omidi, A., & Khatami, M. (2019). A review on metal-organic frameworks: Synthesis and applications. *TrAC Trends in Analytical Chemistry*, *118*, 401-425.

Saha, S., & Sinha, A. (2018). Review on Treatment of Acid Mine Drainage with Waste Materials: A Novel Approach. *Global Nest Journal*, *20*, 512-528.

Sahoo, P. K., Tripathy, S., Equeenuddin, S. M., & Panigrahi, M. K. (2012). Geochemical characteristics of coal mine discharge vis-à-vis behavior of rare earth elements at Jaintia Hills coalfield, northeastern India. *Journal of Geochemical Exploration*, *112*, 235-243.

Sampaio, R. M. M., Timmers, R. A., Xu, Y., Keesman, K. J., & Lens, P. N. L. (2009). Selective precipitation of Cu from Zn in a pS controlled continuously stirred tank reactor. *Journal of Hazardous Materials*, *165*(1), 256-265.

Sánchez España, J., López Pamo, E., Santofimia, E., Aduvire, O., Reyes, J., & Barettino, D. (2005). Acid mine drainage in the Iberian Pyrite Belt (Odiel river watershed, Huelva, SW Spain): Geochemistry, mineralogy and environmental implications. *Applied Geochemistry*, *20*(7), 1320-1356.

Schulz, K. J., DeYoung, J. H., Seal, R. R., & Bradley, D. C. (2018). *Critical mineral resources of the United States: economic and environmental geology and prospects for future supply*. Geological Survey.

Seo, E. Y., Cheong, Y. W., Yim, G. J., Min, K. W., & Geroni, J. N. (2017). Recovery of Fe, Al and Mn in acid coal mine drainage by sequential selective precipitation with control of pH. *CATENA*, *148*, 11-16.

Serre, C., Millange, F., Thouvenot, C., Nogues, M., Marsolier, G., Louër, D., & Férey, G. (2002). Very Large Breathing Effect in the First Nanoporous Chromium (III)-Based Solids: MIL-53 or CrIII (OH)⊙{O2C− C6H4− CO2}⊙{HO2C− C6H4− CO2H} x⊙ H2O y. *Journal of the American Chemical Society*, *124*(45), 13519-13526.

Seyyed Alizadeh Ganji, S. M., Shafaie, S., & Goudarzi, N. (2016). Investigation of performances of solvents D2EHPA, Cyanex272, and their mixture system in separation of some rare earth elements from a Nitric Acid solution. *Journal of Mining and Environment*, *7*(2), 143-148.

Shahbazi, A., Younesi, H., & Badiei, A. (2011). Functionalized SBA-15 mesoporous silica by melamine-based dendrimer amines for adsorptive characteristics of Pb(II), Cu(II) and Cd(II) heavy metal ions in batch and fixed bed column. *Chemical Engineering Journal*, *168*(2), 505-518.

Shahbazi, A., Younesi, H., & Badiei, A. (2013). Batch and fixed-bed column adsorption of Cu (II), Pb (II) and Cd (II) from aqueous solution onto functionalised SBA-15 mesoporous silica. *The Canadian Journal of Chemical Engineering*, *91*(4), 739-750.

Sheng, G., Dong, H., Shen, R., & Li, Y. (2013). Microscopic insights into the temperature-dependent adsorption of Eu (III) onto titanate nanotubes studied by FTIR, XPS, XAFS and batch technique. *Chemical Engineering Journal*, *217*, 486-494.

Sheng, G., Yang, S., Zhao, D., Sheng, J., & Wang, X. (2012). Adsorption of Eu (III) on titanate nanotubes studied by a combination of batch and EXAFS technique. *Science China Chemistry*, *55*, 182-194.

Shi, X., Xiao, C., Ni, H., Gao, Q., Han, L., Xiao, D., & Jiang, S. (2023). Pore structure and pore size change for tight sandstone treated with supercritical CO2 fluid. *Energy Reports*, *9*, 2286-2299.

Silva, L. F., Wollenschlager, M., & Oliveira, M. L. (2011). A preliminary study of coal mining drainage and environmental health in the Santa Catarina region, Brazil. *Environmental Geochemistry and Health*, *33*(1), 55-65.

Simate, G. S., & Ndlovu, S. (2014). Acid mine drainage: Challenges and opportunities. *Journal of Environmental Chemical Engineering*, *2*(3), 1785-1803.

Singovszka, E., Balintova, M., & Junakova, N. (2020). The impact of heavy metals in water from abandoned mine on human health. *SN Applied Sciences*, *2*(5), 934.

Smith, Y. R., Bhattacharyya, D., Willhard, T., & Misra, M. (2016). Adsorption of aqueous rare earth elements using carbon black derived from recycled tires. *Chemical Engineering Journal*, *296*, 102-111.

Song, S., Sun, W., Wang, L., Liu, R., Han, H., Hu, Y., & Yang, Y. (2019). Recovery of cobalt and zinc from the leaching solution of zinc smelting slag. *Journal of Environmental Chemical Engineering*, *7*(1), 102777.

Song, Y., Li, X., Li, C., Li, J., Dong, Z., Zhang, M., . . . Jiang, K. (2020). Exploring and comparing the roles of Ca2+ and Mg2+ in small-sized natural organics-induced charged nanofiltration membrane fouling. *Separation and Purification Technology*, *251*, 117415.

Sosa Lucio, M. D., Oh, E.-J., Ha, J.-H., Lee, J., Lee, H.-J., & Song, I.-H. (2023). Effects of Processing Conditions on the Properties of Porous Diatomite Granules Prepared by Sodium Alginate Gelation. *Applied Sciences*, 13(16), 9474.

Souza, P. R., Dotto, G. L., & Salau, N. P. G. (2017). Detailed numerical solution of pore volume and surface diffusion model in adsorption systems. *Chemical Engineering Research and Design*, *122*, 298-307.

Sun, Y., Chen, C., Tan, X., Shao, D., Li, J., Zhao, G., . . . Wang, X. (2012). Retracted Article: Enhanced adsorption of Eu (III) on mesoporous Al2O3/expanded graphite composites investigated by macroscopic and microscopic techniques. *Dalton Transactions*, *41*(43), 13388-13394.

Suzuki, M., & Suzuki, M. (1990). *Adsorption engineering* (Vol. 14). Kodansha Tokyo.

Tan, Q., & Li, J. (2019). Rare earth metal recovery from typical e-waste. In *Waste Electrical and Electronic Equipment (WEEE) Handbook* (pp. 393-421). Elsevier.

Tan, X., Fang, M., Li, J., Lu, Y., & Wang, X. (2009). Adsorption of Eu(III) onto TiO2: Effect of pH, concentration, ionic strength and soil fulvic acid. *Journal of Hazardous Materials*, *168*(1), 458-465.

Thallapally, P. K., Elsaidi, S., Sinnwell, M., Devaraj, A., Droubay, T., Nie, Z., . . . McGrail, B. (2018). Extraction of Rare Earth Elements using Magnetite@MOF Composites. *Journal of Materials Chemistry A*, *6*.

Tsuji, H., Ishii, Y., Shin, M., Taniguchi, K., Arai, H., Kurihara, M., . . . Hayashi, S. (2019). Factors controlling dissolved 137Cs concentrations in east Japanese Rivers. *Science of The Total Environment*, *697*, 134093.

Ujaczki, É., Zimmermann, Y. S., Gasser, C. A., Molnár, M., Feigl, V., & Lenz, M. (2017). Red mud as secondary source for critical raw materials–extraction study. *Journal of Chemical Technology & Biotechnology*, *92*(11), 2835-2844.

Vass, C. R., Noble, A., & Ziemkiewicz, P. F. (2019). The Occurrence and Concentration of Rare Earth Elements in Acid Mine Drainage and Treatment By-products: Part 1—Initial Survey of the Northern Appalachian Coal Basin. *Mining, Metallurgy & Exploration*, *36*(5), 903-916.

Vaziri Hassas, B., Rezaee, M., & Pisupati, S. V. (2020). Precipitation of rare earth elements from acid mine drainage by CO2 mineralization process. *Chemical Engineering Journal*, *399*, 125716.

Vera, Y. M., & Braga, F. d. S. (2019). Separation of gadolinium and europium from chloride media by the solvent extraction technique. *REM-International Engineering Journal*, *73*, 59-68.

Vicente-Beckett, V. A., Taylor McCauley, G. J., & Duivenvoorden, L. J. (2016). Metal speciation in sediments and soils associated with acid-mine drainage in Mount Morgan (Queensland, Australia). *Journal of Environmental Science and Health, Part A*, *51*(2), 121-134.

Vijayaraghavan, R., Ellappan, V., Dharmar, P., & Lakshmanan, U. (2018). Preferential adsorption of uranium by functional groups of the marine unicellular cyanobacterium Synechococcus elongatus BDU130911. *3 Biotech*, *8*, 1-9.

Viltres, H., López, Y. C., Gupta, N. K., Leyva, C., Paz, R., Gupta, A., & Sengupta, A. (2020). Functional metal-organic frameworks for metal removal from aqueous solutions. *Separation & Purification Reviews*, 1-22.

Wadekar, S. S., Hayes, T., Lokare, O. R., Mittal, D., & Vidic, R. D. (2017). Laboratory and pilot-scale nanofiltration treatment of abandoned mine drainage for the recovery of products suitable for industrial reuse. *Industrial & Engineering Chemistry Research*, *56*(25), 7355-7364.

Wakao, N., & Funazkri, T. (1978). Effect of fluid dispersion coefficients on particle-to-fluid mass transfer coefficients in packed beds: correlation of Sherwood numbers. *Chemical Engineering Science*, *33*(10), 1375-1384.

Wan, K., Wang, G., Bo, W., Xue, S., & Miao, Z. (2023). A Sandwich Structure of Fulvic Acid and PMIDA-Modified LDHs for the Simultaneous Removal of Cu2+ and Aniline in Multicomponent Solutions. *Langmuir*, *39*(7), 2537-2547.

Wang, L., Cao, T., Dykstra, J. E., Porada, S., Biesheuvel, P., & Elimelech, M. (2021). Salt and water transport in reverse osmosis membranes: Beyond the solution-diffusion model. *Environmental Science & Technology*, *55*(24), 16665-16675.

Wang, Q.-C., Wang, P., Qiu, Y., Dai, T., & Chen, W.-Q. (2020). Byproduct Surplus: Lighting the Depreciative Europium in China's Rare Earth Boom. *Environmental Science & Technology*, *54*(22), 14686-14693.

Wang, S., Wang, K., Dai, C., Shi, H., & Li, J. (2015). Adsorption of Pb2+ on amino-functionalized core–shell magnetic mesoporous SBA-15 silica composite. *Chemical Engineering Journal*, *262*, 897-903.

Wang, X., Zhai, L., Wang, Y., Li, R., Gu, X., Yuan, Y. D., . . . Zhao, D. (2017). Improving water-treatment performance of zirconium metal-organic framework membranes by postsynthetic defect healing. *ACS Applied Materials & Interfaces*, *9*(43), 37848-37855.

Warsinger, D. M., Swaminathan, J., Guillen-Burrieza, E., & Arafat, H. A. (2015). Scaling and fouling in membrane distillation for desalination applications: A review. *Desalination*, *356*, 294-313.

Wehbi, M., Mehdi, A., Alaaeddine, A., Jaber, N., & Ameduri, B. (2020). Solid–Liquid Europium Ion Extraction via Phosphonic Acid-Functionalized Polyvinylidene Fluoride Siloxanes. *Polymers*, *12*(9), 1955.

Wongsawa, T., Traiwongsa, N., Pancharoen, U., & Nootong, K. (2020). A review of the recovery of precious metals using ionic liquid extractants in hydrometallurgical processes. *Hydrometallurgy*, 105488.

Wu, Wang, L., Zhao, L., Zhang, P., El-Shall, H., Moudgil, B., . . . Zhang, L. (2018). Recovery of rare earth elements from phosphate rock by hydrometallurgical processes – A critical review. *Chemical Engineering Journal*, *335*, 774-800.

Wu, Yin, X., Zhang, Q., Wang, W., & Mu, X. (2014). The recycling of rare earths from waste tricolor phosphors in fluorescent lamps: A review of processes and technologies. *Resources, Conservation and Recycling*, *88*, 21-31.

Wu, J., Zhou, J., Zhang, S., Alsaedi, A., Hayat, T., Li, J., & Song, Y. (2019). Efficient removal of metal contaminants by EDTA modified MOF from aqueous solutions. *Journal of Colloid and Interface Science*, *555*, 403-412.

Xiaoqi, S., Huimin, L., Mahurin, S. M., Rui, L., Xisen, H., & Sheng, D. (2016). Adsorption of rare earth ions using carbonized polydopamine nano carbon shells. *Journal of Rare Earths*, *34*(1), 77-82.

Xing, X.-S., Fu, Z.-H., Zhang, N.-N., Yu, X.-Q., Wang, M.-S., & Guo, G.-C. (2019). High proton conduction in an excellent water-stable gadolinium metal–organic framework. *Chemical Communications*, *55*(9), 1241-1244.

Xu, Y., Li, J., Tan, Q., Peters, A. L., & Yang, C. (2018). Global status of recycling waste solar panels: A review. *Waste Management*, *75*, 450-458.

Yadav, A., Labhasetwar, P. K., & Shahi, V. K. (2021). Membrane distillation using low-grade energy for desalination: A review. *Journal of Environmental Chemical Engineering*, *9*(5), 105818.

Yang, W., Li, X., Li, Y., Zhu, R., & Pang, H. (2019). Applications of metal–organic-framework-derived carbon materials. *Advanced Materials*, *31*(6), 1804740.

Yang, X., Debeli, D. K., Shan, G., & Pan, P. (2020). Selective adsorption and high recovery of La3+ using graphene oxide/poly (N-isopropyl acrylamide-maleic acid) cryogel. *Chemical Engineering Journal*, *379*, 122335.

Yang, Y., Walton, A., Sheridan, R., Güth, K., Gauß, R., Gutfleisch, O., . . . Jones, P. T. (2017). REE recovery from end-of-life NdFeB permanent magnet scrap: a critical review. *Journal of Sustainable Metallurgy*, *3*(1), 122-149.

Yoshitake, H. (2005). Highly-Controlled Synthesis of Organic Layers on Mesoporous Silica: Their Structure and Application to Toxic Ion Adsorptions. *New Journal of Chemistry*, *29*.

Yu, F., Cui, T., Yang, C., Dai, X., & Ma, J. (2019). κ-Carrageenan/Sodium alginate double-network hydrogel with enhanced mechanical properties, anti-swelling, and adsorption capacity. *Chemosphere*, *237*, 124417.

Zhang, D.-r., Chen, H.-r., Nie, Z.-y., Xia, J.-l., Li, E.-p., Fan, X.-l., & Zheng, L. (2020). Extraction of Al and rare earths (Ce, Gd, Sc, Y) from red mud by aerobic and anaerobic bi-stage bioleaching. *Chemical Engineering Journal*, *401*, 125914.

Zhang, H., McDowell, R. G., Martin, L. R., & Qiang, Y. (2016). Selective Extraction of Heavy and Light Lanthanides from Aqueous Solution by Advanced Magnetic Nanosorbents. *ACS Appl. Mater. Interfaces*, *8*(14), 9523.

Zhang, M., Yang, K., Cui, J., Yu, H., Wang, Y., Shan, W., . . . Xiong, Y. (2020). 3D-agaric like core-shell architecture UiO-66-NH2@ZIF-8 with robust stability for highly efficient REEs recovery. *Chemical Engineering Journal*, *386*, 124023.

Zhang, N., Yuan, L.-Y., Guo, W.-L., Luo, S.-Z., Chai, Z.-F., & Shi, W.-Q. (2017). Extending the use of highly porous and functionalized MOFs to Th (IV) capture. *ACS Applied Materials & Interfaces*, *9*(30), 25216-25224.

Zhang, R., Liu, Y., An, Y., Wang, Z., Wang, P., Zheng, Z., . . . Huang, B. (2019). A water-stable triazine-based metal-organic framework as an efficient adsorbent of Pb (II) Ions. *Colloids and Surfaces A: Physicochemical and Engineering Aspects*, *560*, 315-322.

Zhang, W., Bu, A., Ji, Q., Min, L., Zhao, S., Wang, Y., & Chen, J. (2019). pKa-Directed Incorporation of Phosphonates into MOF-808 via Ligand Exchange: Stability and Adsorption Properties for Uranium. *ACS Applied Materials & Interfaces*, *11*(37), 33931-33940.

Zhang, W., He, X., Ye, G., Yi, R., & Chen, J. (2014). Americium (III) capture using phosphonic acid-functionalized silicas with different mesoporous morphologies: adsorption behavior study and mechanism investigation by EXAFS/XPS. *Environmental Science & Technology*, *48*(12), 6874-6881.

Zhang, W., & Honaker, R. Q. (2018). Rare earth elements recovery using staged precipitation from a leachate generated from coarse coal refuse. *International Journal of Coal Geology*, *195*, 189-199.

Zhang, Y., Xiong, Z., Yang, L., Ren, Z., Shao, P., Shi, H., . . . Luo, X. (2019). Successful isolation of a tolerant co-flocculating microalgae towards highly efficient nitrogen removal in harsh rare earth element tailings (REEs) wastewater. *Water research*, *166*, 115076.

Zhao, Cong, Z., Sun, H., & Ren, D. (2007). The geochemistry of rare earth elements (REE) in acid mine drainage from the Sitai coal mine, Shanxi Province, North China. *International Journal of Coal Geology*, *70*(1-3), 184-192.

Zhao, Duan, X., Azhar, M. R., Sun, H., Fang, X., & Wang, S. (2020). Selective adsorption of rare earth ions from aqueous solution on metal-organic framework HKUST-1. *Chemical Engineering Journal Advances*, *1*, 100009.

Zhao, Repo, E., Song, Y., Yin, D., Hammouda, S. B., Chen, L., . . . Sillanpää, M. (2017). Polyethylenimine-cross-linked cellulose nanocrystals for highly efficient recovery of rare earth elements from water and a mechanism study. *Green Chemistry*, *19*(20), 4816-4828.

Zhao, D., & Yu, S. (2015). A review of recent advance in fouling mitigation of NF/RO membranes in water treatment: pretreatment, membrane modification, and chemical cleaning. *Desalination and Water Treatment*, *55*(4), 870-891.

Zhao, F., Cong, Z., Sun, H., & Ren, D. (2007). The geochemistry of rare earth elements (REE) in acid mine drainage from the Sitai coal mine, Shanxi Province, North China. *International Journal of Coal Geology*, *70*(1), 184-192.

Zhao, M., Huang, Z., Wang, S., Zhang, L., & Zhou, Y. (2019). Design of L-cysteine functionalized UiO-66 MOFs for selective adsorption of Hg (II) in aqueous medium. *ACS Applied Materials & Interfaces*, *11*(50), 46973-46983.

Zhao, S., Ba, C., Yao, Y., Zheng, W., Economy, J., & Wang, P. (2018). Removal of antibiotics using polyethylenimine cross-linked nanofiltration membranes: Relating membrane performance to surface charge characteristics. *Chemical Engineering Journal*, *335*, 101-109.

Zheng, M., Ji, H., Duan, J., Dang, C., Chen, X., & Liu, W. (2020). Efficient adsorption of europium (III) and uranium (VI) by titanate nanorings: Insights into radioactive metal species. *Environmental Science and Ecotechnology*, *2*, 100031.

Zheng, M., Zhao, X., Wang, K., She, Y., & Gao, Z. (2019). Highly efficient removal of Cr (VI) on a stable metal–organic framework based on enhanced H-bond interaction. *Industrial & Engineering Chemistry Research*, *58*(51), 23330-23337.

Zheng, X., Wang, C., Dai, J., Shi, W., & Yan, Y. (2015). Design of Mesoporous Silica Hybrid Materials as Sorbents for the Selective Recovery of Rare Earth Metals. *J. Mater. Chem. A*, *3*(19), 10327.

Zhong, C.-M., Xu, Z.-L., Fang, X.-H., & Cheng, L. (2007a). Treatment of acid mine drainage (AMD) by ultra-low-pressure reverse osmosis and nanofiltration. *Environmental engineering science*, *24*(9), 1297-1306.

Zhong, C.-M., Xu, Z.-L., Fang, X.-H., & Cheng, L. (2007b). Treatment of Acid Mine Drainage (AMD) by Ultra-Low-Pressure Reverse Osmosis and Nanofiltration. *Environmental Engineering Science - ENVIRON ENG SCI*, *24*, 1297-1306.

Zoungrana, A., Çakmakci, M., Zengin, İ. H., İnoğlu, Ö., & Elcik, H. (2016). Treatment of metal-plating waste water by modified direct contact membrane distillation. *Chemical Papers*, *70*(9), 1185-1195.

Zulfikar, M., Novita, E., Hertadi, R., & Djajanti, S. (2013). Removal of humic acid from peat water using untreated powdered eggshell as a low cost adsorbent. *International Journal of Environmental Science and Technology*, *10*(6), 1357-1366.

Zuo, L., Yu, S., Zhou, H., Jiang, J., & Tian, X. (2011). Adsorption of Eu (III) from aqueous solution using mesoporous molecular sieve. *Journal of Radioanalytical and Nuclear Chemistry*, *288*(2), 579-586.